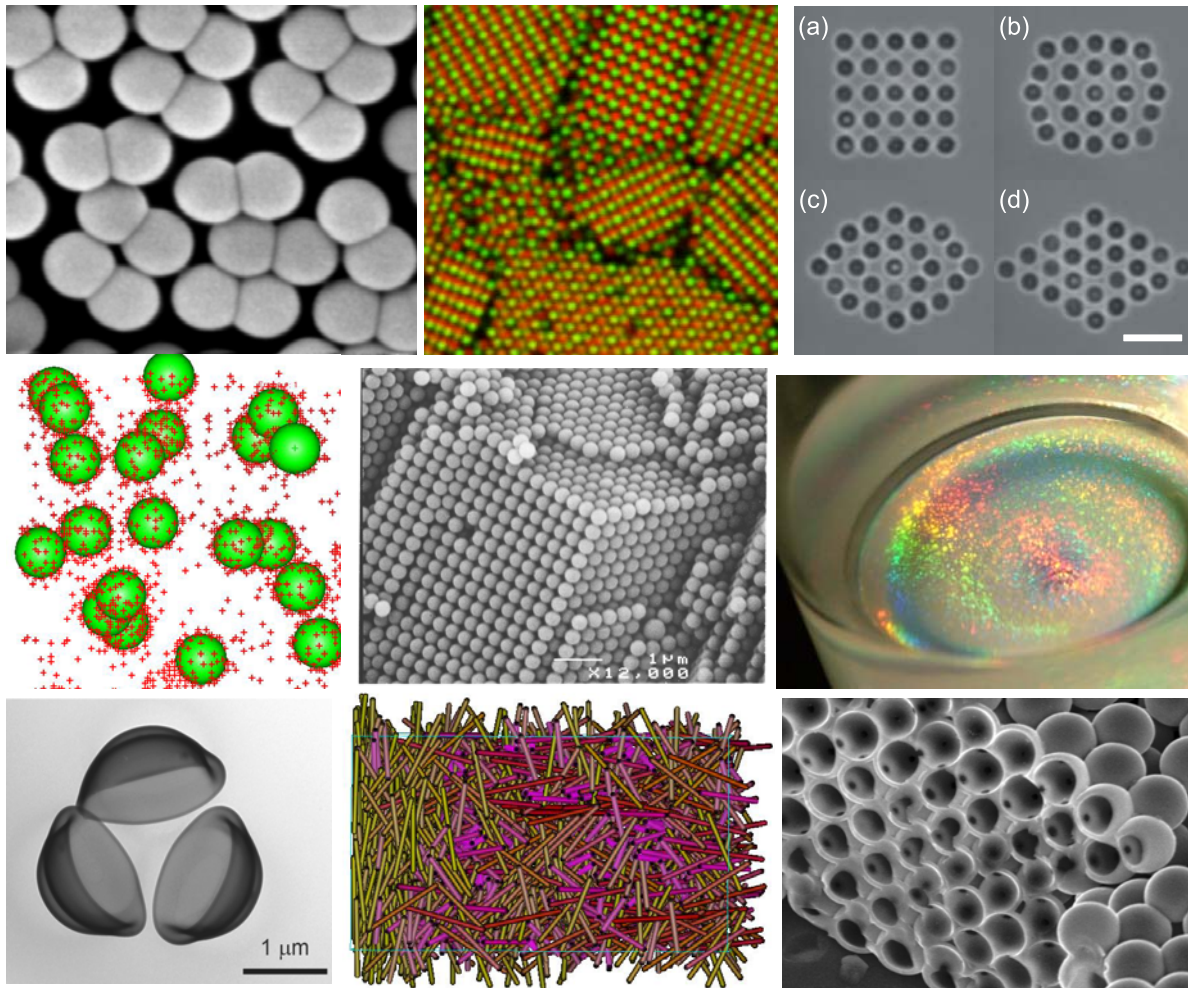


Soft Condensed Matter



Contents

1.	Introduction to soft condensed matter	1
2.	Classical ensemble theory	21
3.	Simple fluids	33
4.	Scattering techniques in soft condensed matter	53
5.	Phase behaviour	81
6.	Interfaces, micelles, and microemulsions	105
7.	Polymers	139
8.	DLVO theory & Measurement of interaction forces	179
	Problem sets	221

1. Introduction to soft condensed matter

Alfons van Blaaderen
Soft Condensed Matter, Debye Institute
Utrecht University

1. Introduction

1.1 Soft Condensed Matter vs. Complex Fluids

An important distinction between conventional or ‘*simple*’ liquids and solids is that the former quickly take the shape of the container in which they are kept, while the latter maintain their shape indefinitely. Almost all ‘*complex fluids*’ are intermediate between a solid and a liquid: while they maintain their shape for some time, they eventually flow. They are solids on a short time scale and liquids at long times: they are *viscoelastic*. Clearly, this rough definition is connected to a human time scale through the designation ‘for some time’. Glaciers do ‘flow’ on geological time scales and solids such as metals creep under large loads by defect motion. Nevertheless, these time scales are so far separated compared to the human lifespan that it does make sense to define a class of materials based upon their ability to flow or not during a (human) experiment, or said in another way, of having mechanical properties in between that of simple liquids and solids. Examples of such ‘complex liquids’ that are also treated in these lectures are: *polymers, colloids, (micro-) emulsions, foams and surfactant solutions*.

There are also complex fluids that change from solid-like to liquid-like, or vice versa, when subjected to a small deformation. Examples of these are different kind of gels that can consist of many of the examples mentioned above. Some fluids change to solids after application of an external electric or magnetic field; these are called electro- or magnetorheological fluids. Classical solids or liquids do not in general change state in response to a weak field.

Another important distinction between classical solids and liquids is that the former have properties that depend on the orientation of the crystallographic axes of the material, these properties, like elastic constants, are *anisotropic*, while the latter are the same in all directions, *isotropic*. Liquid Crystals (LC’s) take the shape of the container they are in immediately, because they flow like liquids, but their mechanical properties are anisotropic like that of crystals (see Fig. 1.1). Just as there are many types of crystalline symmetries, there are also many types of liquid crystal phases depending on the number of degrees of freedom that are solid- or liquid- like. These macroscopic anisotropic properties are the manifestation of some kind of microscopic anisotropy. This can be the shape of the molecules forming the

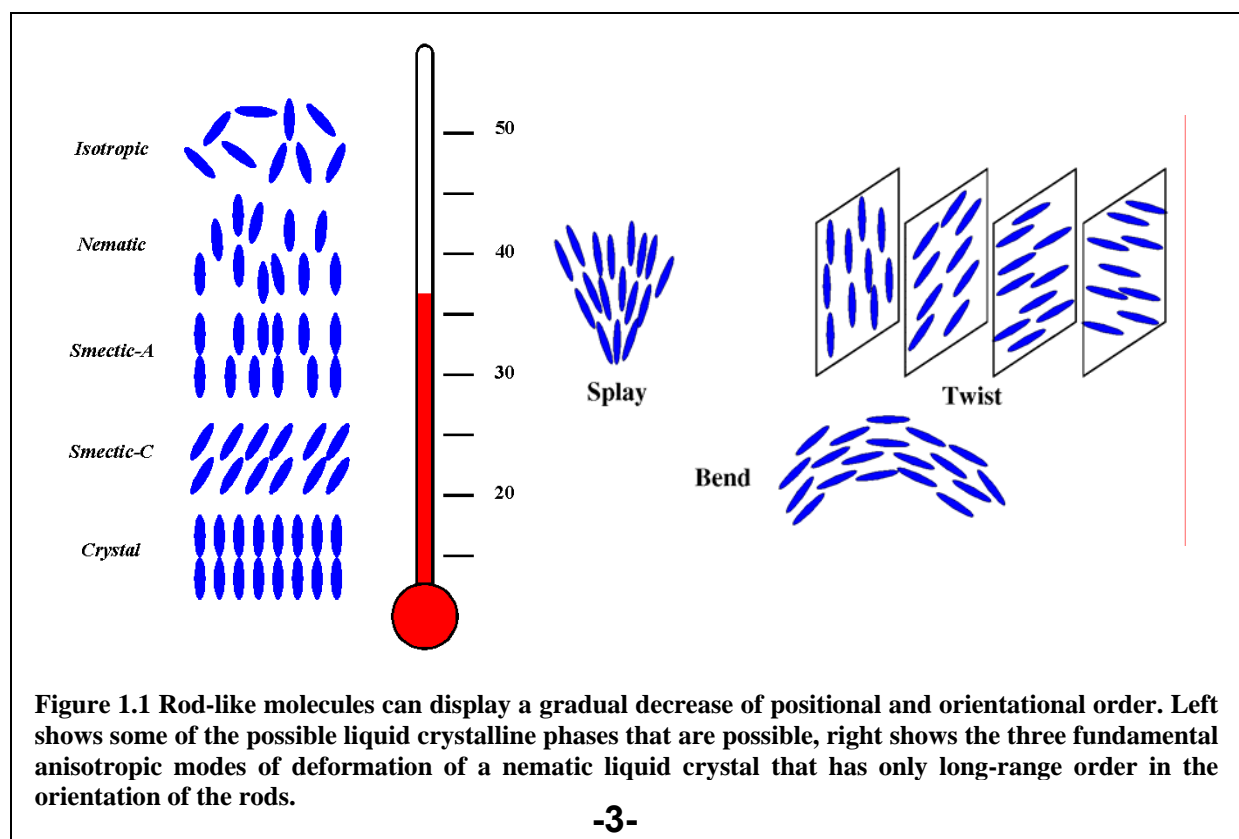


Figure 1.1 Rod-like molecules can display a gradual decrease of positional and orientational order. Left shows some of the possible liquid crystalline phases that are possible, right shows the three fundamental anisotropic modes of deformation of a nematic liquid crystal that has only long-range order in the orientation of the rods.

liquid crystal, but can also be on larger length scales involving self-organized subunits of surfactant molecules or colloidal particles as will be explained below.

A distinguishing feature of complex fluids compared to ordinary condensed matter is, that there always is a length scale involved that is large with respect to the size of individual atoms or small molecules. This separation of length scales makes it possible to integrate out many degrees of freedom and give a more simplified description of the problem. It basically means that the ordinary approach of statistical mechanics to treat a complicated many-body system, such as simple liquids, is taken a few steps further. Usually simplifying the description. Essential to our definition of complex fluids or soft matter is that a final description can be based on statistical mechanics. This sets a limit on the larger end of the length scale that can be included as will become clear below and from the rest of the course. Crossing this upper length scale gets us into the domain of granular matter. In this very interesting and, active field a simple connection with a statistical thermodynamic description cannot be made (at present). It should therefore be mentioned that there are researchers that also include slurries, like cement or wet sand, and foams with mm size air pockets to the realm of complex liquids. Through the general definition given above one can argue that they do belong to this class. However, as mentioned we would like to treat these granular matter systems as separate from the systems that can be dealt with using a thermodynamic description. In a strict sense liquid crystals consisting of small anisotropic molecules do not have a large length scale associated with them, nevertheless the defect structures that are part of these phases determine in a lot of cases their properties (and thus most of the times also their behavior in applications). The length scales of the defects include many molecular sizes

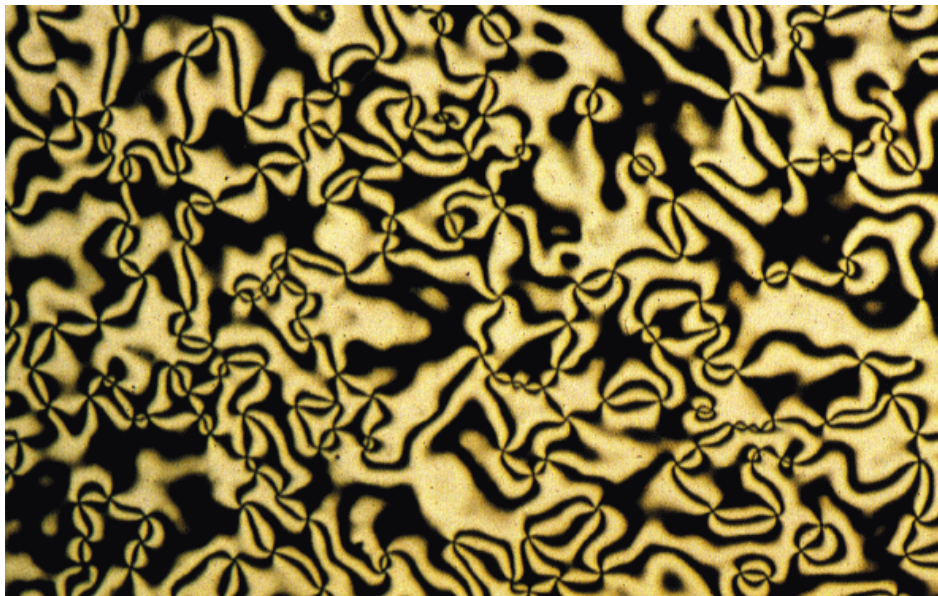
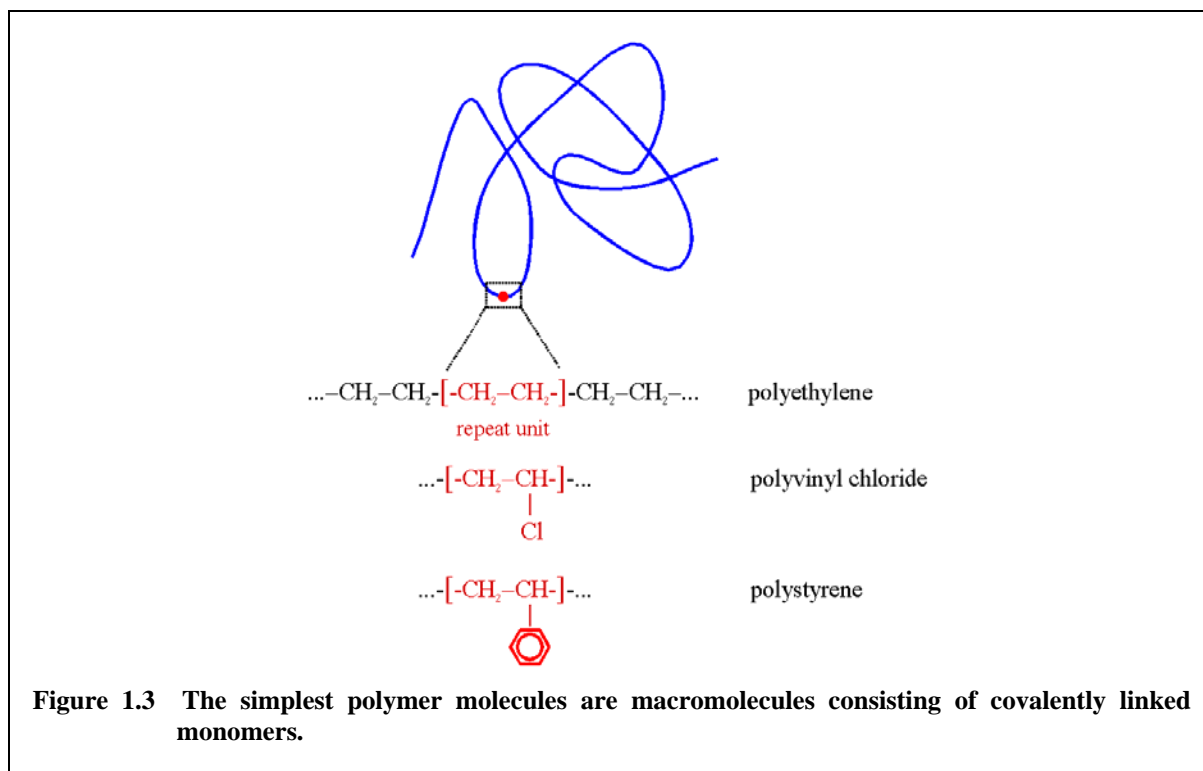


Figure 1.2 Defect structures made visible through crossed polarizers. Different intensities are caused by different local orientation of the molecules, image several mm².

(Fig. 1.2).

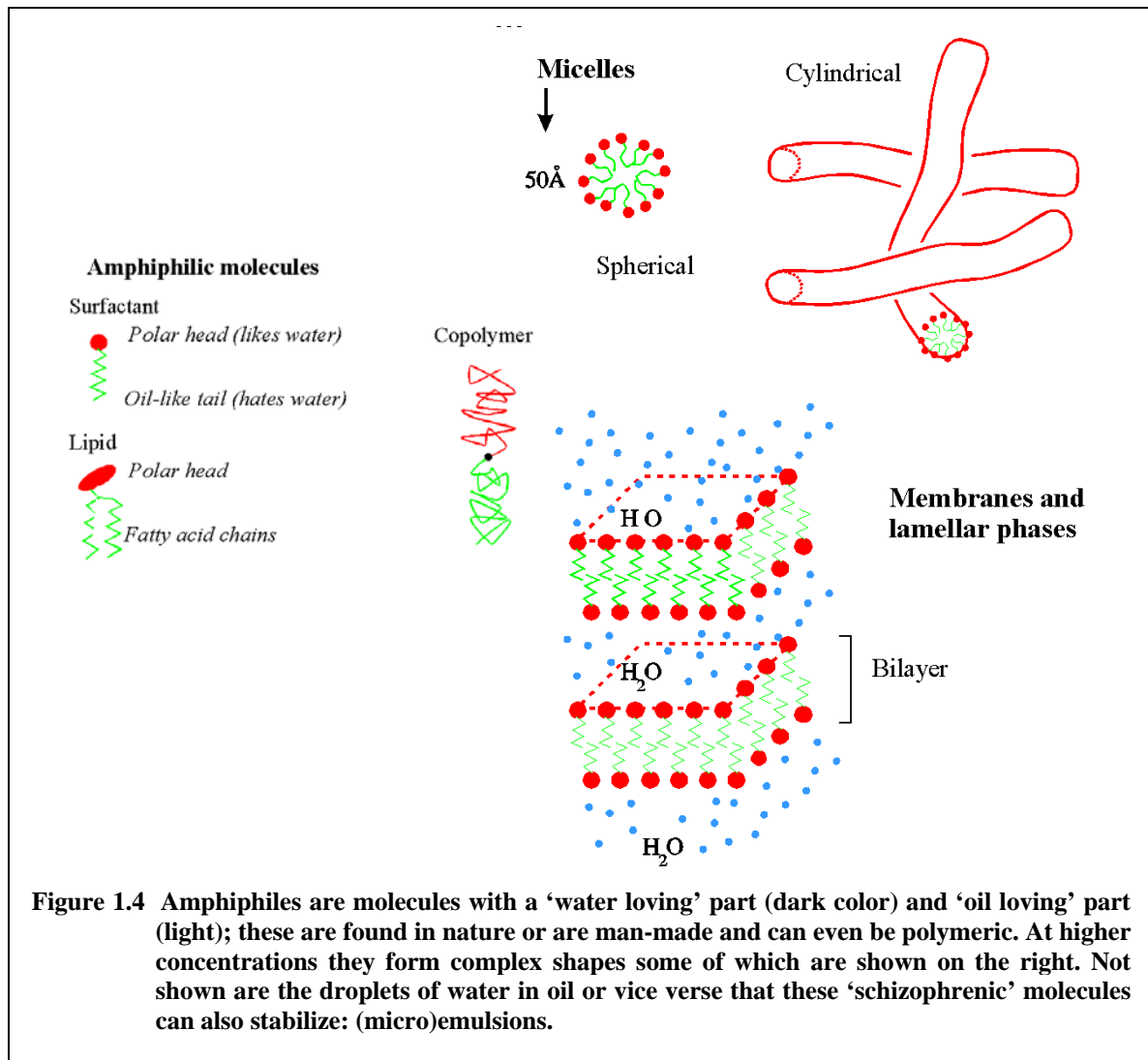
Colloidal particles dispersed in a medium encompass a large class of complex fluids. They are ‘solutions’ of one phase of matter (solid, liquid, gas), the colloidal particle, into another that acts as the continuous phase (liquid, gas). Roughly, the sizes of the particles are between several nm and several μm (see the section below on time and length scales). The name for solutions of particles in this size range is a *dispersion*; in the case that the

continuous phase is a gas such a dispersions is also called an *aerosol*. In case the particle is a liquid the colloidal system is called an (*micro*)-*emulsion*. The distinction between micro-emulsion and ‘ordinary’ emulsion is made on its thermodynamic stability. Micro-emulsions are thermodynamically stable and form spontaneously; emulsions need input of external free energy (e.g., in the form of violent stirring) to be formed and are metastable (although they can be very long lived). Dispersions of a gas in a liquid are called *foams*, while one can also disperse gases in gases through (*soap*) *films*. Again, for completion we mention that, based on the colloidal size range, some researchers also consider porous matter (liquid dispersed in a solid), solid suspensions (solid in a solid, e.g. wood) and solid foams (gas in a solid) as part of colloidal systems. We do not, because also in this case the description of these systems can generally not be made by a (coarse grained) thermodynamical approach.



Polymers are macromolecules that consist of many subunits connected to each other through chemical bonds (Fig. 1.3). More and more complex polymers are manmade, but still by far the most advanced types are found in nature. In the cell polymers are not only the carriers of the genetic code (DNA, RNA) they also catalyze or, literally, do all the work in the form of proteins. When polymer chains are in a collapsed state they form so-called polymer colloids or latex particles. However, the distinction between a polymer in a solution is not so clear. Generally, the synthetic pathways man has developed to make polymers renders them with a relatively broad length distribution, i.e., they are *polydisperse* in length. This is in stark contrast with many biopolymers which are exact copies of one another, a property referred to as *monodisperse*. However, recent new synthetic approaches making use of self-similar structures called dendrimers or architectures where polymer arms are attached to a central core-unit (so called star polymers) can also lead to monodisperse polymer colloids.

Surfactants are molecules with a ‘schizophrenic’ character in the sense that part of the molecule is happy in oil, usually an alkane-like tail, while another part of the molecule, usually with dissociable or polar groups, likes water (Fig. 1.4). The distinction between ‘oil’ and a polar solvent, usually water, is made because generally liquids that have such a large difference in polarity, pay a large enthalpic price if they would mix and that is why they will not, despite the favorable entropic contribution to mixing. This explains the word *amphiphile* (from the greek ‘loving both’) that is often also used to describe these molecules. Therefore, if an oil and immiscible polar liquid like water are into contact the amphiphilic molecules go to the interface with their polar part in the water and apolar part in the oil (chapter 3). In the process they lower the free energy of the interface between the two phases significantly, i.e.,



they lower the surface tension. In the case where the surface tension gets really low and almost vanishes, the entropy of mixing can become large enough that even a thermodynamically stable mixture of water droplets in oil or oil droplets in water (water should be read here as ‘immiscible polar solvent’) can result: a micro-emulsion. For this to occur, it turns out that the droplets need to be very small (~nm’s) to give enough mixing entropy and the surface free energy very small as the created interface surface is large. Under some conditions the amount of the phase of oil or water inside the droplets can be extremely small or even absent. In the case of solutions of surfactant in pure liquids; the colloidal entities that than form are called *micelles* (Fig. 1.4). The more general term referring to these

kind of systems, which do not necessarily need to be spheres is: *association colloids*. The non-droplet phases that can form, are characterized by the symmetry of the way the one phase is dispersed in the other or, in the case of only one solvent, according to the shape of the association colloid. Thus bi-continuous or even liquid crystalline arrangements of surfactant arranged matter is known. To distinguish the liquid crystals made up from self-organized amphiphiles from those consisting of anisotropic molecules, the former are referred to as *lyotropic* ('placement of liquid') and the second as *thermotropic*. The term thermotropic comes from the principle way to change the phase behavior: a change in temperature. And as mentioned, there are also liquid crystals where the smallest anisotropic units giving rise to the liquid crystalline behavior are colloidal particles; consequently these LC's are called colloidal liquid crystals (chapter 12).

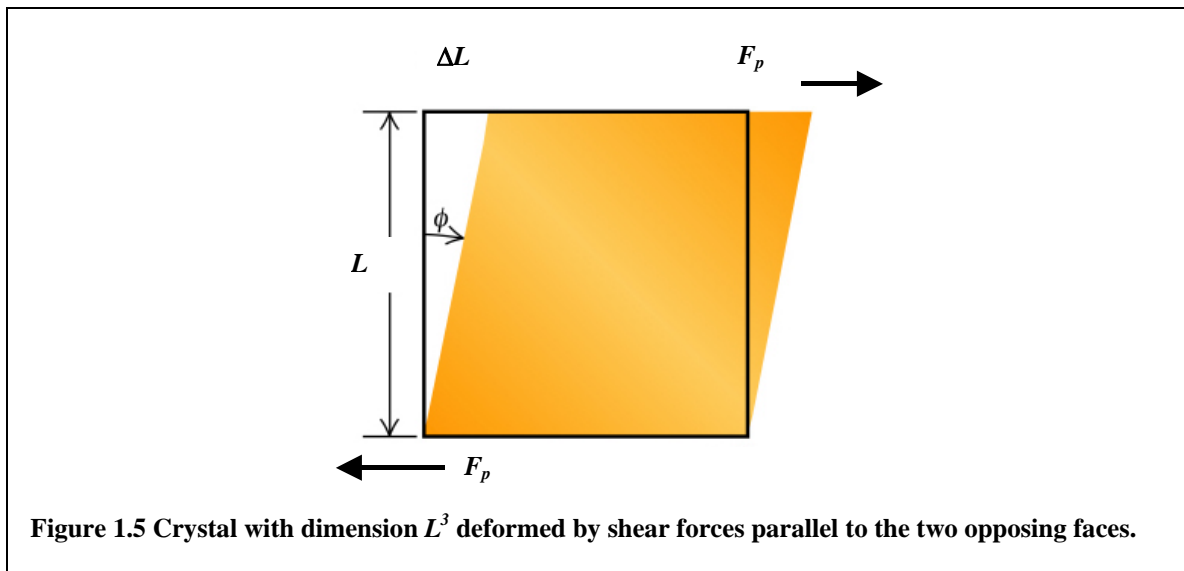
Droplets for which the surface tension is not low enough that they form thermodynamically stable phases can still be dispersed in another liquid by the action of surface-active molecules. In this case mechanic energy is needed to overcome the energy barrier necessary to form the surface between the two phases. As the amount of forces that can be applied on a liquid droplet in a violently flowing liquid determines the size of the droplets, they can generally not be smaller in size than ~100 nm and have usually a broad distribution in sizes (are polydisperse). Because these emulsion droplets would lower their free energy by merging together and reduce the total surface area, a mechanism needs to be in place preventing two droplets from coming into contact and coalesce. This is achieved either by charge repulsion or a so-called steric repulsion between the surfactant molecules, or a combination of both these two mechanisms.

All the examples of complex fluids mentioned above will be introduced in these lectures. The trend nowadays is however, mostly because of increased level of our ability to synthesize and control these systems on an ever-increasing level, to 'mix' these basic soft matter constituents in all kinds of new ways. Some of which will be mentioned briefly in chapter 15 of these lecture notes that deals with new materials made from soft matter and the use of colloids as condensed matter model system. Examples of these more complex complex fluids are: emulsions of thermotropic liquid crystals, amphiphilic and self-associating polymers, polymers with liquid crystalline (side) groups, dispersions of colloidal particles inside thermotropic liquid crystals, emulsions stabilized by colloidal particles etc. etc.

The use of the term *complex fluids* to describe the field as explained above can also be seen in a more negative light. With some exaggeration: physicists are used to describing the hydrogen atom and consider anything larger as 'complex'. This is a like the author that just finished his new textbook and proudly names it 'Modern Mathematics' to set it aside from everything written previously. Because of this possible negative connotation, we prefer the term *soft matter* to describe this research field. Our preference may also indicate that we are from Europe, as there is a strong preference on this side of the Atlantic for use of the term *soft matter*, while Americans usually prefer *complex fluids*. In any case, also the term soft matter needs an explanation, which we will give by focusing on the high-density phases of colloidal particles. The explanation has to do with the large length scale that is, as argued above, also a characteristic of soft matter. Colloidal particles at sufficiently high osmotic pressure, the equivalent in the colloidal domain of mechanical pressure (see Section 1.2), will crystallize forming 3D regular structures in ways that are completely analogous to how molecules freeze as will be explained in more detail in chapter 12 of these notes. Next to having lattice constants that are now in the range of the wavelength of visible light and time scales of crystallization that are much closer to the human time scale, there is another important consequence of the very large size of colloidal particles compared to atomic dimensions. Compared to molecular crystals colloidal crystals are tremendously soft. Nothing will happen to a collection of salt crystals if you put them in a jar and shake it. A colloidal crystal will not

survive such a treatment and will be completely destroyed. This dramatic difference is caused by the $\sim 10^{12}$ difference in the characteristic quantities, the elastic moduli, that determine the strength of a crystal. A solid is characterized by the fact that it keeps its shape if a small force is applied to it. The proportionality constant between the deformation or *stress* and the applied force per unit area or *strain* are called elastic moduli. Depending on the direction of the forces with respect to the deformation, one can distinguish different kind of constants describing the relation between stress and strain. These are the 3D analogs of the spring constant that according to Hook's law describes the proportionality between the force and displacement from its equilibrium position for a harmonic spring. In case the force per area (stress) is given as in Fig. 1.5, the resulting relative deformation (strain) is a twisting of the body that does not change its volume. This kind of stress-strain situation is called *shear*. The elastic constant describing it is called the *shear modulus*, μ , and is defined by:

$$\frac{F_p}{L^2} = \mu \frac{\Delta L}{L} \quad (1.1)$$



Here F_p is the shear force of a crystal with linear size L and ΔL is the crystal deformation (Fig. 1.5). Thus, the shear modulus has the dimension of a pressure or energy/(length)³. Intuitively, it is clear that the strength of a crystal is originating from the forces that bind the particles together in their 3D arrangement. This energy density is proportional to the number of these bonds in the crystal per unit of volume. As colloidal particles are about 10^3 - 10^4 as large as atoms, the elastic modulus is a factor 10^9 - 10^{12} less; soft matter indeed!

The association of small energy densities with large length scales is similar in other manifestations of soft matter and is accompanied by a dramatically increased sensitivity to external fields such as the already mentioned flow fields (shear), or electric and gravitational fields.

1.2 Historical notes

It goes much too far to give here a detailed historic account of the main sub fields of soft matter. It is however, important to know something about when certain phenomena were first studied, why certain names were given to certain fields and what the impact was of understanding gained in one field to other disciplines. Again, because of space we can only

touch upon these issues and have to refer to text books for a more elaborate description. However, really historical accounts dealing specifically with soft matter are rare. We also arbitrarily do not mention those developments here that took place less than 50 years ago.

Therefore, although particle systems were important for human civilization much through all of history, be it in the form of making ceramics, paints, inks or later to make steel, it is appropriate to start by the researcher who coined the word colloid. This was Thomas Graham who in 1861 studied solutions and classified that what could pass through, what we would now call a semi-permeable, membrane and what did not. What did not pass he called colloids after the Greek $\kappa\omicron\lambda\lambda\alpha$ meaning glue. This reflected the fact that many of the substances that Graham dissolved and that did not pass his membrane were polymeric in nature and often displayed a sticky behavior when dried.

As a small aside, we mention here some other experiments performed with semi-permeable membranes, in this case on dilute molecular solutions, because they lead in the mid-1880's van 't Hoff in Amsterdam to a law that now bears his name:

$$\Pi V = nRT \quad (1.2)$$

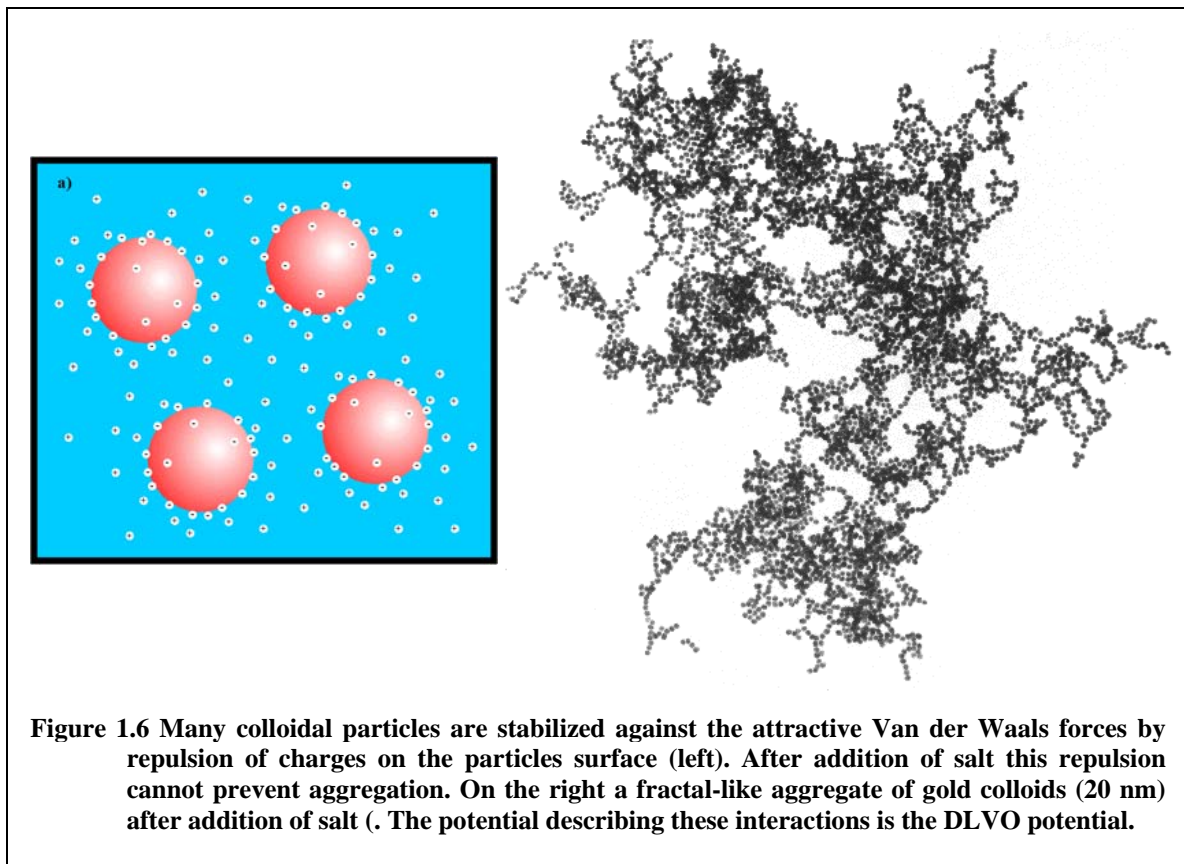
This equation, which bears great resemblance to the ideal gas law, describes the relation, for a dilute amount of n moles of dissolved molecules, between the osmotic pressure, Π , the volume, V , and the temperature, T . So what *is* the osmotic pressure? It is the excess pressure that is needed to achieve equilibrium between a solution containing n moles of molecules that cannot pass a (stiff) membrane that separates this solution with a compartment containing pure solvent. When brought into contact with each other through the membrane, solvent will start to stream from the compartment with the pure liquid into the compartment containing the dissolved species, thereby increasing the pressure, until equilibrium is reached. This excess pressure is called the osmotic pressure and assures that the flows of solvent going both ways through the membrane become equal again. It is no coincidence that van 't Hoff's law states that this excess pressure exactly equals the pressure an amount of n moles of ideal gas would have exerted were it to be placed in a compartment of the same volume and temperature.

However, before the term 'colloid' was coined by Graham, important experiments with colloidal particles had already been performed. In 1827 the botanist Robert Brown studied the thermal motion of pollen grains he observed through a microscope. Contrary to others who had tried to explain this erratic motion before him, he correctly concluded by studying a range of finely divided substances that this motion had nothing to do with life or a 'life force'. It took till Albert Einstein derived in 1905 the relationship between the diffusive Brownian motion and the thermal energy of the solvent molecules that causes it (see Eq. (1.8) in the next Section) this correct conclusion was given a theoretical basis. It is much less known that in the same year, and independently, W. Sutherland from Australia derived the same relation. Despite this fact Eq. (1.8) is generally referred to as the Stokes-Einstein relation. In 1910 Perrin used it to experimentally determine Avogadro's number by analyzing the diffusive motion observed through a microscope of a model dispersion of colloidal spheres he had painstakingly had made monodisperse by repeated centrifugation. These and other experiments he performed to determine this fundamental quantity earned him in 1926 the Nobel prize in Physics for putting '*a definite end to the long struggle regarding the real existence of molecules*' (committee report).

Important experiments before Graham were also performed by Faraday (1791-1867) on gold sols which he flocculated by adding salt. Without salt however, they can be quite stable; several of Faraday's gold sols are still on display in the British museum. Faraday also discovered that small particles could be detected by focusing light into a conical region. This led to the development of the ultramicroscope by Zsigmondy & Siedentopf in 1903, later

used by Perrin. The theory for the scattering of particles small compared to the wavelength was developed by Lord Rayleigh (1881) and finally as a general solution to Maxwell's equations by G. Mie (1908). Because of the increased length scale characterizing soft matter (light) scattering is an important technique that will also be treated in these notes in chapter 5.

It took until after the development of Quantum Mechanics in the 1940's before the first general description of the interaction forces between two colloidal particles were given. This theory was developed independently of each other by Derjaguin and Landau in the former Soviet Union and Verwey and Overbeek in the Netherlands. This so-called DLVO theory describes the interactions resulting from the (between identical particles) attractive Van der Waals forces and the (between identical particles) repulsive forces resulting from charges residing on the particles surfaces (Fig. 1.6). This potential is still a cornerstone of colloid science and experimental ways to measure it will be presented in chapter 9, together with its derivation.



Significant contributions on the study of surfactants (chapter 3) can be traced back to Benjamin Franklin's observations in 1757 of pouring oil on turbulent waters. He noticed that the wakes behind ships were calmed after the cook dumped greasy material in the water. Although he did obtain patents on this effect, they did not turn out to be too practical. It was Agnes Pockels who at the end of the 19th century studied and build the apparatus to measure the pressure versus area curves for monolayers of surfactants. This set the stage for Langmuir's work on the same subject in the beginning of the 20th century and our ability to characterize and understand the very complex phase behavior of amphiphiles.

In 1920 H. Staudinger showed that polymers (chapter 6) are not micellar aggregates, but real macromolecules, in which the monomers from which they formed are held together by covalent bonds. In 1931 Carothers produces the first nylon polymers. Soon thereafter W. Kuhn derives in 1934 the probability distribution for the average size and shape of a random coil.

Early studies on liquid crystals include those of another botanist L. Reinitzer who in 1888 observed two separate melting temperatures in cholesterol nonanoate. The term liquid crystal was coined by the physicist Otto Lehmann, who demonstrated that Reinitzer's phase changes were thermodynamic transitions. In the early 1920's work on the identification of many of the new LC phases took place, while also a description of the unusual defects and textures present in these phases was started. Most notably among the scientists studying LC's at that time was G. Friedel.

1.3 Separation of Time- and Length-Scales: Coarse Graining and Characteristic Forces

In this section we will focus on colloidal spheres with a radius R , but a lot of the reasoning is valid for most of the other soft matter systems as well. The fact that in the description of the properties of a dispersion one can take a so-called *coarse grained* approach is actually what defines the *colloidal domain*, as Evans and Wennerström call the size range between a few nm and a few μm . It also sets it apart from the molecular world on the one hand and granular matter on the other. If there is still a well-defined set of thermodynamical variables, the following approach in the statistical mechanical description can be taken. Coarse graining means averaging over a set of variables. If there is a large separation of length and time scales between the variables describing the constituents of the dispersed phase (the liquid or gas) and that what is dispersed in it (the colloid) one can average over, in other words trace-out, the fast variables that change on small length scales. This means we can, for instance, use continuum descriptions of the mechanical response of the dispersion medium (hydrodynamics). This approach simplifies both theories describing structure and dynamics of colloidal matter as it does computer simulations of these systems. On the other hand it is equally important for describing these properties and for that matter of what we define to be soft matter that not *all* thermodynamic variables are integrated out. In a physical description it means that there is a connection between the thermodynamics of the continuous phase with that of the dispersed particles. For instance, by linking the same fluctuations that cause Brownian motion to the dissipation that is characterized by the viscosity (first example of a fluctuation-dissipation relationship). It is exactly this loss of connection that makes 'sand in water' not a colloidal dispersion and instead a granular matter system; contrary to a solution of glass beads the size of $1\ \mu\text{m}$. It also means that the description of sand piles or slurries of sand in water is much harder and actually at this moment in time even lacks a general accepted theoretical framework to tackle this problem. The description of the properties of the ~ 1000 times smaller glass colloids, on the other hand, can be dealt with through the usual statistical mechanical approach. This is also why the first chapters (2-3) of these lecture notes on soft matter will start with both a recapitulation of statistical mechanics and an introduction to the description of liquids. These theoretical foundations are necessary to understand the methods for deriving, for instance, potentials between colloidal particles that do not contain the details of the liquid in which they are dispersed. In the case of charged colloids interacting through Van der Waals forces and (screened) Coulombic forces from charges residing on the particle surface, we will perform, or more accurately stated, sketch, such a derivation resulting in the DLVO potential after those that first derived it (Derjaguin, Landau, Verwey and Overbeek, chapter 9).

Interestingly, the size range that is defined as *colloidal* is dependant on those who do the observations, not through a collapse of a wave function, but by defining the time scale of experimental observations. Statistical mechanics shows that if an object has a well-defined thermodynamic temperature it has $0.5\ kT$ of kinetic energy per degree of freedom (equipartition theorem) where k stands for Boltzmann's constant ($1,381 \times 10^{-23}\ \text{J/K}$) and T the absolute temperature. This thermal energy leads on the scale of molecules to kinetic chaos

that on the particle level, characterized by a radius R , can be interpreted as a *Brownian force* with a magnitude of $O(kT/R)$. Before we can continue our analysis of relevant time and length scales and the role of different interactions that are of importance in a colloidal dispersion, we first have to take a short digression to that part of continuum physics that describes the laws of Newton in a continuous medium like a fluid or gas: hydrodynamics.

First, let us consider what happens to a fluid of which the density does not change, a so-called incompressible fluid ($\nabla \cdot U = 0$, usually a very good approximation), when we apply the same shear stress F_p/L^2 as in the shear deformation of the crystal mentioned above in Section 1.1. In the deformation of the solid described by Eq. (1.1) in that section we saw that the shear strain was, for small values, proportional to the shear strain. In a fluid the shear strain increases continuously and without limit as long as the force is applied: a fluid flows (Fig. 1.7). Therefore, the stress does not depend on the shear strain, but on its rate of change also called the strain rate or the shear rate (usually depicted by $\dot{\gamma}$). The *viscosity* of a fluid, η , is defined as the ratio of the shear stress, to the strain rate:

$$\eta = \frac{F_p/L^2}{v/L} = \frac{\text{Shear stress}}{\text{Strain rate}} \quad (1.3)$$

For a *Newtonian fluid* the viscosity does not depend on the speed v (or the shear rate) making the speed directly proportional to the applied force (stress). The viscosity, or as it is also called the ‘internal friction’, determines for a fluid how easy a liquid will flow by an applied force and how much energy is dissipated as heat. Viscous forces oppose the motion of one portion of a liquid relative to another. The equations that describe an incompressible

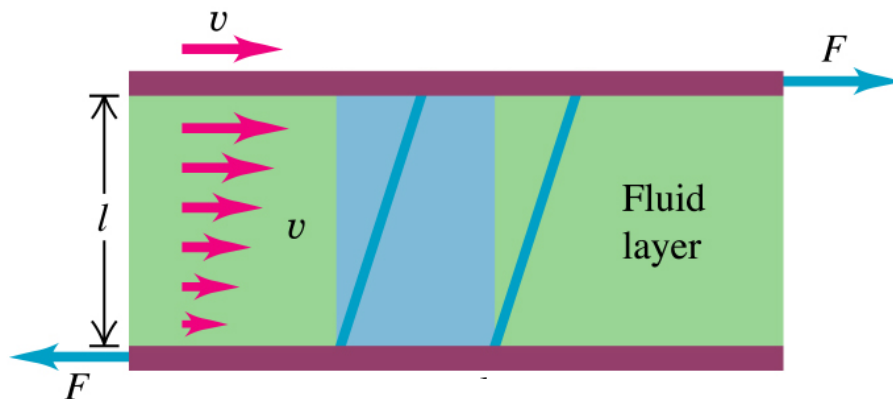


Figure 1.7 Shear forces applied onto a liquid lead to a shear rate characterized by a viscosity.

Newtonian liquid are called the *Navier-Stokes* equations. These describe the momentum conservation principles of elementary physics, for a system that includes friction, as applied to a stationary control volume through which fluid may enter or leave. Similarly as in Eq. (1.3), a sphere with a stick boundary condition on which a constant force is applied will obtain a constant speed. A stick boundary condition means that the fluid just adjacent to the particles surface does not move with respect to the particle. Again the proportionality constant is given by the viscosity and by the particle size. This friction factor, f , has Stokes’ name associated with it, because it follows as a solution to the *Stokes hydrodynamic equations*.

$$f = 6\pi\eta R \quad (1.4)$$

The Stokes equations are a limit of the Navier-Stokes equations and are obtained by neglecting effects of inertia. Inertia and viscous forces affect a mechanical mass-point system in similar ways as in a hydrodynamical description. The *Brownian time*, τ_B , is defined as the relaxation time of momentum of a particle. It is given by the ratio of the mass and the friction factor and describes the time it takes a particle with mass m on which a force works to obtain its steady state velocity as dictated by the Stokes friction factor:

$$\tau_B = \frac{m}{f} = \frac{m}{6\pi\eta R} \quad (1.5)$$

The importance of inertia, as given by $O(R^2\rho U^2)$, with U a typical velocity, relative to viscous forces, $O(\eta RU)$, is given by the dimensionless group called the *Reynolds* number:

$$R_e \equiv \frac{\rho UR}{\eta} \quad (1.6)$$

If we fill in some typical numbers (see Table 1.1 for values chosen) we find 2×10^{-10} s for the Brownian time and 10^{-6} for the Reynolds number. Because of its small mass, momentum transferred to a Brownian particle is very quickly lost and inertial effects can be neglected for all relevant velocities. As our day-to-day experience with hydrodynamics, for instance while swimming or paddling a canoe, is in the limit where inertia effects cannot be neglected, one has to be careful when applying human intuition to the colloidal domain. For instance, if we shrink a person swimming to the size of a μm , his mass is so small that it becomes impossible to swim. Swimming relies heavily on pushing oneself off against the water to gain forward momentum, something that is not possible in the colloidal domain.

Filling in Eq. (1.5) for a solvent molecule tells us that on the molecular scale momentum is relaxed in 10^{-15} s. This is the time scale on which the solvent exerts forces on the colloidal particle. Before Perrin scientists tried to infer from the Brownian motion observed through a microscope the mean velocities of the particle. In principle the mean kinetic energy of a colloidal particle $\langle 0.5mv^2 \rangle = 1.5kT$, $0.5kT$ per degree of translational freedom as stated earlier. However, through our estimates of the relevant time and length scales we can now see that this method of analyzing Brownian motion is doomed to fail. It would mean accessing the particle displacements on time scales much shorter than τ_B , and length scales much shorter than can be resolved through a light microscope. What one observes through a microscope is already the result of many different uncorrelated forces on the particle. A process that is characterized by a great many realizations of uncorrelated events is a diffusion process characterized by a diffusion coefficient D_0 . We will revisit diffusion not only in chapter 13 on the dynamics of colloids, but also find that it describes the basic shape of a polymer molecule (chapter 6). The subscript ‘0’ here designates that we are dealing with single particle diffusion, not influenced by other particles. In a diffusion process particle displacements are not proportional to time as in Newtonian free flight, but instead scale with the square root of time:

$$\langle x^2(t) \rangle = 2D_0t \quad (1.7)$$

Eq. (1.7) describes the mean square displacement, $\langle x^2(t) \rangle$, as a function of time, t , for a 1D process. For each extra dimension a factor 2 needs to be added. It was Einstein who was the

first to derive a value for the diffusion coefficient by connecting the random diffusion process with the average kinetic energy of the colloids:

$$D_0 = \frac{kT}{f} = \frac{kT}{6\pi\eta R} \quad (1.8)$$

In his derivation Einstein used the Stokes friction factor, Eq. (1.4), van 't Hoff's law, Eq. (1.2) and the fact that Brownian motion is described by a diffusion process, Eq. (1.7).

The time it takes a Brownian particle to diffuse a distance $2R$, τ_i , is thus given by:

$$\tau_i = \frac{2R^2 f}{kT} = \frac{12\pi R^3 \eta}{kT} \quad (1.9)$$

This time is sometimes called the interaction time and we can use it to calculate the mean particle velocity resulting from the Brownian force as manifested through the irregular bombardment of solvent molecules, we find: $kT/(Rf)$ and thus indeed that the Brownian force is of $O(kT/R)$.

The interaction time, τ_i , also has physical meaning in a concentrated dispersion; it is the time it takes for a collectoin of colloidal particles that are close together to significantly change their configuration. The colloids experience direct interactions with their neighbors in addition to hydrodynamic friction in the process. This is not to say that the presence of the neighbors is not felt at shorter times. On the contrary, because hydrodynamic interactions are very long-range and very fast, as we will see shortly, the Brownian particle feels already the presence of the other particles on the so-called hydrodynamic time scale, τ_H :

$$\tau_H = \frac{\rho R^2}{\eta} \quad (1.10)$$

This hydrodynamic time, which is on the order of the time it takes a hydrodynamic shear wave to traverse a distance R , comes naturally out of the (Navier-Stokes) equations describing the hydrodynamics in which temporal accelerations are taken into account. After some thought it is not surprising that this hydrodynamic time, after some rearrangements turns out to be of the same order as the Brownian time, τ_B , defined earlier. Similarly as we did before we can calculate that the distance a Brownian particle diffuses in this time, l_B , equals:

$$l_B = \frac{\sqrt{2mkT}}{f} \quad (1.11)$$

Filling in our usual assumptions gives, $l_B \approx 0.1$ nm, which is as was already stated, very short. Thus, for times (much) longer than τ_B and distances (much) further than l_B we can forget about the transients and consider velocities as determined by the friction factor. Said in another way: for distances longer than l_B colloidal motions are overdamped. These facts make the calculation of hydrodynamic effects, which is still a formidable, many body problem, a lot easier and is also at the basis of a computer simulation technique called Brownian dynamics (chapters 7 & 12).

As we will see in chapter 9 it is actually almost always the case that particles dispersed in a liquid acquire a net charge. Although we will also derive in that chapter that the interaction between two charged spheres is mediated in important ways by the ions in solution

that reside around the particle because of its electric potential, an order of magnitude estimate from just a Coulombic repulsion of two spheres with a surface potential of ζ , is given by $\epsilon\epsilon_0\zeta^2$, here ϵ_0 is the dielectric permittivity of free space (8.85×10^{-12} C/Vm). As seen in Table 1.1 the electrical forces are usually larger than the Brownian forces thus explaining why these repulsions can protect two colloids from the attractive Van der Waals forces. As we will also see in chapter 9, additivity of the Van der Waals forces between molecules will lead to interactions between colloids that are always attractive between identical particles and that are characterized by the Hamaker constant, A_{eff} . This constant, which has a unit of [energy], depends on the dielectric properties of both the particles and the intervening dispersion medium and gives rise to a Van der Waals force of $O(A_{eff}/R)$.

Lastly, as was already mentioned, soft matter is much more amenable to external fields than conventional condensed matter. Here we will look at one field, gravity, that on earth is always present and is an important factor limiting experiments on particles that are larger than several μm , next of course to the time restraint a human lifetime puts on the time an experiment can run. The result of gravity is sedimentation: and the velocity a single colloidal sphere in a dilute dispersion will attain either moving down or up under the influence of this external field is given by the sedimentation velocity, U_s . If $\Delta\rho$ is the density difference between the particle and the solvent, the gravitational force is $O(R^3\Delta\rho g)$ with g the gravitational acceleration (9.89 m/s^2), then balancing frictional and gravitational forces gives:

$$U_s = \frac{2R^2\Delta\rho g}{9\eta} \quad (1.12)$$

With Eq. (1.6) we can check that indeed for typical values the Reynolds number is still small for all sedimentation processes. Another dimensionless number the *Peclet* number, here for sedimentation, gives the relative importance of diffusion as compared to sedimentation:

$$P_e = \frac{2RU_s}{D_0} \quad (1.13)$$

Even gas molecules experience the gravitational pull of the earth resulting in a barometric height distribution in which the gas density is characterized by an exponential. The decay length of this exponential distribution is called the gravitational length, l_g , and gives the height one has to lift a particle of (buoyant) mass Δm to raise its potential energy in the gravitational field by kT :

$$l_g = \frac{kT}{\Delta mg} \quad (1.14)$$

For an ideal gas this equation is easily derived by assuming local mechanical equilibrium: the gas pressure at a certain height should be the same as the weight of the gas above that point, i.e., hydrostatic pressure balance. Similarly, but now taking the osmotic pressure as given by Van 't Hoff's law instead of the ideal gas law, we can derive an exponential density distribution for colloids if they behave ideally as well. However, while for an ideal gas the gravitational height is several km, for colloids it can be even on the order of a particle size or smaller. Measuring the gravitational height of a colloidal dispersion was another way in which Perrin determined Avogadro's number.

Table 1.1 summarizes the importance of several forces for our chosen example parameters. Firstly, for all colloids inertia effects can generally be neglected and for almost all time and length scales one can assume diffusive motions and velocities governed by a friction factor. As mentioned, electrical forces keep it suspended and stable against aggregation by attractive Van der Waals forces, while stirring or a modest speed results in viscous forces that are of the same order as those exerted on the particle by thermal motion of the solvent molecules. Gravity effects are not dominant, but can in the long run not be neglected. However useful these quick order-of-magnitude estimates are, it should also not be forgotten that all the forces mentioned have very different dependencies on distance, decaying with different power laws or even exponentially. This is why the derivation of some of these laws will be dealt with in coming chapters as well as the experimental methods to measure them.

Table 1.1 *Order of Magnitude of Characteristic Forces:*
 $R = 1 \mu\text{m}$, $\eta = 10^{-3} \text{ kg/ms}$, $U = 1 \mu\text{m/s}$, $\rho = 10^3 \text{ kg/m}^3$, $\Delta\rho/\rho = 10^{-2}$,
 $g = 10 \text{ m/s}^2$, $A_{\text{eff}} = 10^{-20} \text{ J}$, $\zeta = 50 \text{ mV}$, $\varepsilon = 10^2$

$\frac{\text{electrical force}}{\text{Brownian force}}$	$\frac{R\varepsilon\varepsilon_0\zeta^2}{kT}$	$\sim 10^2$
$\frac{\text{Van der Waals force}}{\text{Brownian force}}$	$\frac{A_{\text{eff}}}{kT}$	~ 1
$\frac{\text{viscous force}}{\text{Brownian force}}$	$\frac{\eta UR^2}{kT}$	~ 1
$\frac{\text{gravitational force}}{\text{Brownian force}}$	$\frac{\Delta\rho R^3 g}{\eta UR}$	$\sim 10^{-1}$
$\frac{\text{inertial force}}{\text{viscous force}}$	$\frac{\rho R^2 U^2}{\eta UR}$	$\sim 10^{-6}$

1.4 Crossroad of Disciplines and Fields

The *Colloidal Domain*: where *Physics, Chemistry, Biology* and *Technology* meet. This is the appropriate title of a recent textbook on colloid science. Even in recent years this statement is gaining more and more momentum, as it is driven by a rapid increase in synthetic methods, increased power of computer simulations and an increasing theoretical understanding combined with powerful methods, including quantitative 3D microscopy, to study and manipulate soft matter. As this course is intended for those who in principle have never heard of complex fluids, our focus is on the physics of both the theoretical basis behind the approach to describe soft matter and on the physics of the experimental and computer simulation tools that are used to study this field. We have limited our focus further to an equilibrium treatment for the Masters subjects (marked with an *), and leave phenomena that have to do with soft matter under flow conditions (shear) and interacting diffusing systems for the advanced part of the course. We can only touch upon the very interesting physical chemical or chemical physical processes that underlie many of the synthetic approaches used to design soft matter systems. The reason is that without a basic understanding of the forces

and phase behavior of the systems in question it is not possible to describe a synthetic pathway in any detail. For instance, the route used most in industry to produce polymers, emulsion polymerization, illustrates this point nicely. The reaction heat that comes free during the chemical routes used to make polymers is large, but more problematically it comes free in a short amount of time. Without going into too much detail, this is mostly due to the fact that the reaction pathways are autocatalytic and therefore have a tendency to ‘run away’. One way to prevent the reactions to get out of hand is to perform them in small droplets of monomers in a sea of an inert (heat absorbing) liquid, such as water. To keep the emulsion droplets from creaming, they have to be stabilized by a surfactant. Subsequently, an initiator has to start the reaction by diffusing from the water phase into the droplets of monomers. A complex set of conditions depending on the diffusion constants of the species involved, the phase behavior of the growing polymer in the monomer liquid and the details of the chemical reactions, etc., now determine the final size of the polymers and the distribution of their length. In short, many synthetic pathways for soft matter components are complicated soft matter research issues where by far not all problems have been solved and where a lot of active research is going on. It is however important to understand how the increased length scale that is present in soft matter systems gives chemical control over the properties. To take colloids as an example: quantum mechanics dictates the interactions between molecules, while for a colloidal spheres with a radius R the interaction potential can be tailored to a very large

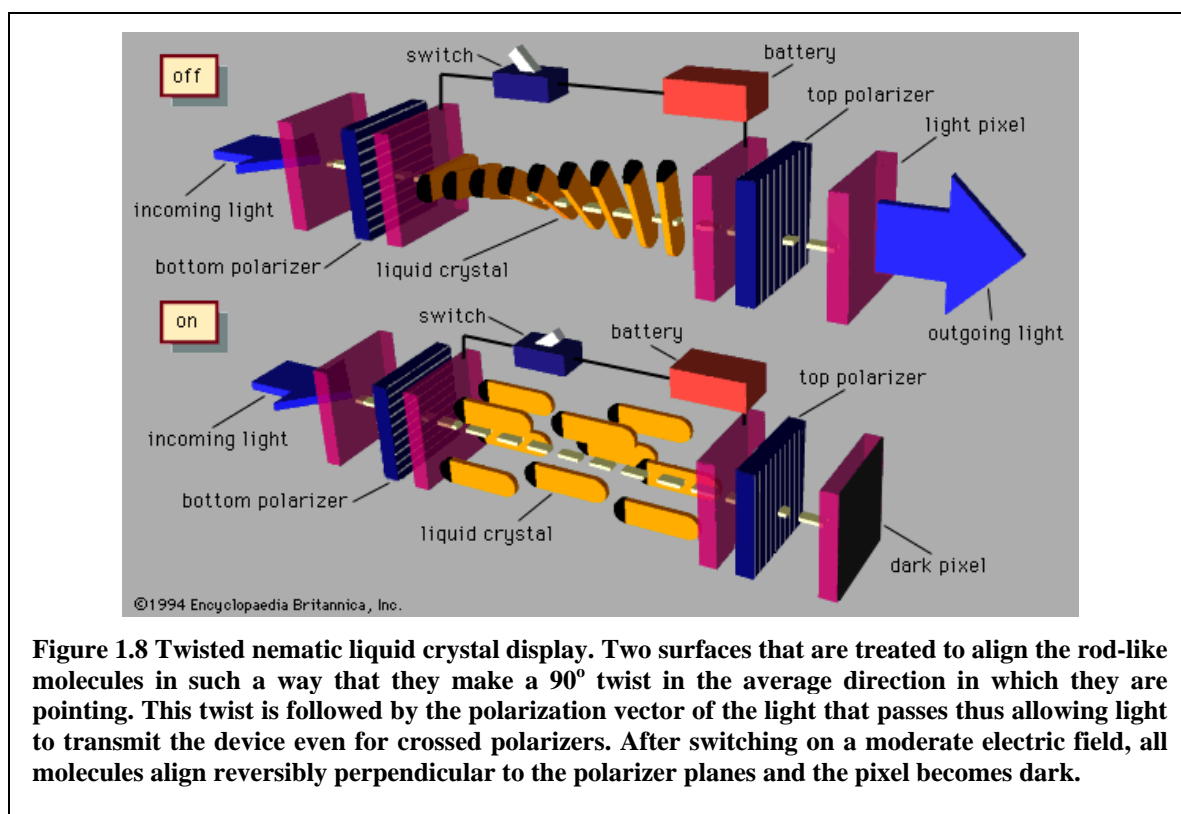


Figure 1.8 Twisted nematic liquid crystal display. Two surfaces that are treated to align the rod-like molecules in such a way that they make a 90° twist in the average direction in which they are pointing. This twist is followed by the polarization vector of the light that passes thus allowing light to transmit the device even for crossed polarizers. After switching on a moderate electric field, all molecules align reversibly perpendicular to the polarizer planes and the pixel becomes dark.

degree both by changing the properties of the particle surface (and/or bulk) and by changing the properties of the dispersion medium. Using particles with core-shell structures even increases the possibilities.

In many industrial processes soft matter systems play a role, this is clear if they are the main components such as in paints, polymers, cosmetics or foods, but is often also less obvious such as in oil recovery, or in the making of IC's. Almost all these systems are very complex involving many soft matter components that all interact with each other. This is why

most of these systems are not treated in this introductory course. It is certainly true however, that progress in the field of soft matter is being made at such a pace that the ‘model’ systems being studied are starting to become more and more complex as well, bridging the gap between the academic and industrial labs. Moreover, the progress mentioned is also creating a whole new class of materials that are directly based on the model systems with their well-controlled properties. These are advanced materials of which the properties can be adjusted dynamically by external stimuli such as: liquid crystal displays (Fig. 1.8), sensors based on photonic crystals or electro-rheological fluids. These materials are also called ‘smart’ materials (chapter 15).

As already mentioned, almost all the important content of every cell falls in the colloidal domain. This includes on the small end proteins and on the large end red blood cells. Despite a lot of recent research that uses almost exclusively theoretical and experimental techniques that were developed by soft matter researches, there is still a lot not known. For instance, even a simple question like: how does the cell or its components exert forces, is largely unknown

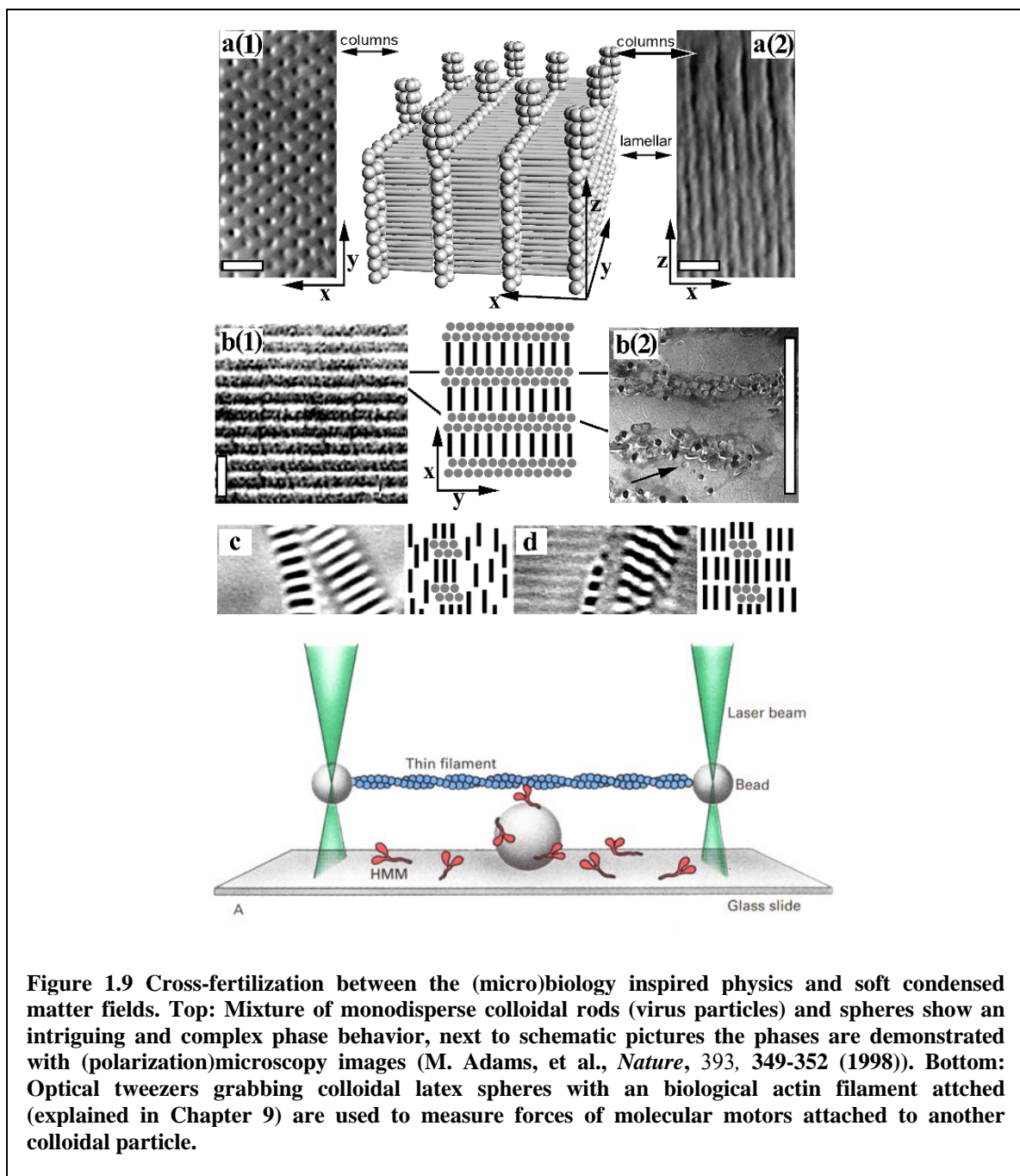
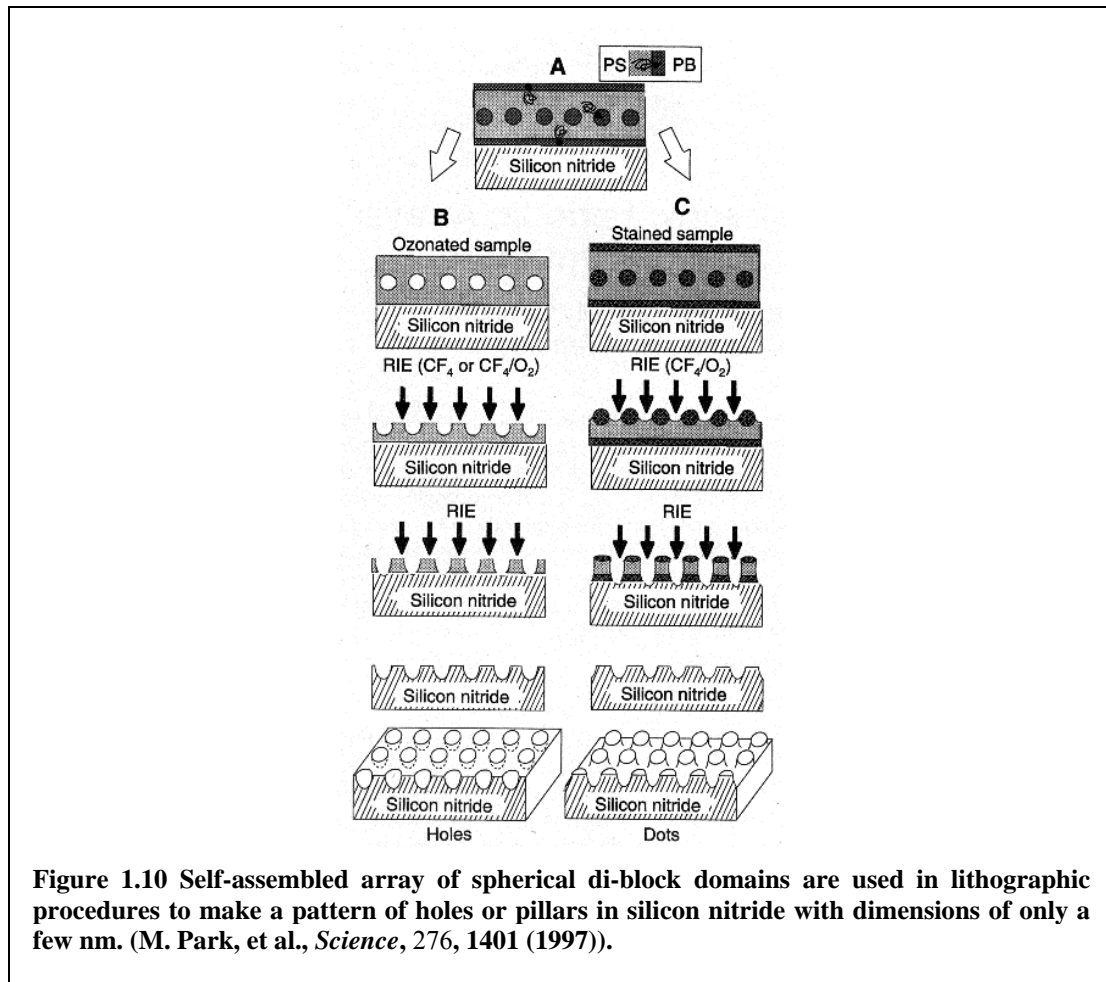


Figure 1.9 Cross-fertilization between the (micro)biology inspired physics and soft condensed matter fields. Top: Mixture of monodisperse colloidal rods (virus particles) and spheres show an intriguing and complex phase behavior, next to schematic pictures the phases are demonstrated with (polarization)microscopy images (M. Adams, et al., *Nature*, 393, 349-352 (1998)). Bottom: Optical tweezers grabbing colloidal latex spheres with an biological actin filament attached (explained in Chapter 9) are used to measure forces of molecular motors attached to another colloidal particle.

and an active field of research. It is fair to say that because of the large number of researchers in this field of biology inspired physics, there is also a flow of knowledge starting to go the other way (Fig. 1.9). One nice example is the possibility to induce specific, temperature reversible, interactions between colloids by coating them with single strands of DNA that will only interact with other particles that are coated with the complementary sequence. Similar cross-fertilization is also starting in the field of biology inspired (soft) materials science.



1.5 Connection with NanoScience and NanoTechnology

The (materials) science ‘buzzword’ at present is certainly anything that has ‘nano’ in it. Not only have the promises of ‘nanoscience’ and ‘nanotechnology’ inspired governments to increase funding in this area, the general public is starting to become aware of this ‘new field’ of science as well. Already, there are serious warnings in editorials in the journal *Nature* to the scientists working in this field that ‘objections and worries about the dangers of this emerging field need to be taken seriously’. By definition anything that has at least one dimension with feature sizes under 100 nm is determined to be part of nano-science. This length scale is chosen completely arbitrarily. Part of the motivation to study systems below this size is that this is roughly the size at which commercial IC’s are produced at the moment. And although it has already been predicted for over 20 years, there will indeed be an end to the doubling of the number of transistors on a silicon chip every (now) two years. Also without the ‘hype’ it is fair to say that the ability to make and design structures below 100 nm

is increasing rapidly. As may be clear from the above, soft matter scientists are playing an important role in this field.

Another reason for increased expectations is that new effects arise when one enters dimension truly close to a nm. For particles of this size one can no longer state that $\hbar = 0$ and quantum mechanical effects manifest itself. This can be understood qualitatively by considering the QM description of an electron in a box. Confinement of the wave function leads to a discrete spectrum of energy levels where the spacing is determined by the size of the box. This explains why metal particles or semiconductor crystals with sizes of several nm have strong size dependant properties and why, for instance their absorption spectrum shows discrete absorption bands. In similar ways as we can tune the interparticle interactions for larger colloids, one can now chemically tune the wave function of these ‘*quantum dots*’ (chapter 8).

What we have hoped to have achieved after following these SCM lectures is the ability to understand why in nano-science is not possible to just scale down a steam engine to a micron size and expect it to still work. It is amazing how many ‘serious’ scientists do not realize this.

(General)Textbooks

- 1) *Colloidal Dispersions*, W. B. Russel, D. A. Saville, W. R. Schowalter, Cambridge Un. Press, Cambridge, 1995.
- 2) *An Introduction to Dynamics of Colloids*, J. K. G. Dhont, in Studies in Interface Science, series Eds. D. Möbius, R. Miller, Elsevier, Amsterdam, 1996.
- 3) *The Colloidal Domain, where physics, chemistry, biology and technology meet*, D. F. Evans, H. Wennerström, in Advances in interfacial engineering series, VCH, New York, 1994.
- 4) *Principles of condensed matter physics*, P. M. Chaikin, T. C. Lubensky, Cambridge Un. Press, Cambridge, 1997.
- 5) *The Structure and Rheology of Complex Fluids*, R. G. Larson, in Topics in Chemical Engineering, Oxford Un. Press, Oxford, 1999.
- 6) *Intermolecular and Surface Forces*, J. Israelachvili, 2nd ed., Academic Press, London, 1992.
- 7) *Foundations of Colloid Science, Volumes I and II*, R. J. Hunter, Clarendon Press, Oxford, 1991.
- 8) *Structured Fluids, polymers, colloids, surfactants*, T.A. Witten, Ph. A. Pincus, Oxford Un. Press., 2004.
- 9) *Soft Condensed Matter*, A. L. Jones, Oxford Un. Press, 2002.

Origin Figures

All figures in this chapter have been obtained from the Timeline of soft condensed matter that was presented at the 100 year APS celebration, a version of this timeline can be found at: <http://www.nat.vu.nl/~fcm/ComplexFluids/ComplexFluids.html>

Chapter 2

Classical ensemble theory

2.1 Phase space

Consider an isolated system of N identical classical particles in a three dimensional volume V . If we assume that each particle has three translational degrees of freedom, then the microscopic state of this system is fully characterised by the $3N$ coordinates $\mathbf{r}^N \equiv \{\mathbf{r}_1, \dots, \mathbf{r}_N\}$ and the $3N$ conjugate momenta $\mathbf{p}^N \equiv \{\mathbf{p}_1, \dots, \mathbf{p}_N\}$ of the particles. The values of these variables define a *phase point* $\Gamma \equiv (\mathbf{r}^N, \mathbf{p}^N)$ in a $6N$ -dimensional *phase space*¹. The time evolution of the system can be seen as a motion of the phase point along its *phase trajectory*. This motion follows from the Hamiltonian $H(\mathbf{r}^N, \mathbf{p}^N)$ of the system, which is written here as

$$H(\mathbf{r}^N, \mathbf{p}^N) = \sum_{i=1}^N \frac{\mathbf{p}_i^2}{2m} + \Phi(\mathbf{r}^N), \quad (2.1)$$

where m is the mass of the particles and $\Phi(\mathbf{r}^N)$ the potential energy, which includes the external potential that defines the volume V . The Hamiltonian thus depends parametrically on the number of particles N and the volume V (or parameters that describe the volume V). This form of the Hamiltonian is not suitable for electro-magnetic systems, with velocity-dependent forces, but the formalism can be extended to include these as well. The Hamilton equations

$$\dot{\mathbf{r}}_i = \frac{\partial H}{\partial \mathbf{p}_i} \quad ; \quad \dot{\mathbf{p}}_i = -\frac{\partial H}{\partial \mathbf{r}_i}, \quad (2.2)$$

together with $6N$ initial conditions, determine the trajectory uniquely and completely. It follows that trajectories in phase space do *not* intersect.

2.2 The Liouville equation

It will turn out to be useful to consider an arbitrary large collection of macroscopically identical systems that only differ by their position in phase space. Such a collection is called an *ensemble*. At a given time t an ensemble is characterised by a cloud of phase points distributed according to a phase space probability density $f(\Gamma, t)$, with $f(\Gamma, t)d\Gamma$ the probability that the system is in a microscopic state lying in the infinitesimal $6N$ dimensional volume element $d\Gamma = d\mathbf{r}^N d\mathbf{p}^N$ around Γ . The time evolution of $f(\Gamma, t)$ is governed by the Liouville equation. This equation is the $6N$ -dimensional analogue of the continuity equation of a fluid; it describes that phase points can neither be created nor destroyed as time evolves, plus how they flow. The Liouville equation can be written compactly as

$$\frac{\partial f(\Gamma, t)}{\partial t} + \frac{\partial}{\partial \Gamma} \cdot (\dot{\Gamma} f(\Gamma, t)) = 0, \quad (2.3)$$

where $\partial/\partial \Gamma$ denotes the phase space gradient operator, and $\dot{\Gamma}$ the $6N$ dimensional vector $(\dot{\mathbf{r}}^N, \dot{\mathbf{p}}^N)$. As it follows directly from the Hamilton equations (2.2) that $\partial/\partial \Gamma \cdot \dot{\Gamma} = 0$, we rewrite Eq.(2.3) as

$$\frac{\partial f(\Gamma, t)}{\partial t} = -\dot{\Gamma} \cdot \frac{\partial f}{\partial \Gamma}$$

¹If each particle has n other internal degrees of freedom (e.g. orientations), then the dimension of the phase space becomes $(6+2n)N$.

$$= \sum_{i=1}^N \left[\frac{\partial H}{\partial \mathbf{r}_i} \frac{\partial f}{\partial \mathbf{p}_i} - \frac{\partial H}{\partial \mathbf{p}_i} \frac{\partial f}{\partial \mathbf{r}_i} \right] \equiv \{H, f\}, \quad (2.4)$$

where $\{, \}$ denotes the Poisson bracket. The Liouville equation is the starting point of most theories of nonequilibrium statistical mechanics. The focus in this course is on equilibrium statistical mechanics, where $f(\Gamma, t)$ is stationary, i.e. $(\partial f / \partial t) = 0$. Equilibrium ensembles are therefore characterised by phase space distributions $f(\Gamma)$ that satisfy $\{H, f\} = 0$. This implies that the Γ -dependence of f can only be through conserved quantities. In most cases of interest here the energy is the only conserved quantity², so that then $f(\Gamma) = \tilde{f}(H(\Gamma))$ for some function \tilde{f} . We will see that important examples include $f(\Gamma) \propto \delta(E - H(\Gamma))$ (microcanonical ensemble) and $f(\Gamma) \propto \exp[-H(\Gamma)/kT]$ (canonical ensemble).

2.3 Time averages and ensemble averages

The aim of equilibrium statistical mechanics is to calculate observables that result from a macroscopic measurement. Such a measurement yields the time average $\bar{\mathcal{A}}$ of a corresponding microscopic function $\mathcal{A}(\Gamma)$ over a sufficiently long time interval $t_0 \leq t \leq t_0 + \tau$ of the phase trajectory, i.e.

$$\bar{\mathcal{A}} = \frac{1}{\tau} \int_{t_0}^{t_0 + \tau} dt \mathcal{A}(\Gamma(t)). \quad (2.5)$$

Even if τ is very large compared to an atomic time scale (say $\tau = 1s$), this average depends, strictly speaking, on the initial time t_0 and on the particular trajectory of the measured system. It is common experience, however, that repeating the measurement on the same equilibrium system at later times t_0 yields an indistinguishable answer. Apparently most values of a phase function (with a macroscopic meaning) are close to their average value on a particular trajectory. Moreover, repeating the measurement on a replica of the original system (i.e. on a different trajectory) often also yields the same answer for $\bar{\mathcal{A}}$. This suggests an alternative microscopic description of a macroscopic equilibrium state: instead of time averaging over a single phase trajectory (as proposed in Eq.(2.5)), we can average over a suitably constructed equilibrium *ensemble* with a corresponding equilibrium probability density $f(\Gamma)$ that does not depend on time explicitly. The ensemble average is now defined as

$$\langle \mathcal{A} \rangle = \int d\Gamma f(\Gamma) \mathcal{A}(\Gamma), \quad (2.6)$$

where the normalisation $\int d\Gamma f(\Gamma) = 1$ is understood. In the next paragraphs we will discuss the standard classical ensembles, characterised by a specific form for $f(\Gamma)$. This form depends on the macroscopic parameters that are chosen to characterise the ensemble.

Remark 1. Systems for which $\bar{\mathcal{A}} = \langle \mathcal{A} \rangle$ for all continuous phase functions $\mathcal{A}(\Gamma)$ are called *ergodic*. Although ergodicity can almost never be proven, it is often assumed to hold. There are, however, manifestly nonergodic systems. Nonergodicity results if trajectories are restricted, for macroscopically long times, to a subspace. This can be caused by the presence of other conserved quantities besides energy (e.g. angular momentum), or due to spontaneous symmetry breaking (e.g. in antiferromagnets). Also systems with an extremely slow dynamics compared to the observation time, e.g. glasses, are nonergodic.

Remark 2. The two type of averages discussed here are also manifest in present day computer simulations of model systems for condensed matter. In Molecular Dynamics simulations the equations of motions (2.2) are integrated numerically for typically $N = 100 - 10000$ particles, starting from some initial configuration. This generates a phase trajectory over which time averages are taken. In Monte Carlo simulations configurations are randomly generated, and then accepted or rejected in such a way that configurations (and hence observables) are sampled with the correct statistical weight $f(\Gamma)$.

2.4 The microcanonical ensemble

2.4.1 The fundamental assumption

The microcanonical ensemble describes the equilibrium properties of a closed ergodic system with fixed energy E , volume V , and number of particles N . It is characterised by

²Linear and angular momentum are not conserved due to collisions with the wall of the container that specifies the volume (unless the wall itself is considered part of the system)

the phase space distribution

$$f_m(\Gamma) = \frac{\delta(E - H(\Gamma))}{\omega(E, V, N)}, \quad (2.7)$$

with the Dirac- δ and with the normalisation

$$\omega(E, V, N) = \int d\Gamma \delta(E - H(\Gamma)). \quad (2.8)$$

This distribution is such that it is zero anywhere except on the $6N-1$ dimensional hypersurface $H(\Gamma) = E$. The hypersurface “area” is $\omega(E, V, N)$. The microcanonical distribution can alternatively be written as the $\Delta E \rightarrow 0$ limit of the distribution

$$f_m(\Gamma) = \begin{cases} \left[\int_{E-\Delta E < H(\Gamma) < E} d\Gamma \right]^{-1} & ; \quad E - \Delta E < H(\Gamma) < E, \\ 0 & \text{otherwise.} \end{cases} \quad (2.9)$$

The systems of the microcanonical ensemble are distributed uniformly in the energy-shell of thickness ΔE below E : each phase point in this shell is equally probable. This is the *fundamental assumption* of statistical mechanics, from which all results in this chapter follow.

2.4.2 Connection with thermodynamics

Consider a small and sufficiently slow volume change of a microcanonical (E, V, N) system, such that the volume V at time t_0 changes to $V + dV$ at time $t_0 + \tau$. The number of particles N remains fixed. During this volume change an amount of work dW is performed *on* the system. Since the volume of the system can be seen as a parameter on which the Hamiltonian depends (through the wall potential), we can write

$$\begin{aligned} dW &= \int_{t_0}^{t_0+\tau} dt \left(\frac{\partial H(\Gamma(t))}{\partial V} \right) \left(\frac{dV}{dt} \right) \\ &= dV \frac{1}{\tau} \int_{t_0}^{t_0+\tau} dt \left(\frac{\partial H(\Gamma(t))}{\partial V} \right) = dV \overline{\left(\frac{\partial H}{\partial V} \right)}, \end{aligned}$$

where we used the time-average defined in Eq.(2.5). We assumed implicitly that $\tau \rightarrow \infty$, i.e. that the volume change is carried out *sufficiently slowly* or *quasi-statically*. If the system is ergodic, we rewrite this as

$$dW = \left\langle \left(\frac{\partial H}{\partial V} \right) \right\rangle_m dV \equiv -pdV, \quad (2.10)$$

where $\langle \cdot \rangle_m$ denotes the microcanonical ensemble average, and p the pressure of the closed system, i.e. the force per unit area exerted on the wall. This will be considered in more detail in one of the problems. We will now use Eq.(2.10), together with the thermodynamic relation (First Law)

$$\begin{aligned} dE &= -pdV + TdS \\ & \quad (+\mu dN, \text{ with } \mu \text{ the chemical potential, but } dN = 0 \text{ here}) \end{aligned} \quad (2.11)$$

to establish a microscopic picture of the thermodynamic (macroscopic) quantity S , the *entropy*.

This identification requires the introduction of the so-called *energy sphere*, the set of phase points Γ with $H(\Gamma) < E$. It is that part of phase space that is “enclosed” by the hypersurface of magnitude $\omega(E, V, N)$ introduced in Eq.(2.8). The (hyper)volume $\Omega(E, V, N)$ of the energy sphere is defined by

$$\Omega(E, V, N) = \int d\Gamma \Theta(E - H(\Gamma; V, N)), \quad (2.12)$$

where we explicitly indicated the volume and particle number dependence of the Hamiltonian, and where $\Theta(x)$ is the Heaviside step function

$$\Theta(x) = \begin{cases} 0 & x < 0 \\ 1 & x \geq 0 \end{cases}. \quad (2.13)$$

Using that $\Theta'(x) = \delta(x)$ (this is a bit loose, but can be made rigorous by regarding $\Theta(x)$ and $\delta(x)$ as distributions), we obtain from Eqs.(2.12) and (2.8) that

$$\frac{\partial\Omega(E, V, N)}{\partial E} \stackrel{(2.12)}{=} \int d\Gamma \delta(E - H(\Gamma; V, N)) \stackrel{(2.8)}{=} \omega(E, V, N) \quad (2.14)$$

and

$$\begin{aligned} \frac{\partial\Omega(E, V, N)}{\partial V} &\stackrel{(2.12)}{=} - \int d\Gamma \delta(E - H(\Gamma; V, N)) \left(\frac{\partial H(\Gamma; V, N)}{\partial V} \right) \\ &\stackrel{(2.7)}{=} -\omega(E, V, N) \int d\Gamma f_m(\Gamma) \left(\frac{\partial H(\Gamma; V, N)}{\partial V} \right) \\ &\stackrel{(2.6)}{=} -\omega(E, V, N) \left\langle \left(\frac{\partial H(\Gamma; V, N)}{\partial V} \right) \right\rangle_m \\ &\stackrel{(2.10)}{=} +\omega(E, V, N)p. \end{aligned} \quad (2.15)$$

In other words, at fixed N ,

$$\begin{aligned} d\Omega &= \omega(E, V, N) (dE + pdV) \\ &\stackrel{(2.11)}{=} \omega(E, V, N) T dS, \end{aligned} \quad (2.16)$$

which implies that

$$T dS = \frac{1}{\left(\frac{\partial\Omega}{\partial E} \right)} d\Omega. \quad (2.17)$$

One should *not* conclude now that $T = (\partial\Omega/\partial E)^{-1}$ and $S = \Omega$, since any function $g(\Omega)$ satisfies

$$\left(\frac{\partial g(\Omega)}{\partial E} \right)^{-1} dg(\Omega) = \left(\frac{\partial\Omega}{\partial E} \right)^{-1} d\Omega. \quad (2.18)$$

We can therefore just conclude that $S = g(\Omega)$, with the function g to be determined yet!

In order to find $g(\Omega)$ for which $dg(\Omega) = dS$ we use that S is extensive, i.e. $S(E, V, N) = 2S(E/2, V/2, N/2)$ for large N . Since one can prove(not here) that $\log[\Omega(E, V, N)/N!] = 2 \log[\Omega(E/2, V/2, N/2)/(N/2)!] + \mathcal{O}(\log N)$, we conclude that $g(\Omega) = k \log[\Omega/N!]$ is the correct expression, with k a constant to be determined. Since Ω has the dimension of (angular momentum) 3N , it is not very elegant to take its logarithm. Division by h^{3N} , with an appropriate dimension for h , does not affect the extensivity condition, and hence we obtain the final relation between the thermodynamic entropy S and the classical phase space volume Ω as

$$S(E, V, N) = k \log \frac{\Omega(E, V, N)}{N! h^{3N}}. \quad (2.19)$$

We will see later that the conventional temperature scale follows by taking $k = k_B$, the Boltzmann constant $k_B = R/N_A$, with R the gas constant and N_A Avogadro's number. Quantummechanics provides Planck's constant as a natural choice for h . The factor $N!$ must be included in order to obtain an extensive entropy. Gibbs included this factor exactly for this reason. It can be interpreted as a correction for counting all $N!$ classical phase space configurations, that result from a permutation of one of them, as distinct states, whereas these $N!$ classical states are quantummechanically indistinguishable. In this sense the entropy is proportional to the logarithm of the *number* of accessible quantummechanical states.

From the thermodynamic definition $1/T = (\partial S/\partial E)_{V, N}$ and Eq.(2.19) it follows that

$$\frac{1}{T} = k \frac{\omega(E, V, N)}{\Omega(E, V, N)} \implies \Omega = kT\omega. \quad (2.20)$$

The proportionality between the "volume" Ω and "surface area" ω is a consequence of the fact that essentially all of the volume of high dimensional convex bodies is concentrated in the surface shell. As

a consequence, we not only have Eq.(2.19) for the entropy, but also the equivalent expressions (in the thermodynamic limit)

$$S(E, V, N) = k \log \frac{\omega(E, V, N)kT}{N!h^{3N}} \quad (2.21)$$

$$= k \log \frac{\omega(E, V, N)\Delta E}{N!h^{3N}}, \quad (2.22)$$

where ΔE is a constant of dimension energy that is arbitrary within extreme bounds.

For later reference we also introduce the intensive function

$$\beta(E, V, N) \equiv \left(\frac{\partial \log \omega(E, V, N)}{\partial E} \right)_{N, V} \quad (2.23)$$

$$= \left(\frac{\partial \log \Omega(E, V, N)}{\partial E} \right)_{N, V}$$

$$= \left(\frac{\partial S(E, V, N)/k}{\partial E} \right)_{N, V} \quad (2.24)$$

$$= \frac{1}{kT}, \quad (2.25)$$

with T the temperature of the microcanonical (E, V, N) ensemble.

2.4.3 Application to ideal gas

For a system of N noninteracting particles in a volume V at fixed energy E the hypervolume Ω reduces from the general form given in Eq.(2.12) to

$$\begin{aligned} \Omega(E, V, N) &= V^N \int d\mathbf{p}^N \Theta\left(E - \sum_{i=1}^N \frac{\mathbf{p}_i^2}{2m}\right) \\ &= V^N \frac{(2\pi mE)^{3N/2}}{\Gamma(\frac{3N}{2} + 1)}, \end{aligned} \quad (2.26)$$

with $\Gamma(x)$ the Euler Γ -function (not to be confused with the $6N$ -dimensional phase point!) defined by

$$\Gamma(x) = \int_0^\infty dt \exp[-t]t^{x-1}. \quad (2.27)$$

This result, together with the property $\log \Gamma(x) = x \log x - x + \mathcal{O}(\log x)$ for $x \rightarrow \infty$ (“Stirling”), will be worked out in detail in one of the problems. Apart from logarithmic corrections the ideal-gas entropy therefore reads,

$$\begin{aligned} S(E, V, N) &= k \log \frac{\Omega(E, V, N)}{N!h^{3N}} \\ &= Nk \log \left[\frac{V}{N} \left(\frac{4\pi mE}{3Nh^2} \right)^{3/2} \right] + \frac{5}{2}Nk. \end{aligned} \quad (2.28)$$

The temperature T , the pressure p , and chemical potential μ follow directly as

$$\begin{aligned} \frac{1}{T} &= \frac{\partial S}{\partial E} = \frac{3Nk}{2E} \implies E = \frac{3}{2}NkT \\ \frac{p}{T} &= \frac{\partial S}{\partial V} = \frac{Nk}{V} \implies pV = NkT \\ \frac{\mu}{T} &= -\frac{\partial S}{\partial N} = -k \log \left[\frac{V}{N} \left(\frac{4\pi mE}{3Nh^2} \right)^{3/2} \right]. \end{aligned} \quad (2.29)$$

These relations show immediately that the constant k should indeed be the Boltzmann constant k_B . We will often omit the index B for notational convenience.

2.5 Thermal equilibrium

Let us consider an isolated system that consists of two subsystems, labeled 1 and 2, with fixed volumes V_1 and V_2 and fixed particle numbers N_1 and N_2 . Also the total energy $E = E_1 + E_2$ is fixed, but energy exchange between the two subsystems is possible, i.e. E_1 and $E_2 = E - E_1$ are not fixed³. The Hamiltonian therefore satisfies

$$H_1(\Gamma_1) + H_2(\Gamma_2) = E. \quad (2.30)$$

We now consider the energy distribution between the two subsystems. Let $W(E_1)dE_1$ be the probability that the energy of subsystem 1 is in the regime between E_1 and $E_1 + dE_1$. Then

$$\begin{aligned} W(E_1) &\propto \int d\Gamma_1 d\Gamma_2 \delta(E_1 - H_1(\Gamma_1)) \delta(E - E_1 - H_2(\Gamma_2)) \\ &\stackrel{(2.8)}{=} \omega_1(E_1, N_1, V_1) \omega_2(E - E_1, V_2, N_2), \end{aligned} \quad (2.31)$$

where we omit, for a while, a normalisation constant (which is, and this is important, independent of E_1). The most probable value of E_1 , say E_1^* , is the one that maximises $W(E_1)$. Since E_1^* also maximises $\log W(E_1)$, we see that $(\partial \log W(E_1)/\partial E_1)|_{E_1^*} = 0$. We rewrite this with Eq.(2.31) as

$$\begin{aligned} 0 &= \frac{\partial}{\partial E_1} \left(\log \omega_1(E_1, V_1, N_1) + \log \omega_2(E - E_1, V_2, N_2) \right) \Big|_{E_1^*} \\ &\stackrel{(2.23)}{=} \beta_1(E_1^*, V_1, N_1) - \beta_2(E - E_1^*, V_2, N_2) \\ &\stackrel{(2.25)}{=} \frac{1}{kT_1} - \frac{1}{kT_2}. \end{aligned} \quad (2.32)$$

As a consequence the most probable energy distribution is the one for which the temperatures T_1 and T_2 of the two subsystems are equal: $T_1 = T_2 \equiv T$. This is consistent with the Zeroth Law of thermodynamics. By rewriting Eq.(2.31) with (2.21) as

$$W(E_1) \propto \exp[S_1(E_1, V_1, N_1)/k + S_2(E - E_1, V_2, N_2)/k], \quad (2.33)$$

we also see that the most likely energy distribution is the one that maximises the total entropy of the system (under the constraint that N_i , V_i and E are fixed). The form of Eq.(2.33) can be used to construct a more explicit form for $W(E_1)$ by Taylor expanding the exponent of Eq.(2.33), $S_1 + S_2$, about $E_1 = E_1^*$. The lowest order term, $S_1(E_1^*) + S_2(E - E_1^*)$ is independent of E_1 and can be absorbed in the normalisation (to be calculated afterwards). The linear term $\mathcal{O}(E_1 - E_1^*)$ vanishes because of the extremum condition Eq.(2.32). The first nontrivial term of the expansion is therefore $\mathcal{O}((E_1 - E_1^*)^2)$. Its coefficient follows from the thermodynamic relation

$$\left(\frac{\partial^2 S(E, V, N)}{\partial E^2} \right) \Big|_{E^*} = \left(\frac{\partial(1/T)}{\partial E} \right) = \frac{-1}{T^2} \frac{1}{C_v}, \quad (2.34)$$

with the (extensive) constant-volume heat capacity $C_v = \partial E / \partial T$. Using Eq.(2.34), and truncating the Taylor expansion beyond the quadratic term, yields the Gaussian distribution

$$W(E_1) \propto \exp \left[\frac{-1}{2kT^2} \left(\frac{1}{C_{v,1}} + \frac{1}{C_{v,2}} \right) (E_1 - E_1^*)^2 \right]. \quad (2.35)$$

The justification of truncating the expansion follows from the fact that the successive next order terms are smaller than the previous term by a factor $\mathcal{O}(1/N)$. The standard deviation of the Gaussian in (2.35) equals $[kT^2 C_{v,1} C_{v,2} / (C_{v,1} + C_{v,2})]^{1/2} \propto \sqrt{N}$. The relative fluctuations in E_1 vanish as $1/\sqrt{N}$ for large systems; the distribution is sharply peaked about $E_1 = E_1^*$, and the average energy $\langle E \rangle$ equals the most probable energy E^* .

³Here we ignore the energy associated with the interactions between particles in the different subsystems. This energy contribution scales with the interface area between subsystem 1 and 2, and is therefore irrelevant in the limits $V_1, V_2 \rightarrow \infty$ that we (implicitly) consider here. Note, however, that the existence of these interactions is crucial for the exchange of energy between the two subsystems.

2.6 The canonical ensemble

We now consider the same, closed, composed system as in the previous section, but now in the extreme limit where subsystem 2 is much bigger than subsystem 1. Yet, however, subsystem 1 is big enough to ignore surface effects etc. In this limit subsystem 2 plays the role of a heat bath, with which subsystem 1 is in thermal contact. As before, the total energy E of the total system is fixed (as are V_1 , N_1 , V_2 , and N_2), but the energy E_1 of subsystem 1 fluctuates. We are interested in the phase space distribution $f_c(\Gamma_1)$ of subsystem 1, and in the energy distribution. The index “c” is for *canonical*, as the ensemble of systems in contact with a heat bath is conventionally called the canonical ensemble.

The *canonical* phase space distribution $f_c(\Gamma_1)$ of subsystem 1 is obtained by integrating the *microcanonical* distribution of the total system, $f_m(\Gamma_1, \Gamma_2) \propto \delta(E - H_1(\Gamma_1) - H_2(\Gamma_2))$ over all configurations of the heat bath. Ignoring the normalisation (for a while) we obtain

$$\begin{aligned} f_c(\Gamma_1) &\propto \int d\Gamma_2 \delta(E - H_1(\Gamma_1) - H_2(\Gamma_2)) \\ &\stackrel{(2.8)}{=} \omega_2(E - H_1(\Gamma_1), V_2, N_2) \\ &\stackrel{(2.23)}{=} \exp[\log \omega_2(E, V_2, N_2) - \beta_2(E, V_2, N_2)H_1(\Gamma_1) + \mathcal{O}(H_1^2/E)], \end{aligned} \quad (2.36)$$

where the Taylor expansion of $\log \omega_2$ about E is justified by the much larger size of subsystem 2. In the limit $N_2/N_1 \rightarrow \infty$ of interest we can ignore the third term in the exponent of Eq.(2.36). Moreover, its first term is independent of Γ_1 and can be absorbed in the normalisation. The canonical distribution function thus satisfies $f_c(\Gamma_1) \propto \exp[-\beta_2 H_1(\Gamma_1)]$. The only effect of the heat bath (subsystem 2) is to fix the value of β_2 , i.e. to fix the temperature. We have seen above that subsystem 1 takes the same temperature in equilibrium.

We can now drop the indices 1 and 2 for the subsystems, and write the normalised canonical distribution function of a system of volume V , number of particles N , phase points Γ , Hamiltonian $H(\Gamma)$, at temperature $T(= 1/k\beta)$ as

$$f_c(\Gamma) = \frac{\exp[-\beta H(\Gamma)]}{N! h^{3N} Z(N, V, T)} \quad (2.37)$$

with the so-called canonical partition sum or partition function

$$Z(N, V, T) = \frac{1}{N! h^{3N}} \int d\Gamma \exp[-\beta H(\Gamma)]. \quad (2.38)$$

The factor h^{3N} is included to make Z dimensionless, and the factor $N!$ to make $\log Z$ extensive, as we will see.

Let us now calculate the energy distribution $W(E)$ of the canonical ensemble (with E playing the role of E_1 above),

$$\begin{aligned} W(E) &= \int d\Gamma f_c(\Gamma) \delta(E - H(\Gamma)) \\ &\stackrel{(2.8)}{=} \frac{1}{N! h^{3N} Z(N, V, T)} \exp[-\beta E] \omega(E, V, N). \end{aligned} \quad (2.39)$$

This distribution is maximal for $E = E^*$ with E^* given by $\beta(E^*, V, N) = \beta$, i.e. for that E^* for which the temperature of the system equals that of the reservoir. Expanding about E^* then yields a Gaussian, just as obtained in Eq.(2.35), which with the correct normalisation, is written as

$$W(E) = (2\pi kT^2 C_v)^{-1/2} \exp\left[-\frac{(E - E^*)^2}{2kT^2 C_v}\right], \quad (2.40)$$

with $C_v = \partial E / \partial T$ the heat capacity. Note that this result is indeed the limit of Eq.(2.35) when $C_{v,2} \gg C_{v,1} \equiv C_v$, i.e. when subsystem 2 is much bigger than subsystem 1. Also note that $C_v > 0$ in order that $E = E^*$ has a maximum probability. It follows directly from (2.40) that the relative energy fluctuations are characterised by

$$\frac{\sqrt{\langle (E - E^*)^2 \rangle}}{E^*} \propto \frac{1}{\sqrt{N}}. \quad (2.41)$$

In the thermodynamic limit these fluctuations become vanishingly small, and then the average energy $\langle E \rangle$ equals the most probable energy E^* . This also implies that the microcanonical and the canonical ensemble are equivalent, for most purposes, in the thermodynamic limit.

The connection with thermodynamics can now be made by integrating Eq.(2.39) over all values of E , and using that the result equals unity by definition. This yields, using the vanishing width of $W(E)$ in the thermodynamic limit, that

$$\begin{aligned} Z(N, V, T) &= \frac{1}{N!h^{3N}} \int_{-\infty}^{\infty} dE \exp[-\beta E] \omega(E, V, N) \\ &= \frac{\omega(E^*)}{N!h^{3N}} \exp[-\beta E^*] \int_{-\infty}^{\infty} dE \exp[-(E - E^*)^2 / (2kT^2 C_v)] \\ &= \exp[S^*/k] \exp[-\beta E^*] (2\pi kT^2 C_v)^{1/2}, \end{aligned} \quad (2.42)$$

where $S^* = S(E^*, V, N) \equiv \langle S \rangle$ the entropy of the (N, V, T) system. Ignoring terms of $\mathcal{O}(\log N)$, it follows that

$$-kT \log Z(N, V, T) \equiv F(N, V, T) = E^* - TS^* = \langle E \rangle - T\langle S \rangle, \quad (2.43)$$

where F is the Helmholtz free energy. As is well known from thermodynamics, $F(N, V, T)$ generates the full thermodynamics of systems with fixed (N, V, T) , just like $S(E, V, N)$ does for systems with fixed (E, V, N) .

Specifically we have for the energy

$$\begin{aligned} E &= \int d\Gamma f_c(\Gamma) H(\Gamma) \\ &= \frac{1}{N!h^{3N} Z(N, V, T)} \int d\Gamma H(\Gamma) \exp[-\beta H(\Gamma)] \\ &= \frac{1}{N!h^{3N} Z(N, V, T)} \frac{-\partial}{\partial \beta} \int d\Gamma \exp[-\beta H(\Gamma)] \\ &= \frac{-\partial \log Z(N, V, T)}{\partial \beta} = \frac{\partial (\beta F(N, V, T))}{\partial \beta}. \end{aligned} \quad (2.44)$$

The pressure and chemical potential are given, respectively, by

$$\begin{aligned} p &= - \left(\frac{\partial F}{\partial V} \right)_{N, T} \\ \mu &= \left(\frac{\partial F}{\partial N} \right)_{V, T}. \end{aligned} \quad (2.45)$$

The Maxwell-Boltzmann velocity distribution is easily obtained in the canonical ensemble, viz.

$$\begin{aligned} f_{MB}(\mathbf{p}) &\equiv \langle \delta(\mathbf{p}_1 - \mathbf{p}) \rangle_c \\ &= \frac{1}{N!h^{3N} Z} \int d\Gamma \delta(\mathbf{p}_1 - \mathbf{p}) \exp[-\beta H(\Gamma)] \\ &= \frac{\exp[-\mathbf{p}^2 / (2mkT)]}{(2\pi mkT)^{3/2}}. \end{aligned} \quad (2.46)$$

The canonical average of momentum independent observables, i.e. observables described by phase functions $\mathcal{A}(\Gamma) = \mathcal{A}(\mathbf{r}^N)$, can be written as

$$\begin{aligned} \langle \mathcal{A} \rangle &= \frac{1}{N!h^{3N} Z(N, V, T)} \int d\Gamma \exp[-\beta H(\Gamma)] \mathcal{A}(\mathbf{r}^N) \\ &= \frac{1}{Q(N, V, T)} \int d\mathbf{r}^N \exp[-\beta \Phi(\mathbf{r}^N)] \mathcal{A}(\mathbf{r}^N), \end{aligned} \quad (2.47)$$

where the *configurational integral* is defined as

$$Q(N, V, T) = \int d\mathbf{r}^N \exp[-\beta \Phi(\mathbf{r}^N)]. \quad (2.48)$$

Note that

$$Z(N, V, T) = \frac{Q(N, V, T)}{N! \Lambda^{3N}}, \quad (2.49)$$

where the thermal (De Broglie) wavelength is defined by

$$\Lambda = \frac{h}{\sqrt{2\pi mkT}}. \quad (2.50)$$

2.6.1 Application to ideal gas

The canonical partition function for N classical noninteracting particles in a volume V at temperature T is given by

$$\begin{aligned} Z(N, V, T) &= \frac{1}{N! h^{3N}} \int d\Gamma \exp[-\beta H(\Gamma)] \\ &= \frac{V^N}{N!} \frac{1}{h^{3N}} \int d\mathbf{p}^N \exp[-\beta \sum_{i=1}^N \frac{\mathbf{p}_i^2}{2m}] \\ &= \frac{V^N}{N! \Lambda^{3N}}, \end{aligned} \quad (2.51)$$

where Λ is defined in Eq.(2.50). The Helmholtz free energy follows as

$$F(N, V, T) = NkT \left[\log \left(\frac{N\Lambda^3}{V} \right) - 1 \right], \quad (2.52)$$

It is easily checked that the energy E , the pressure p , and the chemical potential μ are given by

$$\begin{aligned} E &= \frac{3}{2} NkT \\ p &= \frac{NkT}{V} \\ \mu &= kT \log \left(\frac{N\Lambda^3}{V} \right). \end{aligned} \quad (2.53)$$

These results are identical to those obtained in the microcanonical ensemble, Eqs.(2.29). Note, however, that the explicit calculation of $Z(N, V, T)$ in Eq.(2.51) is much simpler than that of $\Omega(E, V, N)$ in the microcanonical case. This is an example that illustrates the more general result that the ensemble used in theoretical calculations can be chosen for calculational convenience; it need not necessarily correspond to the experimental situation.

2.7 The grand canonical ensemble

Although many physical systems can be characterised by fixed (N, V, T) , and therefore by the canonical ensemble, there are also many cases where the number of particles N can fluctuate because of the permeability of the walls or surface of the system. Examples include membrane equilibria (where some chemical species can and others cannot cross a semi-permeable membrane) or gas-liquid coexistence (where particles can move from the liquid to the gas and vice versa through the meniscus). One can also consider a system that is a part of a bigger system, e.g. a subvolume that contains a fluctuating number of particles. The ensemble of systems that can exchange energy and particles with their environment is called the *grand canonical ensemble*. This ensemble can be constructed by considering a bipartitioned microcanonical ensemble of fixed total energy E , volume V , and number of particles N . If the wall that separates the two fixes V_1 and $V_2 = V - V_1$ conducts heat and is permeable to the particles, then the energy E_1 and the number of particles N_1 of subsystem 1 fluctuates (and that of subsystem 2 as well, with $E_2 = E - E_1$ and $N_2 = N - N_1$). In what follows we assume that subsystem 2 is a reservoir with which 1 is in contact, i.e. we assume that $E_2 \gg E_1$, $V_2 \gg V_1$, and $N_2 \gg N_1$; we ignore terms $\mathcal{O}(N_1/N)$ compared to $\mathcal{O}(N_1)$ terms. Implicitly we also ignore the interaction energy between the two subsystems, which implies that V_1 is large enough to neglect surface contributions.

The grand canonical phase space distribution of subsystem 1, $f_g(\Gamma_1, N_1)$, depends explicitly on N_1 , and follows by integrating the microcanonical distribution of the total system over the phase Γ_2 of subsystem 2. Recalling the definition of $\omega(E, V, N)$ from Eq.(2.8), which we rewrite here as $\omega(E, V, N) = \int d\Gamma_1 d\Gamma_2 \delta(E - H_1(\Gamma_1) - H_2(\Gamma_2))$, we can write

$$\begin{aligned} f_g(\Gamma_1, N_1) &= \left(\frac{N!}{N_1!(N - N_1)!} \right) \frac{\int d\Gamma_2 \delta(E - H_1(\Gamma_1) - H_2(\Gamma_2))}{\omega(E, V, N)} \\ &= \frac{N!h^{3N}}{\omega(E, V, N)} \frac{1}{N_1!h^{3N_1}} \frac{\omega_2(E - H_1(\Gamma_1), V_2, N - N_1)}{(N - N_1)!h^{3(N - N_1)}} \\ &\propto \frac{1}{N_1!h^{3N_1}} \exp \left[\log \left(\frac{\omega_2(E - H_1(\Gamma_1), V_2, N - N_1)}{(N - N_1)!h^{3(N - N_1)}} \right) \right] \end{aligned} \quad (2.54)$$

The bracketed factor in the first line of Eq.(2.54) is of combinatorial nature, and denotes the number of possible ways to divide N particles into two sets of N_1 and $N - N_1$ particles. The second line follows from the first one by rearrangement of terms. Its first term is independent of N_1 and Γ_1 , and hence serves as a mere normalisation that is ignored in the third line but will be restored later. A more explicit form of f_g is obtained by a Taylor expansion of the argument of the exponent in the third line of Eq.(2.54) about $E_2 = E$ and $N_2 = N$,

$$\left[\log \left(\frac{\omega_2(E, V_2, N)}{N!h^{3N}} \right) - \beta_2 H_1(\Gamma_1) + \beta_2 \mu_2 N_1 + \mathcal{O}(N_1/N, H_1/E) \right], \quad (2.55)$$

where the dominant term is again a scaling factor as it is independent of N_1 and Γ_1 ; it will be absorbed by the normalisation. The quantities β_2 and μ_2 are the reservoir quantities defined by

$$\begin{aligned} \beta_2 &= \frac{\partial \log \omega_2(E, V_2, N)}{\partial E} \\ \beta_2 \mu_2 &= - \frac{\partial \log \omega_2(E, V_2, N)/N!h^{3N}}{\partial N} = - \frac{\partial S_2(E, V_2, N)/k}{\partial N}. \end{aligned} \quad (2.56)$$

We have seen already that $\beta_2 = 1/kT_2$, and μ_2 is called the *chemical potential*. Ignoring the small $\mathcal{O}(N_1/N)$ terms, we conclude that $f_g(\Gamma_1, N_1) \propto \exp[-\beta_2 H_1(\Gamma_1) + \beta_2 \mu_2 N_1]/(N_1!h^{3N_1})$. Restoring the normalisation, setting the fixed reservoir quantities $\beta_2 = \beta$ and $\mu_2 = \mu$, and dropping all indices (we now focus only on the system that we previously called subsystem 1) yields

$$f_g(\Gamma, N) = \frac{1}{N!h^{3N} \Xi(\mu, V, T)} \exp[-\beta H(\Gamma) + \beta \mu N] \quad (2.57)$$

with the so-called grand canonical partition function

$$\begin{aligned} \Xi(\mu, V, T) &= \sum_{N=0}^{\infty} \frac{\exp[\beta \mu N]}{N!h^{3N}} \int d\Gamma \exp[-\beta H(\Gamma)] \\ &\stackrel{(2.38)}{=} \sum_{N=0}^{\infty} \exp[\beta \mu N] Z(N, V, T). \end{aligned} \quad (2.58)$$

The grand canonical ensemble can be regarded as a linear combination of canonical ensembles with different numbers of particles. (Similarly one can regard the canonical ensemble as a linear combination of microcanonical ensembles with different energies).

The probability distribution $W(N)$ to find N particles in a grand canonical ensemble is given by

$$\begin{aligned} W(N) &= \int d\Gamma f_g(\Gamma, N) \\ &\stackrel{(2.57)}{=} \frac{\exp[\beta \mu N]}{N!h^{3N} \Xi(\mu, V, T)} \int d\Gamma \exp[-\beta H(\Gamma)] \\ &\stackrel{(2.58)}{=} \frac{\exp[\beta \mu N] Z(N, V, T)}{\Xi(\mu, V, T)}. \end{aligned} \quad (2.59)$$

This distribution is maximal for that value of N , say N^* , for which $(\partial \log W(N)/\partial N) = 0$. This implies, from Eqs.(2.43) and (2.59), that

$$\left(\frac{\partial F(N, V, T)}{\partial N} \right) \Big|_{N^*} = \mu, \quad (2.60)$$

i.e. the most probable number of particles, N^* , is such that the chemical potential equals that of the reservoir. The distribution can now be obtained explicitly by a Taylor expansion of N about N^* , with the result

$$\begin{aligned} W(N) &= \exp \left[\log W(N) \right] \\ &\stackrel{(2.59)}{=} \frac{\exp[\beta\mu N^* - \beta F^*]}{\Xi(\mu, V, T)} \exp \left[-\frac{1}{2} \beta \left(\frac{\partial \mu}{\partial N} \right)_{V, T, N=N^*} (N - N^*)^2 \right] \end{aligned} \quad (2.61)$$

with $F^* = F(N^*, V, T)$. Neglecting the $\mathcal{O}((N - N^*)^3)$ terms is justified provided $(\partial N/\partial \mu) > 0$; this is a well known thermodynamic stability requirement. One checks that the relative width of the distribution,

$$\frac{\sqrt{\langle (N - N^*)^2 \rangle}}{N^*} \propto \frac{1}{\sqrt{N^*}}, \quad (2.62)$$

vanishes in the thermodynamic limit, unless $(\partial \mu/\partial N)_{V, T} = 0$ as is the case for phase coexistence. In the one-phase regime, $(\partial \mu/\partial N)_{V, T} > 0$, the average number of particles, $\langle N \rangle$, equals the most probable number N^* . It also implies that the grand canonical ensemble is equivalent, thermodynamically, to the canonical and microcanonical ensemble (unless $(\partial N/\partial \mu) \leq 0$).

An interesting result is obtained by considering the variance of the Gaussian distribution (2.61), which is given by

$$\begin{aligned} \langle (N - \langle N \rangle)^2 \rangle &= \frac{kT}{\left(\frac{\partial \mu}{\partial N} \right)_{V, T, N=N^*}} \\ &= \frac{kT \langle N \rangle}{\left(\frac{\partial p}{\partial \rho} \right)_T}, \end{aligned} \quad (2.63)$$

where we used that the thermodynamic result that

$$\begin{aligned} \left(\frac{\partial N}{\partial \mu} \right)_{V, T} &= V \left(\frac{\partial \rho}{\partial \mu} \right)_T \\ &= V \left(\frac{\partial \rho}{\partial p} \right)_T \left(\frac{\partial p}{\partial \mu} \right)_T \\ &= N \left(\frac{\partial \rho}{\partial p} \right)_T. \end{aligned} \quad (2.64)$$

The relative variance in the number of particles is therefore related to the compressibility through

$$\frac{\langle N^2 \rangle - \langle N \rangle^2}{\langle N \rangle} = kT \left(\frac{\partial \rho}{\partial p} \right)_T. \quad (2.65)$$

The relation between the grand canonical ensemble and thermodynamics is obtained by integrating (adding) the left- hand right hand side of Eq.(2.61) over all values of N . By definition the left hand side yields unity, while the right hand side yields $\exp[\beta\mu N^* - \beta F^* - \log \Xi + \mathcal{O}(\log N)]$, where the $\mathcal{O}(\log N)$ term (that follows from the Gaussian integration) is vanishingly small compared to the other three when $N \rightarrow \infty$. Consequently we have

$$\begin{aligned} \log \Xi(\mu, V, T) &= \beta\mu \langle N \rangle - \beta F(\langle N \rangle, V, T) \\ &= \beta p(\mu, T) V, \end{aligned} \quad (2.66)$$

with $p(\mu, T)$ the pressure of the (μ, V, T) system⁴. The average number of particles is given by

$$\begin{aligned}
\langle N \rangle &= \sum_{N=0}^{\infty} NW(N) \\
&\stackrel{(2.59)}{=} \frac{1}{\Xi(\mu, V, T)} \sum_{N=0}^{\infty} N \exp[\beta\mu N] Z(N, V, T) \\
&= \frac{1}{\Xi(\mu, V, T)} \frac{\partial}{\partial \beta\mu} \left(\sum_{N=0}^{\infty} \exp[\beta\mu N] Z(N, V, T) \right)_{V, T} \\
&\stackrel{(2.58)}{=} \left(\frac{\partial \log \Xi(\mu, V, T)}{\partial \beta\mu} \right)_{V, T}. \tag{2.67}
\end{aligned}$$

For later reference we define the *fugacity*

$$z = \frac{\exp[\beta\mu]}{\Lambda^3}, \tag{2.68}$$

which is, for any temperature T , one-to-one related to μ . In terms of z Eq.(2.67) is rewritten as

$$\langle N \rangle = z \left(\frac{\partial \log \Xi(z, V, T)}{\partial z} \right)_{V, T}. \tag{2.69}$$

2.7.1 Application to the ideal gas

The grand canonical partition function for a system of classical noninteracting particles in a volume V at temperature T and chemical potential μ is given by

$$\begin{aligned}
\Xi(\mu, V, T) &\stackrel{(2.58)}{=} \sum_{N=0}^{\infty} \exp[\beta\mu N] Z(N, V, T) \\
&\stackrel{(2.51)}{=} \sum_{N=0}^{\infty} \frac{1}{N!} \left(\frac{V \exp[\beta\mu]}{\Lambda^3} \right)^N \\
&\stackrel{(2.68)}{=} \exp[zV]. \tag{2.70}
\end{aligned}$$

It follows from Eqs.(2.66) and (2.69) that, for the ideal gas, $\beta p = z$ and $N = zV$, which is consistent with all ideal-gas results previously obtained in Eqs.(2.29) and (2.53).

⁴ $\mu N - F$ only equals pV in homogeneous bulk systems. It does not hold for e.g. an ideal gas in a gravity field, or for systems for which the pressure is of tensorial character due to surface effects.

Chapter 3

Simple Fluids

3.1 Some experimental facts

The classical ideal-gas laws $pV = NkT$ and $E = \frac{3}{2}NkT$ do not hold for real gases at finite density $\rho = N/V$ because of the interactions between the atoms or molecules of the gas. Over the years many empirical “laws” have been introduced that account for these deviations from ideality. One of the most fundamental of these is due to Kamerlingh-Onnes, who introduced, on empirical grounds, the so-called virial expansion for the pressure. It is written as

$$p(\rho, T) = kT(\rho + B_2(T)\rho^2 + B_3(T)\rho^3 + \dots), \quad (3.1)$$

where the temperature dependent virial coefficients $B_n(T)$ can be obtained by fitting to the observed deviations from ideal-gas behaviour. In this chapter we will *derive* the functional form of Eq.(3.1) using the ensemble formalism of the previous chapter, and find explicit expressions for the virial coefficients in terms of the interaction potential between the particles.

There are more phenomena in real, interacting, gases that do not occur in ideal gases. By lowering the temperature or increasing the pressure, a real gas can be transformed into a dense liquid or crystalline solid phase. The transformation from one phase to another is called a *phase transition*. The phase behaviour of a substance can be characterised by a phase diagram. A sketch of the phase diagram of a monoatomic substance like Argon is depicted in Fig.3.1, both in the density-temperature and in the pressure-temperature representation. The curves denote the phase boundaries, i.e. the state points where two phases coexist. These curves are also called *binodals*. Fig.3.1 shows that above the *critical temperature*

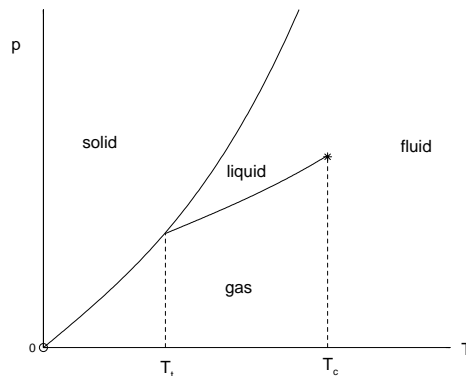


Figure 3.1: (a) Phase diagram of a simple fluid like Argon.

T_c a gas can be compressed continuously up to the dense crystalline phase, while density-jumps occur at temperatures below T_c . For $T_t < T < T_c$ a liquid phase exists in between the dilute gas and the crystal, and below the triple temperature T_t the dilute gas can coexist with the crystal. At $T = T_t$ the three

phases can coexist simultaneously. The calculation of such binodals, and the analysis of the critical point, is possible within the framework of statistical mechanics, as we will see in this chapter.

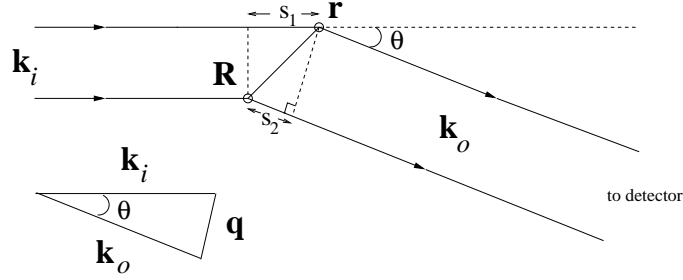


Figure 3.2: Schematic setup of a scattering experiment.

Experimentally it is possible to measure *correlations* in a gas or liquid by neutrons or X-ray scattering. Imagine a sample of gas or liquid irradiated by a coherent X-ray beam, say, of wavelength λ . The wavevector of the incident radiation is called \mathbf{k}_i , with $|\mathbf{k}_i| = 2\pi/\lambda \equiv k$ the wavenumber. Due to the presence of particles in the sample, radiation will be scattered in all directions, and its intensity $I(\theta)$ can be detected far from the sample as a function of the angle θ with respect to the incident beam, as illustrated in Fig.3.2. Scattered radiation in a particular direction θ , with outgoing wavevector \mathbf{k}_o , satisfies $|\mathbf{k}_o| = k$ for elastic scattering. Consider now the path length difference $\Delta s = s_1 - s_2$ between the path “source $\rightarrow \mathbf{R} \rightarrow$ detector”, with \mathbf{R} an arbitrary point in the sample, and the path “source $\rightarrow \mathbf{r} \rightarrow$ detector”, where \mathbf{r} is the position of a scattering particle. It follows from the geometry that $ks_1 = \mathbf{k}_i \cdot (\mathbf{r} - \mathbf{R})$ and $ks_2 = \mathbf{k}_o \cdot (\mathbf{r} - \mathbf{R})$. From this the phase difference $\Delta\psi$ of the two paths at the detector is obtained as

$$\begin{aligned} \Delta\psi &= \frac{2\pi\Delta s}{\lambda} = k\Delta s = (\mathbf{k}_o - \mathbf{k}_i) \cdot (\mathbf{r} - \mathbf{R}) \\ &= \mathbf{q} \cdot (\mathbf{r} - \mathbf{R}), \end{aligned} \quad (3.2)$$

where we defined the momentum transfer $\mathbf{q} \equiv \mathbf{k}_o - \mathbf{k}_i$ in the scattering process. The contribution from this particle to the field amplitude \mathcal{A} at the detector is proportional to $\exp[i\Delta\psi]$. The total amplitude at the detector is given by the contribution from all particles, and can be written as

$$\mathcal{A}(\theta) \propto \sum_{i=1}^N \exp[i\mathbf{q} \cdot (\mathbf{r}_i - \mathbf{R})], \quad (3.3)$$

for some static configuration of N particles in the irradiated volume. The measured intensity is the ensemble or time average of the squared modulus of the amplitude, and can be written as

$$I(\theta) = \langle |\mathcal{A}(\theta)|^2 \rangle \propto \left\langle \sum_{i,j}^N \exp[i\mathbf{q} \cdot \mathbf{r}_{ij}] \right\rangle \propto S(q), \quad (3.4)$$

where $\mathbf{r}_{ij} = \mathbf{r}_i - \mathbf{r}_j$, and where the *structure factor* $S(q)$ is defined as

$$\begin{aligned} S(q) &\equiv \left\langle \frac{1}{N} \sum_{i,j}^N \exp[i\mathbf{q} \cdot \mathbf{r}_{ij}] \right\rangle \\ &= 1 + \left\langle \frac{1}{N} \sum_{i \neq j}^N \exp[i\mathbf{q} \cdot \mathbf{r}_{ij}] \right\rangle. \end{aligned} \quad (3.5)$$

Note that q is directly related to θ through $q \equiv |\mathbf{q}| = 2k \sin(\theta/2)$ from elementary geometry. It is implicitly assumed that the fluid of interest is homogeneous and isotropic, so that only the modulus q is relevant and not the direction of \mathbf{q} . A typical liquid structure factor is shown in Fig.3.3.

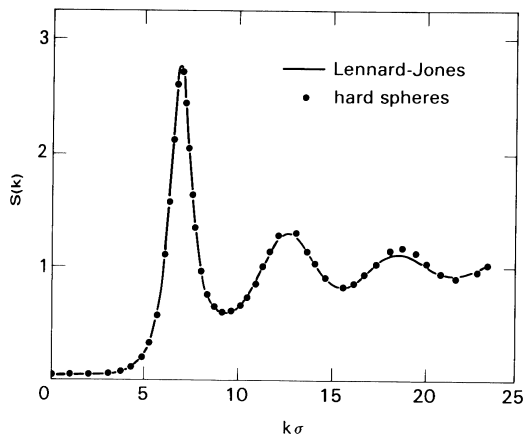


Figure 3.3: Structure factor of a simple fluid close to its triple point.

3.2 Interactions

The phenomena of the previous section are all caused, in one way or another, by the fact that particles in real gases or liquids are not ideal but *interact* with each other. In theoretical descriptions it is often assumed that the interactions are *pairwise additive*, i.e. the interaction energy is a sum of pairwise terms, each of which is characterised by a pair potential $\phi(\mathbf{r}_i - \mathbf{r}_j)$ that depends on the relative coordinates of particle i and j . For so-called simple fluids the pair potential is radially symmetric, which means that the Hamiltonian can be written as

$$H(\Gamma) = \sum_{i=1}^N \frac{\mathbf{p}_i^2}{2m} + \sum_{i<j}^N \phi(r_{ij}), \quad (3.6)$$

with $r_{ij} = |\mathbf{r}_i - \mathbf{r}_j|$ the radial distance between particle i and j . Radial symmetry is a good approximation for the noble gases, and a fair approximation for small molecules like CH_4 (methane), N_2 and O_2 . The typical form of $\phi(r)$ is depicted in Fig.3.4. We distinguish two important features:

- The interaction is steeply repulsive for $r < \sim \sigma$, with σ a measure for the diameter of the particle. For simple fluids σ is typically 2-5Å. This short-ranged repulsion is due to Pauli exclusion (and Coulomb repulsion) of outer shell electrons of two particles in close proximity.
- The interaction is attractive for $r > \sim \sigma$, with Van der Waals interactions $\phi(r) \propto -r^{-6}$ when $r \gg \sigma$. These attractions are caused by correlated (induced) dipole fluctuations in the two particles. The range of these attractions is typically $\simeq 2\sigma$, and the depth of the minimum, $-\epsilon$, that occurs at $r \simeq \sigma$, depends on the chemical species.

A convenient, successful, and famous parameterisation for $\phi(r)$ is the Lennard-Jones form

$$\phi_{LJ}(r) = 4\epsilon \left[\left(\frac{\sigma}{r} \right)^{12} - \left(\frac{\sigma}{r} \right)^6 \right], \quad (3.7)$$

which gives good agreement with many experiments by adjusting the well depth ϵ and “size” σ . A less realistic, but an analytically more tractable form is the square well potential

$$\phi_{SW}(r) = \begin{cases} \infty & r < \sigma \\ -\epsilon & \sigma < r < \lambda\sigma \\ 0 & r > \lambda\sigma \end{cases}, \quad (3.8)$$

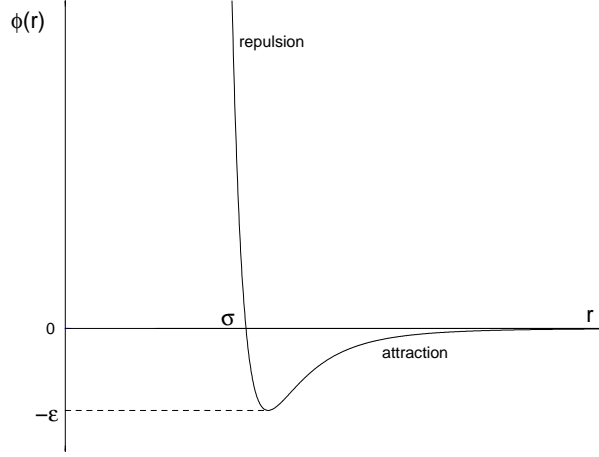


Figure 3.4: Typical pair potential of a simple fluid.

where σ denotes the hard-core diameter, and where $\lambda > 1$ is a measure for the range of the attractive well. Another important potential is the hard-sphere potential

$$\phi_{HS}(r) = \begin{cases} \infty & r < \sigma \\ 0 & r > \sigma \end{cases}, \quad (3.9)$$

where σ is the hard-sphere diameter. The hard-sphere system does not contain any attraction, but does describe the short-ranged atomic repulsions crudely. This neglect of attractions may seem unphysical at first sight, but we will see that the hard-sphere fluid plays a crucial role as a reference zeroth order approximation in perturbation theory of liquids, where the attractions are treated as a perturbation of the purely repulsive short-ranged interactions. For this reason the hard-sphere fluid has been of great theoretical importance. Moreover, due to advances in the synthesis of colloidal particles (mesoscopic solid particles with diameter in the range from 1nm to $1 \mu\text{m}$), experimental realisations of hard-sphere systems actually exist in the form of colloidal suspensions.

The question we will address in this chapter is how these nonzero microscopic interactions are related to macroscopic observables such as the pressure, and to phenomena such as liquid condensation and freezing.

3.3 Corrections to the ideal-gas law

3.3.1 The Mayer expansion

We consider a gas described by a Hamiltonian of the form (3.6) in a fixed volume V . It turns out to be convenient to consider this system grand canonically, i.e. at fixed temperature T (with $\beta = 1/kT$) and fixed chemical potential μ (or fixed fugacity $z = \exp[\beta\mu]/\Lambda^3$, see Eq.(2.68)). Starting point of our analysis is the grand partition function, which takes the form

$$\begin{aligned} \Xi(\mu, V, T) &= \sum_{N=0}^{\infty} \frac{\exp[\beta\mu N]}{N! \Lambda^{3N}} \int_V d\mathbf{r}^N \exp \left[-\beta \sum_{i < j}^N \phi(r_{ij}) \right] \\ &= \sum_{N=0}^{\infty} \frac{z^N}{N!} Q(N, V, T) \\ &\equiv 1 + Q_1 z + \frac{1}{2} Q_2 z^2 + \frac{1}{3!} Q_3 z^3 + \dots, \end{aligned} \quad (3.10)$$

where we defined the configurational integral

$$Q_N \equiv Q(N, V, T) = \int_V d\mathbf{r}^N \exp \left[-\beta \sum_{i < j}^N \phi(r_{ij}) \right]. \quad (3.11)$$

It follows from Eq.(3.10), together with the Taylor expansion $\log(1+x) = \sum_{n=1}^{\infty} \frac{(-1)^{n+1}}{n} x^n$ that

$$\log \Xi = V \sum_{j=1}^{\infty} b_j z^j, \quad (3.12)$$

where the first few coefficients are given explicitly by

$$\begin{aligned} b_1 &= \frac{1}{V} Q_1 = 1 \\ b_2 &= \frac{1}{2!V} (Q_2 - Q_1^2) \\ b_3 &= \frac{1}{3!V} (Q_3 - 3Q_2 Q_1 + 2Q_1^3) \\ b_4 &= \frac{1}{4!V} (Q_4 - 4Q_3 Q_1 - 3Q_2^2 + 12Q_2 Q_1^2 - 6Q_1^4). \end{aligned} \quad (3.13)$$

Even though the expressions for b_j become more cumbersome as j increases, it is possible to write down a general formula for b_j in terms of the Q_i 's; we will not do that here as we focus on the lowest few terms only. Note that we implicitly assumed that the expansion of Eq.(3.12) exists.

Inserting the expansion of Eq.(3.12) into the expressions for p (Eqs(2.66)) and $N = \rho V$ (Eq.(2.69)) yields

$$p(z, T) = kT \sum_{j=1}^{\infty} b_j z^j \quad (3.14)$$

$$\rho(z, T) = \frac{z}{V} \frac{\partial \log \Xi}{\partial z} = \sum_{j=1}^{\infty} j b_j z^j. \quad (3.15)$$

Now we have both p and ρ as a power series in z , whereas much experimental data involves the density dependence of the pressure, see e.g. Eq.(3.1). It is our task now to eliminate z between the Eqs.(3.14) and (3.15). This can be accomplished algebraically by writing

$$z = a_1 \rho + a_2 \rho^2 + a_3 \rho^3 + \dots, \quad (3.16)$$

where the yet unknown coefficients a_j follow by inserting Eq.(3.16) into Eq.(3.15) and equating the resulting coefficients of each power of ρ on both sides of the equation. This gives

$$\begin{aligned} a_1 &= 1 \\ a_2 &= -2b_2 \\ a_3 &= -3b_3 + 8b_2^2. \end{aligned} \quad (3.17)$$

Higher order terms become more complicated but are, in principle, tractable as well. Inserting the density expansion of z , given by the Eqs.(3.16) and (3.17), into the fugacity expansion of p , Eq.(3.14), yields a density expansion of the pressure as phenomenologically given in Eq.(3.1), but now with explicit expressions for the virial coefficients,

$$B_2(T) = -b_2 \quad (3.18)$$

$$B_3(T) = 4b_2^2 - 2b_3. \quad (3.19)$$

These expressions will be worked out in detail below.

3.3.2 The second virial coefficient $B_2(T)$

The second virial coefficient is given by

$$\begin{aligned}
 B_2(T) &\stackrel{(3.18)}{=} -b_2 \\
 &\stackrel{(3.13)}{=} -\frac{1}{2V} \left(\int d\mathbf{r}_1 d\mathbf{r}_2 (\exp[-\beta\phi(r_{12})] - 1) \right) \\
 &= -\frac{1}{2} \int d\mathbf{r} f(r),
 \end{aligned} \tag{3.20}$$

where we used translational invariance of the pair interaction, ignored (small) surface effects that arise when \mathbf{r}_1 and/or \mathbf{r}_2 are close to the wall of the container, and where we introduced the Mayer function (named after the first who performed this analysis)

$$f(r) = \exp[-\beta\phi(r)] - 1. \tag{3.21}$$

We have now expressed the lowest order correction to the ideal-gas pressure in terms of the pair interaction $\phi(r)$. The Mayer function is temperature dependent, and is shown in Fig.(3.5) for the Lennard-Jones potential (3.7). We first remark that $f(r)$ for $r < \sigma$ is very insensitive for the details of $\phi(r)$; it equals -1

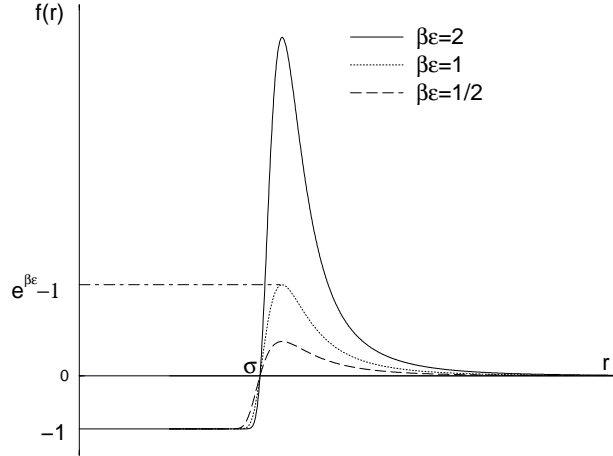


Figure 3.5: Mayer function $f(r)$ for the Lennard-Jones potential, at several temperatures.

as long as $\phi(r) \gg kT$. At $r \approx \sigma$ the Mayer function changes sign quite abruptly, goes through a positive maximum and decays to zero as $f(r) \simeq -\beta\phi(r)$ for $r \gg \sigma$. The latter implies that B_2 exists, i.e. is finite, if $\phi(r)$ decays to zero more rapidly than r^{-3} . Although this convergence criterion excludes application of the Mayer theory to the important cases of Coulombic fluids (electrolytes, plasmas) as well as dipolar fluids (water, magnetic colloids), it shows that systems interacting through e.g. Lennard-Jones, square-well, hard-sphere, and screened-Coulomb potentials can be treated within this framework. Note that the temperature dependence of $f(r)$ implies that $B_2(T)$ can change sign at the so-called Boyle temperature T_B , i.e. $B_2(T_B) = 0$. At low temperatures $T < T_B$ we have $B_2(T) < 0$, signifying that the Van der Waals attractions reduce the pressure with respect to the ideal-gas pressure. At temperature $T > T_B$ the hard-core repulsions increase the pressure beyond the ideal-gas pressure.

3.3.3 The third virial coefficient $B_3(T)$

The third virial coefficient is calculated as follows.

$$B_3(T) \stackrel{(3.19)}{=} 4b_2^2 - 2b_3$$

$$\begin{aligned}
& \stackrel{(3.13)}{=} -\frac{1}{3V} [(Q_3 - 3Q_2Q_1 + 2Q_1^3) - 3Q_1^{-1}(Q_2 - Q_1^2)^2] \\
& = -\frac{1}{3V} [Q_3 - 3Q_1^{-1}Q_2^2 + 3Q_1Q_2 - Q_1^3] \\
& = -\frac{1}{3V} \int d\mathbf{r}_1 d\mathbf{r}_3 d\mathbf{r}_3 \left(\exp[-\beta(\phi_{12} + \phi_{13} + \phi_{23})] \right. \\
& \quad \left. - 3 \exp[-\beta(\phi_{12} + \phi_{13})] + 3 \exp[-\beta\phi_{12}] - 1 \right) \\
& = -\frac{1}{3V} \int d\mathbf{r}_1 d\mathbf{r}_3 d\mathbf{r}_3 f(r_{12})f(r_{13})f(r_{23}), \tag{3.22}
\end{aligned}$$

where we used the shorthand notation $\phi_{ij} = \phi(r_{ij})$, the fact that $Q_1 = V$, and that \mathbf{r}_i are dummy integration variables. The product of three Mayer functions in Eq.(3.22) implies that $B_3(T)$ involves three particles, and since $f(r_{ij})$ vanishes if particle i and j are separated, the product will vanish unless all three particles are simultaneously close to each another.

3.3.4 Higher order virial coefficients and diagrams

The analysis of higher order virial coefficients becomes increasingly difficult, and the expressions increasingly involved. To keep track of the bookkeeping a pictorial technique has been developed, whereby integrals of Mayer functions are represented by *cluster diagrams*. These diagrams, or graphs, consist of points (representing coordinates \mathbf{r}_i , \mathbf{r}_j , etc.) and lines connecting points (representing $f(r_{ij})$). Using this we can write

$$\begin{aligned}
B_2(T) &= -\frac{1}{2V} \int d\mathbf{r}_1 d\mathbf{r}_2 \text{ --- } \bullet \text{---} \bullet \\
B_3(T) &= -\frac{1}{3V} \int d\mathbf{r}_1 d\mathbf{r}_2 d\mathbf{r}_3 \text{ --- } \bullet \text{---} \bullet \text{---} \bullet \\
B_4(T) &= -\frac{1}{8V} \int d\mathbf{r}_1 d\mathbf{r}_2 d\mathbf{r}_3 d\mathbf{r}_4 \left(3 \text{ --- } \bullet \text{---} \bullet \text{---} \bullet \text{---} \bullet + 6 \text{ --- } \bullet \text{---} \bullet \text{---} \bullet \text{---} \bullet + \text{ --- } \bullet \text{---} \bullet \text{---} \bullet \text{---} \bullet \right) \tag{3.23}
\end{aligned}$$

It has been proven that all diagrams appearing in the integrand of the virial coefficients are *doubly connected*, i.e. are still connected when *any* point and all of its associated lines are removed. This means that diagrams like



do not occur. We remark that in most of the literature the integral symbol and the integral measure $d\mathbf{r}_1 \cdots d\mathbf{r}_n$ are ignored when the diagrams are defined, and often even the prefactors, like the “3” and the “6” in the expression for B_4 , are absorbed in the definitions. We will not pursue this here.

The number of diagrams for B_n increases rapidly with n , e.g. 468 in B_7 . For the hard-sphere potential (diameter σ) B_2 , B_3 , B_4 are known analytically,

$$\begin{aligned}
B_2 &= \frac{2\pi}{3} \sigma^3 \equiv b_0 \\
B_3 &= \frac{5\pi^2}{18} \sigma^6 = \frac{5}{8} b_0^2 \\
B_4 &= \left(-\frac{89}{280} + \frac{219\sqrt{2}}{2240\pi} + \frac{4131}{2240\pi} \arccos\left(\frac{1}{\sqrt{3}}\right) \right) b_0^3 \\
&\simeq 0.28695 b_0^3, \tag{3.24}
\end{aligned}$$

while higher order terms have been calculated by various numerical techniques (e.g. Monte Carlo methods),

$$B_5 = 0.1097(3)b_0^4 ; B_6 = 0.0386(4)b_0^5 ; B_7 = 0.0138(4)b_0^6. \tag{3.25}$$

The convergence of the hard-sphere virial expansion can be judged from Fig.3.6, where the numbers 2, 3, etc. label the second, third, etc. virial approximation, and where the full curve is the “exact” result as obtained from computer simulations. Obviously the deviations between the exact equation of state and

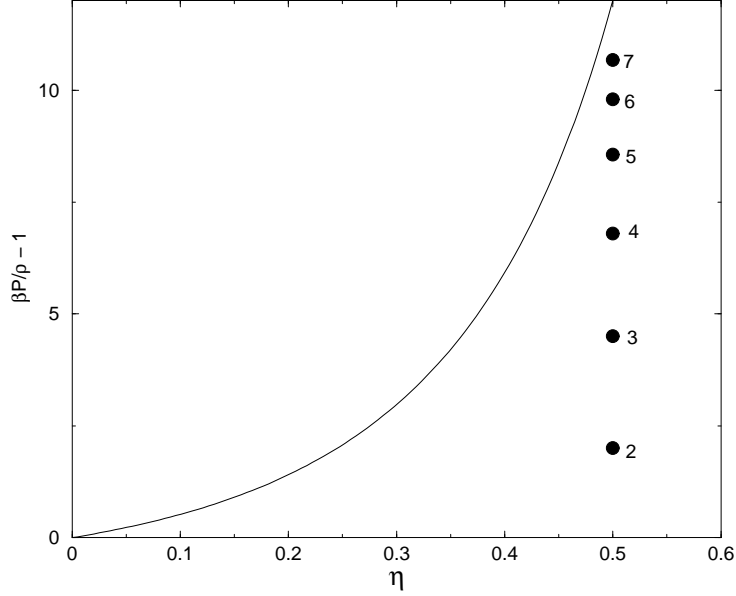


Figure 3.6: Equation of state of hard-sphere fluid as a function of the dimensionless density $\eta = (\pi/6)\sigma^3\rho$ (the packing fraction). The black dots labeled by $n = 2, 3, \dots, 7$ denote the results from the n -th order virial expansion at $\eta = 0.5$

the truncated virial expansions become more pronounced as η increases, and the 7th order expansion gives a good account up to moderate packing fractions $\eta \simeq 0.3$, say. Since not even the diagrams have been generated for B_8 and higher virial coefficients, we can also conclude from Fig.3.6 that the virial expansion is *not* suitable to describe liquids quantitatively, since a typical liquid density is $\eta \simeq 0.5$. Another reason why the virial expansion is cumbersome when applied to liquids is that the virial coefficients are generally T -dependent, so that lengthy calculations must be performed at many values of T . This contrasts the hard-sphere case, where the virial coefficients are temperature independent. For these reasons other methods have been devised to deal with dense liquids.

The virial expansion is, nevertheless, a valuable tool in the study of dilute or moderately dense gases. For instance, much of our knowledge of atomic pair potentials stems from measurements of virial coefficients. Although we focused on the application of the virial expansion to a one-component, classical, monoatomic gas, it is possible to extend these results to more components, polyatomic molecules, and to quantum effects.

3.3.5 The Helmholtz free energy

For later reference we also calculate the density expansion

$$\frac{F - F_{id}}{VkT} = f - f_{id} = f_{ex} = \sum_{n=2}^{\infty} C_n(T)\rho^n \quad (3.26)$$

of the excess (over ideal) Helmholtz free energy density (per kT) f_{ex} , with $C_n(T)$ the coefficients to be determined. Recalling that $p/kT = -f + \rho(\partial f/\partial\rho)_T$, we have

$$\frac{p - p_{id}}{kT} = -f_{ex} + \rho \left(\frac{\partial f_{ex}}{\partial \rho} \right)_T = \sum_{n=2}^{\infty} (n-1)C_n(T)\rho^n, \quad (3.27)$$

which in combination with the virial expansion for the pressure, Eq.(3.1), yields

$$C_n(T) = \frac{B_n(T)}{n-1} \quad n \geq 2. \quad (3.28)$$

The Helmholtz free energy can thus be written as

$$\frac{F}{VkT} = f = \rho \log(\rho\Lambda^3) - \rho + B_2(T)\rho^2 + \frac{B_3(T)}{2}\rho^3 + \dots, \quad (3.29)$$

with the virial coefficients $B_n(T)$ given in Eqs.(3.20) and (3.22).

3.4 Dense fluids

3.4.1 The pair correlation function

The rapidly increasing complexity of higher order virial coefficients prohibits practical applications of the virial expansion to dense fluids such as liquids. In fact, the problem is not only practical but also fundamental, as it is not guaranteed that the radius of convergence of the virial series is large enough to include the high densities of interest. Moreover, the virial expansion does not take into account the true nature of a liquid, in which each molecule constantly interacts strongly with all its neighbours. Other approaches have therefore been devised to deal with dense fluids. A key role in these theories is played by the distribution functions

$$\rho^{(1)}(\mathbf{r}) = \left\langle \sum_{i=1}^N \delta(\mathbf{r} - \mathbf{r}_i) \right\rangle \quad (3.30)$$

$$\rho^{(2)}(\mathbf{r}, \mathbf{r}') = \left\langle \sum_{i=1}^N \sum_{j \neq i}^N \delta(\mathbf{r} - \mathbf{r}_i) \delta(\mathbf{r}' - \mathbf{r}_j) \right\rangle, \quad (3.31)$$

which are called the one-particle distribution and the pair distribution function, respectively. Higher order distributions can be defined accordingly, but we do not need them here because we restrict attention to pairwise interactions. The angular brackets in Eqs.(3.30) and (3.31) denote an ensemble average, either canonical or grand canonical. $\rho^{(1)}(\mathbf{r})$ is a measure for the probability density that a particle is present at position \mathbf{r} . Because of the normalisation $\int d\mathbf{r} \rho^{(1)}(\mathbf{r}) = N$, we see that $\rho^{(1)}(\mathbf{r})$ is the local density, and equals $\rho = N/V$ in a homogeneous bulk system. $\rho^{(2)}(\mathbf{r}, \mathbf{r}')$ is called the pair distribution function, and is a measure for the probability that there is a particle at position \mathbf{r} and *another* one at \mathbf{r}' *simultaneously*. Within the canonical ensemble, we obtain from Eq.(3.31) that

$$\begin{aligned} \rho^{(2)}(\mathbf{r}, \mathbf{r}') &= \frac{1}{Q_N} \int d\mathbf{r}^N \exp[-\beta\Phi(\mathbf{r}^N)] \left(\sum_{i=1}^N \sum_{j \neq i}^N \delta(\mathbf{r} - \mathbf{r}_i) \delta(\mathbf{r}' - \mathbf{r}_j) \right) \\ &= \frac{N(N-1)}{Q_N} \int d\mathbf{r}^N \exp[-\beta\Phi(\mathbf{r}^N)] \delta(\mathbf{r} - \mathbf{r}_1) \delta(\mathbf{r}' - \mathbf{r}_2) \\ &= \frac{N(N-1)}{Q_N} \int d\mathbf{r}_3 \cdots d\mathbf{r}_N \exp[-\beta\Phi(\mathbf{r}, \mathbf{r}', \mathbf{r}_3, \dots, \mathbf{r}_N)]. \end{aligned} \quad (3.32)$$

Recall the definition of the configuration integral

$$Q_N = Q(N, V, T) = \int d\mathbf{r}^N \exp[-\beta\Phi(\mathbf{r}^N)]. \quad (3.33)$$

At sufficiently long distances $|\mathbf{r} - \mathbf{r}'|$ these probabilities become uncorrelated, and we have $\rho^{(2)}(\mathbf{r}, \mathbf{r}') \rightarrow \rho^{(1)}(\mathbf{r})\rho^{(1)}(\mathbf{r}')$. In isotropic, homogeneous systems such as liquids and gases we can use translational invariance to define the *radial distribution function* $g(r)$ by

$$\rho^{(2)}(\mathbf{r}, \mathbf{r}') = \rho^2 g(|\mathbf{r} - \mathbf{r}'|). \quad (3.34)$$

Note that $\rho g(r)$ is the average particle density at a distance r from a fixed particle. Also note that $\lim_{r \rightarrow \infty} g(r) = 1$. For systems with pairwise additive interactions the thermodynamics follows completely from $g(r)$, that is from $g(r; \rho, T)$ in the canonical ensemble or from $g(r; \mu, T)$ in the grand canonical

ensemble. There are three independent routes from $g(r)$ to thermodynamics, viz.

$$p = \rho kT - \frac{\rho^2}{6} \int d\mathbf{r} r \phi'(r) g(r) \quad (\text{virial route}) \quad (3.35)$$

$$\frac{E}{V} = \frac{3}{2} \rho kT + \frac{\rho^2}{2} \int d\mathbf{r} \phi(r) g(r) \quad (\text{caloric route}) \quad (3.36)$$

$$kT \left(\frac{\partial \rho}{\partial p} \right)_T = 1 + \rho \int d\mathbf{r} (g(r) - 1) \quad (\text{compressibility route}) \quad (3.37)$$

The virial and caloric route follow straightforwardly from the canonical partition function of a pairwise additive system, as will be shown in one of the problems. The compressibility route is necessarily derived grand canonically, and follows directly from the normalisation $\int d\mathbf{r} d\mathbf{r}' \rho^{(2)}(\mathbf{r}, \mathbf{r}') = N(N-1) = \langle N^2 \rangle - \langle N \rangle^2$ and Eq.(2.65).

Knowledge of $g(r)$ does not only lead to the thermodynamics of the fluid, but also to the structure factor $S(q)$ (that can be measured in scattering experiments). The relation between $S(q)$ and $g(r)$ is obtained as follows,

$$\begin{aligned} S(q) &\stackrel{(3.5)}{=} 1 + \left\langle \frac{1}{N} \sum_{i \neq j}^N \exp[i\mathbf{q} \cdot \mathbf{r}_{ij}] \right\rangle \\ &= 1 + \frac{1}{NQ_N} \int d\mathbf{r}^N \exp[-\beta\Phi(\mathbf{r}^N)] \sum_{i \neq j}^N \exp[i\mathbf{q} \cdot \mathbf{r}_{ij}] \\ &= 1 + \frac{1}{N} \int d\mathbf{r}_1 d\mathbf{r}_2 \exp[i\mathbf{q} \cdot \mathbf{r}_{12}] \\ &\quad \left(\frac{N(N-1)}{Q_N} \int d\mathbf{r}_3 \cdots d\mathbf{r}_N \exp[-\beta\Phi(\mathbf{r}^N)] \right) \\ &\stackrel{(3.32)}{=} 1 + \frac{1}{N} \int d\mathbf{r}_1 d\mathbf{r}_2 \exp[i\mathbf{q} \cdot \mathbf{r}_{12}] \rho^{(2)}(\mathbf{r}_1, \mathbf{r}_2) \\ &\stackrel{(3.34)}{=} 1 + \rho \int d\mathbf{r} \exp[i\mathbf{q} \cdot \mathbf{r}] g(r), \end{aligned} \quad (3.38)$$

i.e. $S(q)$ is essentially the Fourier transform of $g(r)$. Since $g(r)$ approaches unity for large r it is convenient to rewrite Eq.(3.38) as

$$S(q) = 1 + \rho \int d\mathbf{r} \exp[i\mathbf{q} \cdot \mathbf{r}] (g(r) - 1) + (2\pi)^3 \rho \delta(\mathbf{q}), \quad (3.39)$$

where the last term is irrelevant as long as the scattering angle θ , and hence the scattering vector \mathbf{q} , do not vanish. Clearly, we can also invert Eq.(3.38) with the result

$$\rho g(r) = \frac{1}{(2\pi)^3} \int d\mathbf{q} (S(q) - 1) \exp[i\mathbf{q} \cdot \mathbf{r}], \quad (3.40)$$

which can be used to deduce $g(r)$ from a measurement of $S(q)$. Typical $g(r)$'s for dense fluids are shown in Figs.3.7 and 3.9.

Although we wish to calculate $g(r)$ in dense fluids eventually, it is useful to consider its low-density behaviour first. Using methods similar to the virial expansion, it is possible to write

$$g(r; \rho, T) = g_0(r; T) + \rho g_1(r; T) + \rho^2 g_2(r; T) + \cdots, \quad (3.41)$$

with

$$g_0(r_{12}; T) = \exp[-\beta\phi(r_{12})] \quad (3.42)$$

$$g_1(r_{12}; T) = \exp[-\beta\phi(r_{12})] \int d\mathbf{r}_3 f(r_{13}) f(r_{32}), \quad (3.43)$$

where $\phi(r)$ is the pair potential and $f(r)$ the Mayer function defined in Eq.(3.21). The lowest order term g_0 is the Boltzmann weight of an isolated pair, as expected for classical particles, and the next order correction describes the effect of a third particle on the pair correlations of the pair (12).

For later reference we define the *potential of mean force* $w(r; \rho, T)$ by

$$w(r_{12}) = -kT \log g(r_{12}) \iff g(r_{12}; \rho, T) = \exp[-\beta w(r_{12}; \rho, T)] \quad (3.44)$$

This name stems from the fact that the gradient $-\nabla_1 w(r_{12})$ is the average force $\mathbf{f}(r_{12})$ acting on particle 1, keeping 1 and 2 fixed and averaging over all the others,

$$\begin{aligned} \nabla_1 w(\mathbf{r}_{12}) &\stackrel{(3.44)}{=} \frac{-kT}{g(r_{12})} \nabla_1 g(r_{12}) \\ &\stackrel{(3.32)}{=} - \frac{\int d\mathbf{r}_3 \cdots d\mathbf{r}_N \exp[-\beta \Phi(\mathbf{r}^N)] (-\nabla_1 \Phi(\mathbf{r}^N))}{\int d\mathbf{r}_3 \cdots d\mathbf{r}_N \exp[-\beta \Phi(\mathbf{r}^N)]} \\ &\equiv -\langle \mathbf{f}(r_{12}) \rangle. \end{aligned} \quad (3.45)$$

3.4.2 Ornstein-Zernike theory

Because of the importance of $g(r)$ in the theory of strongly interacting, dense fluids, many approaches have been devised to calculate (approximations to) this function, either analytically or numerically. Methods go by the names of “Kirkwood integral equation”, “BBGKY hierarchy”, and “Ornstein-Zernike” theory. The latter one will be discussed here heuristically. Rigorous derivations require extensive graph analysis or, a bit more modern, functional techniques that are too involved for the present course.

It is convenient to define the *total correlation function*

$$h(r_{12}) = g(r_{12}) - 1, \quad (3.46)$$

which is a measure for the “influence” of molecule 1 on molecule 2 a distance r_{12} away. In 1914 Ornstein and Zernike proposed to split this influence into two contributions, a direct part and an indirect part. The direct contribution is *defined* to be given by what is called the *direct correlation function*, denoted $c(r_{12})$. The indirect part is due to the direct influence of molecule 1 on a third molecule, labeled 3, which in turn influences molecule 2, directly and indirectly. Clearly, this indirect effect must be weighted by the density of particle 3, and averaged over all its possible positions. Mathematically this decomposition can be written as

$$h(r_{12}) = c(r_{12}) + \rho \int d\mathbf{r}_3 c(r_{13}) h(r_{32}), \quad (3.47)$$

which is called the Ornstein-Zernike (OZ) equation. It can be viewed as the defining equation for the direct correlation function $c(r)$. One may also argue, however, that we have rewritten a function we wish to calculate, $h(r)$, in terms of another function that we do not know, $c(r)$. In that sense Eq.(3.47) can be viewed as a single equation with two unknowns, which can only be solved if another relation between $c(r)$ and $h(r)$ is given. Such an additional relation is called the *closure*. The power of the decomposition given by Ornstein and Zernike is that approximate closures can be given, that allow for explicit calculation of $c(r)$ and $h(r)$ at a given density and temperature.

Before discussing an example of such a closure, we remark that the OZ equation (3.47) can be rewritten in terms of the Fourier transforms $\hat{h}(q)$ and $\hat{c}(q)$ of $h(r)$ and $c(r)$, respectively, as

$$\hat{h}(k) = \hat{c}(k) + \rho \hat{c}(k) \hat{h}(k), \quad (3.48)$$

from which we obtain that

$$\hat{c}(q) = \frac{\hat{h}(q)}{1 + \rho \hat{h}(q)} \quad ; \quad \hat{h}(q) = \frac{\hat{c}(q)}{1 - \rho \hat{c}(q)}. \quad (3.49)$$

From Eqs.(3.39) and (3.49) we find that $\hat{c}(q)$ is related to the structure through

$$S(q) = \frac{1}{1 - \rho \hat{c}(q)}. \quad (3.50)$$

A very successful and relatively simple closure is named after Percus and Yevick (PY). It consists of the *approximation* that

$$c(r) \stackrel{PY}{\approx} g(r)(1 - \exp[+\beta \phi(r)]). \quad (3.51)$$

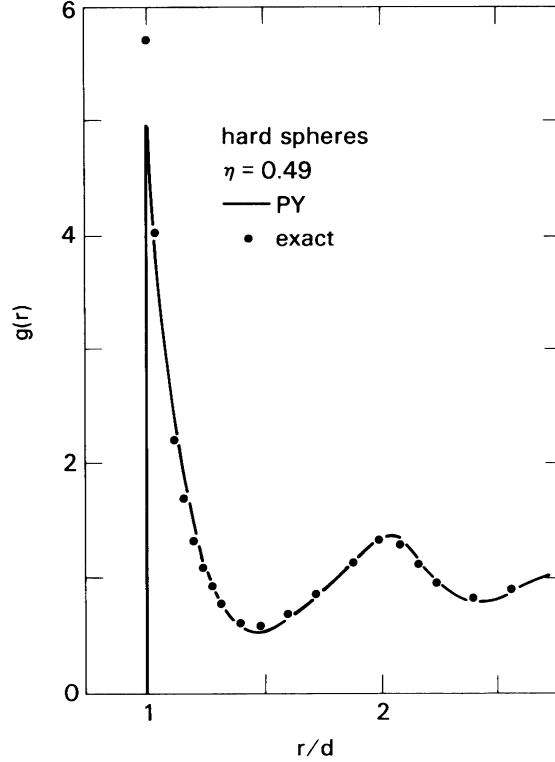


Figure 3.7: Radial distribution function $g(r)$ of a dense hard-sphere fluid.

The physical motivation behind the PY closure is as follows. First we note that the direct correlation $c(r)$ can be seen as the difference between the (total) pair correlation $g(r) \equiv \exp[-\beta w(r)]$ (see Eq.(3.44)) and an *indirect* term $g_{\text{indirect}}(r)$. This indirect term, which is *defined* as $g_{\text{indirect}}(r) = g(r) - c(r)$, is now *approximated* as $g_{\text{indirect}}(r) = \exp[-\beta(w(r) - \phi(r))] = g(r) \exp[+\beta\phi(r)]$, i.e. as the Boltzmann factor of $w(r) - \phi(r)$. Eq.(3.51) then follows readily. Having in mind that $w(r)$ is the (total) potential of mean force, while $\phi(r)$ is the pair potential, this approximation indeed captures the idea that the indirect contribution is *not* due to direct pair interactions. Other, more technical motivations for the PY closure can also be given, e.g. in terms of ignoring some subclasses of diagrams in the diagrammatic expansion of $c(r)$, but this is beyond the present goals.

The OZ equation (3.47) with the PY closure (3.51) constitutes two independent equations that can be solved for the two unknown functions $h(r)$ and $c(r)$, at least in principle. In practise this can often only be done numerically, but for the important case of the hard-sphere potential (3.9) analytic results have been found. Independently from each other Wertheim and Thiele showed, in 1963, that the PY closure to the OZ equation of a hard sphere fluid (diameter σ) at the dimensionless density $\eta = (\pi/6)\rho\sigma^3$ (i.e. the packing fraction) yields for the direct correlation function

$$c(r) = \begin{cases} \frac{-(1+2\eta)^2 + 6\eta(1+\frac{1}{2}\eta)^2\left(\frac{r}{\sigma}\right) - \frac{1}{2}\eta(1+2\eta)^2\left(\frac{r}{\sigma}\right)^3}{(1-\eta)^4} & r < \sigma \\ 0 & r > \sigma \end{cases} \quad (3.52)$$

This can be analytically Fourier transformed, from which the structure factor follows using Eq.(3.50). Unfortunately $g(r)$ cannot be written down analytically, but a numerical Fourier transform of $S(q)$ is straightforward, and from Eq.(3.38) $g(r)$ follows. The result is in very good agreement with computer simulations of $g(r)$ of hard spheres for $0 < \eta < \simeq 0.5$. This is illustrated in Fig.3.7. Since the hard-sphere fluid freezes at $\eta \approx 0.494$, the PY closure is accurate in the whole fluid regime of hard spheres. In one of the problems we will calculate that the explicit form (3.52) for $c(r)$ leads to the pressure p_c via the

compressibility route (3.37), and to p_v via the virial route (3.35), where

$$\begin{aligned}\frac{p_c}{\rho kT} &= \frac{1 + \eta + \eta^2}{(1 - \eta)^3} \\ \frac{p_v}{\rho kT} &= \frac{1 + 2\eta + 3\eta^2}{(1 - \eta)^2}.\end{aligned}\tag{3.53}$$

The difference between these two expressions increases with increasing η , but both give good account of the pressure that results from simulations. The (slight) inconsistency that results from the different routes is due to the PY approximation; an exact theory would lead to fully consistent thermodynamics. It turns out that the linear combination $p_{CS} = (2p_c + p_v)/3$, which is named after Carnahan and Starling, is indistinguishable from the simulations up to $\eta = 0.5$,

$$\frac{p_{CS}}{\rho kT} = \frac{1 + \eta + \eta^2 - \eta^3}{(1 - \eta)^3}.\tag{3.54}$$

In one of the problems it will be worked out that the Helmholtz free energy, F_{CS} , that follows from p_{CS} reads

$$\frac{F_{CS}}{NkT} = \log \rho \Lambda^3 - 1 + \frac{4\eta - 3\eta^2}{(1 - \eta)^2},\tag{3.55}$$

where the first two terms are ideal gas terms (see Eq.(2.52)), and the last one the excess term due to the hard-sphere interactions.

Because a typical triple point density, ρ_{tr} , of a simple fluid like argon satisfies $\rho_{tr}\sigma^3 \approx 1$, it is interesting to compare the triple-point structure with that of hard spheres at $\rho\sigma^3 \simeq 1$, i.e. $\eta \simeq 0.5$. Fig.3.8 shows

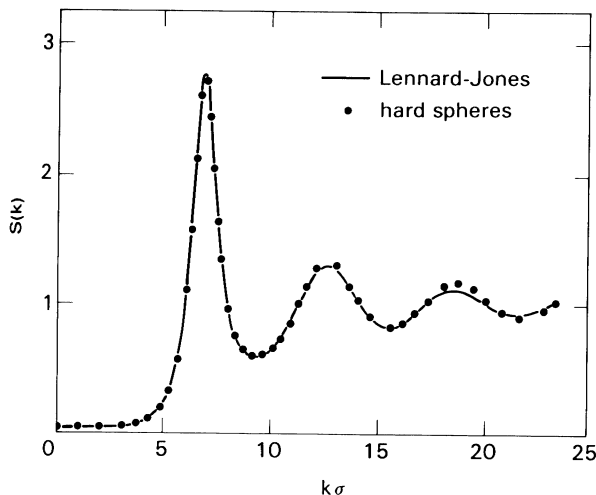


Figure 3.8: Structure factor of a Lennard-Jones fluid close to its triple point ($\rho\sigma^3 = 0.844$, $kT/\epsilon = 0.72$, and that of a hard-sphere fluid close to freezing ($\eta = 0.495$), as obtained from computer simulations.

such a comparison: the structure of a real dense fluid is qualitatively, and actually almost quantitatively, identical to that of a dense hard-sphere fluid! This implies that the fluid structure is mainly determined by the short-ranged repulsions, while the attractions hardly affect the high-density structure¹. This is further illustrated in Fig.3.9, where the liquid structure factor (close to the triple point) of Argon is shown. The similarity with Fig.3.7 for $g(r)$ of hard spheres is striking.

This notion is a crucial ingredient of the perturbation theory to be discussed in the next paragraph.

¹The attractions are important for the structure of a dilute gas, see e.g. Eq.(3.42).

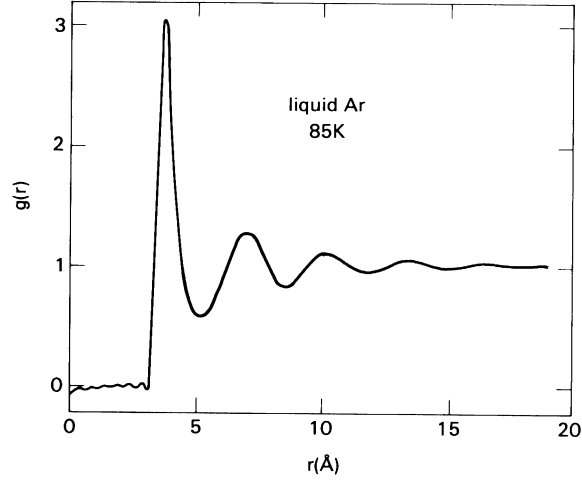


Figure 3.9: Radial distribution function of triple-point liquid Argon as measured by neutron scattering. The ripples at small r are artefacts of the data analysis.

3.5 Thermodynamic perturbation theory

We have seen that ensemble theory provides a formal framework to calculate thermodynamic properties starting from a microscopic Hamiltonian. Such a calculation always involves, in one way or another, the explicit calculation of the partition function, which is usually intractable analytically. Low-density expansion are possible, but these are not applicable in the regime of dense fluids. Here we present a method that does allow for realistic calculations of the Helmholtz free energy $F(N, V, T)$, and hence the full thermodynamics, of dense fluids.

We consider a Hamiltonian of the form (2.1), and decompose the interaction part Φ , formally, into a reference part Φ_0 and a perturbation Φ_1 . At this stage the decomposition is arbitrary, but a typical one would be to include the repulsions into Φ_0 and the attractions into Φ_1 . We define the auxiliary Hamiltonian

$$H_\lambda(\Gamma) = \sum_{i=1}^N \frac{\mathbf{p}_i^2}{2m} + \Phi_0(\mathbf{r}^N) + \lambda\Phi_1(\mathbf{r}^N) \equiv H_0(\Gamma) + \lambda\Phi_1(\mathbf{r}^N), \quad (3.56)$$

where H_0 is the *reference Hamiltonian*, and $\lambda \in [0, 1]$ a *coupling constant* or a *switching* parameter that switches H_λ from the reference Hamiltonian at $\lambda = 0$ to the Hamiltonian of interest at $\lambda = 1$. The Helmholtz free energy F_λ of the system with Hamiltonian H_λ can be written as

$$\begin{aligned} \exp[-\beta F_\lambda(N, V, T)] &= \frac{1}{N!h^{3N}} \int d\Gamma \exp[-\beta H_\lambda(\Gamma)] \\ &= \frac{1}{N!\Lambda^{3N}} \int d\mathbf{r}^N \exp[-\beta\Phi_0(\mathbf{r}^N) - \beta\lambda\Phi_1(\mathbf{r}^N)]. \end{aligned} \quad (3.57)$$

Taking the derivative with respect to λ on both sides of Eq.(3.57), and rearranging terms gives

$$\begin{aligned} \frac{\partial F_\lambda(N, V, T)}{\partial \lambda} &= \frac{\int d\mathbf{r}^N \exp[-\beta(\Phi_0 + \lambda\Phi_1)]\Phi_1(\mathbf{r}^N)}{\int d\mathbf{r}^N \exp[-\beta(\Phi_0 + \lambda\Phi_1)]} \\ &\equiv \langle \Phi_1 \rangle_\lambda, \end{aligned} \quad (3.58)$$

where the angular brackets $\langle \cdot \rangle_\lambda$ denote the canonical ensemble average of systems with Hamiltonian H_λ . The Helmholtz free energy of interest can with Eq.(3.58) be written as

$$F(N, V, T) = F_0(N, V, T) + \int_0^1 d\lambda \langle \Phi_1 \rangle_\lambda, \quad (3.59)$$

with F_0 the free energy of the reference system. Note that Eq.(3.59) is an exact result. Thermodynamic perturbation theory is based on a λ -expansion of the integrand of Eq.(3.59) about $\lambda = 0$. It follows from Eq.(3.58) that

$$\begin{aligned}
\langle \Phi_1 \rangle_\lambda &= \frac{\int d\mathbf{r}^N \exp[-\beta\Phi_0] (1 - \beta\lambda\Phi_1 + \frac{1}{2}\beta^2\lambda^2\Phi_1^2 + \dots)\Phi_1}{\int d\mathbf{r}^N \exp[-\beta\Phi_0] (1 - \beta\lambda\Phi_1 + \frac{1}{2}\beta^2\lambda^2\Phi_1^2 + \dots)} \\
&= \frac{\langle \Phi_1 \rangle_0 - \lambda\beta\langle \Phi_1^2 \rangle_0 + \frac{1}{2}\lambda^2\beta^2\langle \Phi_1^3 \rangle_0 + \dots}{1 - \lambda\beta\langle \Phi_1 \rangle_0 + \frac{1}{2}\lambda^2\beta^2\langle \Phi_1^2 \rangle_0 + \dots} \\
&= \langle \Phi_1 \rangle_0 - \lambda\beta(\langle \Phi_1^2 \rangle_0 - \langle \Phi_1 \rangle_0^2) + \frac{\lambda^2}{2}\beta^2\langle (\Phi_1 - \langle \Phi_1 \rangle_0)^3 \rangle_0 \\
&\quad + \mathcal{O}(\lambda^3),
\end{aligned} \tag{3.60}$$

where $\langle \cdot \rangle_0$ is a canonical average over the ensemble of reference systems. Using Eq.(3.59) we have

$$\begin{aligned}
\beta F(N, V, T) &= \beta F_0(N, V, T) + \beta\langle \Phi_1 \rangle_0 - \frac{\beta^2}{2}\langle (\Phi_1 - \langle \Phi_1 \rangle_0)^2 \rangle_0 \\
&\quad + \mathcal{O}((\beta\Phi_1)^3).
\end{aligned} \tag{3.61}$$

This is often called the *high-temperature expansion*. This name is not entirely appropriate, since β does not only appear explicitly in the prefactors of the successive terms, but also implicitly in the average of the reference system.

Let us now focus on the case that $\Phi(\mathbf{r}^N)$ can be written as a sum of pair potentials, with

$$\begin{aligned}
\Phi_0(\mathbf{r}^N) &= \sum_{i<j}^N \phi_0(r_{ij}) \\
\Phi_1(\mathbf{r}^N) &= \sum_{i<j}^N \phi_1(r_{ij}),
\end{aligned} \tag{3.62}$$

i.e. the pair potential of interest is $\phi(r) = \phi_0(r) + \phi_1(r)$. Then

$$\begin{aligned}
\langle \Phi_1 \rangle_\lambda &\stackrel{(3.58)}{=} \frac{N(N-1)}{2} \frac{\int d\mathbf{r}_1 d\mathbf{r}_2 \phi_1(r_{12}) d\mathbf{r}_3 \dots d\mathbf{r}_N \exp[-\beta(\Phi_0 + \lambda\Phi_1)]}{\int d\mathbf{r}^N \exp[-\beta(\Phi_0 + \lambda\Phi_1)]} \\
&\stackrel{(3.32)}{=} \frac{1}{2} \int d\mathbf{r}_1 d\mathbf{r}_2 \rho_\lambda^{(2)}(\mathbf{r}_1, \mathbf{r}_2) \phi_1(r_{12}) \\
&\stackrel{(3.34)}{=} \frac{V}{2} \rho^2 \int d\mathbf{r} g_\lambda(r) \phi_1(r),
\end{aligned} \tag{3.63}$$

where the last step only holds for uniform, isotropic systems in the thermodynamic limit. The Helmholtz free energy is

$$\begin{aligned}
F(N, V, T) &= F_0(N, V, T) + \frac{V\rho^2}{2} \int_0^1 d\lambda \int d\mathbf{r} g_\lambda(r) \phi_1(r) \\
&= F_0(N, V, T) + \frac{V\rho^2}{2} \int_0^1 d\lambda \int d\mathbf{r} [g_0(r) + \lambda g'_0(r) + \dots] \phi_1(r) \\
&= F_0(N, V, T) + \frac{V\rho^2}{2} \int d\mathbf{r} [g_0(r) + \frac{1}{2}g'_0(r) + \dots] \phi_1(r),
\end{aligned} \tag{3.64}$$

where $g'_0(r) = (\partial g_\lambda(r)/\partial \lambda)_{\lambda=0}$.

The crucial point of the perturbation theory for a dense liquid like triple point Argon, e.g. a liquid described by a pair potential of the form shown in Fig.3.4, is that its radial distribution function $g(r)$ hardly differs from that of the corresponding hard-sphere fluid, see Fig.3.8. This implies that the decomposition

$$\phi_0(r) = \phi_{HS}(r) \quad ; \quad \phi_1(r) = \phi(r) - \phi_{HS}(r) \tag{3.65}$$

is such that $g'_0(r)$ (and also higher order derivatives with respect to λ) is small. Consequently the free energy is given accurately by first order perturbation theory about the hard-sphere reference fluid, viz.

$$\begin{aligned} F(N, V, T) &= F_{HS}(N, V, T) + \frac{V\rho^2}{2} \int d\mathbf{r} g_{HS}(r) (\phi(r) - \phi_{HS}(r)) \\ &= F_{HS}(N, V, T) + \frac{V\rho^2}{2} \int_{r>\sigma_{HS}} d\mathbf{r} g_{HS}(r) \phi(r), \end{aligned} \quad (3.66)$$

where we used that $g_{HS}(r) = 0$ for $r < \sigma_{HS}$, the hard-sphere diameter. One can now use the Carnahan-Starling free energy of Eq.(3.55) as a very accurate representation of F_{HS} , and the PY radial distribution for $g_{HS}(r)$, to describe the thermodynamics of dense fluids quantitatively correctly. Note that there is some freedom to choose σ_{HS} .

3.6 Van der Waals theory

We can simplify the thermodynamic perturbation theory in order to recover Van der Waals' theory for gas-liquid coexistence. In his thesis of 1873 Van der Waals proposed two corrections to the ideal-gas law $p = NkT/V$. Firstly, he argued that the actual volume available to a molecule is smaller than the total volume V of the container because the finite diameter (or volume) of each molecule excludes some volume, say b , to all the others. Secondly, he argued that the attractions between the molecules reduce the pressure p by an amount $-a\rho^2$, where $a > 0$ is a measure of the strength of the attractions. So Van der Waals wrote

$$p = \frac{NkT}{V - Nb} - a\rho^2 = \frac{\rho kT}{1 - \rho b} - a\rho^2 = \frac{kT}{v - b} - \frac{a}{v^2}, \quad (3.67)$$

with volume per particle $v = 1/\rho = V/N$ and phenomenological parameters a and b . Note that the very existence of molecules was not generally accepted in Van der Waals' days, let alone that their interactions were understood (it actually takes quantummechanics to understand them as we have seen). Yet van der Waals did get the essential features of short-ranged repulsions (giving the excluded volume b) and the long-ranged attractions (parameterised by a) right. Moreover, his splitting of these two effects into two separate contributions is fully consistent with the perturbation theory about a hard-sphere reference fluid as we will see.

Fig.3.10 shows a plot of the pressure as a function of density at several temperatures that follows from Van der Waals' expression (3.67). At high enough temperatures, $T > T_c$, the pressure increases

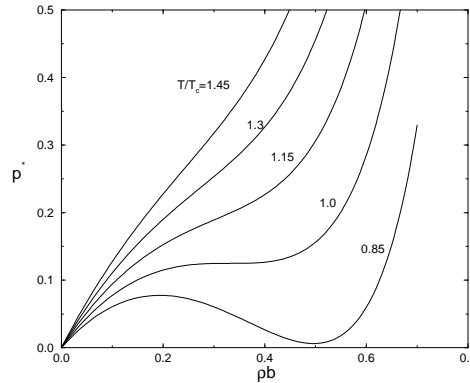


Figure 3.10: Van der Waals' pressure p^* , in arbitrary units, as a function of the density for temperatures T above, at, and below the critical temperature T_c .

monotonically with density, whereas at low enough temperatures, $T < T_c$, there is a density regime with $(\partial p/\partial \rho)_T < 0$. The critical isotherm, at temperature T_c , separates these two regimes, and shows a point of inflection with zero slope at the critical density ρ_c . The critical point (ρ_c, T_c) follows from the

conditions

$$\left. \begin{aligned} \left(\frac{\partial p}{\partial \rho}\right)_{T_c} &= 0 \\ \left(\frac{\partial^2 p}{\partial \rho^2}\right)_{T_c} &= 0 \end{aligned} \right\} \implies \begin{aligned} \rho_c b &= \frac{1}{3} \\ kT_c &= \frac{8a}{27b}. \end{aligned} \quad (3.68)$$

This result will be worked out in detail in one of the exercises.

A negative slope in the isotherm $p(\rho)$, i.e. a negative compressibility, is unphysical, and signifies a thermodynamic instability. It is a consequence of the implicit assumption in the calculation that the fluid is homogeneous, with the density equal to the imposed density $\rho = N/V$. We will show now, following Van der Waals, that the system can reduce its total free energy by splitting into two subsystems (the gas and the liquid), *if* the temperature is below T_c . The starting point of this analysis is the Helmholtz free energy F_{VdW} that underlies Van der Waals equation of state (3.67). From $p = -(\partial F/\partial V) = -f + \rho(\partial f/\partial \rho)_T$, with $f = F/V$ the free energy density, it follows from a straightforward integration that

$$f_{VdW} \equiv \frac{F_{VdW}}{V} = \rho kT \left(\log \frac{\rho \Lambda^3}{1 - b\rho} - 1 \right) - a\rho^2, \quad (3.69)$$

where the integration constant is chosen such that the ideal-gas free energy is obtained in the limit $\rho \rightarrow 0$. A plot of f_{VdW} , in arbitrary units, is shown in Fig.3.11. The convexity of these curves is directly related

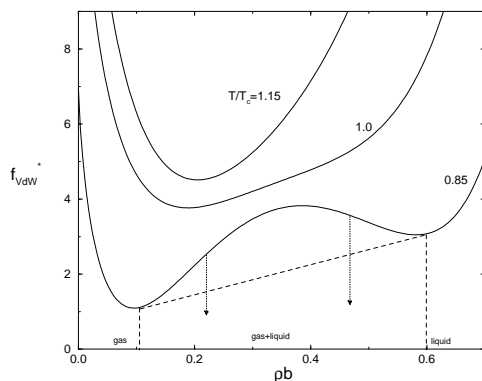


Figure 3.11: Van der Waals' free energy density f^* , in arbitrary units, as a function of the density for temperatures T above, at, and below the critical temperature T_c .

to the slopes of the equation of state in Fig.(3.10) since

$$\left(\frac{\partial p}{\partial \rho}\right)_T = \frac{\partial}{\partial \rho} \left(-f + \rho \left(\frac{\partial f}{\partial \rho}\right)_T \right) = \rho \left(\frac{\partial^2 f}{\partial \rho^2}\right)_T. \quad (3.70)$$

A negative compressibility is therefore equivalent to a concave part in $f(\rho)$. The set of points $\rho(T)$ for which $(\partial^2 f/\partial \rho^2)_T = 0$ is called the *spinodal*. The spinodal densities at $T = 0.85T_c$ are indicated by the arrows in Fig.3.11.

We will now show that the existence of a spinodal at some fixed temperature allows the system to lower its total free energy in some density regime by means of *phase separation* into a phase that is dilute (the gas phase, density ρ_1 , occupied volume V_1) and a phase that is dense (the liquid phase, density ρ_2 , occupied volume V_2) compared to the overall density $\rho = N/V$ of the system. Of course the constraints $V = V_1 + V_2$ and $\rho V = \rho_1 V_1 + \rho_2 V_2$ must be satisfied, which implies that the relative volume occupied by the liquid is given by

$$\frac{V_2}{V} = \frac{\rho - \rho_1}{\rho_2 - \rho_1}. \quad (3.71)$$

Clearly this expression only makes sense if $\rho_1 \leq \rho \leq \rho_2$. The total Helmholtz free energy of the phase-separated system is given by $F_M = V f_M = V_1 f(\rho_1) + V_2 f(\rho_2)$, where surface terms have been ignored,

and where the index “M” stands for “Maxwell”. From the constraints and from Eq.(3.71) it then follows that the free energy density is, still at a fixed temperature,

$$f_M(\rho) = f(\rho_1) + \left(\frac{\rho - \rho_1}{\rho_2 - \rho_1} \right) (f(\rho_2) - f(\rho_1)), \quad \rho \in [\rho_1, \rho_2], \quad (3.72)$$

i.e. a function that linearly interpolates between $f(\rho_1)$ and $f(\rho_2)$. If $f(\rho)$ is convex, i.e. if $T > T_c$, then $f_M(\rho) > f(\rho)$ for any choice of ρ_1 and ρ_2 . This implies that the free energy would increase upon phase separation, and hence the homogeneous phase at the imposed density ρ has the lowest free energy: *no* gas-liquid separation occurs for $T > T_c$. If, however, $f(\rho)$ is not entirely convex, i.e. $T < T_c$, then there is a density regime where $f_M(\rho) < f(\rho)$ for suitable values of ρ_1 and ρ_2 . The system can then reduce its total free energy by a phase separation into a dilute and a dense phase. The values of ρ_1 and ρ_2 are determined by the requirement that the total free energy of the system be minimised. It is seen from the geometry in Fig.3.11 that the lowest possible $f_M(\rho)$ is obtained if ρ_1 and ρ_2 satisfy the conditions

$$\left. \frac{\partial f}{\partial \rho} \right|_{\rho_1} = \left. \frac{\partial f}{\partial \rho} \right|_{\rho_2} = \frac{f(\rho_2) - f(\rho_1)}{\rho_2 - \rho_1}. \quad (3.73)$$

The first equality implies that the chemical potential in the gas, $\mu(\rho_1)$, and that in the liquid phase, $\mu(\rho_2)$, are the same, since $\mu = (\partial F / \partial N)_{V,T} = (\partial f / \partial \rho)_T$. Combination of $\mu(\rho_1) = \mu(\rho_2) \equiv \mu_{12}$ with the second equality then yields that the pressures in the two phases are the same, since

$$\begin{aligned} p(\rho_1) - p(\rho_2) &= -(f(\rho_1) - f(\rho_2)) + \rho_1 \mu(\rho_1) - \rho_2 \mu(\rho_2) \\ &= (\rho_1 - \rho_2) \left(\mu_{12} - \frac{f(\rho_2) - f(\rho_1)}{\rho_2 - \rho_1} \right) = 0. \end{aligned} \quad (3.74)$$

This lowest possible f_M and the corresponding coexistence densities ρ_1 and ρ_2 are indicated by the dashed lines in Fig.3.11. The total free energy density of the system, at temperatures $T < T_c$, is therefore given by $f(\rho)$ if $\rho < \rho_1$ and $\rho > \rho_2$, and by $f_M(\rho)$ for $\rho_1 \leq \rho \leq \rho_2$. The system is in the pure gas phase for $\rho < \rho_1$, in the pure liquid state for $\rho > \rho_2$, and in gas-liquid coexistence for $\rho_1 \leq \rho \leq \rho_2$. The set of points $\rho_1(T)$ is the gas branche of the *coexistence curve*, and the set $\rho_2(T)$ the liquid branche. The coexistence curve is also called the *binodal*. At the critical temperature the binodal and spinodal coalesce into the *critical point*. The reconstruction of the original free energy density f by f_M is known as the “common tangent construction” or the “Maxwell construction”. Note that such a construction is impossible if $f(\rho)$ is entirely convex; for $T > T_c$ there is no gas-liquid coexistence.

The parameters a and b in Van der Waals’ theory provide a phenomenological description of the attractions and repulsions between molecules. Since the perturbation theory we discussed before is also based on a separation of the interactions into attractions and repulsions, we can obtain (approximate) microscopic expressions for a and b by comparing f_{VdW} in Eq.(3.69) with the first order perturbation result given in Eq.(3.66). The last term in both expressions accounts for the attractions, the other terms for the (hard-sphere) repulsions. Using the low-density result $g_{HS}(r) = 1 + \mathcal{O}(\rho)$ for $r > \sigma_{HS}$ (see Eqs.(3.41) and (3.42)) we can identify

$$a = - \int_{r > \sigma_{HS}} d\mathbf{r} \phi(r), \quad (3.75)$$

i.e. a is the negative of the spatially-integrated strength of the attractive interactions, and hence $a > 0$ is indeed a measure for the attraction strength. The parameter b can be obtained by comparing the low-density expansion of F_{HS}/V with that of the first term of f_{VdW} . Both expressions reduce to the ideal-gas limit as $\rho \rightarrow 0$, and their $\mathcal{O}(\rho^2)$ terms are equal provided

$$b = B_2 \stackrel{(3.24)}{=} \frac{2\pi\sigma_{HS}^3}{3}. \quad (3.76)$$

With these identifications it is not surprising that the predictions that follow from the perturbation theory, Eq.(3.66), are merely more accurate than those of Van der Waals in comparison with experiments and simulations, but the essential physics of gas-liquid coexistence is contained within Van der Waals’ theory. An exception is the critical point, where both Van der Waals and perturbation theory fail dramatically. A detailed study of critical phenomena is beyond the scope of this course, but a few remarks can be made.

First, it follows from Eq.(2.65) that upon approach of the critical point the fluctuations in the number of particles diverge². These critical density fluctuations show up experimentally in the enhancement (and in fact divergence) of small-angle scattering experiments, since from Eqs.(3.37) and (3.39)

$$\lim_{q \rightarrow 0} S(q) = kT \left(\frac{\partial \rho}{\partial p} \right)_T \rightarrow \infty \text{ at the critical point.} \quad (3.77)$$

²In a canonical system with fixed N and V the overall density cannot fluctuate, but it can (and does) fluctuate in macroscopic subvolumes

4. Scattering techniques in soft condensed matter

Arnout Imhof
Soft Condensed Matter
Utrecht University

4.1. Introduction

Scattering techniques form an important class of tools for the study of soft condensed matter. Most laboratories have equipment for doing light scattering measurements, and many commercial instruments (in electrophoresis or particle sizing equipment) use light scattering internally. A light source is used to illuminate the sample and the scattered light is measured as a function of the angle between the incident beam and the detector. Light scattering is a suitable technique for soft condensed matter because the typical length scales (the particle size or the average distance between particles) is on the order of the wavelength of visible light. A few other types of radiation are also used, namely neutrons and X-rays. These scattering techniques are analogous to light scattering, but the wavelength is typically much shorter (0.1 – 10 nm). This makes these techniques useful for systems containing small particles. Even when the particles are not small, however, X-rays and neutrons are still useful when the samples scatter light too strongly (think of milk for example). As we shall see later, the information in this case is contained at small scattering angles (up to a few degrees), and the techniques are called small-angle X-ray or neutron scattering, or SAXS and SANS in short.

Wave scattering is a general phenomenon that occurs whenever the medium through which the wave propagates is inhomogeneous. Sound waves scatter if the medium contains objects with a different sound velocity, X-rays scatter from inhomogeneities in electron density, and light scatters from inhomogeneities in the refractive index. In this chapter we will concentrate on scattering of light, but scattering of other types of waves is almost completely analogous so that the theory we will develop applies equally well to those other types of radiation.

Suppose that an electromagnetic wave is incident on an object. Matter is composed of discrete electric charges, electrons and protons. They are set into oscillatory motion by the electric field of the incident electromagnetic wave. From electrodynamics it is known that the accelerated electric charges must radiate waves in all directions. This secondary radiation is called the radiation *scattered* by the object. Apart from scattering, part of the incident wave may also be converted to other forms of energy, such as heat. This process is called *absorption*. Both scattering and absorption remove light energy from the primary beam, which is thereby attenuated. Together, they are called *extinction*.

The light scattered by a particle in an otherwise homogeneous medium consists of the sum of wavelets scattered by all the subvolumes making up the particle. It is the *interference* between all these wavelets that leads to a characteristic angular dependence of the scattered light. This is the reason that light scattering can be used to measure the properties (size and shape) of colloidal particles. If there are other particles near the first particle then the waves scattered by different particles will also interfere with each other. Then the angular dependence also contains information on the average interparticle distances. As we shall see later, this angular dependence is directly proportional to the structure factor of the dispersion. Because of thermal motion the positions of the scattering particles relative to each other fluctuates continuously. By measuring the time dependence of the scattered light (*Dynamic Light Scattering*) we can obtain information on the dynamics of the scattering particles.

Why doesn't light scatter when it propagates through a homogeneous medium like, say, glass or water? Surely, the charges in these materials also start oscillating and must radiate in all directions! In fact they do, but it should be remembered that the scattered wave seen by an observer is the sum of wavelets originating from every little subvolume illuminated by the light beam. In a homogeneous medium there always exists a second subvolume, about half a wavelength away, which scatters exactly out of phase with a given subvolume. This leads to complete cancellation in all directions but the forward direction. Only when the medium is

inhomogeneous this cancellation does not take place, because half a wavelength away there is a different material. This means that some light is now scattered away from the forward direction. Of course, no medium except vacuum is truly homogeneous. Glass, water and air all consist of atoms and molecules, and therefore even these media scatter light, albeit only very weakly.

We now know that light scattered by a particle depends on the incident wave. In practice, scattering media contain many particles. Thus, the light incident on a given particle is the sum of the primary wave and the waves scattered by all the other particles. This seems like a hopeless problem, but we can simplify it if the total amount of scattered light is small enough so that it does not contribute significantly to the wave seen by the scattering particles. This is called *single scattering*, because a light wave scattered by a single particle does not scatter again from any of the other particles. The assumption is valid if the distance between the particles is large enough or if the amplitude of the scattered wave is very small compared to that of the incident wave. *Multiple scattering* takes place in systems in which this condition is not met. Examples are milk and clouds.

In the cases we shall consider the scattered light has a frequency equal to that of the incident wave. This is called *elastic scattering*. The angle-dependence gives information on the spatial structure of the sample. In *inelastic scattering* the frequencies of the scattered waves are measured in addition to the angle dependence. This gives information on dynamic processes, such as diffusion or relaxation. Many forms of inelastic scattering exist, such as Brillouin scattering and Raman scattering in which the scattered light contains both higher and lower frequencies. And in X-ray scattering the so-called Compton modified scattering is lowered in frequency. In dynamic light scattering the frequency changes are only very small (but not strictly zero), so it is sometimes also called quasi-elastic light scattering.

4.2. Measures of scattered light

In light scattering experiments the sample, containing particles suspended in a medium, is irradiated with a beam of light and light scattered at different angles is measured. We will call the direction of the incident beam the z -direction. Scattered light is measured by simply placing the detector on a rotation stage. In general, there are two angles to be varied, θ and ϕ , but in most instruments only θ is varied (see Figure 4.1). The yz -plane is defined to be the plane containing the incident beam and the detector and is called the *scattering plane*. A special scattering angle is zero degrees, where one measures the sum of the incident wave and the forward scattered wave. This is what one would measure in a normal transmission spectrophotometer. But what are the measured quantities? The *intensity* of the light, of course. (Or, to be more precise: the *irradiance*, the units are $\text{J}\cdot\text{m}^{-2}\cdot\text{s}^{-1}$.) But to completely characterize the scattered light the polarization state and the phase are also needed. Phases cannot be directly measured, but the polarization state must be carefully characterized by placing polarizers in the incident beam and/or in front of the detector¹.

First, let us consider a sample with only one particle. If we describe the angle dependence of the scattered intensity I_s with the function $F(\theta, \phi)$ then the intensity measured by a detector placed at a large distance r from the sample can be written as

$$I_s(\theta, \phi) = \frac{I_0 F(\theta, \phi)}{k^2 r^2} \quad (4.1)$$

¹ A complete discussion of polarization dependent scattering would complicate the discussion considerably. However, in most (but not all) cases relevant for soft condensed matter experiments the two polarization components shown in Figure 4.1 are independent. This is the case when the particles scatter light only weakly. Since this is already a requirement for single scattering it does not impose extra restrictions.

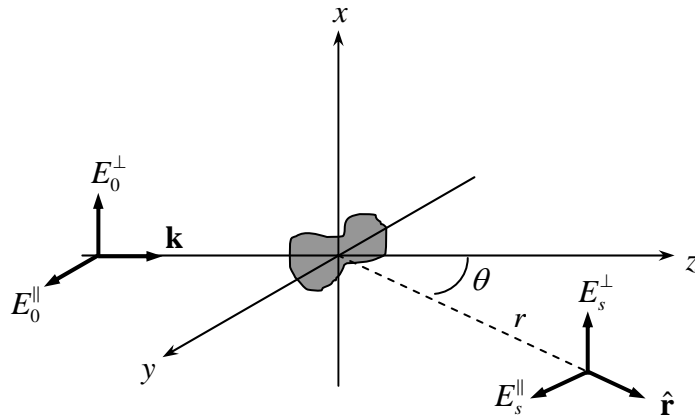


Figure 4.1. The scattering geometry.

I_0 is the intensity of the incident beam. The factor $1/r^2$ arises because the total scattered intensity over the surface of a sphere must be independent of its radius². Further, $k = 2\pi/\lambda$ is the length of the *wave vector* of the light (measured in the medium). The factor $1/k^2$ is included to make F a dimensionless function. If we integrate (4.1) over the surface of a sphere with radius r we get the total *power* of scattered light P_s . The scattered power per unit incident intensity has units of area and is called the *scattering cross section* of the particle:

$$C_{sca} = \frac{P_s}{I_0} = \frac{1}{k^2} \int_{4\pi} F(\theta, \varphi) d\Omega \quad (4.2)$$

where $d\Omega = \sin\theta d\theta d\varphi$ is shorthand for the infinitesimal element of solid angle. What is the physical significance of C_{sca} ? Conservation of energy dictates that the power removed from the incident beam must equal the total scattered power (if there is no absorption). Therefore the power in the light beam is lowered by an amount $C_{sca}I_0$. This is just as if the particle “casts a shadow” of area C_{sca} on a detector placed in the transmitted beam. If there is also absorption then the power received by the transmission detector is reduced by a further $C_{abs}I_0$. The total reduction of the light power must be the sum of scattering and absorption, and is given by the *extinction cross section*:

$$C_{ext} = C_{sca} + C_{abs} \quad (4.3)$$

Now consider a sample containing many identical particles at number density ρ . Every particle in the beam reduces the power in the beam further. Assuming only single scattering as usual, it is clear that every particle reduces the power by the amount $C_{ext}I(z)$, and that a thin slab of thickness dz reduces it by $C_{ext}I(z)\rho Adz$, with A the cross sectional area of the beam. Therefore,

$$dI = -\rho C_{ext} I(z) dz.$$

Integrating from 0 to L , the thickness of the sample, we see that the transmitted intensity is given by

$$I_t = I_0 e^{-\rho C_{ext} L}. \quad (4.4)$$

If there is no absorption and the number density of particles is known then their scattering cross section can be measured with a transmission measurement, using (4.4).

² This assumes that the medium is nonabsorbing.

A small detector placed not in the transmitted beam, but at an angular position (θ, φ) sees an intensity per particle given by (4.1). If the detector intercepts light coming from a sample volume V_s (the scattering volume) then the quantity that is often used to measure the scattered light is the *Rayleigh ratio*, defined as

$$R(\theta, \varphi) \equiv \frac{r^2 I_s(\theta, \varphi)}{V_s I_0} = \frac{\rho}{k^2} F(\theta, \varphi) \quad (4.5)$$

Another quantity that is often encountered in the literature is the *differential scattering cross section* $dC_{sca}/d\Omega$:

$$\frac{dC_{sca}}{d\Omega} \equiv \frac{r^2 I_s(\theta, \varphi)}{N I_0} = \frac{1}{k^2} F(\theta, \varphi), \quad (4.6)$$

where $N = \rho V_s$ is the number of scattering particles. It is called this way because (compare with (4.2)) it is the power received by the detector per unit incident intensity and per unit solid angle, but the notation should *not* be interpreted as the derivative of a function C_{sca} .

4.3. Light scattering by single particles

We will now consider scattering by a single particle placed at the origin and embedded in a homogeneous medium. It is illuminated with a monochromatic plane wave with angular frequency ω . The situation is again shown in Figure 4.1. The angle θ is the angle between the incident beam and the direction of the detector. We start with a particle that has a size much smaller than the wavelength in the medium λ . This means that the particle behaves approximately like a point dipole. The incident wave is denoted in complex notation³ by its electric field vector

$$\mathbf{E}(\mathbf{r}, t) = \mathbf{E}_0 e^{i\mathbf{k}\cdot\mathbf{r} - i\omega t}. \quad (4.7)$$

The wave vector \mathbf{k} points in the direction of propagation of the wave and has length $|\mathbf{k}| = k = 2\pi/\lambda$. The velocity of the wave in the medium is $c = \omega/k$. We will take the particle to be in the origin. The electric field of the incident beam will give rise to an induced dipole moment $\mathbf{p} = \alpha \mathbf{E}$ with α the polarizability of the particle. Far from the particle, at a distance r , the electric field of the wave radiated by this oscillating dipole is (see for example Griffiths, page 457):

$$\mathbf{E}_s = \frac{1}{4\pi\epsilon_m c^2 r} \left[\hat{\mathbf{r}} \times (\hat{\mathbf{r}} \times \ddot{\mathbf{p}}(t - r/c)) \right].$$

Here $\hat{\mathbf{r}}$ is a unit vector in the direction of the detector. The two dots on \mathbf{p} mean the second time derivative, which should be evaluated at time $t - r/c$. Thus, we obtain

$$\mathbf{E}_s = -\alpha \frac{k^2}{4\pi\epsilon_m r} \left[\hat{\mathbf{r}} \times (\hat{\mathbf{r}} \times \mathbf{E}_0) \right] e^{i\mathbf{k}\cdot\mathbf{r} - i\omega t}, \quad (4.8)$$

where we have used $\omega = ck$. We decompose the electric field in components perpendicular and parallel to the scattering plane (see Figure 4.1). The result is then

$$\begin{pmatrix} E_s^\parallel \\ E_s^\perp \end{pmatrix} = \alpha \frac{k^2}{4\pi\epsilon_m r} e^{i\mathbf{k}\cdot\mathbf{r} - i\omega t} \begin{pmatrix} E_0^\parallel \cos\theta \\ E_0^\perp \end{pmatrix} \quad (4.9)$$

³ In complex notation the real electric field is the real part of the complex electric field, $\mathbf{E}_r = \text{Re}(\mathbf{E}) = \mathbf{E}_0 \cos(\mathbf{k} \cdot \mathbf{r} - \omega t)$. The intensity of the wave is proportional to the square of the modulus of the complex electric field: $|\mathbf{E}|^2 = \mathbf{E} \cdot \mathbf{E}^*$.

This describes a spherical wave: in every direction it looks like a plane wave with an amplitude that falls like $1/r$. Also note that at 90 degrees the scattered light has complete perpendicular polarization. At this angle the dipole has a vanishing component in the E_s^{\parallel} direction.

The polarizability for a particle with volume V_p and permittivity ϵ_p in a medium with permittivity ϵ_m (both linear and isotropic) is given by the Clausius-Mosotti (or Lorentz-Lorenz) relation

$$\begin{aligned}\alpha &= 3\epsilon_m \frac{\epsilon_p - \epsilon_m}{\epsilon_p + 2\epsilon_m} V_p \\ &= 3\epsilon_m \frac{m^2 - 1}{m^2 + 2} V_p \quad \text{with } m = \frac{n_p}{n_m}\end{aligned}\tag{4.10}$$

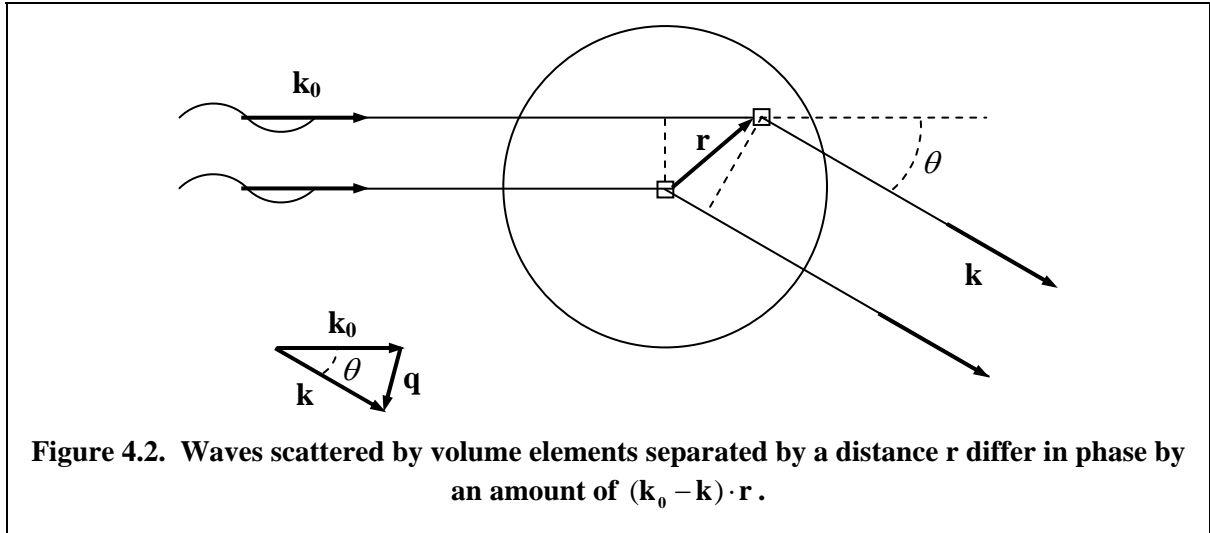
m is the ratio of the refractive indices of the particle and the medium. In general, α depends on the frequency; at frequencies where the particle absorbs it becomes a complex number.

The scattered intensity is $I_s \sim |\mathbf{E}_s|^2$ so that for unpolarized incident light

$$\begin{aligned}I_s(\theta) &= I_0 \frac{k^4}{32\pi^2 \epsilon_m^2 r^2} |\alpha|^2 (1 + \cos^2 \theta) \\ &= I_0 \frac{9\pi^2}{2\lambda^4 r^2} \left| \frac{m^2 - 1}{m^2 + 2} \right|^2 V_p^2 (1 + \cos^2 \theta)\end{aligned}\tag{4.11}$$

This result was derived by Rayleigh, and scattering by particles much smaller than the wavelength is therefore called Rayleigh scattering. Two things about (4.11) are important to notice. Firstly, the scattered intensity depends on the inverse *fourth* power of the wavelength. This means that short wavelengths are scattered much more strongly than long wavelengths. Molecules in the air scatter only slightly, but they scatter blue much more strongly than red. This is why the sky looks blue. The setting sun looks red because a good deal of the blue light has scattered out of the rays by the time they reach your eyes. (Why doesn't the sun look red during most of the day?) Another important thing about (4.11) is that the scattered intensity increases with the square of the volume, i.e. the *sixth* power of the diameter of a particle! Finally, if a particle and its environment have the same refractive index ($m=1$) then the scattered intensity vanishes. In this case the particle is said to be *index matched*.

Now we move on to consider light scattering by particles that are not small compared to the wavelength. When the plane wave (4.7) is incident upon such a particle every volume element becomes an oscillating dipole with the same frequency ω . But since the dipoles are at different positions they each carry a different phase. The scattered wave seen by a detector is the superposition of the dipole fields radiated by all the dipoles. At this point we have to make an approximation. Each dipole responds to the field incident upon it according to (4.8). Since the field incident on a volume element is the superposition of the primary beam with the fields coming from all the other dipoles, the problem becomes extremely complicated. Only for a few types of particles exactly solving the complete Maxwell equations can solve the problem. (For spherical particles this is called Mie theory, after the person who first solved this in 1908. The solution is in the form of infinite series that must be evaluated using a computer.) The approximation that we will make is that the field incident on a volume element can be approximated by the field of the primary beam. The fields from the other dipoles are neglected. In quantum mechanical scattering problems this is called the 1st order Born approximation; in light scattering the Rayleigh-Gans-Debye theory. The conditions for validity are the following:



$$\begin{aligned}
 |m-1| &\ll 1 \\
 kd|m-1| &\ll 1
 \end{aligned}
 \tag{4.12}$$

where d is a characteristic linear dimension of the particles. The first condition means that the scattering is weak so that the intensity of the incident beam is hardly attenuated inside the particles. This way, all dipoles experience the same incident field and radiate only a little. The second condition means that the phase fronts do not become distorted on passage through the particle.

With this approximation we can sum the waves of equation (4.9) over all volume elements in the particle. Figure 4.2 shows how to take the phase differences into account. The incident wave is characterized by a wave vector \mathbf{k}_0 . Two volume elements $d\mathbf{r}$ are shown. One sits in the origin, the other at position \mathbf{r} . Each scatters a wave with wave vector \mathbf{k} towards the detector, which is at a large distance R . The phase difference between these two waves is

$$\begin{aligned}
 \Delta\phi &= -\mathbf{k} \cdot \mathbf{r} + \mathbf{k}_0 \cdot \mathbf{r} \\
 &= -(\mathbf{k} - \mathbf{k}_0) \cdot \mathbf{r} \\
 &\equiv -\mathbf{q} \cdot \mathbf{r}
 \end{aligned}
 \tag{4.13}$$

We call $\mathbf{q} = \mathbf{k} - \mathbf{k}_0$ the *scattering vector*. It is the difference between the scattered and incident wave vectors. Since we are considering elastic scattering these both have length $2\pi/\lambda$. It is then easy to show that

$$q = |\mathbf{q}| = \frac{4\pi}{\lambda} \sin(\theta/2)
 \tag{4.14}$$

Remember that λ is the wavelength in the medium, not in vacuum!

The field scattered by the element at \mathbf{r} , as seen by the detector, is then

$$dE_s^\perp = \frac{k^2}{2\pi R} (m(\mathbf{r}) - 1) E_0^\perp e^{ikR - i\mathbf{q} \cdot \mathbf{r} - i\omega t} d\mathbf{r}.
 \tag{4.15}$$

Since m is close to unity we have simplified $(m^2 - 1)/(m^2 + 2) \approx \frac{2}{3}(m - 1)$. We also allow that the particle is inhomogeneous, so m can depend on position. The parallel component of the field has an extra factor $\cos\theta$. This must be integrated over the volume of the particle V_p to get the total field scattered in the direction of \mathbf{k} :

$$E_s^\perp = \frac{k^2}{2\pi R} E_0^\perp e^{ikR - i\omega t} f(\mathbf{q})
 \tag{4.16}$$

with

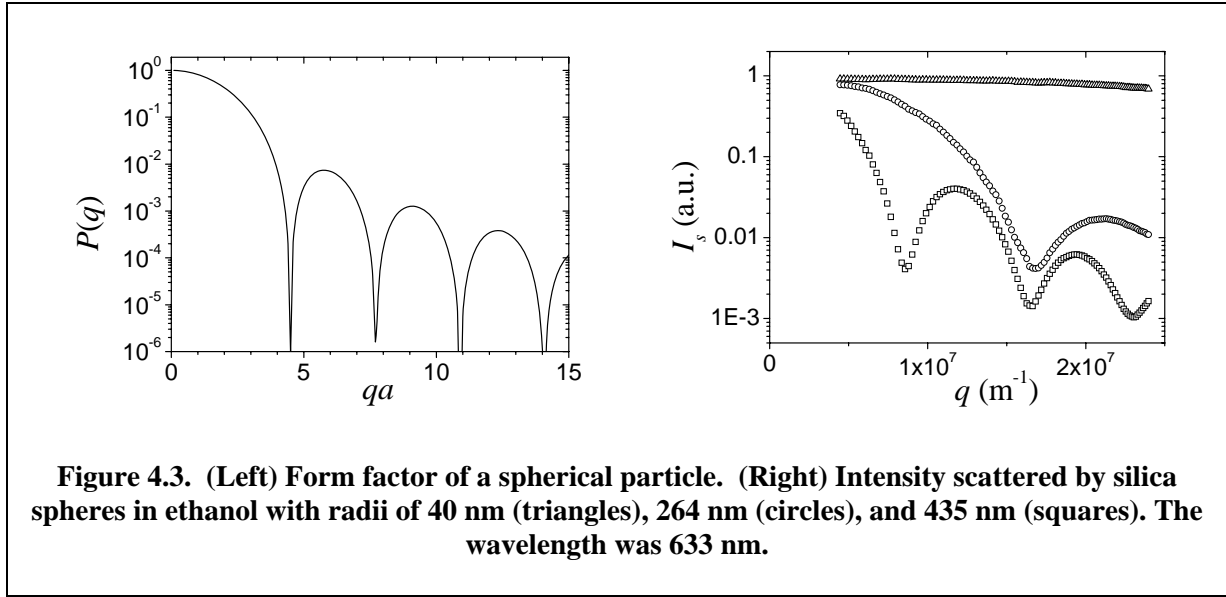


Figure 4.3. (Left) Form factor of a spherical particle. (Right) Intensity scattered by silica spheres in ethanol with radii of 40 nm (triangles), 264 nm (circles), and 435 nm (squares). The wavelength was 633 nm.

$$f(\mathbf{q}) = \int_{V_p} (m(\mathbf{r}) - 1) e^{-i\mathbf{q}\cdot\mathbf{r}} d\mathbf{r}. \quad (4.17)$$

We have separated the interesting part $f(\mathbf{q})$ from the boring constants. It can be interpreted as the amplitude of the wave scattered at wave vector \mathbf{q} by the particle as a whole. Finally, the square of the modulus gives us the scattered intensity. After a bit of rearranging we find

$$I_s = I_0 \frac{k^4 V_p^2 |\bar{m} - 1|^2}{8\pi^2 R^2} P(\mathbf{q}) (1 + \cos^2 \theta) \quad (4.18)$$

with

$$P(\mathbf{q}) = \frac{|f(\mathbf{q})|^2}{|f(\mathbf{0})|^2} = \frac{\left| \int_{V_p} (m(\mathbf{r}) - 1) e^{-i\mathbf{q}\cdot\mathbf{r}} d\mathbf{r} \right|^2}{\left| \int_{V_p} (m(\mathbf{r}) - 1) d\mathbf{r} \right|^2} \quad (4.19)$$

Here \bar{m} is the value of m averaged over the volume of the particle. The prefactor in the formula gives the absolute scattered intensity and has just the same properties as in the Rayleigh formula. The part that interests us more is the *form factor* $P(\mathbf{q})$ of the particle, which describes the angular dependence of the scattering⁴. The form factor is determined only by the size and shape of the particle and is normalized in the forward direction (where $\mathbf{q}=\mathbf{0}$). By measuring the angular dependence of the scattered light we can immediately obtain the form factor and learn about the particle properties. We must then compare this with a model.

The simplest model is of course the sphere. For a sphere with radius a the form factor can be calculated by choosing the z -axis along \mathbf{q} and first integrating over the angles. The result is

$$P(q) = \left[3 \frac{\sin(qa) - qa \cos(qa)}{(qa)^3} \right]^2. \quad (4.20)$$

This function is shown in Figure 4.3. Note that the form factor depends only on the product qa , so there is in principle no limit to the number of oscillations. Of course, q can never be larger than $4\pi/\lambda$, so the number of oscillations in the range of scattering angles between 0 and 180° is a sensitive function of the particle radius. This can be used to measure the size of

⁴ In the crystallography literature it is often the function $f(\mathbf{q})$ which is called the form factor.

spheres. If the particles are monodisperse the minima and maxima can be observed in the scattered intensity, as is also shown in Figure 4.3. Also note the strong forward scattering for large particles.

Equations (4.18) and (4.19) as they stand describe scattering by a single particle with a fixed and given orientation in space. In practice we almost always measure the light scattered by a large number of particles which each have a different (and constantly fluctuating) orientation. In a dilute suspension all the particles scatter incoherently so that we can add the intensities scattered by each particle. The scattered intensity thus becomes N times larger and the form factor must be averaged over the orientations of the particles. Results are known for a number of particle shapes, such as ellipsoids, rods and disks. These formulas can be found in the scattering literature.

We will not study all the consequences of particle anisotropy, but just consider the case of small particles. This is a useful case because many particles are much smaller than the wavelength of the light used to study them, for example most polymers, proteins, nanocrystals and micelles. In this case $\mathbf{q} \cdot \mathbf{r}$ is small so that we can only measure the initial part of the form factor. What we get in return is that the particles are allowed to be nonspherical and polydisperse. First, we must decide on an origin for an irregularly shaped particle. (Since only differences in phase are important this choice should not influence the result.) The easiest choice is the center of mass:

$$\mathbf{R}_{cm} = \frac{1}{V_p} \int \mathbf{r} d\mathbf{r} = \mathbf{0}$$

We can now expand the exponent in the form factor (4.19) in a Taylor series. The first order term is zero due to our choice of the origin. This leads to

$$P(\mathbf{q}) = \left| 1 - \frac{1}{2} \left\langle \frac{\int_{V_p} (m-1)(\mathbf{q} \cdot \mathbf{r})^2 d\mathbf{r}}{\int_{V_p} (m-1) d\mathbf{r}} \right\rangle + \dots \right|^2 \approx 1 - \frac{\int_{V_p} (m-1) q^2 r^2 \langle \cos^2 \theta \rangle d\mathbf{r}}{\int_{V_p} (m-1) d\mathbf{r}}$$

The angled brackets $\langle \dots \rangle$ indicate an average over the ensemble of particles. Since the particles have random orientations $\langle \cos^2 \theta \rangle = 1/3$. The result is the *Guinier approximation*:

$$P(q) = 1 - \frac{1}{3} q^2 R_g^2 + \dots \quad (4.21)$$

with the *radius of gyration* defined as

$$R_g^2 = \frac{\int_{V_p} (m-1) r^2 d\mathbf{r}}{\int_{V_p} (m-1) d\mathbf{r}} \quad (4.22)$$

Note that this is still a volume integral and that r is the distance of a volume element to the particle's center of mass. For spheres it is easy to derive that $R_g = \sqrt{3/5} a$, but the result is most useful for irregularly shaped particles, because it provides a uniquely defined particle size that is directly measurable and which can be compared to a model. For example, a rodlike particle with length L has $R_g = L/\sqrt{12}$ and a Gaussian polymer coil of n random chain (or Kuhn) segments of length l has $R_g = l\sqrt{n/6}$.

4.4. Light scattering by an ensemble of particles

Next, we consider scattering by a more concentrated suspension. This means that many particles in the scattering volume V_s contribute to the wave scattered towards the detector. To do this we take exactly the same approach as in the case of the not-so-small particle. We again assume that every volume element scatters a dipole field, and that the field incident on a given particle can be approximated by the external field. The waves scattered by the other particles are neglected. This is the same as saying that there is only *single* scattering. If a concentrated suspension is measured the scattered intensity per particle must be very small. This is the case for very small particles or if $m \approx 1$. The latter condition can sometimes be satisfied if the refractive index of the medium is adjusted so that it almost equals that of the particles (*index-matching*).

Assuming that the single scattering assumption is satisfied we again refer to Figure 4.2. This time, imagine that the large circle is the entire scattering volume V_s , which contains a large number of particles N . The volume elements $d\mathbf{r}$ can lie either in a particle or in the medium. The waves scattered towards the distant detector are once more summed, taking their phases into account:

$$E_s^\perp = \frac{k^2}{2\pi R} E_0^\perp e^{ikR-i\omega t} \int_{V_s} (m(\mathbf{r})-1) e^{-i\mathbf{q}\cdot\mathbf{r}} d\mathbf{r} \quad (4.23)$$

Only volume elements lying in the particles have a nonzero $m-1$ and contribute to the integral. We can thus separate the integral into contributions coming from each particle:

$$E_s^\perp = \frac{k^2}{2\pi R} E_0^\perp e^{ikR-i\omega t} \sum_{j=1}^N \int_{V_j} (m(\mathbf{r})-1) e^{-i\mathbf{q}\cdot\mathbf{r}} d\mathbf{r} \quad (4.24)$$

where V_j is the volume occupied by particle j . Let \mathbf{r}_j denote the position of the center of particle j . The integration variable \mathbf{r} can then be written as $\mathbf{r} = \mathbf{r}_j + \mathbf{r}'$. The new integration variable \mathbf{r}' ranges over the volume of the particle with its center translated to the origin. Equation (4.24) now becomes

$$E_s^\perp = \frac{k^2}{2\pi R} E_0^\perp e^{ikR-i\omega t} \sum_{j=1}^N f_j(\mathbf{q}) e^{-i\mathbf{q}\cdot\mathbf{r}_j} . \quad (4.25)$$

We have recognized the integral appearing in (4.17). It describes the interference of waves scattered by one particle. The exponential functions containing the position coordinates \mathbf{r}_j describe interference of light scattered by different particles. Because the particles move continuously the latter kind of interference leads to rapid fluctuations in the scattered light (typically to μs to ms). What is measured in a *static light scattering* experiment is the light scattered from a large sample volume containing very many particles, and averaged over times of the order of 1 s. In other words the measured quantity is the ensemble averaged intensity $I_s \sim \langle \mathbf{E}_s \cdot \mathbf{E}_s^* \rangle$. We will assume that all N particles are identical⁵. Remembering that the parallel field component has a factor $\cos\theta$ we obtain

$$I_s(\mathbf{q}) = I_0 \frac{Nk^4 V_p^2 |\bar{m}-1|^2}{8\pi^2 R^2} P(\mathbf{q}) S(\mathbf{q}) (1 + \cos^2 \theta), \quad (4.26)$$

with

⁵ The expression can be generalized for a mixture of nonidentical particles, but the result can no longer be separated into the product of a form factor and a structure factor. This also the case for nonspherical particles. In that case, identical particles with different orientations also have different f_j 's.

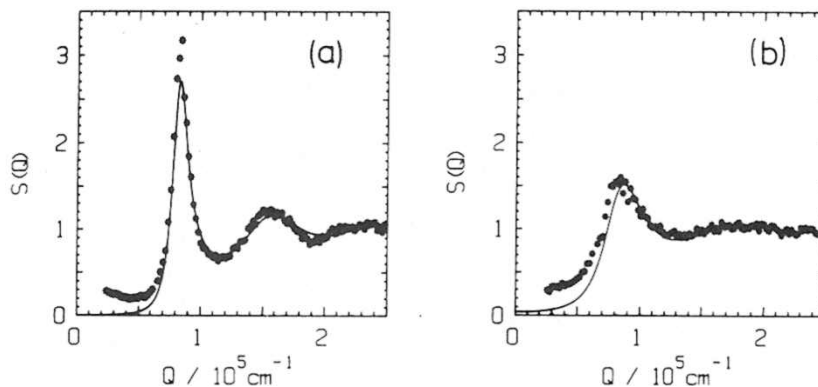


Figure 4.4. Structure factors of 80 nm diameter polystyrene spheres in water measured with light scattering. The particles surfaces carry ionizable $-\text{SO}_3\text{H}$ groups. The concentration was 1.8×10^{18} particles/ m^3 . (a) $3.1 \mu\text{mol/L}$ NaOH added; (b) $3.1 \mu\text{mol/L}$ NaCl added. The drawn lines are fits using the rescaled mean spherical approximation (RMSA). From: Härtl and Vermold, *Langmuir* 8, 2885 (1992).

$$S(\mathbf{q}) = \frac{1}{N} \left\langle \sum_{j=1}^N \sum_{k=1}^N e^{i\mathbf{q} \cdot (\mathbf{r}_k - \mathbf{r}_j)} \right\rangle. \quad (4.27)$$

This is the *structure factor* from Chapter 4.

This result means that the structure factor can be measured in a scattering experiment as follows. The scattered intensity of the sample under study, which has particle number density ρ , is measured as a function of angle. Then a small amount is diluted to ρ_{dil} by a large factor, say 100 times, so that its structure factor becomes equal to unity. The scattered intensity is again measured. Call this I_{dil} . The structure factor of the original sample is then found from

$$S(\mathbf{q}) = \frac{\rho_{\text{dil}}}{\rho} \frac{I_s(\mathbf{q})}{I_{\text{dil}}(\mathbf{q})}. \quad (4.28)$$

Some examples of measured structure factors are given in Figure 4.4. The large oscillations imply strong liquid-like ordering. Remember that a peak in the structure factor at wave vector q implies that there exists a (sinusoidal) density fluctuation with wavelength

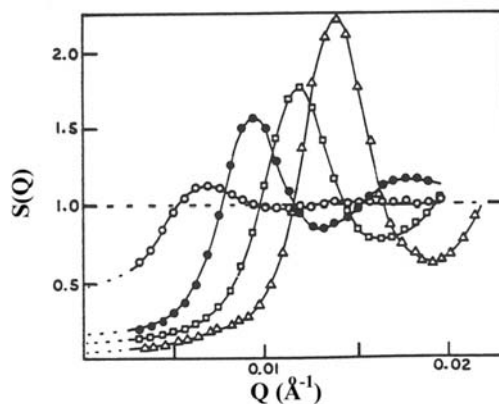
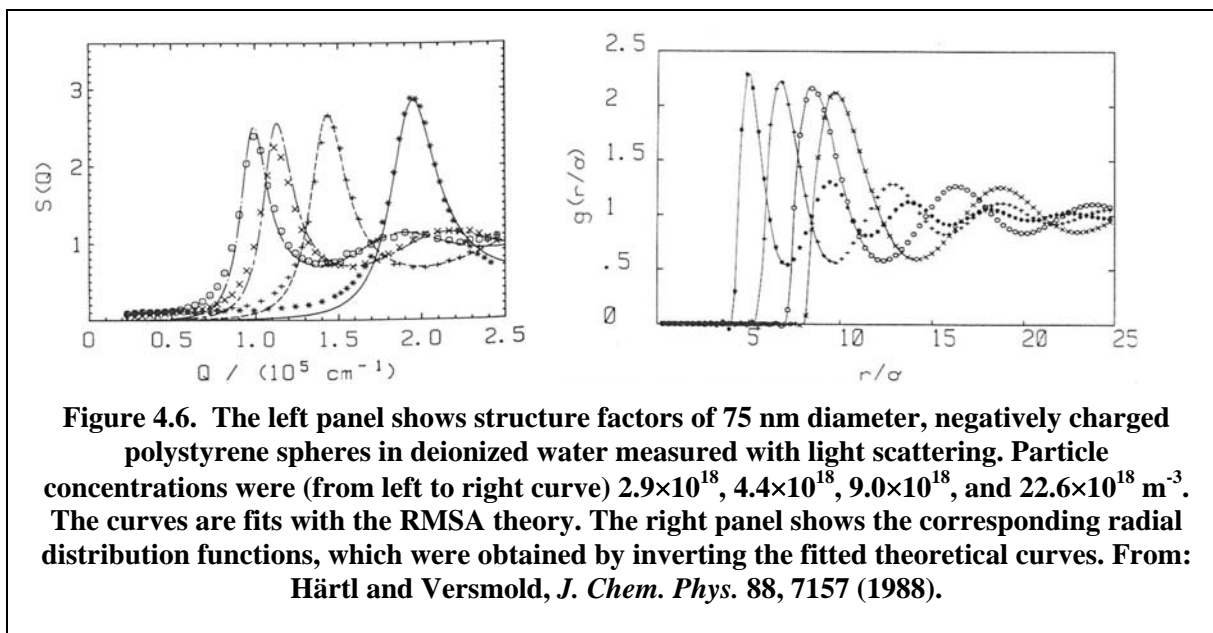


Figure 4.5. Structure factors measured with SANS of 16 nm radius polystyrene spheres in water containing 10^{-4} mol/L NaCl. Particle volume fractions were 0.01, 0.04, 0.08, and 0.13. From: Goodwin et al. *Makromol. Chem. Suppl.* 10/11, 499 (1985).



$2\pi/q$. The particles in this experiment were negatively charged. Addition of NaOH ionizes all the sulfonate groups on the surfaces, but does not reduce the Debye length because the H^+ counterions are merely replaced by Na^+ . Addition of an equal concentration of NaCl, on the other hand, reduces the Debye length making the liquid-like structure less pronounced. The dependence of the structure factor on the particle concentration is demonstrated in Figure 4.5 for charged polystyrene spheres with more salt added. It is clear that as the concentration is increased the liquid-like structure becomes much more pronounced. Also the first peak shifts to larger q , corresponding to smaller average interparticle distances.

In principle, it should be possible to Fourier invert the structure factor and obtain the radial distribution function. In practice, however, this turns out to be very difficult. The reason is that $S(q)$ can only be measured over a limited range of q , and the data become more noisy at larger q . Instead one therefore often finds a suitable fit of the structure factor with an appropriate theory and one then inverts the theoretical curve. This is done in Figure 4.6. Again, the increase in particle concentration leads to a shift of the structure factor peak to larger q , while the primary peak in $g(r)$ moves to smaller r . In this case the height of the peaks does not increase very much with concentration. This is because in a deionized dispersion most ions present in the system are the ions dissociated from the particle surfaces. As the particle concentration is increased the ionic strength of the solvent is also increased leading to more effective screening.

As an example of the relation between scattering and thermodynamics we show in Figure 4.7 measurements of the value of $S(q=0)$ for a colloidal dispersion of particles that behave like hard spheres. According to the well-known compressibility equation (Chapter 4) this must be proportional to the osmotic compressibility of the system:

$$S(q=0) = kT \left(\frac{\partial \rho}{\partial \Pi} \right)_T \quad (4.29)$$

The data are described correctly by the Percus-Yevick equation. This has been an important test of this theory, and demonstrated at the same time that silica spheres coated with stearyl alcohol and dispersed in cyclohexane behave like true hard spheres. The values of $S(q=0)$ are extrapolated from a plot of $S(q)$ versus q^2 . Great care should be taken to ensure that the measurements are not affected by the presence of dust or clusters of particles, which contribute mainly to the scattering at low q .

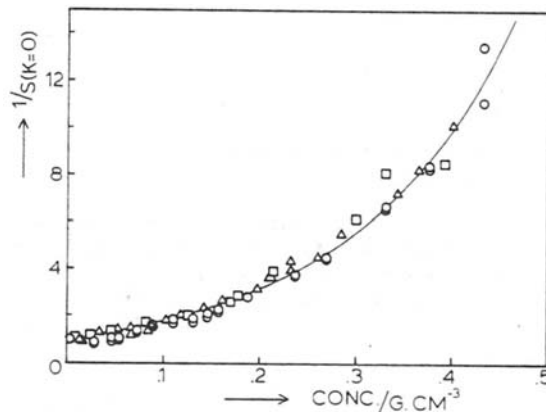


Figure 4.7. Scattering measurements of the structure factor extrapolated to zero wave vector on a system of stearyl alcohol coated silica spheres dispersed in cyclohexane. These particles behave like hard spheres. The data agree with the Percus-Yevick expression for the compressibility (drawn line). Triangles are light scattering data on particles with radius 35 nm, squares are SANS measurements on the same particles. Circles are light scattering data on spheres with a radius of 22 nm. From: De Kruif, Jansen, and Vrij, In: ‘Physics of Complex and Supramolecular Fluids’, Wiley, New York, 1987.

In many cases, for example molecular weight determinations in polymers or the measurement of particle sizes in association colloids, one is not so much interested in the form of the structure factor but instead treats it as a correction of the scattering for the finite concentration of the sample. In such cases a range of weight concentrations c is prepared and each sample measured over a range of q . The scattered intensity at low q and low ρ can be approximated as:

$$\frac{K\rho}{I(q)} \approx \left(1 + \frac{1}{3}R_g^2q^2\right)(1 + 2B_2\rho). \quad (4.30)$$

Zimm has proposed a method to perform the double extrapolation in a so-called Zimm-plot, and thus to obtain the radius of gyration and the second virial coefficient from the slopes. Since $\rho = cN_{av}/M$ the molecular weight M can be determined from the intercept provided all the constants in the factor K are correctly accounted for.

4.5. Scattering by crystals

As a special case we consider the structure factor of a crystalline array of particles. This is usually called diffraction. You may recognize the equations that we shall derive from the theory of X-rays diffraction by molecular crystals. In the previous paragraph we have seen that the peaks in the structure factor become sharper when the particles are forced to occupy a smaller volume. This reflects the tendency of the particles to order in order to use space more efficiently. It is therefore not hard to imagine that when the system starts to develop periodic order the structure factor peaks become very high and narrow, while it is zero in between the peaks. Of course, this transition cannot be truly continuous because a first order phase transition takes place during the process. The peaks in the structure factor are the Bragg spots that appear in the diffraction pattern. Two examples are shown in Figure 4.8: one made with light scattering, the other with small-angle x-ray diffraction.

By definition a crystal has translational symmetry along three independent axes. The basis vectors describing these translations are denoted \mathbf{a}_1 , \mathbf{a}_2 , and \mathbf{a}_3 . Together they define the unit cell, which when translated makes up the whole crystal. We will assume that the crystal

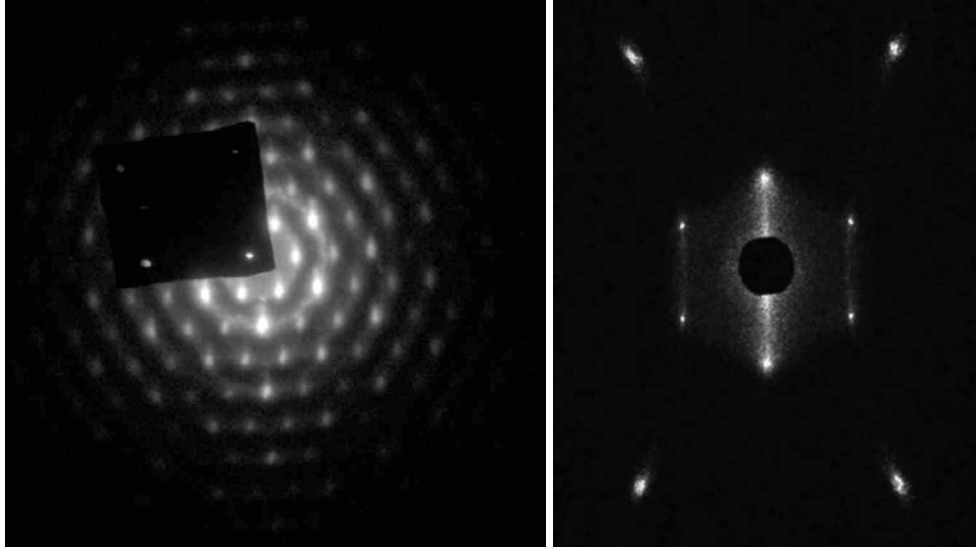


Figure 4.8. Diffraction patterns from colloidal crystals. (Left) Small-angle x-ray diffraction on an fcc crystal of silica spheres in water, (Right) Laser light diffraction on a body-centered tetragonal crystal of silica spheres in a water/DMSO mixture. The black square and circle are beam stops that block the transmitted beam.

is finite, extending a number of M_1 , M_2 , and M_3 unit cells along the three basis vectors, respectively. It therefore has the shape of a parallelepiped. Since each unit cell is identical we can write the location of a particle i sitting at position \mathbf{R}_p relative to the origin of a unit cell as $\mathbf{r}_i = \mathbf{R}_p + m_1\mathbf{a}_1 + m_2\mathbf{a}_2 + m_3\mathbf{a}_3$, with the m 's integer numbers. For simplicity, we will again assume that all particles are identical, but it is easy to generalize to unit cells with more than one particle. Expression (4.27) tells us to take the sum of $\exp(-i\mathbf{q}\cdot\mathbf{r}_i)$ over all particles, and then multiply the result by its complex conjugate and divide it by the total number of particles. So, first we write down the sum, as follows:

$$\sum_{i=1}^N e^{-i\mathbf{q}\cdot\mathbf{r}_i} = \sum_{p=1}^n e^{-i\mathbf{q}\cdot\mathbf{R}_p} \sum_{m_1=0}^{M_1-1} e^{-im_1\mathbf{q}\cdot\mathbf{a}_1} \sum_{m_2=0}^{M_2-1} e^{-im_2\mathbf{q}\cdot\mathbf{a}_2} \sum_{m_3=0}^{M_3-1} e^{-im_3\mathbf{q}\cdot\mathbf{a}_3} \quad (4.31)$$

The sum over p runs over all the n particles in a single unit cell. The other sums run over all the unit cells. So the total number of particles is $nM_1M_2M_3$. Notice that each of the sums over the m 's have the form of a geometric progression

$$\sum_{m=0}^{M-1} x^m = \frac{1-x^M}{1-x}.$$

where x is of the form $\exp(-i\mathbf{q}\cdot\mathbf{a})$. We might as well multiply this by its complex conjugate at once. The result is

$$\frac{1-\exp(-iM\mathbf{q}\cdot\mathbf{a})}{1-\exp(-i\mathbf{q}\cdot\mathbf{a})} \cdot \frac{1-\exp(iM\mathbf{q}\cdot\mathbf{a})}{1-\exp(i\mathbf{q}\cdot\mathbf{a})} = \frac{2-2\cos(M\mathbf{q}\cdot\mathbf{a})}{2-2\cos(\mathbf{q}\cdot\mathbf{a})} = \frac{\sin^2(\frac{1}{2}M\mathbf{q}\cdot\mathbf{a})}{\sin^2(\frac{1}{2}\mathbf{q}\cdot\mathbf{a})}$$

We do this for all the factors so that

$$S(\mathbf{q}) = \frac{1}{M_1M_2M_3} F(\mathbf{q}) \frac{\sin^2(\frac{1}{2}M_1\mathbf{q}\cdot\mathbf{a}_1)}{\sin^2(\frac{1}{2}\mathbf{q}\cdot\mathbf{a}_1)} \frac{\sin^2(\frac{1}{2}M_2\mathbf{q}\cdot\mathbf{a}_2)}{\sin^2(\frac{1}{2}\mathbf{q}\cdot\mathbf{a}_2)} \frac{\sin^2(\frac{1}{2}M_3\mathbf{q}\cdot\mathbf{a}_3)}{\sin^2(\frac{1}{2}\mathbf{q}\cdot\mathbf{a}_3)} \quad (4.32)$$

with

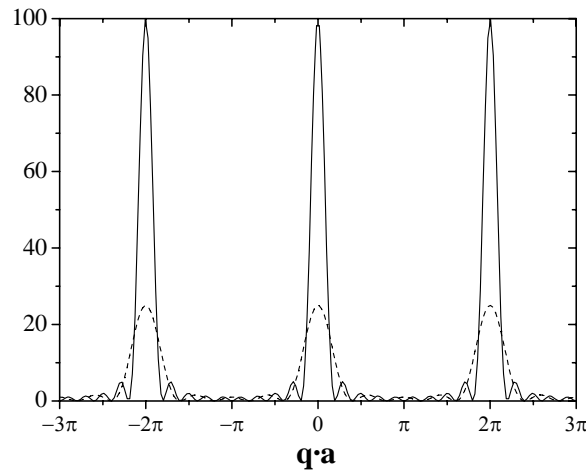


Figure 4.9. The function $\sin^2(\frac{1}{2}M\mathbf{q} \cdot \mathbf{a}) / \sin^2(\frac{1}{2}\mathbf{q} \cdot \mathbf{a})$ for $M=5$ (dashed) and $M=10$ (solid).

$$F(\mathbf{q}) = \frac{1}{n} \left| \sum_{p=1}^n e^{-i\mathbf{q} \cdot \mathbf{R}_p} \right|^2 \quad (4.33)$$

Note that the function $F(\mathbf{q})$ is just the structure factor of the unit cell⁶.

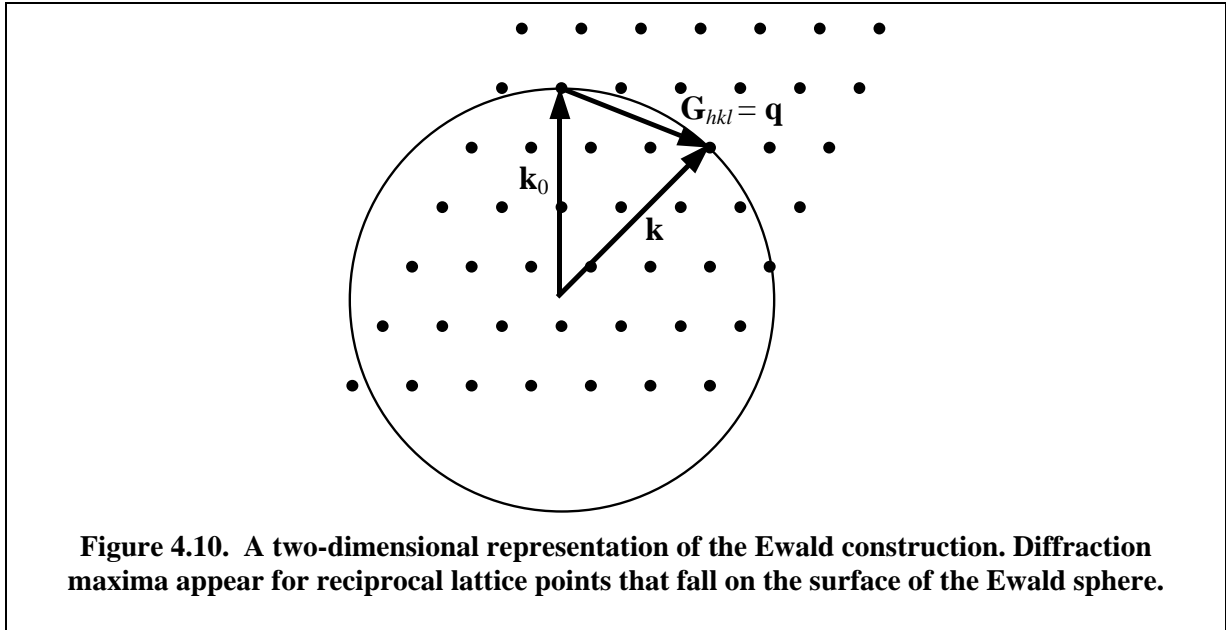
Let us interpret this result by first taking a look at the function $\sin^2(\frac{1}{2}Mx) / \sin^2(\frac{1}{2}x)$. It is plotted in Figure 4.9 for $M=5$ and $M=10$. It is seen that this function is sharply peaked around x values of an integer times 2π . The height of the peaks is M^2 and their width is $2\pi/M$. This means that for a crystal with more than a few unit cells the scattered intensity is always zero except for those values of \mathbf{q} which satisfy the following conditions simultaneously:

$$\begin{aligned} \mathbf{q} \cdot \mathbf{a}_1 &= 2\pi h \\ \mathbf{q} \cdot \mathbf{a}_2 &= 2\pi k \\ \mathbf{q} \cdot \mathbf{a}_3 &= 2\pi l \end{aligned} \quad (4.34)$$

Here h , k , and l must be integers. These equations are called the *Laue equations*. They are equivalent to the Bragg law, which we will show later. For a given crystal with basis vectors \mathbf{a}_i they determine the angles where diffraction is observed. The physical basis for this result is that because all unit cells scatter equivalently they must all scatter in phase if there is to be diffraction. Otherwise, even the smallest phase difference will cause complete cancellation of the wave sum, due to the large number of cells. “Fortuitous” constructive interference only occurs at very special angles, which are characteristic for the crystal. This of course forms the basis for structure identification in crystallography. For small crystallites some light also ends up in a small angular range around the peaks, so that the width of the peaks can sometimes be used to estimate the size of the crystals.

We now understand why only particular diffraction peaks are seen in crystals. But note that equation (4.32) also contains the factor $F(\mathbf{q})$, describing interference between the particles within the unit cell. If this cell contains only a single particle then it is equal to unity.

⁶ In the crystallography literature it is the complex function $\sum_{p=1}^n f_p \exp(-i\mathbf{q} \cdot \mathbf{R}_p)$ that is called the structure factor. But in expressions for the diffracted intensity only its modulus squared appears.



But if it contains two or more particles then F determines the relative strengths of the diffraction peaks. It could even equal zero at a \mathbf{q} value which otherwise satisfies (4.34). In this case a diffraction, which is allowed by the periodicity of the lattice, disappears because it is not allowed by the symmetry of the unit cell. One speaks of *systematic vanishings*. It may seem unlikely that the few \mathbf{q} values allowed by (4.34) would happen to coincide exactly with a zero in $F(\mathbf{q})$, but it is in fact a common occurrence in many lattice types, as we will demonstrate shortly in the example of a face centered cubic lattice. Systematic vanishings are an important aid for crystallographers in recognizing the lattice type.

From crystallography we know that with every crystal lattice we can associate a *reciprocal lattice*. The basis vectors of the reciprocal lattice are cunningly defined as⁷

$$\mathbf{b}_1 = 2\pi \frac{\mathbf{a}_2 \times \mathbf{a}_3}{\mathbf{a}_1 \cdot \mathbf{a}_2 \times \mathbf{a}_3}, \quad \mathbf{b}_2 = 2\pi \frac{\mathbf{a}_3 \times \mathbf{a}_1}{\mathbf{a}_1 \cdot \mathbf{a}_2 \times \mathbf{a}_3}, \quad \mathbf{b}_3 = 2\pi \frac{\mathbf{a}_1 \times \mathbf{a}_2}{\mathbf{a}_1 \cdot \mathbf{a}_2 \times \mathbf{a}_3}, \quad (4.35)$$

so that we have

$$\mathbf{a}_i \cdot \mathbf{b}_j = 2\pi \delta_{ij}. \quad (4.36)$$

In other words, the each reciprocal lattice vectors is orthogonal to two of the basis vectors of the direct lattice. Every vector in reciprocal space, such as the \mathbf{q} belonging to a particular diffraction peak, can now be represented by the linear combination

$$\mathbf{q} = p_1 \mathbf{b}_1 + p_2 \mathbf{b}_2 + p_3 \mathbf{b}_3.$$

The p 's are the components of \mathbf{q} along the three axes. By virtue of (4.36) they can be determined by taking the dot product with the basis vectors of the real lattice, for example

$$\mathbf{q} \cdot \mathbf{a}_1 = 2\pi p_1.$$

Comparing this with the Laue conditions we see that for diffraction to occur we must have $p_1 = h$, and similarly for p_2 and p_3 . Thus, we find that

$$\mathbf{q} = h\mathbf{b}_1 + k\mathbf{b}_2 + l\mathbf{b}_3 \equiv \mathbf{G}_{hkl}. \quad (4.37)$$

The integers hkl are called the *Miller indices* belonging to the particular diffraction. Every reciprocal lattice point is labeled by a set of Miller indices. Thus, equation (4.37) tells us that the scattering vector \mathbf{q} must precisely coincide with a reciprocal lattice vector \mathbf{G} . This is the

⁷ Contrary to what is common practice in solid state physics most crystallographers define the reciprocal lattice vectors without the factor 2π .

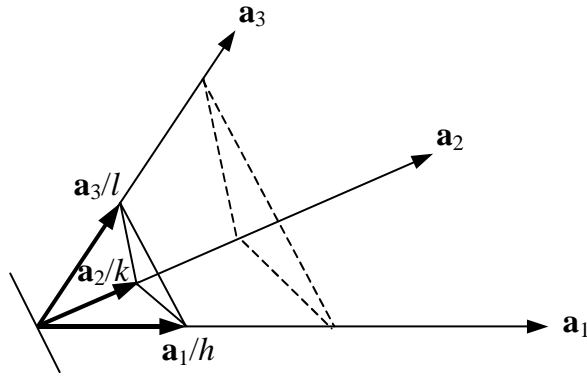


Figure 4.11. Real space representation of the crystallographic planes hkl .

basis for the *Ewald construction* (see Figure 4.10), which says that if we place the incident wave vector \mathbf{k}_0 with its head pointing at the origin of reciprocal space and draw a sphere around it, then diffracted waves \mathbf{k} occur wherever this sphere intersects with a reciprocal lattice point. By rotating the crystal with respect to the incident beam we can scan (a part of) reciprocal space in search of diffractions.

The real space interpretation of the Miller indices is that of a set of parallel equidistant planes, one of which passes through the origin, and the next nearest intercepts the \mathbf{a}_1 axis at a_1/h , the \mathbf{a}_2 axis at a_2/k , and the \mathbf{a}_3 axis at a_3/l (see Figure 4.11). These planes are perpendicular to \mathbf{G}_{hkl} , because so are two independent vectors in the planes: $\mathbf{a}_1/h - \mathbf{a}_2/k$ and $\mathbf{a}_2/k - \mathbf{a}_3/l$. (To see this, take the dot product of each of these vectors with \mathbf{G}_{hkl} as given by (4.37)). A normal vector to the lattice planes is then $\mathbf{G}_{hkl} / |\mathbf{G}_{hkl}|$. The distance between two planes of the set d_{hkl} can thus be found from

$$d_{hkl} = \frac{\mathbf{a}_1 \cdot \mathbf{G}_{hkl}}{h |\mathbf{G}_{hkl}|} = \frac{2\pi}{|\mathbf{G}_{hkl}|}. \quad (4.38)$$

Using this result in (4.37) and (4.14) we finally obtain the familiar Bragg law:

$$2d_{hkl} \sin(\theta/2) = \lambda. \quad (4.39)$$

The factor $1/2$ in the sine probably appears unfamiliar, but that is only because crystallographers define their scattering angle as 2θ instead of θ .

We conclude this section with an example: diffraction by a face centered cubic (*fcc*) lattice. This type of lattice is common in colloidal crystals. The unit cell contains 4 particles. The basis vectors of this cubic lattice are simply

$$\mathbf{a}_1 = a\hat{\mathbf{x}}, \quad \mathbf{a}_2 = a\hat{\mathbf{y}}, \quad \mathbf{a}_3 = a\hat{\mathbf{z}}. \quad (4.40)$$

Using (4.35) the reciprocal lattice vectors are found to be

$$\mathbf{b}_1 = \frac{2\pi}{a}\hat{\mathbf{x}}, \quad \mathbf{b}_2 = \frac{2\pi}{a}\hat{\mathbf{y}}, \quad \mathbf{b}_3 = \frac{2\pi}{a}\hat{\mathbf{z}}. \quad (4.41)$$

The diffraction condition (4.37) tells us that diffraction peaks may be expected at scattering vectors \mathbf{q} that are linear combinations of integer multiples of these three vectors. The corresponding diffraction angles can be found by taking the modulus squared on both sides of (4.37), and using (4.14) and (4.41):

$$\left(\frac{2 \sin(\theta/2)}{\lambda} \right)^2 = \frac{h^2 + k^2 + l^2}{a^2}. \quad (4.42)$$

So we may expect a large number of diffraction peaks. But it turns out that many of them are missing due to systematic vanishings. This can be seen by calculating the structure factor using Eq. (4.33). The position of a particle in its unit cell can be written as $\mathbf{R} = x\mathbf{a}_1 + y\mathbf{a}_2 + z\mathbf{a}_3$, and \mathbf{q} is given by the diffraction condition (4.37). Then for a diffraction hkl we have

$$\mathbf{q} \cdot \mathbf{R} = 2\pi(hx + ky + lz). \quad (4.43)$$

If one particle is located at $(x,y,z)=(0,0,0)$ then other particles are present at $(\frac{1}{2},\frac{1}{2},0)$, $(\frac{1}{2},0,\frac{1}{2})$ and $(0,\frac{1}{2},\frac{1}{2})$. The structure factor (4.33) is then

$$\begin{aligned} F(\mathbf{q}) &= \frac{1}{4} \left| 1 + e^{-i\pi(k+l)} + e^{-i\pi(h+l)} + e^{-i\pi(h+k)} \right|^2 \\ &= \frac{1}{4} \left(1 + (-1)^{k+l} + (-1)^{h+l} + (-1)^{h+k} \right)^2 \\ &= \begin{cases} 4 & hkl \text{ all even or all odd} \\ 0 & \text{otherwise} \end{cases} \end{aligned} \quad (4.44)$$

We see that not all combinations of hkl give rise to diffraction. Hence, the *fcc* lattice can be recognized by the fact that all diffractions with one odd or one even Miller index vanish systematically. If we are dealing with an unknown crystal we list $(2\sin(\theta/2)/\lambda)^2$ of the various diffractions and look for a common divisor $(1/a)$ that produces small integers. These integers equal $h^2 + k^2 + l^2$ if the crystal is cubic. The missing hkl values tell us whether the structure is really *fcc*⁸.

The reason for the fact that systematic vanishings are not so unlikely at all is seen to lie in the special position of the particles within the unit cell. In fact, only unit cells with special positions of the particles can be repeated periodically to fill all space. These crystal lattices are called the *Bravais lattices*, and there exist only 14 of them.

4.6. Dynamic light scattering

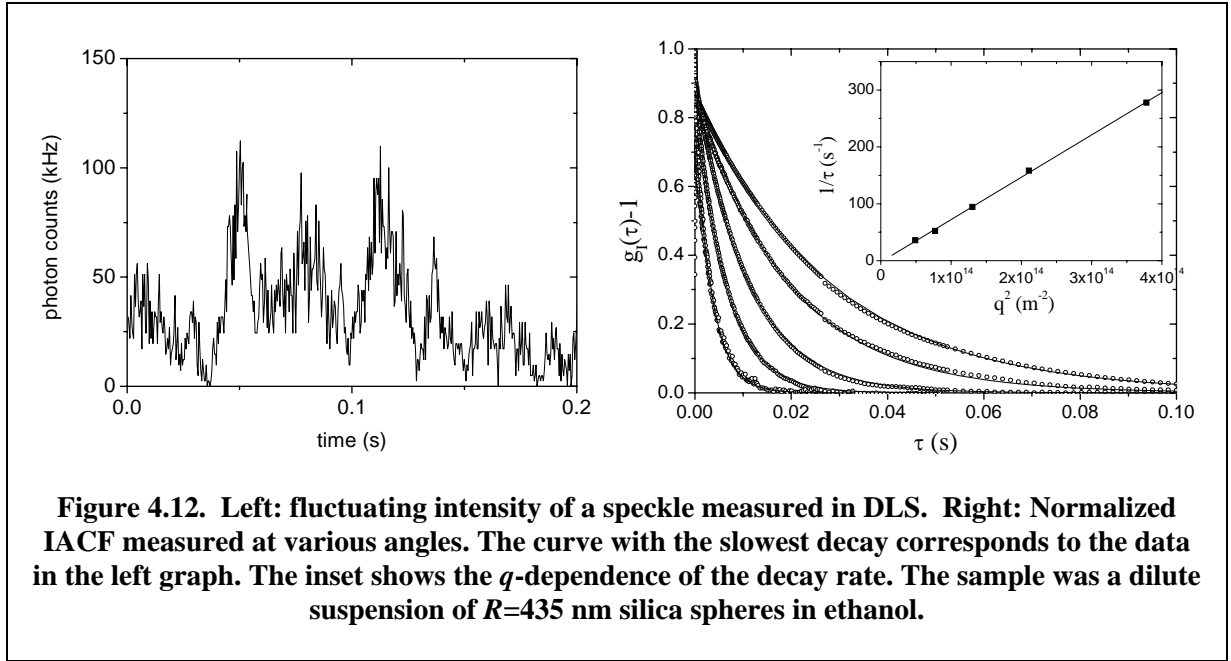
In the previous sections it was mentioned in passing that the particles in soft matter systems are in constant thermal motion (*Brownian motion*). In principle this may be expected to lead to fluctuations in the scattered intensity. In *dynamic light scattering* (DLS)⁹ these fluctuations are measured. This provides information on the dynamics of particles in solution. In dilute suspensions DLS has become a standard technique for the characterization of particle size and polydispersity. Also, the dynamics of internal degrees of freedom can be studied, such as chain fluctuations in polymers and shape fluctuations of microemulsion droplets. When applied to concentrated suspensions DLS provides information on the length and time scale dependent dynamics of particles.

4.6.1. Fluctuations in the scattered intensity

In static light scattering a wide beam is used (typically a few mm) which illuminates very many particles. This leads to the ensemble average in Eqs. (4.26) and (4.27). Since the structure factor describes interference of waves scattered by different particles and these particles are constantly moving it is clear that there must also be fluctuations in the scattered intensity. In dynamic light scattering a much smaller beam of coherent radiation is used: about 0.1 mm, but still containing many particles. The fluctuations are then readily

⁸ In crystallography comparing the relative intensities of the diffraction peaks with their calculated values must then further validate the proposed structure.

⁹ Other names are Photon Correlation Spectroscopy (PCS) and Quasi-Elastic Light Scattering (QELS).



visible to the naked eye: If we use a white screen as the detector we see a field containing many bright spots in a dark background. This is known as (*laser*) *speckle*. The origin of the speckle pattern can be understood as follows: Each particle scatters a spherical wave toward the screen with a phase that depends sensitively on its position, shape, and orientation. At each point on the screen the intensity is determined by the sum of all these scattered waves:

$$E_s(t) = \sum_{j=1}^N f_j(\mathbf{q}, t) \exp(-i\mathbf{q} \cdot \mathbf{r}_j(t)) \quad (4.45)$$

At some points the waves happen to cancel each other, while at others they reinforce each other. Particles only need to move over about one wavelength to let individual speckles blink on and off. The idea of dynamic light scattering is now to measure the (average) rate at which the speckles blink, and relate this to the rate with which particles change their relative positions. This is done by making the detector also very small, by placing a pinhole in front of it, such that it collects light in only a single speckle.

The angular size (in radians) of a speckle is determined only by the ratio of the wavelength and the apparent diameter $d \sin \theta$ of the scattering volume as seen by the detector:

$$\Delta\theta_{\text{speckle}} \approx \frac{\lambda}{d_{\text{app}}} = \frac{\lambda}{d \sin \theta} \quad (4.46)$$

This is the same as the width of the primary diffraction maximum of a slit. For wavelengths in the visible and a scattering volume of 0.5 mm this is $\sim 10^{-3}$ rad, or 0.05° . With a detector placed at a distance of 20 cm the pinhole size should be about 200 μm . Incidentally, we now see that the fact that fluctuations are small in static light scattering lies not in the larger number of illuminated particles, but in the larger number of (very small) speckles collected by the detector. In SLS we can therefore also get away with using an incoherent light source (though monochromatic). In fact, this even improves the speckle averaging. In DLS the use of a coherent light source is required.

Mathematical functions that are used for studying fluctuating quantities are so-called correlation functions. In the case of DLS we measure the *intensity autocorrelation function*, or IACF:

$$g_I(\mathbf{q}, \tau) = \langle I(\mathbf{q}, t) I(\mathbf{q}, t + \tau) \rangle \quad (4.47)$$

This means that the intensity measured at a fixed time t is multiplied with the intensity measured a time τ later. This is repeated for a large number of speckles and averaged to form the ensemble average, as indicated by the angled brackets. In practice, of course, instead of moving the detector to a different speckle a great number of times (while keeping \mathbf{q} almost constant!), we prefer to keep the detector fixed and to take a time average¹⁰. The measurement in Figure 4.12 illustrates how this works. The intensity looks completely random, but there is a characteristic time scale associated with the fluctuations: The intensity never jumps from a maximum to a minimum in an instant, but this takes a finite amount of time. At very short times τ , when the particles have not had enough time to move much, the intensity is unchanged, so that $g_I(0) = \langle I^2 \rangle$. After a somewhat longer time the particles have moved enough to let the intensity change and the IACF begins to decay. After a sufficiently long time a speckle's intensity has changed so much that it has become completely uncorrelated with its initial value. The average of the product in (4.47) is then equal to the product of the averages, making $g(\tau \rightarrow \infty) = \langle I \rangle^2$. It is clear that $\langle I^2 \rangle \geq \langle I \rangle^2$. In fact, if only a single speckle is measured it can be shown that $\langle I^2 \rangle = 2\langle I \rangle^2$. In other words, after one correlation time the speckle has become a different speckle. The ensemble average is obtained by measuring during a time interval equal to many times ($>10^4$) this correlation time.

4.6.2. Brownian diffusion

Fluctuations in the scattered light are primarily caused by random displacements of the particles resulting from the constant bombardment by solvent molecules, known as Brownian motion (but in general also by rotations or shape fluctuations). We will now make a short detour and derive a few results to describe Brownian displacements, which we need to calculate the IACF. We will follow the ingenious and simple argument used by Einstein (1905).

Consider an equilibrium system of non-interacting particles suspended in a liquid. A steady external force \mathbf{K} derivable from a potential $\Phi(\mathbf{r})$ acts on the particles and drives them to an impermeable boundary. (Think of the force of gravity driving the particle to the bottom of the container.) The velocity imparted to the particles by this force will be \mathbf{K}/γ where γ is called the friction factor. Random movements due to thermal agitation drive the particles away from the boundary. In this state of thermal equilibrium the probability density for the position of the particles is given by the Boltzmann distribution as

$$P(\mathbf{r}) = P_0 \exp(-\Phi/kT), \quad (4.48)$$

where P_0 is a normalization constant. In equilibrium the particle flux caused by the external force, $P\mathbf{K}/\gamma$, must be balanced by the flux due to Brownian diffusion at every position in the system:

$$-(P/\gamma)\nabla\Phi - D_0\nabla P = 0. \quad (4.49)$$

Substitution of (4.48) then shows that the diffusion coefficient must have the value

$$D_0 = \frac{kT}{\gamma}, \quad (4.50)$$

¹⁰ This assumes that the system is ergodic, so that time averages and ensemble averages are equal. For nonergodic systems we have no choice but to measure different speckles, although tricks exist to make this process more efficient.

which is known as the Einstein relation. For spherical objects the hydrodynamic friction factor γ was calculated by Stokes:

$$D_0 = \frac{kT}{6\pi\eta a}. \quad (4.51)$$

Here η is the shear viscosity of the solvent.

It is interesting to note that the particle flux caused by Brownian motion is the same as if a steady force acted on the particles opposite to the external force. In view of (4.49) this so-called Brownian, or thermodynamic, force is equal to

$$\mathbf{F}_{\text{Br}} = -kT\nabla \ln P \quad (4.52)$$

This does not mean, of course, that the collisions of solvent molecules really cause the exertion of a steady force on the particle. It just means that when the probability density is non-uniform the mean Brownian displacement is such as to cause a diffusive flux equal to that caused by a steady external force \mathbf{F}_{Br} .

The above arguments are equally valid for particles on which no external force is acting. If a suspension is non-uniform initially then the only particle flux is the diffusive flux $\mathbf{J} = -D\nabla P$. Particle conservation demands that its divergence must be equal to the (negative) rate of change of the local density, as expressed by the continuity equation

$$\frac{\partial P}{\partial t} = -\nabla \cdot \mathbf{J}. \quad (4.53)$$

Combining this with the diffusive flux results in the diffusion equation

$$\frac{\partial P}{\partial t} = D_0 \nabla^2 P. \quad (4.54)$$

In one of the problems you will be asked to solve this equation subject to the initial condition that the particles all start diffusing from the origin. (It would be wise, however, not to attempt this until after reading the next paragraph.) An important and characteristic property of the solution is that the mean-square displacement of the particles increases linearly with time:

$$\langle \Delta r^2 \rangle = 6D_0 t. \quad (4.55)$$

4.6.3. Dilute suspensions

We will now make the discussion a little more precise and derive the form of the IACF for a suspension of independent, but identical particles. Particles are independent if they do not interact with each other. This is the case if a suspension is sufficiently dilute. We will also assume that the particles have orientational degrees of freedom. If (4.45) is then substituted in (4.47) we get

$$g_I(\tau) = \left\langle f^4 \sum_{j,k,l,m=1}^N \exp\left(-i\mathbf{q} \cdot [\mathbf{r}_j(0) - \mathbf{r}_k(0) - \mathbf{r}_l(\tau) + \mathbf{r}_m(\tau)]\right) \right\rangle. \quad (4.56)$$

When particles are independent the average of a product is equal to the product of the averages. So, if only one of the numbers $ijklm$ is different from any of the others the IACF will contain a factor of the form $\langle \exp(-i\mathbf{q} \cdot \mathbf{r}_j(\tau)) \rangle$. This average is zero, since the particles are distributed randomly so that the phase is a random quantity (except in the uninteresting case $\mathbf{q}=\mathbf{0}$). As a result, only three kinds of terms survive: (i) N^2 terms for which $j=k, l=m$, (ii) N^2-N terms for which $j=m, k=l, j \neq k$, and (iii) N^2-N terms for which $j=l, k=m, j \neq k$. In case (i) the terms equal unity. Terms of type (ii) give

$$\left\langle \exp(i\mathbf{q} \cdot [\mathbf{r}_j(\tau) + \mathbf{r}_j(0)]) \right\rangle \left\langle \exp(-i\mathbf{q} \cdot [\mathbf{r}_k(\tau) + \mathbf{r}_k(0)]) \right\rangle.$$

Both these averages are zero for the same reason as before: their phase depends on the absolute position of the particle, which is random. Finally, terms of type (iii) give

$$\left\langle \exp(i\mathbf{q} \cdot [\mathbf{r}_j(\tau) - \mathbf{r}_j(0)]) \right\rangle \left\langle \exp(-i\mathbf{q} \cdot [\mathbf{r}_k(\tau) - \mathbf{r}_k(0)]) \right\rangle.$$

These terms are *not* zero, because they depend on particle *displacements*, which are small for small τ and large for large τ . Taking these things together we obtain

$$g_I(\tau) = N^2 f^4 + (N^2 - N) f^4 \left\langle \exp(i\mathbf{q} \cdot \Delta\mathbf{r}_j(\tau)) \right\rangle^2,$$

where $\Delta\mathbf{r}_j(\tau) = \mathbf{r}_j(\tau) - \mathbf{r}_j(0)$. Because $\langle I \rangle = Nf^2$ and $N^2 \gg N$ we finally get for the IACF:

$$g_I(\tau) = \langle I \rangle^2 \left[1 + \left\langle \exp(i\mathbf{q} \cdot \Delta\mathbf{r}_j(\tau)) \right\rangle^2 \right]. \quad (4.57)$$

We now need to evaluate the ensemble average in (4.57) for particles in Brownian motion. Let $P(\Delta\mathbf{r}, t)$ be the probability of finding that a given particle has undergone a displacement $\Delta\mathbf{r}$ in a time t . The equation of motion for this process is the diffusion equation (4.54) with the initial condition that the particle has not moved at time $t = 0$:

$$\begin{cases} \frac{\partial P(\Delta\mathbf{r}, t)}{\partial t} = D_0 \nabla^2 P(\Delta\mathbf{r}, t) \\ P(\Delta\mathbf{r}, t = 0) = \delta(\Delta\mathbf{r}) \end{cases} \quad (4.58)$$

We first recognize that the average we want to calculate is

$$\left\langle \exp(-i\mathbf{q} \cdot \Delta\mathbf{r}) \right\rangle = \int P(\Delta\mathbf{r}, t) \exp(-i\mathbf{q} \cdot \Delta\mathbf{r}) d(\Delta\mathbf{r}).$$

But this is just the Fourier transform of P with respect to $\Delta\mathbf{r}$. Thus, we Fourier transform Eq. (4.58), giving

$$\begin{cases} \frac{\partial P(\mathbf{q}, t)}{\partial t} = -q^2 D_0 P(\mathbf{q}, t) \\ P(\mathbf{q}, t = 0) = 1 \end{cases},$$

with the simple solution

$$P(\mathbf{q}, t) = \exp(-q^2 D_0 t).$$

Substitution into Eq. (4.57) then yields the result

$$g_I(\tau) = \langle I \rangle^2 \left[1 + \exp(-2q^2 D_0 t) \right]. \quad (4.59)$$

This result tells us that the IACF of particles in (independent) Brownian motion is an exponential with a characteristic time $1/2q^2 D_0$. This is the behavior seen in the experiment of Figure 4.12. The IACF will decay faster if the particles diffuse faster, as expected. There is also a strong q -dependence (slow decay at small angles). This is because q^{-1} can be seen as the distance over which particles need to diffuse in order to cause the IACF to decay. Since in a diffusion process mean-square displacements are proportional to time this leads to a q^{-2} dependence.

Equation (4.59) is often used to measure the diffusion coefficient of particles in a dilute solution. This value is then related to an (average) particle radius, using (4.51). The radius obtained from this equation is usually called the *hydrodynamic radius*, because it is the hydrodynamic friction on the sphere that determines its diffusion coefficient. If a layer of solvent close to the particle is entrained the hydrodynamic radius may be somewhat larger than the actual radius. This can be significant if the particles are rough, or if they contain a stabilizing coating of long polymer molecules. Non-spherical particles have of course a more complicated relation between D_0 and R . Results have been derived for different geometric shapes.

An important application of DLS is the measurement of the particle size distribution of polydisperse suspensions. In essence, the decay of the IACF becomes multi-exponential due to the presence of particle with different sizes. It can be inverted using numerical methods to obtain the size distribution, which is used routinely on all commercial instruments.

4.6.4. Concentrated suspensions

In concentrated suspensions the particles are no longer independent and the average in Eq. (4.56) cannot be factorized so easily. Nevertheless, it is possible to derive some general results. We will state the most important results and refer to the literature cited at the end of this chapter for details and derivations. It can be shown that under certain general assumptions the *Siegert relation* is valid:

$$g_I(\tau) = \langle I \rangle^2 + |g_E(\tau)|^2, \quad (4.60)$$

where the electric field autocorrelation function (EACF) g_E is defined by

$$g_E(\tau) = \langle E_s(t) E_s^*(t+\tau) \rangle. \quad (4.61)$$

The assumptions are that (i) the scattering volume contains a large number of particles, (ii) the scattering volume is much larger than the range over which the particles are correlated, and (iii) the system is ergodic. For most systems these assumptions are easily satisfied¹¹. By inserting Eq. (4.45) it is seen that

$$g_E(\tau) = \langle I \rangle \left\langle \frac{1}{N} \sum_{j,k=1}^N \exp(i\mathbf{q} \cdot [\mathbf{r}_j(0) - \mathbf{r}_k(\tau)]) \right\rangle. \quad (4.62)$$

The factor between angled brackets is called the *dynamic structure factor* (or intermediate scattering function). Notice that it equals the (static) structure factor, Eq. (4.27), at $\tau = 0$. Also notice that for independent particles the only nonzero terms are those with $j=k$, so that we obtain (4.57) again.

The analysis of the measured IACF is much more complicated than in the dilute case. Particle correlations affect both the decay rate and the q -dependence of the IACF. This is described phenomenologically with an equation similar to (4.59) but with a q and t dependent *collective* diffusion coefficient D_c :

$$g_I(\tau) = \langle I \rangle^2 \left[1 + \exp(-2q^2 D_c(q,t)t) \right] \quad (4.63)$$

Note that this does *not* mean that the IACF still decays according to a single exponential. Also, there is no longer a pure q^{-2} dependence. How then should the collective diffusion coefficient be interpreted? Remember that thermal motion of particles constantly creates and dissipates small fluctuations in the particle number density. These fluctuations have a (Fourier) spectrum of wavelengths. The collective diffusion coefficient can be interpreted as describing the relaxation of a sinusoidal density wave with a wavelength $2\pi/q$. D_c is also time dependent because at short times particles move only a small distance relative to each other (much less than a particle diameter). But on longer time scales particles must increasingly ‘pass each other’ in order to make progress. Thus, the diffusion coefficient relevant to mean-square displacements at longer times is decreased.

¹¹ The electric field seen by the detector is then a Gaussian random variable.

As an illustration of these ideas we will conclude this section with a few examples, namely that of concentrated suspensions of spherical colloids. Figure 4.13 shows a number of dynamic structure factors (curves 1-3) of charged spheres measured at different q . It is clear that the decay is not single-exponential (curve 2), contrary to what is measured at low volume fractions (curve 4). However, in the limit of short times a single exponential can still describe the initial decay. The inverse of the ‘short-time’ diffusion coefficients assigned to the data in this way are also shown in Figure 4.13 together with the static structure factor. It is seen that the shape of the $1/D_c(q)$ -curve looks similar to that of the structure factor. Apparently, density fluctuations with a length scale similar to the mean interparticle spacing relax slowly (at short times). Diffusion on shorter and longer length scales is more rapid. Although DLS results from various kinds of soft matter can be quite different this same behavior is generally found: diffusion on length scales with strong particle ordering is slow and vice versa.

The collective diffusion coefficient tells us how particles move collectively to dissipate spontaneous density fluctuations. It can be much more insightful to consider the motion of individual particles in the suspension. This is described by the self-diffusion coefficient. It can be measured with DLS by adding a small number of strongly scattering ‘tracer’ particles to a suspension containing a large number of index-matched ‘host’ particles. Because the tracers are the only particles that scatter light the only nonzero terms in (4.62) are those for which j and k both refer to a tracer particle. Since the tracers are very small in number they behave independently (i.e. they almost never interact with each other). Thus, the averages of terms with $j \neq k$ separate into products, producing zero as before. Only terms with $j = k$ survive, and these lead to

$$g_E = \langle I \rangle \langle \exp(i\mathbf{q} \cdot \Delta\mathbf{r}(\tau)) \rangle. \quad (4.64)$$

Accordingly, we can write

$$g_I(\tau) = \langle I \rangle^2 \left[1 + \exp(-2q^2 D_s(t)) \right], \quad (4.65)$$

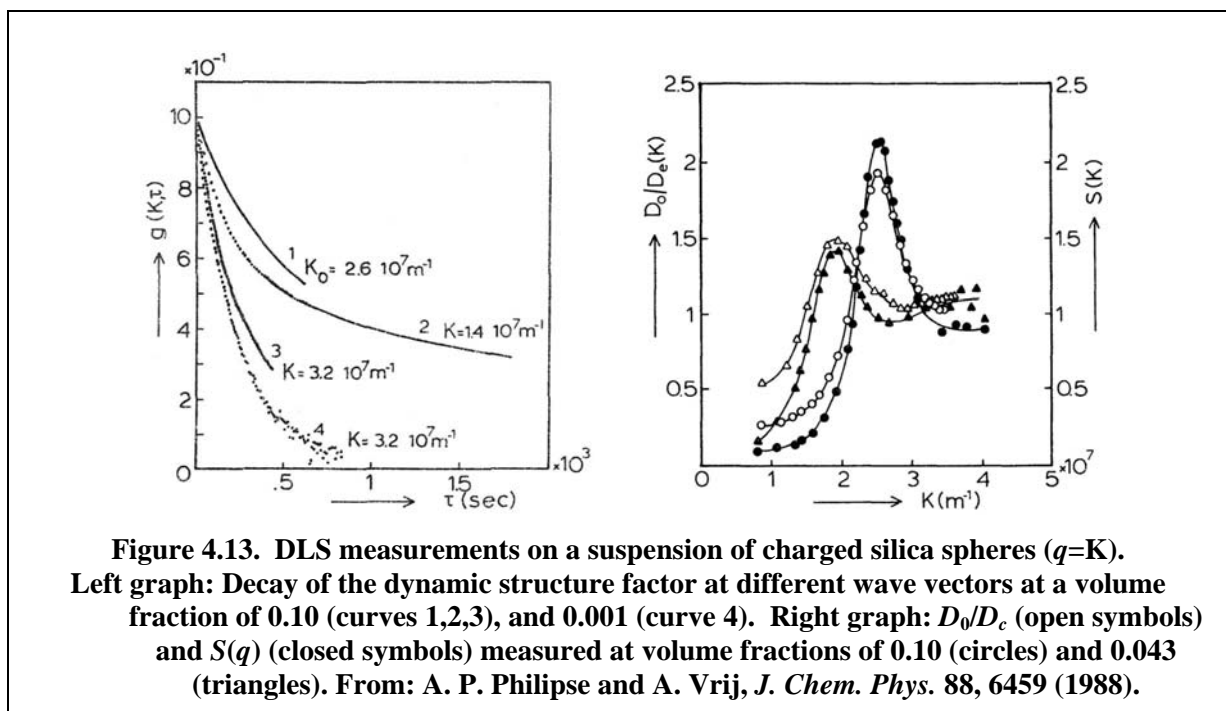
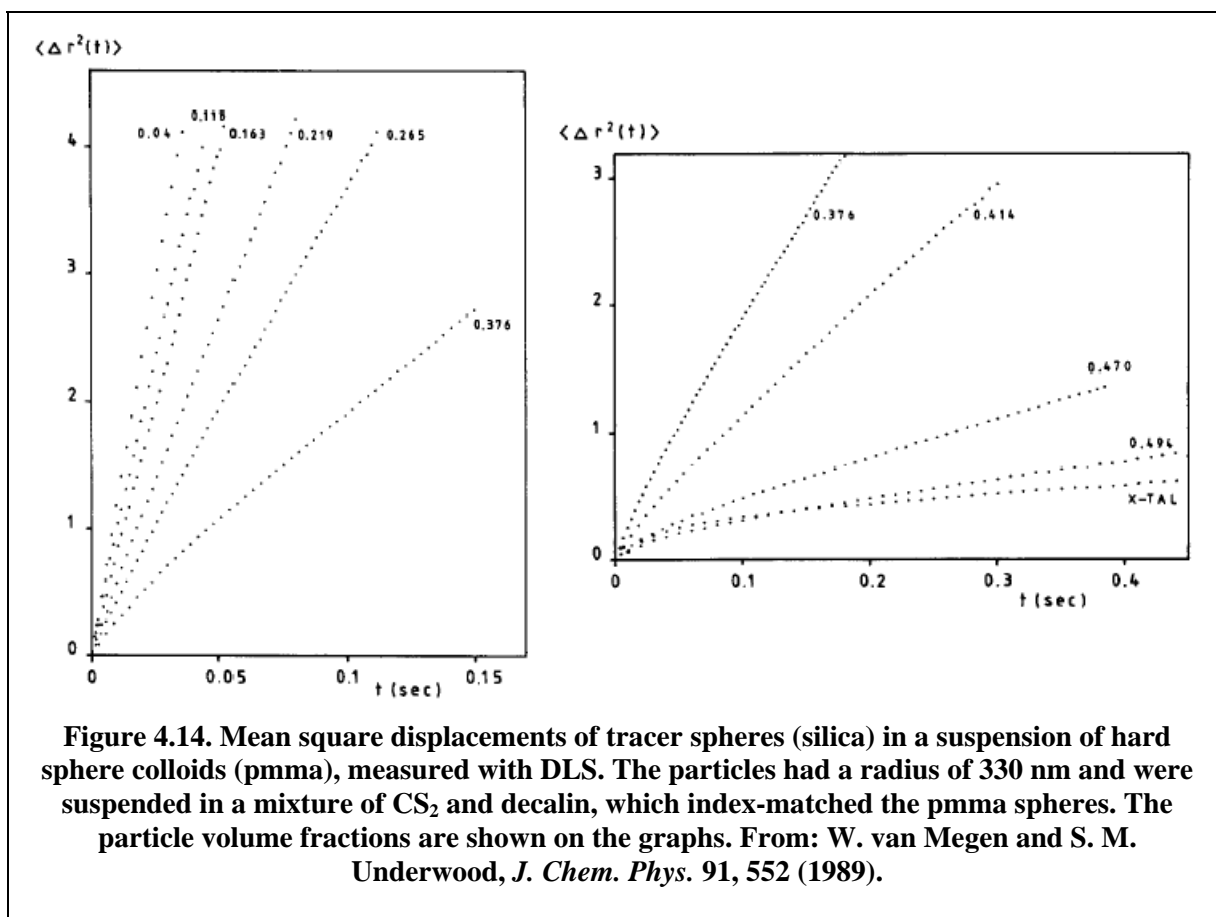


Figure 4.13. DLS measurements on a suspension of charged silica spheres ($q=K$).
Left graph: Decay of the dynamic structure factor at different wave vectors at a volume fraction of 0.10 (curves 1,2,3), and 0.001 (curve 4). Right graph: D_0/D_c (open symbols) and $S(q)$ (closed symbols) measured at volume fractions of 0.10 (circles) and 0.043 (triangles). From: A. P. Philipse and A. Vrij, *J. Chem. Phys.* 88, 6459 (1988).



where D_s is the *self-diffusion coefficient*. It does not depend on q because distances between the independent tracers do not play a role. D_s is time dependent, however, because the tracer particles do still feel their nonscattering neighbors. Some experimental results are shown in Figure 4.14 for concentrated suspensions of hard sphere colloids. They are presented in terms of mean square displacements (msd) as a function of time. It can be seen that at low volume fractions the msd increases linearly with time, as expected for normal diffusion. But at higher volume fractions there is a crossover from a short-time to a slower long-time regime. In the crossover regime the tracer particles start feeling the presence of their neighbors, which slow down their progress. On very long time scales these particle interactions have averaged out and the msd increases linearly with time again, but much more slowly. One therefore speaks of short-time and long-time self-diffusion coefficients, equal to one-sixth the slope of the msd.

In the experiments shown effort was taken to make the interactions between the tracer and host particles identical, so that it may be assumed that the motion of the tracers is identical to that of the host particles. This is not necessary, however. Similar experiments are performed in a wide variety of systems. For example, tracers can be added to polymer solutions, or attached to cell membranes. The dynamics of the tracers then provides information about the properties of the host material, such as the local viscosity or elasticity.

4.7. Scattering of other types of radiation

As mentioned before not only light can be used to obtain information on the structure of matter, but in principle type of information is obtained with other types of radiation. Of these, X-rays and neutrons are routinely used in the study of soft condensed matter and, indeed, in

the study of all kinds of condensed matter. We discuss some of the differences and advantages compared to light scattering.

4.7.1. X-rays

The wavelength of X-rays is typically on the order of 0.1 nm, which places us in the large q limit. Information on the structure of larger particles therefore appears at small angles, on the order of 1° . This application of X-rays is therefore called small-angle X-ray scattering, or SAXS. To reach such small angles the detector is placed at large distance from the sample, typically ~ 10 m. Smaller length scales such as polymer segments and intracellular structure are studied at wider angles (WAXS). Length scales that can therefore be probed with X-ray scattering range from 0.01 to 10^3 nm. Since the refractive index of most materials at these short wavelengths is very close to unity (to within 10^{-6} to 10^{-4}) multiple scattering is absent even in samples that strongly scatter light. Since X-rays are electromagnetic radiation they are scattered by charged particles, usually electrons. Because of their short wavelength the scattering strength is related not to the polarizability of bulk matter but to the scattering strength of an electron. For an individual electron which oscillates in the e.m. field the scattered intensity is again a dipole field (*Thomson scattering*):

$$I_s = I_0 \left(\frac{e^2}{4\pi\epsilon_0 m_e c^2 R} \right)^2 \frac{1 + \cos^2 \theta}{2}. \quad (4.66)$$

Here m_e and e are the electron mass and charge, and c the speed of light. To calculate scattering by larger objects such as atoms, polymer molecules or colloidal particles we sum the fields scattered by the electrons taking into account the proper phase differences, as explained before. It is clear that the resulting formulas will be completely analogous to those for visible light. Because heavy elements contain many more electrons than light elements scattering by the former dominates the measured intensity. This may make it difficult to measure light elements in a sample.

Classically, X-rays are produced in X-ray tubes, in which a metal foil is bombarded with electrons. The resulting X-rays have a well-defined wavelength and can be used to irradiate samples. Since X-rays are hard to focus and reflect from mirrors a collimated beam must be produced with a narrow slit. This seriously limits the available power. Stronger X-ray beams are available from modern synchrotrons in which magnetic bending or undulation of a relativistic electron beam produces an almost collimated beam containing a “white” spectrum of wavelengths (typically 0.05 to 0.2 nm). The extremely high irradiance makes it possible to study weakly scattering samples, even after monochromation and collimation. Worldwide a growing number of synchrotrons is available at national or international facilities. European synchrotrons with international access are in Grenoble (“European Synchrotron Radiation Facility”), Daresbury (“Daresbury Synchrotron Radiation Source”), Hamburg (“Hamburger Synchrotronstrahlungslabor”), Villigen (“Swiss Light Source”), and Aarhus (“Institute for Storage Ring Facilities”).

Although the X-rays produced in synchrotrons (like those from tubes) are incoherent the beams are so intense that a small pinhole can be placed in the beam to produce a nearly coherent source. In this way Dynamic X-ray Scattering (DXS) has become possible in recent years.

4.7.2. Neutrons

Neutrons interact with matter mainly through two types of interaction. The magnetic dipole of the neutron interacts with the magnetic field of unpaired electrons. Although this is very important in the study of magnetic materials it does not usually play a role in soft condensed matter systems. The other interaction is the strong nuclear interaction between the

neutron and the atomic nuclei. Despite the word “strong” the scattering cross sections of atoms (*i.e.* of their nuclei) are very small, so neutrons have a high penetrating power and multiple scattering is of no concern. Neutrons are produced in nuclear reactors. Some of the neutrons are needed to continue the nuclear fission process, while others need to be transported out. In reactors used for scientific research these neutrons are channeled into relatively well-collimated beams. Neutrons are described as a matter wave with De Broglie wave vector

$$k = \frac{1}{\hbar} \sqrt{2m_n E} . \quad (4.67)$$

E is the kinetic energy of the neutrons and \hbar Planck’s constant divided by 2π . This energy depends on the reactor and is often given in terms of the neutron temperature, as $E = \frac{3}{2} kT$. In many reactors the neutrons have undergone many collisions with the nuclei present in the moderator and will have “thermalized” upon leaving the reactor, so that their temperature is about 300 K. These neutrons have a wavelength of 0.2 nm. (By using a cooled moderator wavelengths of up to 2 nm are accessible.) This is the same order of magnitude as that of X-rays, so that neutron scattering provides information on the same length scales. Correspondingly, small angle neutron scattering is called SANS.

Since the strong interaction is very short range the atomic nuclei can be considered point scatterers for neutrons at room temperature or below. Thus the neutron waves scattered by each atomic nucleus has a form similar to the oscillating dipole in light and X-ray scattering. Scattering by larger objects follows by summing over all nuclei including the correct phase, just like before. The strength of scattering is expressed as a *scattering length*, which depends on the number of protons and neutrons in the nucleus, but not in a systematic way. This has the advantage that light elements may scatter as much as heavy elements. Even different isotopes of the same element may have completely different scattering lengths. Since the isotopes will be distributed randomly through the sample, and their nuclear spins normally have a random orientation, the scattered intensity contains an often-large background of so-called incoherent scattering. An important difference with electromagnetic scattering is that neutron scattering lengths for some elements, most notably ^1H , are *negative*. The analogous thing in light scattering would be to have a negative f_j in equation (4.25) for certain components of the sample. By mixing normal solvents with deuterated solvents (^2H has a positive scattering length) the scattering contribution from selected parts of the sample can be made to vanish while minimally affecting the chemical composition. This process is called *contrast variation* and is an important technique in neutron scattering. In light scattering contrast variation is only possible by replacing the solvent by one with a refractive index equal to that of the selected part of the sample. (In equation (4.25) the f_j of this part would become zero.) But this always comes at the price of changing the chemical makeup of the system under study, which is almost certain to lead to other, unwanted, changes.

Several nuclear reactors provide beamlines for scientific research. In the Netherlands test reactors offering neutron beamlines to researchers are located in Delft (“Interfacultair Reactor Instituut”) and in Petten (“Energieonderzoek Centrum Nederland”). More powerful neutron sources open to European researchers are in Jülich (“Forschungszentrum Jülich”) and in Grenoble (“Institut Laue-Langevin”).

4.8. More reading

The derivation of the field radiated by an oscillating dipole can be found in:

- Griffiths, D. J., *Introduction to Electrodynamics* (3rd ed., Prentice Hall, Upper Saddle River, 1999).

or in most other textbooks on electrodynamics.

Famous books on light scattering and absorption by individual particles are:

- H. C. van de Hulst, *Light Scattering by Small Particles* (Wiley, New York, 1957)
- M. Kerker, *The scattering of light and other electromagnetic radiation* (Academic Press, New York, 1969).
- C. F. Bohren and D. R. Huffman, *Absorption and scattering of light by small particles* (John Wiley & Sons, New York, 1983).

Note that these books only treat scattering by single particles. For discussions of structure factors we refer to textbooks on soft condensed matter, which are listed elsewhere in this syllabus.

A classic text on dynamic light scattering is

- B. J. Berne and R. Pecora, *Dynamic Light Scattering – With applications to chemistry, biology, and physics* (Wiley, New York, 1976).

5. Phase Behaviour

Marjolein Dijkstra
Soft Condensed Matter, Debye Institute
Utrecht University

Contents

5.1	Introduction	3
5.2	Steric stabilised colloidal suspensions	4
5.3	Charge-stabilised Colloidal Suspensions	8
5.3.1	Free energy calculation of the solid phase	10
5.3.2	Free energy calculation of the fluid phase	11
5.3.3	Kofke integration method	12
5.3.4	Phase diagram	13
5.4	Sedimentation	13
5.5	Colloid-Polymer Mixtures	16
5.6	Binary hard sphere mixtures	19

5.1 Introduction

Colloidal suspensions are complex fluids that consist of mesoscopic particles suspended in a solvent (e.g. water). The colloidal particles are significantly larger than the solvent molecules, but small enough to show Brownian motion. In the case that the linear dimension R of the colloids is in the regime of $10 \text{ nm} < R < 1000 \text{ nm}$, no significant sedimentation occurs in Earth's gravity. Examples of colloidal particles are viruses, proteins, synthetic polymeric particles (latex, PMMA), micelles, etc. Suspensions of these particles play an important role in biology, e.g. blood, but also many industrial products are essentially colloidal suspensions, e.g. paints, inks, food, detergents, cosmetics.

Due to fluctuating dipole moments, an attractive 'dispersion' force, or Van der Waals force, acts between every pair of atoms separated by a distance r . Summing over all pairs of atoms in two colloidal particles gives rise to a strong Van der Waals attraction between the colloids, which can be larger by orders of magnitude than the thermal energy $k_B T$. This may lead to irreversible aggregation of the colloids. In order to stabilise a colloidal suspension against irreversible aggregation two mechanisms are common: charge and steric stabilisation. In the case of charge stabilisation, the colloidal particles have ionisable groups on their surfaces, which dissociate when the particles are suspended in a polar liquid. The colloidal particles then acquire a net surface charge Ze , with e the elementary charge and Z the charge number typically in the range $10^2 < |Z| < 10^5$. The released counterions form a diffuse layer of thickness κ^{-1} around each colloidal particle, where κ^{-1} is the Debye screening length. The approach of two charged colloids leads to overlap of these so-called electric double layers, and causes a repulsive force that can stabilise the particles against aggregation [1]. In the case of steric stabilisation the colloidal particles are coated with a polymer layer. When two coated colloidal particles approach each other sufficiently closely, the polymer layers interpenetrate and overlap, which leads to a reduction of the polymer entropy, and hence to an effective repulsive force between the colloids. This repulsion leads again to stabilisation of the particles against aggregation.

Often other components, such as salt ions, polymers or smaller colloids, are present in suspension as well. In the case of charged colloids, the addition of electrolyte or salt changes the Debye screening length κ^{-1} . On the other hand, the addition of free polymer coils or smaller colloids to a steric stabilised colloidal suspension induces a depletion interaction between colloids which is mainly attractive and of a range of the size of the depletant [2, 3]. The concentration of added salt, or the size and concentration of added free polymers or smaller colloids, can therefore be used as control

parameters with which the effective interactions between the colloids can be tailored. The possibility of tailoring the effective interactions enriches the physics of colloidal systems compared to simple (atomic) fluids, and leads to a wide range of practical applications.

Most theoretical treatments of soft matter systems are based on a coarse-grained view in which the solvent is regarded as an inert, structureless continuum characterised by a density and a dielectric constant. In this approach, the colloids are described by effective interparticle potentials and classical statistical physics, combined with standard theories developed for simple liquids and solids, can then be used to calculate the phase behaviour and structure of such a suspension. In Section 12.2, we first discuss steric stabilised colloidal suspensions, in which the particles interact via hard-sphere like pair potentials. Computer simulations have shown a well-defined freezing transition in a system of pure hard spheres. We explain this freezing transition with a simple theory and we discuss some experiments on colloidal hard spheres that exhibit indeed this freezing transition. In Section 12.3, we discuss the phase behaviour of charge-stabilised colloidal suspensions using an effective one-component description of the suspension. A model system that is well-studied experimentally and theoretically is the hard-sphere system.

In Section 12.5 we show explicitly that the effective interactions between colloidal particles can change due to the addition of polymer coils. The addition of polymer can lead to a phase separation into a phase which is dilute in colloids (gas-like) and a phase which is dense in colloids (liquid-like). The mechanism of this phase separation is due to the so-called depletion mechanism, which leads to attractive effective interactions between the colloids. This phenomena has many practical applications, e.g. creaming of rubber latex, isolating virus particles, creaming of oil droplets, etc. Finally, in Section 12.6, the phase behaviour of binary mixtures of large and small steric stabilised colloidal suspensions are discussed.

5.2 Steric stabilised colloidal suspensions

In the case of steric stabilisation, the colloidal particles are coated with a polymer layer, which leads to a steep repulsive interaction between the colloids when they approach each other; the colloidal pair potential can therefore be regarded as hard-sphere like. The hard-sphere system has been studied in great detail. The first computer simulations were performed by Alder and Wainwright and Wood and Jacobson in 1957 [4]. They showed, using this new technique for studying many-body systems, that a system with purely repulsive hard spheres has a well-defined freezing point. How-

ever, both the computer simulations as a new tool as well as the freezing transition in hard spheres were disputed for a long time. Even after a long discussion of 17 eminent physicists with several Noble Prize laureates, the situation was still unsettled as many people found it hard to believe that a crystalline phase can appear without any attraction. Nowadays, it is generally accepted that a hard-sphere system has a fluid-solid transition and indeed colloidal particles that interact with hard-sphere potentials show a clear fluid-solid transition. Below we show that this fluid-solid transition can be explained using the Carnahan-Starling expressions for the fluid phase and a cell theory for the solid phase. The Carnahan-Starling expression for the Helmholtz free energy of a fluid of hard spheres with diameter σ is given by:

$$f_{CS}(\eta) = \frac{F_{CS}\pi\sigma^3}{6V} = kT \left[\eta \log\left(\frac{6\eta\Lambda^3}{\pi\sigma^3}\right) - \eta + \frac{4\eta^2 - 3\eta^3}{(1-\eta)^2} \right] \quad (5.1)$$

where we define the packing fraction $\eta = \pi\sigma^3 N/6V$. The chemical potential and pressure can easily be obtained from the Helmholtz free energy:

$$\mu(\eta) = \frac{\partial f}{\partial \eta} \quad p(\eta) = \frac{-6}{\pi\sigma^3} \left(f(\eta) - \eta \frac{\partial f}{\partial \eta} \right) \quad (5.2)$$

and the Carnahan-Starling expressions for the chemical potential and the pressure read

$$\mu_{CS}(\eta) = kT \left[\log\left(\frac{6\eta\Lambda^3}{\pi\sigma^3}\right) + \frac{8\eta - 9\eta^2 + 3\eta^3}{(1-\eta)^3} \right] \quad (5.3)$$

$$p_{CS}(\eta) = kT \frac{6}{\pi\sigma^3} \left[\frac{\eta(1 + \eta + \eta^2 - \eta^3)}{(1-\eta)^3} \right] \quad (5.4)$$

We already mentioned in Chapter 3 that the Carnahan-Starling equation of state is indistinguishable from simulation results up to $\eta = 0.5$. Fig.5.1 shows that also the equation of state derived experimentally by Piazza *et al.* from equilibrium sedimentation profiles of colloidal hard spheres shows good agreement with the Carnahan-Starling equation of state. The good agreement found with simulations and experiments justifies the use of the Carnahan-Starling expressions for the fluid phase.

For the solid phase we can employ a simple cell theory. In this theory for solids, the particles are localised around given lattice sites. We assume that the particles are confined to cells centered at lattice sites. In a FCC solid with a lattice constant a , the particles are confined to dodecahedral cells with a volume $v = a^3/\sqrt{2} = V/N$. At close packing the volume of the dodecahedral cell is given by $v_{cp} = \sigma^3/\sqrt{2}$. The canonical partition

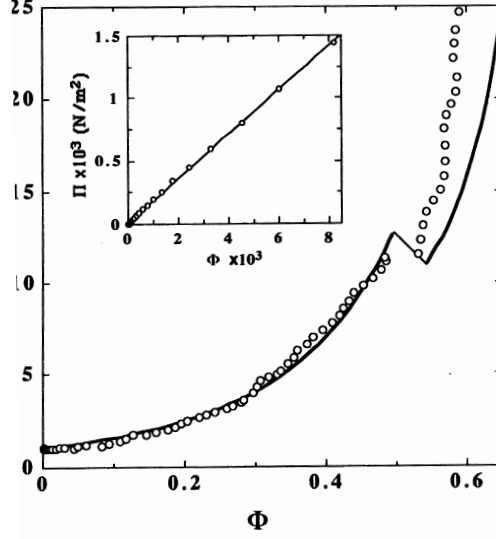


Figure 5.1: The pressure $\Pi/Nk_B T$ versus the packing fraction Φ obtained experimentally from the sedimentation profile of colloidal hard spheres (Piazza *et al.*, Phys. Rev. Lett. **71**, 4267 (1993)). The solid line denotes the Carnahan-Starling equation of state for the fluid phase and an empirical fit to simulation data for the solid phase.

function (2.38) reads

$$\begin{aligned}
 Z_{\text{cell}} &= \frac{N!}{N! \Lambda^{3N}} \int_{v_1} d\mathbf{r}_1 \cdots \int_{v_N} d\mathbf{r}_N \exp[-\beta \sum_{i < j}^N \phi(r_{ij})] \\
 &\simeq \left(\frac{v_{\text{free}}}{\Lambda^3} \right)^N
 \end{aligned} \tag{5.5}$$

where $N!$ in the numerator equals the number of distinct ways that N colloids can be distributed over N cells and where v_{free} is the volume in which the colloid can move freely, i.e.

$$\begin{aligned}
 v_{\text{free}} &= \frac{(a - \sigma)^3}{\sqrt{2}} \\
 &= \left(\frac{\pi \sigma^3}{6\eta} \right) \left(1 - \left(\frac{\eta}{\eta_{cp}} \right)^{1/3} \right)^3
 \end{aligned} \tag{5.6}$$

The Helmholtz free energy reads

$$\begin{aligned} f_{\text{cell}} &= \frac{\pi\sigma^3 F_{\text{cell}}}{6V} = -\frac{\pi\sigma^3 kT \log Z_{\text{cell}}}{6V} \\ &= \eta kT \log \left[\frac{6\eta\Lambda^3}{\pi\sigma^3} \left(1 - \left(\frac{\eta}{\eta_{cp}} \right)^{1/3} \right)^{-3} \right] \end{aligned} \quad (5.7)$$

Using Eq. (5.2) we find that the chemical potential and pressure for the solid are given by

$$\begin{aligned} \mu_{\text{cell}}(\eta) &= \frac{kT}{1 - \left(\frac{\eta}{\eta_{cp}} \right)^{1/3}} \\ &+ kT \log \left[\frac{6\eta\Lambda^3}{\pi\sigma^3} \left(1 - \left(\frac{\eta}{\eta_{cp}} \right)^{1/3} \right)^{-3} \right] \end{aligned} \quad (5.8)$$

$$p_{\text{cell}}(\eta) = \frac{6\eta}{\pi\sigma^3} \frac{kT}{1 - \left(\frac{\eta}{\eta_{cp}} \right)^{1/3}} \quad (5.9)$$

Fig. 5.2 shows the free energy for the fluid phase $f_{CS}(\eta)$ and the solid phase $f_{\text{cell}}(\eta)$ as a function of η . A fluid phase and a solid phase with packing fractions η_f and η_s are in thermodynamic equilibrium at fixed temperature T if

$$p_{CS}(\eta_f) = p_{\text{cell}}(\eta_s) \quad (5.10)$$

$$\mu_{CS}(\eta_f) = \mu_{\text{cell}}(\eta_s) \quad (5.11)$$

Combining Eq. (5.2) with Eq. (5.10) and (5.11) we find that

$$\frac{f_{\text{cell}}(\eta_s) - f_{CS}(\eta_f)}{\eta_s - \eta_f} = \left(\frac{\partial f_{CS}}{\partial \eta} \right) \Big|_{\eta=\eta_f} = \left(\frac{\partial f_{\text{cell}}}{\partial \eta} \right) \Big|_{\eta=\eta_s} \quad (5.12)$$

which is equivalent to the common tangent construction. The common tangent construction in Fig. 5.2 shows that there is a coexistence between a fluid phase with $\eta_f = 0.609$ and a solid phase with $\eta_s = 0.661$ at a pressure $\beta p\sigma^3 = 17.84$. A more accurate equation of state for the solid phase due to computer simulations give a freezing transition at $\beta p\sigma^3 = 11.69$ with coexisting densities $\eta_f = 0.494$ and $\eta_s = 0.545$ for the fluid and solid phase, respectively. Indeed, experiments by Pusey and Van Megen (Nature **320**, 340 (1986).) on colloidal hard spheres show a homogeneous fluid phase for packing fractions $\eta < 0.494$ and a homogeneous solid phase for packing

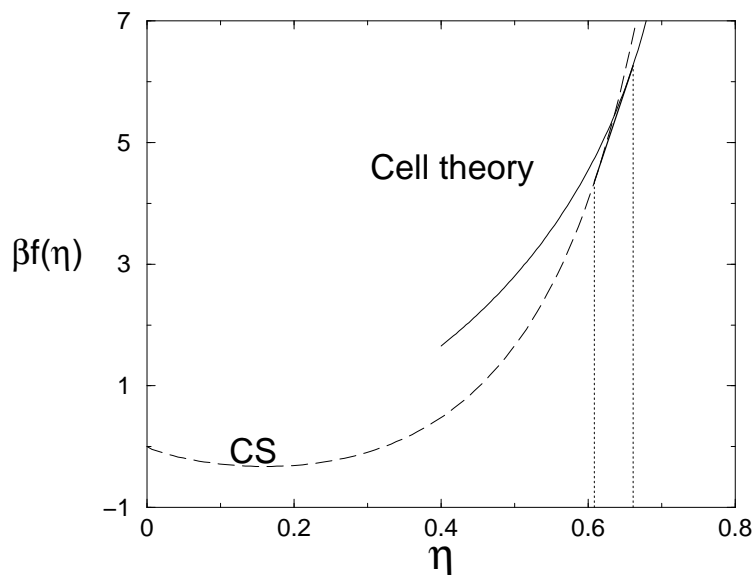


Figure 5.2: The Helmholtz free energy for the fluid phase (Carnahan-Starling) and the solid phase (Cell theory) as a function of the packing fraction η .

fractions $\eta > 0.545$. For packing fractions $0.494 < \eta < 0.545$, the samples show coexistence between a fluid and a solid phase with a clear meniscus between the crystalline phase at the bottom of the test tube and the fluid phase on top. For packing fractions $\eta > 0.58$, a colloidal glass is found. However, this glass transition is absent in microgravity experiments by NASA of colloidal hard spheres in a space shuttle (J.X. Zhu *et al.*, *Nature* **387**, 883 (1997).) . Fig. 5.3 summarises the phase behaviour of purely repulsive hard spheres.

5.3 Charge-stabilised Colloidal Suspensions

Charge-stabilised colloidal suspensions consist of (spherical or anisotropic) mesoscopic colloidal particles suspended in a polar solvent with co- and counterions. The radius of the co- and counterions is comparable to that of the solvent molecules, i.e. of the order of 0.1-0.3 nm. A statistical mechanics description of these highly asymmetric multicomponent fluids represent a major challenge as very different length and time scales are involved for the various species. This is the reason why attempts to treat the mesoscopic

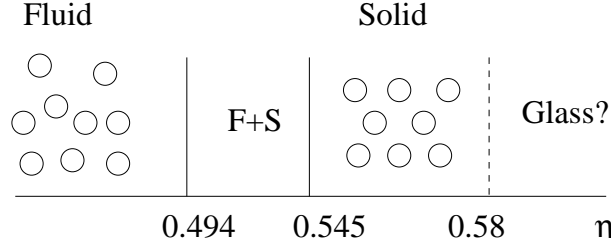


Figure 5.3: The phase diagram of purely repulsive hard spheres.

colloids and the microscopic salt and solvent particles on an equal footing usually fail. It is therefore not surprising that the present understanding of these systems is based on simplified models, in which the degrees of freedom of the microscopic particles have been integrated out, and the mesoscopic particles interact with an effective (usually pairwise) potential resulting in a coarse-grained effective one-component description of the suspension. The standard and very successful effective one-component description of charged colloidal suspensions dates back to the 1940's and is due to Derjaguin-Landau-Verwey-Overbeek (DLVO) [1]. The DLVO theory is the cornerstone of colloid science; it not only describes the diffuse double layer of thickness κ^{-1} of co- and counterions surrounding the charge surfaces of colloidal particles, but it also predicts effective screened Coulomb repulsions (or Yukawa repulsions), with decay length κ^{-1} , between pairs of colloids:

$$\beta u(r) = \beta u_{hs}(r) + \beta u_{yuk}(r) \quad (5.13)$$

where the hard-sphere pair potential reads

$$\beta u_{hs}(r) = \begin{cases} \infty, & r < \sigma \\ 0, & r > \sigma \end{cases}, \quad (5.14)$$

and where the Yukawa pair potential is given by

$$\beta u_{yuk}(r) = \begin{cases} 0, & r < \sigma \\ \beta \epsilon \frac{\exp[-\kappa \sigma (r/\sigma - 1)]}{r/\sigma}, & r > \sigma \end{cases}, \quad (5.15)$$

$\beta \epsilon$ is the value of the pair potential at contact per $k_B T$, and σ is the hard-core diameter of the colloids. The contact value $\beta \epsilon$ reads

$$\beta \epsilon = \frac{Z^2}{(1 + \kappa \sigma / 2)^2} \frac{\lambda_B}{\sigma}, \quad (5.16)$$

where Z is the charge of the colloids and $\lambda_B = \beta e^2 / \epsilon_s$ is the Bjerrum length of the solvent with dielectric constant ϵ_s [1]. The total potential energy of N particles is given by the sum over all pairs i.e.,

$$U(\mathbf{r}^N) = \sum_{i < j}^N u(r_{ij}) \quad (5.17)$$

where $r_{ij} = |\mathbf{r}_i - \mathbf{r}_j|$. The phase diagram consists of stable regions of fluid, bcc and fcc phases that are bounded by coexistence regions between any two phases. Therefore, the determination of the phase diagram reduces to the calculation of the coexistence lines. Points on the coexistence line can be determined by calculating, for each phase, the Helmholtz free energy per volume as a function of density and using the common tangent construction to obtain the densities of the coexisting phases.

5.3.1 Free energy calculation of the solid phase

As the free energy can not be measured directly in a Monte Carlo (MC) simulation, we used thermodynamic integration to relate the free energy of the system interacting with a potential energy function given by Eq. (5.17) to that of a reference system at the same density. The Helmholtz free energy of the solid phases is calculated using the Frenkel-Ladd method [5]. To this end we introduce the auxiliary potential energy function.

$$U_{\text{solid}}(\mathbf{r}^N) = \sum_{i < j}^N u(r_{ij}) + \lambda \sum_{i=1}^N (\mathbf{r}_i - \mathbf{r}_{0,i})^2 / \sigma^2. \quad (5.18)$$

where $\mathbf{r}_{0,i}$ is the lattice position of particle i , and λ the dimensionless switching parameter. In Eq. (5.18), particles are coupled to their lattice sites with harmonic springs: for $\lambda = 0$ we recover the system of interest, while for a sufficiently high value of λ , say $\lambda = \lambda_m$, the particles do not feel each other and the system reduces to that of a noninteracting Einstein solid with Madelung energy $U(\mathbf{r}_0)$, i.e., the potential energy of a crystal with all particles at their lattice positions. It is a standard result that [34,36]

$$\begin{aligned} \beta F_{\text{solid}}(N, V, T) &= \beta F_{\text{Ein}}^{CM}(N, V, T, \lambda_m) + \beta F_{\text{corr}}(N, V, T) \\ &\quad - \int_0^{\lambda_m} d\lambda \left\langle \sum_{i=1}^N (\mathbf{r}_i - \mathbf{r}_{0,i})^2 / \sigma^2 \right\rangle_{\lambda}^{CM}, \end{aligned} \quad (5.19)$$

where the superscript CM on the ensemble average denotes that it is calculated for a crystal with fixed center of mass. The free energy of an Einstein

crystal with fixed center of mass is given by.

$$\begin{aligned} \beta F_{E_{in}}^{CM}(N, V, T, \lambda_m) &= \beta U(\mathbf{r}_0^N) - \frac{3(N-1)}{2} \ln \left[\frac{\pi}{\lambda_m} \right] \\ &+ (N-1) \ln \left[\frac{\Lambda^3}{\sigma^3} \right], \end{aligned} \quad (5.20)$$

where Λ is the de Broglie wavelength. The correction term F_{corr} arises when the constraint on the center of masses is released, i.e., the Helmholtz free energy difference between the unconstrained and constrained crystal:

$$\beta F_{corr}(N, V, T) = \ln \left[\frac{\Lambda^3}{VN^{1/2}} \right] \quad (5.21)$$

5.3.2 Free energy calculation of the fluid phase

The Helmholtz free energy of the fluid phase is calculated using the λ integration with the hard-sphere fluid as a reference state [5]. To this end, we introduce an auxiliary potential energy function

$$U_{\text{fluid}}^\lambda(\mathbf{r}^N) = \sum_{i<j}^N u_{hs}(r_{ij}) + \lambda \sum_{i<j}^N u_{yuk}(r_{ij}), \quad (5.22)$$

where $0 \leq \lambda \leq 1$ is the coupling parameter: at $\lambda = 0$ the interaction reduces to that of a fluid of N hard spheres, while at $\lambda = 1$ it is the potential energy function of interest (for fixed V). The Helmholtz free energy is

$$F_{\text{fluid}}(N, V, T) = F_{\text{fluid}}^{hs}(N, V, T) + \int_0^1 \left\langle \sum_{i<j}^N u_{yuk}(r_{ij}) \right\rangle_\lambda d\lambda, \quad (5.23)$$

where F_{fluid}^{hs} is the free energy of a hard-sphere fluid, for which we use the Carnahan-Starling expression [6]

$$\frac{\beta F_{\text{fluid}}^{hs}}{N} = \ln \left[\frac{N\Lambda^3}{V} \right] - 1 + \frac{\eta(4-3\eta)}{(1-\eta)^2}. \quad (5.24)$$

where $\eta = \pi\sigma^3 N/6V$.

In most experiments on charge-stabilized colloidal suspensions, one makes several assumptions for charge Z and the inverse Debye screening length $\kappa\sigma$. Charge Z is often replaced by a so-called renormalized or saturated charge that depends both on $\kappa\sigma$ and on the packing fraction η [7, 8]. Furthermore, one often considers a $\kappa\sigma$ that depends on Z , η , and on the added

salt concentration [9]. This means that the relationship between $\beta\epsilon$, $\kappa\sigma$, and η is complicated. However, an η and Z independent $\kappa\sigma$ can be realized by coupling the system to a salt reservoir and considering $\kappa\sigma$ to be that of the reservoir. In addition, we take the value of $\beta\epsilon$ to be fixed, which can later be related to experimental system parameters through Eq. (5.16). In this way, $\beta\epsilon$ and $\kappa\sigma$ are independent variables, i.e., independent of each other and of the colloid packing fraction η , and we calculate the phase behavior in the three dimensional space $(\beta\epsilon, \kappa\sigma, \eta)$ spanned by them. This means that two phases in coexistence have, as usual, equal pressure p and equal chemical potential μ , but have also equal $\kappa\sigma$ and equal $\beta\epsilon$, while η is different. For a given $\beta\epsilon$ and $\kappa\sigma$, coexistence can be determined by calculating, the Helmholtz free energy for many different η for the fluid, bcc, and fcc phase and employing the common tangent construction.

5.3.3 Kofke integration method

In principle this could be repeated for every $\kappa\sigma$ to obtain a smooth coexistence line. However, this would be computationally very demanding and, as it turns out, not even necessary. The reason for this is that once one point on the coexistence line is known, the rest of the line can be calculated without performing additional free energy calculations. This can be achieved by employing a numerical method first proposed by Kofke [10]. We are interested in calculating phase coexistence lines in the $(\eta, \kappa\sigma)$ plane for a fixed $\beta\epsilon$. In this case, the Kofke's method amounts to integrating

$$dp = - \frac{\langle \beta U' / N \rangle_1 - \langle \beta U' / N \rangle_2}{\langle V / N \sigma^3 \rangle_1 - \langle V / N \sigma^3 \rangle_2} d(\kappa\sigma), \quad (5.25)$$

(for the derivation see Ref. [11]) from a known starting point $(p, \kappa\sigma)$. Note that the two phases in coexistence have the same p , $\beta\epsilon$ and $\kappa\sigma$ but different η . In Eq. (5.25), $p = \beta P \sigma^3$ is the dimensionless pressure, $\langle \dots \rangle_i$ denotes ensemble average of the i th phase ($i = 1, 2$) and U' is the partial derivative of the total potential energy with respect to $\kappa\sigma$. In practice Eq. (5.25) is integrated as follows. The differentials dp and $d(\kappa\sigma)$ are replaced by finite differences Δp and $\Delta(\kappa\sigma)$. Starting from a known coexistence point with p and $\kappa\sigma$, Monte Carlo (MC) simulations [5] are performed for both phases in the NPT -ensemble to calculate the ensemble averages in Eq. (5.25). This gives us a prediction for the slope in the coexistence line in the $(p, \kappa\sigma)$ plane. Changing $\kappa\sigma$ to $\kappa\sigma + \Delta(\kappa\sigma)$ we perform MC simulations for both phases at pressure $p + \Delta p$ predicted by Eq. (5.25) and we calculate again the ensemble averages in Eq. (5.25). Continuing in this manner gives us a series of points $\{p_j, (\kappa\sigma)_j\}$ that lie on the coexistence line. At each point

the packing fractions of the two phases are determined using the ensemble averages $\eta_i = \frac{\pi}{6}\sigma^3 N/\langle V \rangle_i$, obtained from the *NPT*-simulations.

5.3.4 Phase diagram

Using the methods described above, the phase behavior of hard-core Yukawa particles is determined. The phase diagrams are calculated for fixed contact values $\beta\epsilon$ and they are given in the $(\eta, 1/\kappa\sigma)$ representation. We calculate the phase diagram for four contact values, $\beta\epsilon = 8, 20, 39$, and 81 , and the results are given in Fig. 12.4. In all the four phase diagrams the gray areas bounded by the solid lines give the coexistence regions (tie lines are horizontal), while the dashed lines give the point Yukawa phase boundaries of Ref. [12]. In Fig. 12.5 we summarize the results from Figs. 12.4 by plotting all the phase diagrams in one figure. We observe from Fig. 12.5 that the low $1/\kappa\sigma$ triple point moves to lower η and higher $1/\kappa\sigma$ with increasing contact value $\beta\epsilon$. Another observation is that the region of stable bcc phase broadens, mainly because the fluid-bcc coexistence line moves to lower packing fractions, while the bcc-fcc coexistence line moves only slightly to higher η and seems to saturate around $\eta \simeq 0.5$.

5.4 Sedimentation

Suspensions of colloidal particles are spatially inhomogeneous in an external field, e.g. gravity. The spatial inhomogeneity is characterized by a density profile $\rho(x, y, z)$. The potential energy of a particle in a gravitational field at height z is given by $V(z) = m_B g z$, where m_B is the buoyant mass of a particle, $k_B T$ the thermal energy, and g the acceleration due to gravity. The buoyant mass of a spherical colloid with diameter σ is according to Archimedes' principle

$$m_B = M - (\pi\sigma^3/6)\rho_{solvent} \quad (5.26)$$

where M is the bare mass of the colloid and $\rho_{solvent}$ the mass density of the solvent.

The gravitational length $\xi = k_B T/m_B g$ can be tuned by changing g , e.g. space shuttle experiments or centrifugation, or by changing the density of the solvent (density-matching). The gravitational lengths in experiments of hard spheres by Pusey and Van Meegen are of order micrometers on earth, and of order meters in space shuttle experiments by Zhu *et al.*. In a gravitational field, a colloidal suspension experiences a competition between minimal potential energy, which favors the particles to be at the bottom of the container, and maximal entropy, i.e. a homogeneous distribution of the

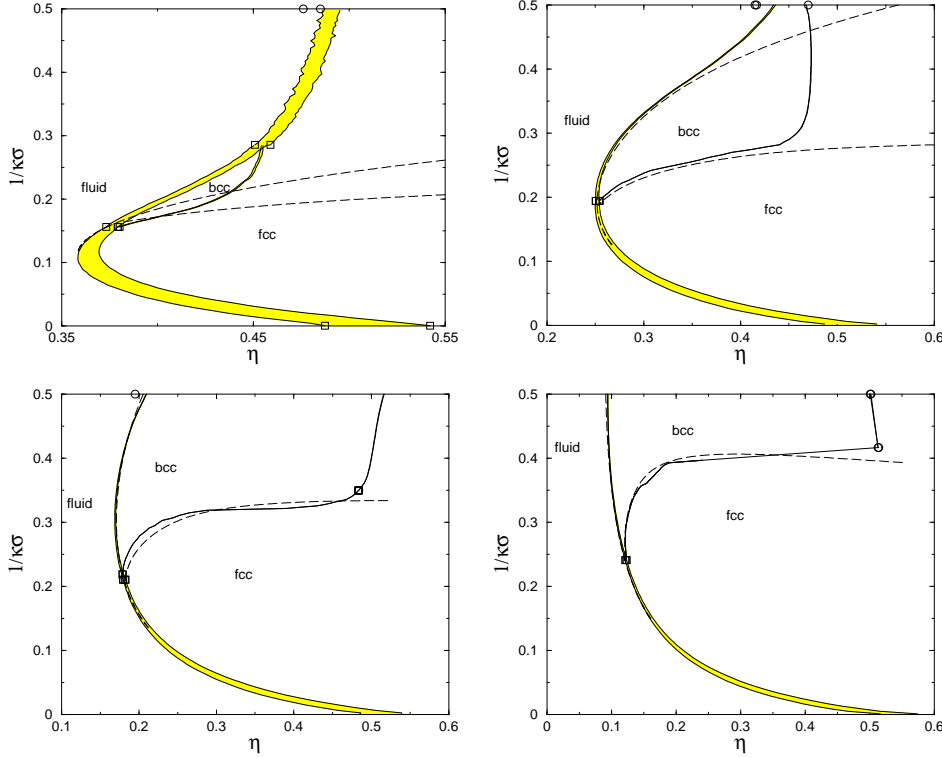


Figure 5.4: Phase diagram for a system in which the particles interact via a hard-core repulsive Yukawa pair potential Eq.5.13 with $\beta\epsilon = 8$ (upper left), 20 (upper right), 39 (bottom left), 80 (bottom right), presented in the (packing fraction η , Debye screening length $1/\kappa\sigma$) plane. In charge-stabilized colloidal suspensions, the lower part of the diagram ($1/\kappa\sigma = 0$) is a high salt regime and the upper part ($1/\kappa\sigma = 0.5$) is a low salt regime. The solid lines are coexistence lines obtained by using the Kofke integration and the gray areas denote the coexistence regions. The tie lines are horizontal. We find a stable fluid phase at low η , a stable face-centered-cubic (fcc) solid at high η , and in between, a stable body-centered-cubic (bcc) solid. The dashed lines are the phase boundaries of the point Yukawa particles by Hamaguchi, Farouki, and Dubin [12]. The squares mark the starting points for the Kofke integration and the circles are checkup points for the coexistence that were obtained using free energy calculations. (Phase diagrams are from A.P. Hynninen and M. Dijkstra, *Phys. Rev. E* **68**, 021407 (2003)).

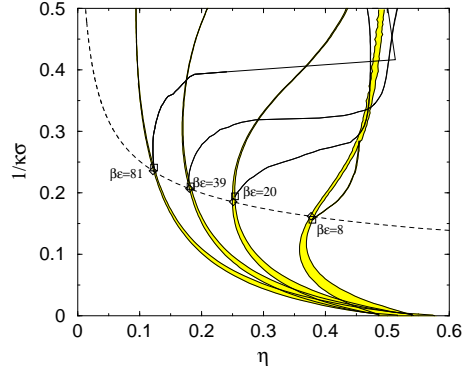


Figure 5.5: Phase diagrams of Fig. 12.4 plotted in one figure. The dashed line gives the line of triple points predicted by the point Yukawa results of Hamaguchi, Farouki, and Dubin [12], the diamonds highlight the triple points at $\beta\epsilon = 8, 20, 39,$ and $81,$ and the squares mark the position of the triple points used in our calculations. (Phase diagrams are from A.P. Hynninen and M. Dijkstra, Phys. Rev. E **68**, 021407 (2003)).

particles. Macroscopically, the density profile $\rho(z)$, which depends on only the z -coordinate in a gravity field, obeys the hydrostatic equilibrium:

$$\frac{dP(z)}{dz} = -m_B g \rho(z) \quad (5.27)$$

The determination of density profiles of suspensions with vitreous spheres allowed Jean Perrin in 1910 to measure Boltzmann's constant and, hence, Avogadro's number. He was awarded the Nobel Prize in Physics in 1926 "for his work on the discontinuous structure of matter, and especially for his discovery of sedimentation equilibrium". Under isothermal conditions, the pressure P depends only on the local density $\rho(z)$, so that Eq. (5.27) can be written as a nonlinear differential equation for $\rho(z)$:

$$\frac{d\rho(z)}{dz} = -\chi_T \beta m g \rho(z) \quad (5.28)$$

where $\chi_T = (\partial\beta P/\partial\rho)_T^{-1}$ is the compressibility of the suspension at density ρ . The integration constant is obtained from the normalization condition

$$\int_{z=0}^{z=\infty} \rho(z) dz = n_s \quad (5.29)$$

where $n_s = N/A$ is the number of particles per unit area. If the pressure is known as a function of the density of the bulk fluid, direct integration of

Eq. (5.27) between $z = 0$ and $z = \infty$ (where the pressure vanishes) and use of the normalization condition gives the following implicit equation for the wall-contact value $\rho_0 = \rho(z = 0)$ of the density profile

$$P(\rho_0) = m_B g n_s \quad (5.30)$$

For a sufficiently dilute fluid, for which the ideal-gas equation of state $\beta P = \rho$ holds, Eq. (5.28) yields the well-known barometric height formula

$$\rho(z) = \rho_0 \exp(-z/\xi) \quad (5.31)$$

where $\rho_0 = n_s/\xi$ is the wall contact value of the density. On the other hand, Equation 5.27 can be used to obtain the equation of state by integrating a known density profile $\rho(z)$. This route was followed by Piazza *et al.* to obtain the equation of state of colloidal hard spheres from an experimentally determined sedimentation profile.

5.5 Colloid-Polymer Mixtures

In this section we show that the addition of polymer can lead to effective attractive interactions between the colloids. We consider a binary mixture of colloids and polymers suspended in a solvent. The solvent is regarded as a continuum inert medium that gives rise to effective interactions between the colloids and polymers. The colloids are treated as hard spheres with diameter σ_c and the interpenetrable, non-interacting polymer coils are treated as point particles but which are excluded from the colloids to a centre-of-mass distance of $(\sigma_c + \sigma_p)/2$, where σ_p is the diameter of the polymer coil. The pairwise potentials in this simple model are given by:

$$\begin{aligned} \phi_{cc}(R_{ij}) &= \infty && \text{for } R_{ij} < \sigma_c \\ &= 0 && \text{otherwise} \\ \phi_{cp}(\mathbf{R}_i - \mathbf{r}_j) &= \infty && \text{for } |\mathbf{R}_i - \mathbf{r}_j| < \frac{1}{2}(\sigma_c + \sigma_p) \\ &= 0 && \text{otherwise} \\ \phi_{pp}(r_{ij}) &= 0 \end{aligned} \quad (5.32)$$

Here \mathbf{R}_i and \mathbf{r}_j are the positions of the centres of the colloids and the polymer coils, respectively, while $R_{ij} = |\mathbf{R}_i - \mathbf{R}_j|$ and $r_{ij} = |\mathbf{r}_i - \mathbf{r}_j|$.

We now determine the effective interactions between two colloids due to the presence of the polymer. It is convenient to treat the polymer grand-canonically as at phase coexistence the chemical potential of the polymer should be equal in the coexisting phases. Fig. 5.6 shows two colloidal

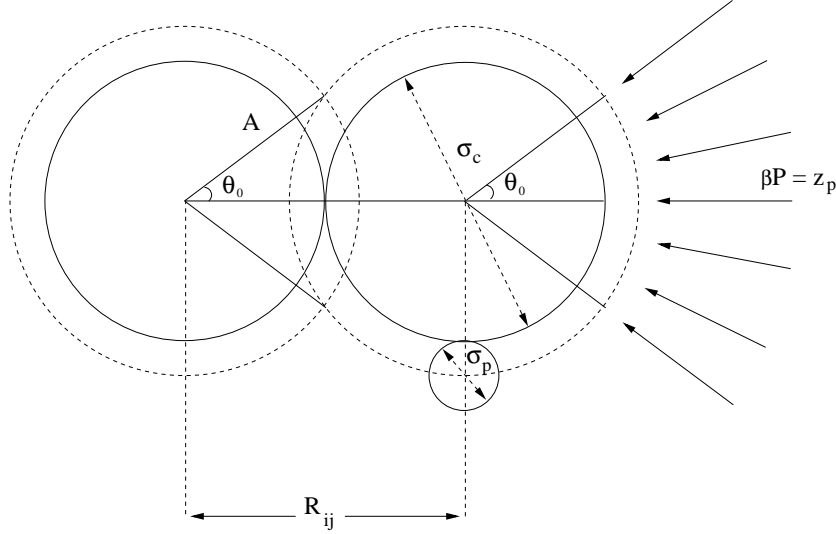


Figure 5.6: Two colloidal particles with diameter σ_c at distance R_{ij} immersed in a sea of ideal polymer with diameter σ_p and fugacity z_p .

particles immersed in a 'sea' of ideal polymers with a fugacity z_p . When the two colloids are close to each other, i.e. $\sigma_c < R_{ij} < (\sigma_c + \sigma_p)$, there is an unbalanced force as no polymer coils are present between the colloids. The unbalanced force is given by

$$\begin{aligned}
 F(R_{ij}) &= - \int_{\theta=0}^{\theta=\theta_0} \int_{\phi=0}^{\phi=2\pi} P \cos \theta A^2 \sin \theta d\theta d\phi \\
 &= -\pi A^2 P \left(1 - \frac{R_{ij}^2}{4A^2} \right) \quad \sigma_c \leq R_{ij} \leq \sigma_c + \sigma_p \quad (5.33)
 \end{aligned}$$

with

$$\begin{aligned}
 \theta_0 &= \arccos \left(\frac{R_{ij}/2}{A} \right) \\
 A &= \frac{\sigma_c + \sigma_p}{2} \quad (5.34)
 \end{aligned}$$

and P the pressure of the 'sea' of ideal polymer, i.e. $\beta P = z_p = \rho_p$. It is worth noting that the unbalanced force is zero for colloid distances $R_{ij} > \sigma_c + \sigma_p$, while colloid distances $R_{ij} < \sigma_c$ are non-existent due to the hard-sphere potential of the colloids. The unbalanced force gives rise to an

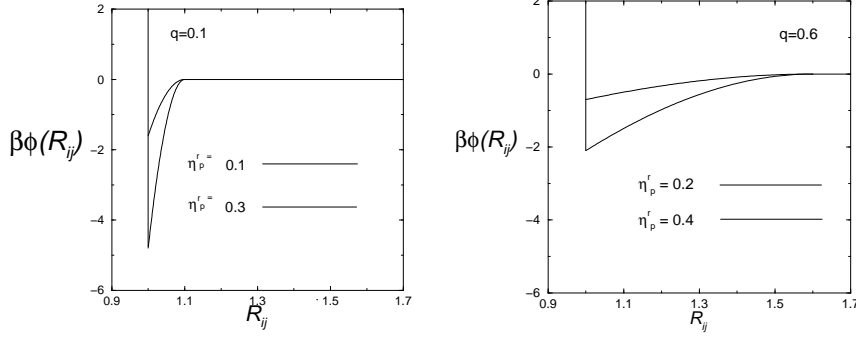


Figure 5.7: The effective pairpotential (5.36) between two colloids due to the presence of polymer in a mixture of colloid and polymers for size ratio $q = \sigma_p/\sigma_c = 0.1$ and 0.6 and varying polymer reservoir packing fraction.

effective attractive potential, which is called depletion potential

$$\begin{aligned} \beta\phi_{\text{dep}}(R_{ij}) &= - \int_{R'_{ij}=\sigma_c+\sigma_p}^{R'_{ij}=R_{ij}} \beta F(R'_{ij}) dR'_{ij} \\ &= -\frac{4}{3} z_p \pi A^3 \left[1 - \frac{3}{4} \frac{R_{ij}}{A} + \frac{1}{16} \left(\frac{R_{ij}}{A} \right)^3 \right] \\ &\quad \text{for } \sigma_c \leq R_{ij} \leq \sigma_c + \sigma_p \end{aligned} \quad (5.35)$$

Fig. 5.7 shows examples of the effective pair interaction of two colloidal hard spheres in a sea of ideal polymer. This effective pair interaction consists of the hard-sphere repulsion between the colloids themselves and the depletion potential due to the presence of the polymer:

$$\beta\phi_{\text{eff}}(R_{ij}) = \beta\phi_{cc}(R_{ij}) + \beta\phi_{\text{dep}}(R_{ij}) \quad (5.36)$$

Note that the range of the attraction becomes longer-ranged when the size ratio $q = \sigma_p/\sigma_c$ is larger and the well-depth becomes deeper upon increasing the polymer fugacities, while the temperature is irrelevant. In these systems, the polymer fugacity or packing fraction of the polymer in the reservoir $\eta_p^r \equiv \pi\sigma_p^3 z_p/6$ with which the system of interest is in contact plays the role of temperature. It is therefore convenient to represent the phase diagram of colloid-polymer mixtures in the $\eta_p^r - \eta_c$ plane, instead of the $T - \rho$ plane.

We can now use the effective pair interaction (5.36) in a Van der Waals theory using Eqs. (3.75) and (3.76). It is straightforward to derive the Van

der Waals parameters

$$\begin{aligned} a &= \frac{8\pi^2 z_p}{3} \left(\frac{A^6}{3} - \frac{\sigma_c^3 A^3}{3} + \frac{3\sigma_c^4 A^2}{16} - \frac{\sigma_c^6}{96} \right) \\ b &= \frac{2\pi\sigma_c^3}{3} \end{aligned} \quad (5.37)$$

Using Eq. (3.68), we find that the critical point is located at

$$\begin{aligned} \eta_c^* &= \frac{\pi\sigma_c^3 \rho_c^*}{6} = \frac{1}{12} \\ \eta_p^{r*} &= \frac{\pi\sigma_p^3 z_p^*}{6} = \frac{27\sigma_p^3 \sigma_c^3}{64A^6 - 64\sigma_c^3 A^3 + 36\sigma_c^4 A^2 - 2\sigma_c^6} \end{aligned} \quad (5.38)$$

and this explains qualitatively a demixing transition in a phase, which is dilute in colloids and a phase, which is dense in colloids upon addition of polymer.

In Fig. 5.8, we show ‘exact’ results for the phase behaviour of colloid-polymer mixtures obtained from simulations in the $\eta_c - \eta_p^r$ representation for varying size ratios $q = \sigma_p/\sigma_c$ using the effective pair potential of Eq. 5.36. For all q , we find at $\eta_p^r = 0$, i.e. no polymer, the freezing transition of pure hard spheres. However, when we add more and more polymer, we find for $q \simeq 0.6$ a phase separation into a phase which is dilute in colloids and a phase which is dense in colloids, i.e. colloidal gas-liquid phase transition. For $q \leq 0.4$, the colloids interact with a short-ranged effective attraction. We do find a colloidal gas-liquid transition, but this transition is metastable with respect to a very broad freezing transition.

5.6 Binary hard sphere mixtures

In the case of mixtures of large and small steric stabilised colloidal particles, the system can be regarded as a binary hard-sphere mixture. In the last decade, it was found that binary hard-sphere mixtures show extremely rich phase behaviour. Spindle, azeotropic, and eutectic type of phase diagrams and complex crystalline superlattice structures are found in theory, simulation, and experiments, when the size ratio $q \equiv \sigma_2/\sigma_1 > 0.4$. Published work in this size ratio regime is reviewed in Ref. [13]. The diameters of the large and small spheres are, respectively, σ_1 and σ_2 . When the size ratio is more asymmetric, the addition of the second component leads to the so-called depletion effect. Understanding the structure and phase equilibria of very asymmetric binary hard-sphere mixtures is a long-standing problem in liquid state physics. These idealized systems provide a natural reference

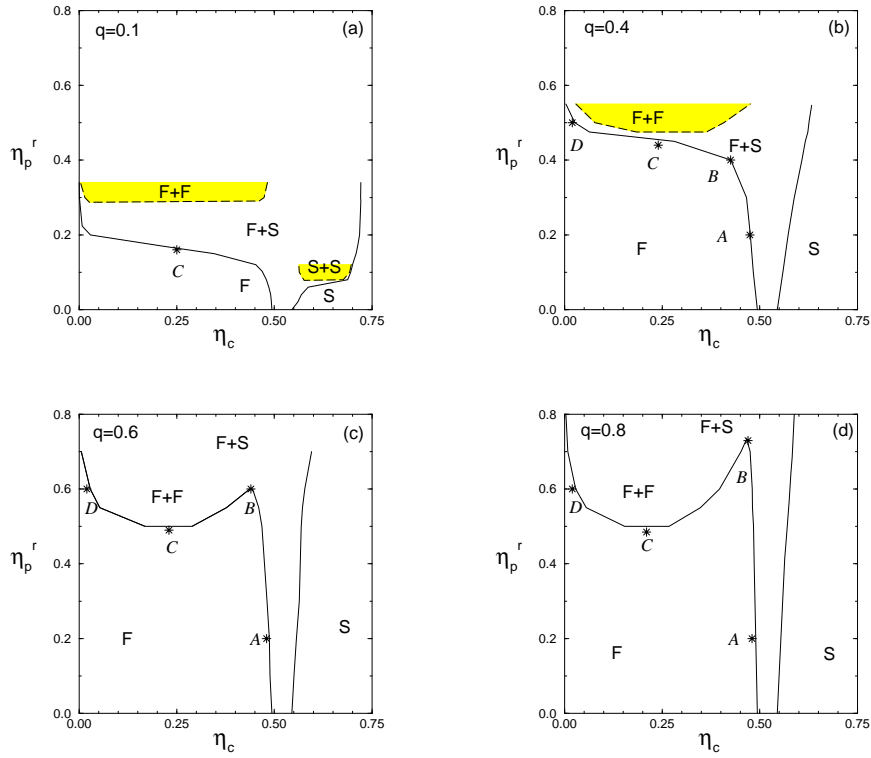


Figure 5.8: Phase diagram of colloid-polymer mixtures with size ratios $q = \sigma_p/\sigma_c = 0.1$ (upper left) $q = 0.4$ (upper right), $q = 0.6$ (bottom left), and $q = 0.8$ (bottom right) as a function of the colloid packing fraction η_c and the ideal polymer coil reservoir packing fraction η_p^r as obtained from simulations using the effective pair potential. F and S denote the stable fluid and solid (fcc) phase. $F+S$, $F+F$, and $S+S$ denote, respectively, the stable fluid-solid, the (meta)stable fluid-fluid and the metastable solid-solid coexistence region. (M. Dijkstra, J.M. Brader, and R. Evans, *J. Phys.: Cond. Matt.* **11**, 10079 (1999).

system for determining the properties of more realistic models of mixtures of simple (atomic) fluids, of colloids and polymers, and of other colloidal systems. A contentious issue, which attracts much attention, is whether fluid-fluid phase separation occurs in this model system. A classic study of Lebowitz and Rowlinson, based on the Percus- Yevick approximation, showed that hard spheres mix at all state points, for any ratio of diameters [14]. In 1991, improved integral equation studies by Biben and Hansen provided evidence for a spinodal instability when $q < 0.2$ [15]. The main reason for the subsequent interest resides in the fact that any mechanism for a demixing transition in hardsphere systems must be purely entropic. In Ref. [15] the depletion effect was identified as the mechanism behind the possible instability. The weakness of the integral equation theories lies in the sensitivity of the existence and location of the spinodal instability to fine details of the theory. Moreover, experimental work on colloidal systems indicates that any demixing is strongly coupled to the freezing transition, whereas these theories are not designed to deal with solid phases. Direct simulations of highly asymmetric binary mixtures are prohibited by slow equilibration when the packing fraction of the small spheres becomes substantial.

Therefore, a different strategy is often followed, in which advantage is taken of the large size asymmetry. In this approach the binary mixture is formally mapped onto an effective one-component system by integrating out the degrees of freedom of the small species in the partition function. An effective Hamiltonian is then obtained for the larger ones, which consists of zero-body, one-body, two-body and higher-body interactions. The effective two-body interactions or depletion potentials have been calculated within hypernetted-chain-based approximations, in simulations, using a virial expansion, integral equation theory, and density functional theory. Depletion potentials have also been measured experimentally. Using this approach and ignoring three-body and higher-body interactions, simulations show the existence of a fluid-fluid demixing transition for size ratios of 1:10 or more extreme. However, this fluid-fluid transition is metastable with respect to the fluid-solid transition that turns out to occur at strikingly low values of the packing fraction of the large spheres. More surprisingly, also an isostructural solid-solid transition at high packing fractions of the large spheres is found. This transition becomes stable for a size ratio $q < 0.05$. Good agreement is found with direct simulations of the true binary hard-sphere mixture, thereby justifying the depletion potential picture.

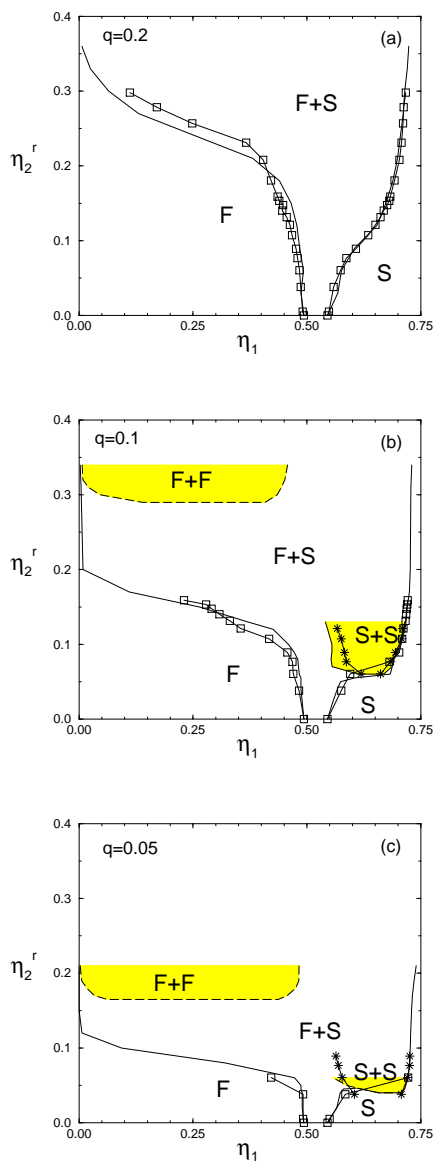


Figure 5.9: Phase diagram of binary hard-sphere mixtures with size ratios (a) $q = 0.2$, (b) $q = 0.1$, and (c) $q = 0.05$ as a function of the large-sphere packing fraction η_1 and the small-sphere reservoir packing fraction η_2^r . F and S denote the stable fluid and solid (fcc) phase. F+S, F+F, and S+S denote, respectively, the stable fluid-solid, the metastable fluid-fluid, and the (meta)stable solid-solid coexistence regions. The solid and dashed lines are the effective one-component results; the squares and the asterisks (joined by lines to guide the eye) denote, respectively, the fluid-solid and the solid-solid transition obtained from direct simulations of the true binary mixture. (M. Dijkstra, R. van Roij, and R. Evans, *Phys. Rev. E* **59**, 5744 (1999)).

Bibliography

- [1] B. Derjaguin and L. Landau, *Acta Physicochim. URSS* **14**, 633 (1941); E.J.W. Verwey and J. Th. G. Overbeek, "Theory of the stability of lyotropic colloids", Amsterdam, Elsevier, 1948; Republication Dover Publications, New York (1999).
- [2] S. Asakura and F. Oosawa, *J. Chem. Phys.* **22**, 1255 (1954).
- [3] A. Vrij, *Pure Appl. Chem.* **48**, 471, (1976).
- [4] W. W. Wood and J. D. Jacobson, *J. Chem. Phys.* **27**, 1207 (1957); B. J. Alder and T. E. Wainwright, *J. Chem. Phys.* **27**, 1208 (1957).
- [5] D. Frenkel and B. Smit, "Understanding Molecular Simulations", 2nd ed. (Academic Press, London, 2002).
- [6] N. F. Carnahan and K. E. Starling, *J. Chem. Phys.* **51**, 635 (1969).
- [7] S. Alexander, P.M. Chaikin, P. Grant, G.J. Morales, and P. Pincus, *J. Chem. Phys.* **80**, 5776 (1984).
- [8] E. Trizac, L. Bocquet, and M. Aubouy, *Phys. Rev. Lett.* **89**, 248301 (2002).
- [9] Y. Monovoukas and A.P. Gast, *J. Colloid Interface Sci.* **128**, 533 (1989).
- [10] D.A. Kofke, *Mol. Phys.* **78**, 1331 (1993); *J. Chem. Phys.* **98**, 4149 (1993).
- [11] F. El Azhar, M. Baus, J.P. Ryckaert, and E.J. Meijer, *J. Chem. Phys.* **112**, 5121 (2000).
- [12] S. Hamaguchi, R.T. Farouki, and D.H.E. Dubin, *Phys. Rev. E* **56**, 4671 (1997).

- [13] M. Dijkstra, R. van Roij, and R. Evans, Phys. Rev. E **59**, 5744 (1999);
M. Dijkstra, R. van Roij, and R. Evans, Phys. Rev. Lett. **82**, 117 (1999);
M. Dijkstra, R. van Roij, and R. Evans, Phys. Rev. Lett. **81**, 2268 (1998).
- [14] J. L. Lebowitz and J. S. Rowlinson, J. Chem. Phys. **41**, 133 (1964).
- [15] T. Biben and J. P. Hansen, Phys. Rev. Lett. **66**, 2215 (1991); J. Phys.:
Condens. Matter **3**, F65 (1991).

6. Interfaces, Micelles, and Microemulsions

Willem K. Kegel
Van't Hoff Laboratory for Physical and Colloid Chemistry
Utrecht University
The Netherlands

January 2012

Contents

1	Interfaces & adsorption	2
1.1	Thermodynamic description of interfaces	2
1.2	Molecular origin of the interfacial tension	3
1.3	Position of the Gibbs dividing plane	5
1.4	Van der Waals theory of interfaces	6
1.5	Gibbs adsorption equation	10
1.6	Problems	14
2	Surfactants and Micelles	16
2.1	Introduction: surfactants	16
2.2	Micelles: The critical micelle concentration (cmc)	17
2.3	Thermodynamics of micelle formation	19
2.4	Influence of molecular properties of the surfactant on the cmc	19
2.4.1	Influence of chain length on cmc	20
2.4.2	Effect of salt on the cmc	21
2.5	Geometry of surfactant molecules and micellar shape.	21
2.6	Problems	24
3	Microemulsions	25
3.1	Introduction	25
3.2	Experimental facts	26
3.3	Generalized Laplace equation	27
3.4	Curvature free energy	28
3.5	A microscopic model for curvature elasticity: incompressible spring model	29
3.6	Interfacial tension between microemulsion- and excess phase	31
3.7	Problems	31
	Bibliography	33

Chapter 1

Interfaces & adsorption

1.1 Thermodynamic description of interfaces

Consider two bulk phases α and β , that are separated by an interface. The bulk phases may be a simple liquid coexisting with a gas phase, but may also be immiscible liquids such as oil and water. Atoms or molecules that are close to the interface will experience interactions with their surrounding that is different from the situation in the bulk-phases. The resulting excess (free) energy per unit area at the interface is referred to as the interfacial tension γ . Hence, we have to account for an additional work term in the thermodynamic description of a two-phase system. In order to increase the surface area σ between the two phases by $d\sigma$, we have to add γ of (free) energy per unit area. The reversible work therefore reads

$$\bar{d}w_{\text{interface}} = \gamma d\sigma. \quad (1.1)$$

Comparison with the general expression for reversible work, $\bar{d}w_{\text{rev}} = Fdx$ ('work equals force times distance'), reveals that interfacial tension also is a force per unit length.

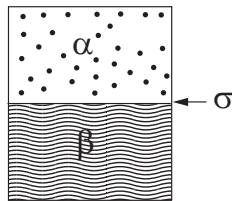


Figure 1.1: Two bulk phases α and β are separated by an interface σ .

Using Eq. 1.1, the change of the Helmholtz free energy of the total system can be written as

$$dA = -SdT - PdV + \sum_i \mu_i dN_i + \gamma d\sigma. \quad (1.2)$$

The change of the Helmholtz free energy of either bulk phases $b = \alpha, \beta$ can be written in its common form

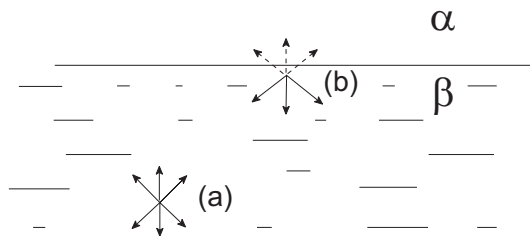


Figure 1.2: The number of attractive interactions is larger in bulk (a) than at the interface (b).

$$dA^b = -S^b dT - PdV^b + \sum_i \mu_i dN_i^b, \quad (1.3)$$

where S^b is the entropy of the respective bulk phases, V^b the volume of the phases, and N_i^b the number of particles of species i in the two phases. In thermal (equal temperatures T), mechanical (equal bulk pressures P), and chemical (equal chemical potentials μ_i) equilibrium of both bulk phases α and β , the change of the Helmholtz free energy of the interface follows from Eq. 1.2 and Eq. 1.3 as

$$dA^\sigma = dA - dA^\alpha - dA^\beta = -S^\sigma dT + \sum_i \mu_i dN_i^\sigma + \gamma d\sigma. \quad (1.4)$$

Here S^σ is the interfacial entropy and N_i^σ the total number of particles of species i at the interface. We have made use of the fact that Helmholtz free energy and the volume are extensive state variables, that is

$$A = A^\alpha + A^\beta + A^\sigma, \quad V = V^\alpha + V^\beta. \quad (1.5)$$

Consequently, in this thermodynamic description the interface has no volume but has to be considered as a (mathematical) plane. This can also be seen from comparison of the expression of the Helmholtz free energy of the bulk phases, Eq. 1.3, to that of the interface, Eq. 1.4. The interfacial work, Eq. 1.1, is a two-dimensional analogue of the volume work, $\vec{d}w_{\text{volume}} = -PdV^b$, in either of the bulk phases.

1.2 Molecular origin of the interfacial tension

Let us consider how the interactions change when transferring a particle from the bulk (a) to the interface (b) in order to provide an estimate of the order of magnitude of the interfacial tension. Since the interactions in bulk are more attractive than at the interface, as shown schematically in Fig 1.2, there is a (free) energy penalty for such a move. To bring a molecule from (a) to (b) we have to perform work against an attractive internal pressure, P_{att} , over a distance d , being typically on the order of a molecular size. The work to increase the interface per unit area roughly amounts to

$$\gamma \sim -P_{\text{att}} d \quad (1.6)$$

We assume that the pressure is given by the van der Waals equation of state. This equation provides two corrections to the ideal gas law. The first one is an

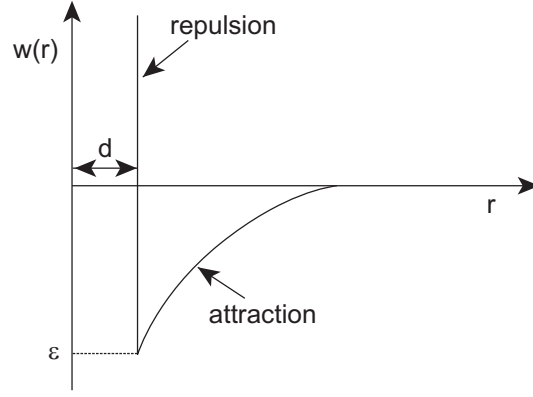


Figure 1.3: The total molecular interaction as a function of distance according to van der Waals. Up to the hard-sphere diameter d the repulsion is infinite, after that the attraction goes as $w(r) = -\epsilon \left(\frac{d}{r}\right)^6$

excluded volume term, b , and the second correction is due to particles experiencing an average attractive interaction, a , with surrounding particles.

$$P_{\text{vdW}} = P_{\text{hs}} + P_{\text{att}} = \frac{Nk_B T}{V - Nb} - a \left(\frac{N}{V}\right)^2, \quad (1.7)$$

where N is the number of particles, k_B Boltzmann's constant and

$$a = -\frac{1}{2} \int_d^\infty w(r) 4\pi r^2 dr. \quad (1.8)$$

The intermolecular potential $w(r)$ has an infinite repulsion up to the hard-sphere diameter d , i.e., as long as $r \leq d$, $w(r) = \infty$. If $r > d$, the intermolecular potential $w(r) = -\epsilon \left(\frac{d}{r}\right)^6$, where ϵ is the value of $w(r)$ at closest approach, shown schematically in Fig 1.3.

From the van der Waals expression for the attractive pressure of Eq. 1.7, we find as an estimate for the interfacial tension, using Eq. 1.6 and Eq. 1.8 with $w(r) = -\epsilon \left(\frac{d}{r}\right)^6$,

$$\gamma \sim a \left(\frac{N}{V}\right)^2 d \sim \epsilon d^3 \left(\frac{1}{d^3}\right)^2 d = \frac{\epsilon}{d^2}. \quad (1.9)$$

This result can be interpreted as follows. By moving a molecule from bulk to the interface, approximately d^2 interfacial area is created for each intermolecular contact with energy ϵ that is lost in the bulk. The required (free) energy to create interface is therefore roughly $\gamma \sim \epsilon/d^2$. Substitution of experimentally obtained ϵ and d yields an estimate for the interfacial tension of 10 - 100 mN/m that is typical for simple liquids.

Example: interfacial tension of liquid Argon with its vapour

It follows from the Lennard-Jones potential of Argon that $\epsilon = 1.71 \cdot 10^{-21}$ J, $d = 0.342$ nm. Substitution in Eq. 1.9 gives as an estimate for the interfacial tension:

$$\gamma \approx \frac{1.65 \cdot 10^{-21}}{(0.34 \cdot 10^{-9})^2} = 14.6 \frac{\text{mN}}{\text{m}}$$

The value at the melting point of Argon at 1 atm ($T_m = 83,78$ K) experimentally observed is $\gamma_m = 13.4$ mN/m. The estimate and the experimental values for the interfacial tension at the melting point, γ_m , for some other substances are given below .

		ϵ/k_B [K]	d [nm]	ϵ/d^2 [mN/m]	γ_m [mN/m]	T_m [K]
Argon	Ar	124	0.342	14.6	13.4	83.78
Benzene	C ₆ H ₆	440	0.527	21.9	30.7	278.6
Bromine	Br ₂	520	0.427	39.4	46.1	265.8
Helium	He ₂	10.2	0.258	2.1	0.36	0.8
Nitrogen	N ₂	91.5	0.368	9.3	12.1	63.29
Tetra	CCl ₄	327	0.588	13.1	32.1	250.2
Hydrogen	H ₂	33.3	0.297	5.2	3.0	14.01
Xenon	Xe	229	0.406	19.2	19.0	161.2
Oxygen	O ₂	113	0.343	13.3	21.8	54.8

Table 1.1: The interfacial tension of some liquids with their vapour (γ_{LG}) and water (γ_{SL}) at 20°C in mN/m.

	γ_{LG}	γ_{SL}		γ_{LG}	γ_{SL}
acetone	23.7	-	hexane	18.4	51.1
benzene	28.9	35.0	hexanol	24.8	6.8
cyclohexane	25	51	mercury	458	375
cyclohexanol	32	4	octane	21.8	50.8
ethanol	22.3	-	octanol	27.5	8.5
ethylether	17.01	10.7	tetra	26.8	45.1
			water	72.8	-

1.3 Position of the Gibbs dividing plane

In Section 1.1 we considered a two-phase system as two bulk volumes separated by a mathematical plane. In reality, however, there will be a smooth transition from concentrations c_i^α in one bulk phase to concentrations c_i^β in the other. A possible concentration profile is given in Fig. 1.4. We now have to *define* a mathematical plane separating the bulk phases. Bulk properties (such as concentrations) are extrapolated up to this chosen plane. In this way we assign an excess amount or deficit to the respective bulk phases. For instance, by extrapolating the concentration c_1^α

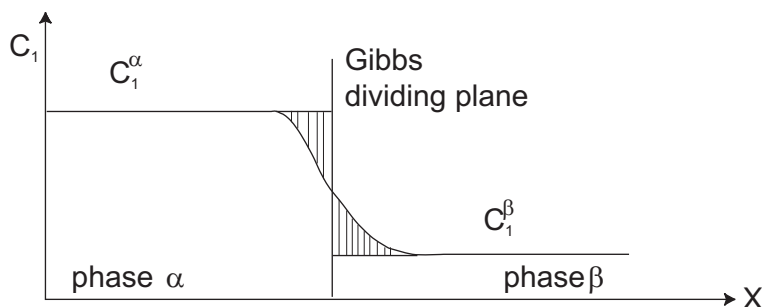


Figure 1.4: The concentration c_1 smoothly changes through the system. The Gibbs plane is assigned where there is no net adsorption at the interface of solvent ‘1’; the hatched areas are equal.

in Fig. 1.4 up to a certain plane, we assign the hatched area on the left as a surplus to phase α . Analogously, we endow phase β the right hatched area too little. The net excess at the interface is:

$$N_i^\sigma = N_i - \left(V^\alpha c_i^\alpha + V^\beta c_i^\beta \right). \quad (1.10)$$

The excess amounts of all components at the interface are established once a plane has been chosen and by that the volumes V^α and V^β are defined. A reasonable choice for the position of the interface is where the excess amount of the solvent vanishes. That is, denoting the solvent as ‘1’, where $N_1^\sigma = 0$. Consequently, from Fig. 1.10 it follows that V^α and V^β are given by:

$$N_1 = V^\alpha c_1^\alpha + V^\beta c_1^\beta = N_1^\alpha + N_1^\beta.$$

This position where there is no excess amount of solvent is the so-called *Gibbs dividing plane*.¹ The Gibbs dividing plane is graphically found where the hatched areas in Fig. 1.4 equal.

Using this choice for the position of the interface the adsorbed amounts N_i^σ of the components $i = 2, 3, \dots$ are found from Eq. 1.10. This can also be done graphically, as shown by the hatched areas in Fig. 1.5. If component i accumulates at the interface, positive adsorption is found, i.e. $N_i^\sigma > 0$. If a component prefers to reside in the solvent and depletes from the interface, we will have that $N_i^\sigma < 0$. This is referred to as negative adsorption.

1.4 Van der Waals theory of interfaces

The spatial dependence of the density profile between a gas and a liquid phase of a single component has first been described by Van der Waals², although its full impact has been acknowledged by Cahn and Hilliard only 65 year later³ for the interface in a phase-separated binary system. Below the critical temperature the

¹First published in *On the Equilibrium of Heterogeneous Substances*, the basis of modern physiscal chemistry, in: J.W. Gibbs, *Trans Conn Acad* **III**, 108–248 (1876), 343–524 (1878). Reprint in *The Scientific Papers*, Vol. 1 (OxBow Press, Woodbridge, 1993)

²J.D. van der Waals, *Verh K Ned Akad Wet Afd Natuurk* **1**, 8 (1893)

³J.W. Cahn en J.E. Hilliard, *J Chem Phys* **28**, 258 (1958)

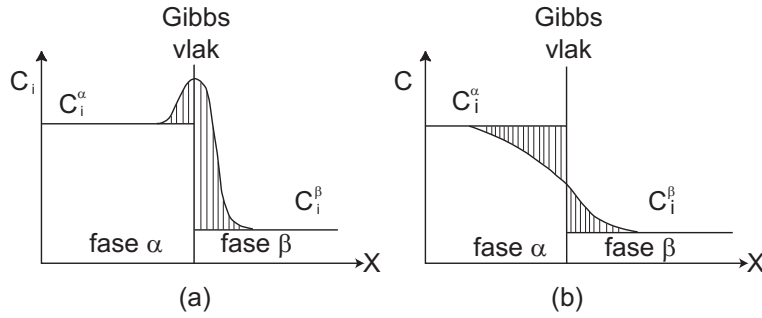


Figure 1.5: The concentration c_i changes smoothly through the system. By extrapolation of the bulk concentrations up to the Gibbs dividing plane, excess amounts of components i can be determined from the hatched areas. Thus we may find (a) positive adsorption ($n_i^\sigma > 0$) and (b) negative adsorption ($n_i^\sigma < 0$).

Helmholtz free energy per unit volume, $A/V = -P(\rho, T) + \mu(\rho, T)\rho$, displays a loop as a function of density $\rho \equiv N/V$. At a given temperature, the loop has a common tangent that connects two of its points. Thermodynamically this implies that these two points possess one common pressure (the intercept) and a common chemical potential (the slope), as indicated in Fig. 1.6a. That is, there is an equilibrium between a phase of a low density (ρ_g ; gas) with a phase of a high density (ρ_l ; liquid).

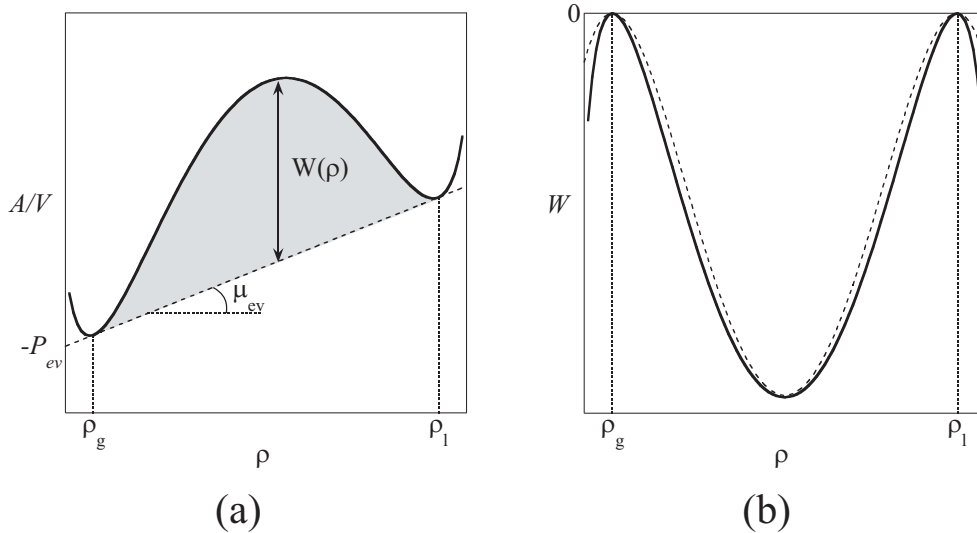


Figure 1.6: (a) The solid curve displays the Helmholtz free energy per unit volume as a function of density. From a common tangent (dashed line) the equilibrium between a gas (ρ_g) and a liquid (ρ_l) phase is found. The enclosed grey area is a measure of the interfacial tension. (b) The full curve is given by the difference $W(\rho)$ between the Helmholtz free-energy curve and the common tangent as a function of density. The dashed line follows from the model expression, Eq. 1.15.

As indicated in Fig. 1.6a, free energy per unit volume equal to $W(\rho)$ is gained when a system of density $\rho_g < \rho < \rho_l$ separates into a gas and liquid with densities ρ_g and ρ_l , respectively. An example of such a free energy gain at a given density is denoted by an arrow in Fig. 1.6a. The gain as a function of the density is given in Fig. 1.6b by the solid line.

The above is still bulk thermodynamics. Let us now pass through the interface between the gas and liquid phase. On every point z in the interface we have a local density $\rho(z)$. The local extra free energy density $\Psi(z)$ of that piece of the interface is not only given by the bulk term, $W[\rho(z)]$, but must also account for the inhomogeneity of the interface. Van der Waals did so by including a *squared gradient* term of the density

$$\Psi(z) = W[\rho(z)] + \frac{1}{2}m \left(\frac{d\rho(z)}{dz} \right)^2. \quad (1.11)$$

The density $\rho(z)$, in a mechanical analogue, can be considered as ‘position’ and the point z as ‘time’. Hence, the additional squared gradient term can be seen as a ‘kinetic energy’ required to pass through the interface. In this analogue W is the potential energy. A more formal derivation of the squared gradient term is possible starting from the contribution of a single molecule to the internal energy. Note that we applied a mean-field approximation since no correlations between the particles have been accounted for in Eq. 1.11.

We have shown in section 1.3 that the Gibbs dividing plane is an obvious choice for the interface in a one-component system, i.e., $N_i^\sigma = 0$. It then follows from Eq. 1.4 that the total Helmholtz free energy of the interface is given by $A^\sigma = \gamma\sigma$. However, it may also be found by integrating the excess free energy density over space: $A^\sigma = \int \Psi(r)d^3r$. It is readily seen that

$$\gamma = \int_{-\infty}^{\infty} \Psi(z)dz = \int_{-\infty}^{\infty} W[\rho(z)] + \frac{1}{2}m \left(\frac{d\rho(z)}{dz} \right)^2 dz. \quad (1.12)$$

The grey area in Fig. 1.6a is therefore a measure for the interfacial tension.

The equilibrium situation is where the Helmholtz free energy, and by that the interfacial work, is minimal. Hence, the equilibrium density profile $\rho(z)$ is the profile in $\Psi(z)$, Eq. 1.11, that minimizes the integral of Eq. 1.12. To calculate that profile, we consider how the interfacial tension responds to a small perturbation $\delta\rho(z)$ to the profile $\rho(z)$

$$\delta\gamma = \int_{-\infty}^{\infty} W[\rho + \delta\rho] + \frac{1}{2}m \left(\frac{d}{dz}(\rho + \delta\rho) \right)^2 dz - \int_{-\infty}^{\infty} W[\rho] + \frac{1}{2}m \left(\frac{d\rho}{dz} \right)^2 dz.$$

We dropped the explicit z -dependence of the density for convenience.

Considering $W[\rho]$ as a function of ρ rather than a functional, series expansion of $W[\rho + \delta\rho]$ up to second order in $\delta\rho$ yields

$$\delta\gamma = \int_{-\infty}^{\infty} \left\{ \left(\frac{dW}{d\rho} \right) \delta\rho + m \left(\frac{d\rho}{dz} \right) \left(\frac{d\delta\rho}{dz} \right) + O(\delta\rho^2) \right\} dz.$$

The second term in the integral can be rewritten by integration by parts as

$$\begin{aligned} \int_{-\infty}^{\infty} \frac{d}{dz} \left(\left(\frac{d\rho}{dz} \right) \delta\rho \right) dz &= \left(\frac{d\rho}{dz} \right) \delta\rho \Big|_{-\infty}^{\infty} = 0 \\ &= \int_{-\infty}^{\infty} \left(\frac{d^2\rho}{dz^2} \right) \delta\rho dz + \int_{-\infty}^{\infty} \left(\frac{d\rho}{dz} \right) \left(\frac{d\delta\rho}{dz} \right) dz, \end{aligned}$$

where we used the fact that the profile levels off in both phases (after all $\rho(z) = \rho_l$ and $\rho(z) = \rho_g$ for $z \rightarrow \pm\infty$), i.e. $d\rho/dz = 0$. Substitution into the variance of the interfacial tension gives

$$\delta\gamma \approx \int_{-\infty}^{\infty} \left\{ \left(\frac{dW}{d\rho} \right) - m \left(\frac{d^2\rho}{dz^2} \right) \right\} \delta\rho dz \equiv \int_{-\infty}^{\infty} \left(\frac{\delta\gamma[\rho]}{\delta\rho} \right) \delta\rho dz.$$

Here we introduced the functional derivative of the interfacial tension, $(\delta\gamma[\rho]/\delta\rho)$. We are looking for the profile that minimizes the interfacial tension, i.e., the profile with the property that the first (functional) derivative vanishes. Hence, the density profile is found from the condition

$$\left(\frac{dW}{d\rho} \right) = m \left(\frac{d^2\rho}{dz^2} \right). \quad (1.13)$$

The mechanical analogue of this Eq. is Newton's law stating that the force equals the derivative of the potential with respect to position.

Multiplying both sides of Eq. 1.13 by the density gradient yields

$$\left(\frac{dW}{d\rho} \right) \left(\frac{d\rho}{dz} \right) = m \left(\frac{d^2\rho}{dz^2} \right) \left(\frac{d\rho}{dz} \right) \Leftrightarrow \left(\frac{dW}{dz} \right) = \frac{1}{2} m \frac{d}{dz} \left(\frac{d\rho}{dz} \right)^2.$$

Since this is generally valid, the arguments of the differential operators must be equal. Alternatively, intergrating using $W[\rho_l] = W[\rho_g] = \left(\frac{d\rho}{dz} \right)_{z \rightarrow -\infty} = \left(\frac{d\rho}{dz} \right)_{z \rightarrow \infty} = 0$ gives

$$W = \frac{1}{2} m \left(\frac{d\rho}{dz} \right)^2. \quad (1.14)$$

Hence, the equilibrium profile is found when the 'potential energy' balances the de 'kinetic energy'.

An explicit density profile can only be obtained from the differential equation Eq. 1.14 if W is known. In general, the free energy density must display a loop below the critical temperature, as illustrated in Fig. 1.6a. The distance to the common tangent W vanishes by definition at the extremes ρ_g and ρ_l . A minimum should always be present in between, as demonstrated by the solid line in Fig. 1.6b. To a good approximation, W will be a fourth order polynomial around the equilibrium densities

$$W(\rho) = \frac{1}{4} B (\rho_l - \rho)^2 (\rho - \rho_g)^2. \quad (1.15)$$

The constant B determines the depth of the loop. The dashed line in Fig. 1.6b shows that this is indeed a fair approximation to W . Upon approaching the critical point B decreases and so does $\rho_l - \rho_g$.

Substitution of Eq. 1.15 into the equilibrium condition, Eq. 1.14, yields

$$\frac{d\rho}{dz} = \sqrt{\frac{B}{2m}} (\rho_l - \rho) (\rho - \rho_g).$$

Introducing the profile thickness ξ (verify this has the units of length)

$$\xi \equiv \sqrt{\frac{2m}{B} \frac{1}{\rho_l - \rho_g}}, \quad (1.16)$$

we find after separation of variables

$$\frac{1}{(\rho_l - \rho)(\rho - \rho_g)} d\rho = \frac{1}{\xi(\rho_l - \rho_g)} dz.$$

integration gives

$$\frac{1}{(\rho_l - \rho_g)} \ln \frac{\rho - \rho_g}{\rho_l - \rho} = \frac{z}{\xi} \frac{1}{(\rho_l - \rho_g)} + C.$$

The integration constant C is found from symmetry considerations. At the Gibbs dividing plane ($z = 0$) we are exactly in between both phases, i.e., $\rho = (\rho_l + \rho_g)/2$. This boundary condition yields $C = 0$ and therefore

$$\ln \frac{\rho - \rho_g}{\rho_l - \rho} = \frac{z}{\xi}. \quad (1.17)$$

From Eq. 1.17 we know the position as a function of the density. Inverting this Eq. gives

$$\rho = \frac{\rho_l e^{z/\xi} + \rho_g}{1 + e^{z/\xi}}.$$

Although the density is now known as a function of position, it is instructive to rewrite the equation. To that end, we multiply both numerator and denominator by $e^{-z/2\xi}$ to obtain

$$\rho = \frac{\rho_l e^{z/2\xi} + \rho_g e^{-z/2\xi}}{e^{-z/2\xi} + e^{z/2\xi}} = \frac{\frac{1}{2}(\rho_l + \rho_g)(e^{z/2\xi} + e^{-z/2\xi}) + \frac{1}{2}(\rho_l - \rho_g)(e^{z/2\xi} - e^{-z/2\xi})}{e^{z/2\xi} + e^{-z/2\xi}}.$$

The density at the interface ($z = 0$) is immediately recovered. Using $\tanh x \equiv (e^x - e^{-x})/(e^x + e^{-x})$, we finally arrive at

$$\rho(z) = \frac{1}{2}(\rho_l + \rho_g) + \frac{1}{2}(\rho_l - \rho_g) \tanh\left(\frac{z}{2\xi}\right). \quad (1.18)$$

This is the famous van der Waals density-profile for two coexisting phases, where ξ is a measure for the profile thickness. Far from the critical point the profile thickness is typically on the order of a molecular diameter and may be determined experimentally from ellipsometry. In the vicinity of the critical point the density difference between gas and liquid becomes increasingly smaller and the free energy loop flattens ($\rho_l - \rho_g$ and B decrease). Hence, from Eq. 1.16 it follows that the profile thickness increases and eventually diverges. A typical density profile is given in Fig 1.7 for the system of Fig. 1.6.

1.5 Gibbs adsorption equation

In order to derive the Gibbs adsorption equation, we consider an infinitesimal change in the excess internal energy dU^σ ,

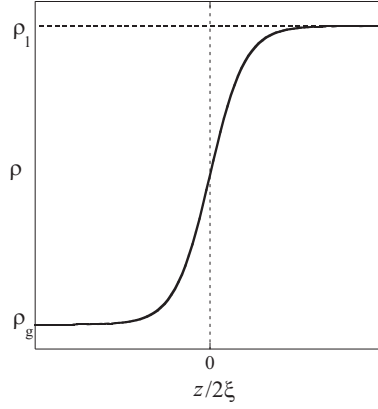


Figure 1.7: The van der Waals density-profile $\rho(z)$ from Eq. 1.18 for inhomogeneous systems, e.g., a gas and a liquid. The profile thickness is determined by ξ from Eq. 1.16.

$$dU^\sigma = \gamma d\sigma + T dS^\sigma + \sum_i \mu_i dN_i^\sigma. \quad (1.19)$$

We may also write Eq. 1.19 as

$$dU = \left(\frac{\partial U}{\partial S} \right)_{\sigma, \{N_i\}} dS + \left(\frac{\partial U}{\partial \sigma} \right)_{S, \{N_i\}} d\sigma + \sum_i \left(\frac{\partial U}{\partial N_i} \right)_{S, \sigma, \{N_{j \neq i}\}} dN_i. \quad (1.20)$$

Where we dropped the superscripts σ for convenience. The Euler theorem for homogeneous functions of the first degree reads

$$f(x_1, x_2, \dots, x_n) = \sum_{i=1}^n \left(\frac{\partial f}{\partial x_i} \right)_{\{x_{j \neq i}\}} x_i, \quad (1.21)$$

so it must be that $U = TS + \gamma\sigma + \sum_i \mu_i N_i$, and

$$dU = T dS + S dT + \gamma d\sigma + \sigma d\gamma + \sum_i \mu_i dN_i + \sum_i N_i d\mu_i. \quad (1.22)$$

Comparing Eqs. 1.20 and 1.19 to Eq. 1.22 and putting the superscripts σ back where appropriate leads to the *Gibbs-Duhem equation* for the surface

$$S^\sigma dT + \sigma d\gamma + \sum_i N_i^\sigma d\mu_i = 0 \quad (1.23)$$

By choosing the interface at the Gibbs dividing plane of the solvent ($N_1^\sigma = 0$), we may write Eq. 1.23 as

$$(d\gamma)_T = - \sum_{i>1} \Gamma_i^{(1)} d\mu_i. \quad (1.24)$$

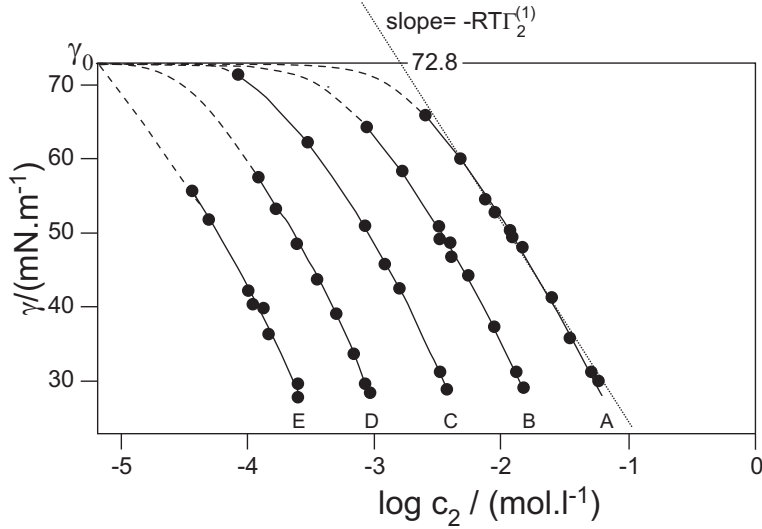


Figure 1.8: The measured interfacial tension of a water surface changes with (the logarithm of) the concentration of alifatic alcohols A, B, C, D en E. The adsorption density can be determined from the slope.

This is the *Gibbs adsorption-equation*⁴, where we implicitly defined the adsorption density of component i as

$$\Gamma_i^{(1)} \equiv \frac{N_i^\sigma}{\sigma} = - \left(\frac{\partial \gamma}{\partial \mu_i} \right)_{T, \mu_{j \neq i}} . \quad (1.25)$$

The superscript (1) indicates that the adsorption density is determined relative to the Gibbs dividing plane defined by a vanishing adsorption density of component (1). The last term in Eq. 1.25 is found from the total differential Eq. 1.24. According to Eq. 1.25 the interfacial tension will decrease upon positive adsorption of component i ($\Gamma_i^{(1)} > 0$). In the case of negative adsorption ($\Gamma_i^{(1)} < 0$) the interfacial tension will increase.

For dilute ideal mixtures we may write for the dissolved component

$$\mu_2 = \mu_2^0 + RT \ln c_2.$$

Substitution into Eq. 1.25 yields

$$\left(\frac{\partial \gamma}{\partial \ln c_2} \right)_T = -RT\Gamma_2^{(1)} \quad (1.26)$$

From this equation the adsorption density can be determined experimentally. This is demonstrated in Fig. 1.8 for the measured interfacial tension of five different alifatic alcohols on water against (the logarithm of) the concentration. For very low concentrations the interfacial tension is equal to that of pure water $\gamma_0 = 72.8$ mN/m.

For dilute systems the adsorption density will be proportional to the concentration of dissolved material

⁴J.W. Gibbs, Trans Conn Acad **III**, 108–248 (1876), 343–524 (1878)

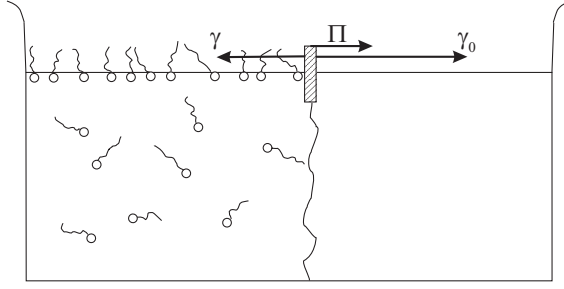


Figure 1.9: The positively adsorbed molecules lower the interfacial tension γ as compared to that of the pure solvent, γ_0 . Consequently, a surface pressure $\Pi = \gamma_0 - \gamma$ acts on the movable barrier.

$$\Gamma_2^{(1)} = Bc_2. \quad (1.27)$$

Substitution into Eq. 1.26 gives

$$\left(\frac{\partial \gamma}{\partial c_2} \right)_T = -RTB.$$

Integration from zero adsorption ($c_2 = 0$, $\gamma = \gamma_0$) to finite adsorption leads to

$$\gamma - \gamma_0 = -RTBc_2 = -RT\Gamma_2^{(1)} = -RT \frac{N_2^\sigma}{\sigma}. \quad (1.28)$$

This eq. is the two-dimensional analogue of the ideal gas law $P = RT \frac{n}{V}$. Here $\Pi \equiv \gamma_0 - \gamma$ is the *surface pressure*: the force per unit length, due to the adsorbed molecules, that act on a barrier. This is shown schematically in Fig. 1.9.

For higher concentrations the adsorption density will no longer be proportional to c_2 , as can be seen in Fig. 1.8. Higher adsorption densities often obey the Langmuir adsorption equation

$$\Gamma_2^{(1)} = \Gamma_m \frac{Kc_2}{1 + Kc_2}, \quad (1.29)$$

where Γ_m is the maximal adsorption density at the surface and $K\Gamma_m = B$ the proportionality constant of Eq. 1.27. Upon substitution in Eq. 1.26 and integration from ($c_2 = 0$, $\gamma = \gamma_0$) to (c_2 , γ), the surface pressure now reads

$$\gamma_0 - \gamma = RT\Gamma_m \ln(1 + Kc_2) \quad (1.30)$$

This equation was found empirically by Von Szyszkowski in 1908. Using the Langmuir adsorption equation, Eq. 1.29, this can be rewritten as

$$\gamma_0 - \gamma = -RT\Gamma_m \ln \left(1 - \frac{\Gamma_2^{(1)}}{\Gamma_m} \right) \quad (1.31)$$

This is the so-called Frumkin equation. The maximum adsorption density can be found by measuring the surface tension as a function of concentration of the dissolved material using the above equations.

Note that for low concentrations ($\Gamma \ll \Gamma_m$) series expansion gives $\ln\left(1 - \frac{\Gamma_2^{(1)}}{\Gamma_m}\right) \approx -\frac{\Gamma_2^{(1)}}{\Gamma_m}$. Substitution in the Frumkin equation, Eq. 1.31, recovers the two-dimensional equivalent of the ideal gas law, Eq. 1.28.

1.6 Problems

1. Consider an intermolecular potential of the form $w(r) = -\epsilon\left(\frac{d}{r}\right)^n$. Show that for $n > 3$, we always have $\gamma \sim \frac{\epsilon}{d^2}$. What happens if $n \leq 3$?
2. Show that for a bulk, one-component system the Gibbs-Duhem relation reads $SdT - Vdp + Nd\mu = 0$, and that $(dp)_T = \rho(d\mu)_T$, with $\rho = N/V$.
3. Measuring the interfacial tensions at 20°C of a series of aqueous solutions of a surface-active agent A yields the following results

[A] [mol/dm ³]	0	0.10	0.20	0.30	0.40	0.50
γ [mN/m]	72.8	70.2	67.7	65.1	62.5	59.5

- a. Determine the adsorption density and surface pressure of the surface active agent at the given concentrations.
 - b. Does the two-dimensional equivalent of the ideal gas law apply to the data?
4. Derive the Langmuir adsorption equation, Eq. 1.29 from equilibrium considerations. To that end, note that the adsorption of (initially) dissolved molecules B at the surface of a solvent A can be considered as an exchange equilibrium, represented as $A_{\text{ads}} + B_{\text{dis}} \rightleftharpoons A_{\text{dis}} + B_{\text{ads}}$, and that the equilibrium constant for this ‘reaction’ can be written as

$$K = \frac{N_{\text{B}}^{\sigma}}{N_{\text{A}}^{\sigma}c_{\text{B}}} = \frac{\Gamma_{\text{B}}}{\Gamma_{\text{A}}c_{\text{B}}}. \quad (1.32)$$

Further, consider a maximum adsorption density, i.e., if every position at the interface is taken by either a solvent molecule A or a dissolved molecule B, the total or maximum adsorption density reads

$$\Gamma_m = \Gamma_{\text{A}} + \Gamma_{\text{B}}. \quad (1.33)$$

What are the assumptions / approximations made?

5. A simple way of looking at so-called *hydrophobic interactions* is by considering objects with hydrophobic surfaces that float around in water. The surface tension between the objects and water is γ .

- a. Prove that if two of these objects stick, the gain in free energy will be $w \approx -2\gamma\sigma_{\text{overlap}}$. Here, σ_{overlap} is the contact area between the objects, i.e., the surface area shielded from water.
- b. It is often found that the strength of the hydrophobic interactions *increases* with temperature, i.e., w gets more negative upon increasing temperature. Assuming that σ_{overlap} is independent of temperature, identify the thermodynamic property of the surface that is responsible for this remarkable temperature dependence. Hint: expand γ around a reference temperature.

Chapter 2

Surfactants and Micelles

2.1 Introduction: surfactants

An important type of molecules that adsorb positively at (water-air or water - oil) interfaces are so-called surface-active agents or briefly *surfactants*. The common characteristic of these materials is that their molecules consist of a polar ‘head’ (hydrophilic part) and a hydrocarbon ‘tail’ (hydrophobic part), as schematically depicted in Fig. 2.1. The amphipolar nature of surfactants makes them adsorb positively at relatively low surfactant concentrations.

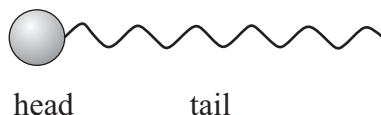


Figure 2.1: The common characteristic of surface active agents, or briefly surfactants, is that they consist of a polar ‘head’ and a hydrocarbon ‘tail’.

Depending on their chemical structure and properties of the head group, a surfactant is called anionic, cationic, amphoteric, or non-ionic.

Classical ‘soaps’ are a well-known example of anionic surfactants. These soaps are usually sodium or potassium salts of fatty acids (carboxylates) with a chain length of typically 10 to 20 hydrocarbon groups; $RCOO^-M^+$, for instance sodium laurate, $C_{11}H_{23}COO^-Na^+$. With increasing tail length, the solubility in water decreases and hence the surface activity increases.

In the case of cationic surfactants, the soap is a cation, i.e., the headgroup is positively charged. Examples are tetra-alkyl ammonium salts such as cetyltrimethyl ammonium bromide (CETAB).

Surfactants containing head groups that have both positive and negative sites are referred to as amphoteric. These surfactants are well-miscible with all other type surfactants and less antagonizing for skin and eyes. Therefore they are frequently encountered in cosmetics. Typical examples are the betaines.

The remaining approximately 21% of the total of surfactants are comprised by non-ionic surfactants. The head group of this type does not contain charges but has a propensity to forming hydrogen bonds. They are well-miscible with all other types of surfactants.

An important class of non-ionic surfactants are the poly(glycol ethers), $R - O(C_2H_4O)_nH$, or C_mE_n . The hydrocarbon tail R is usually linear and is abbreviated as C_m . The ethylene oxide head-group is frequently denoted as E_n . For small head-groups ($n = 1 - 6$) these surfactants are frequently applied as oil/water emulsifiers. Intermediate ethylene oxide head-group ($n = 6 - 15$) are found in detergents, whereas large head-groups ($n > 15$) in special emulsifiers.

Positive adsorption at interfaces decreases the interfacial tension as dictated by the Gibbs adsorption equation. However, beyond a certain surfactant concentration, the critical micelle concentration (cmc), the interfacial tension remains more or less constant. The situation has been shown schematically in Fig. 2.2.

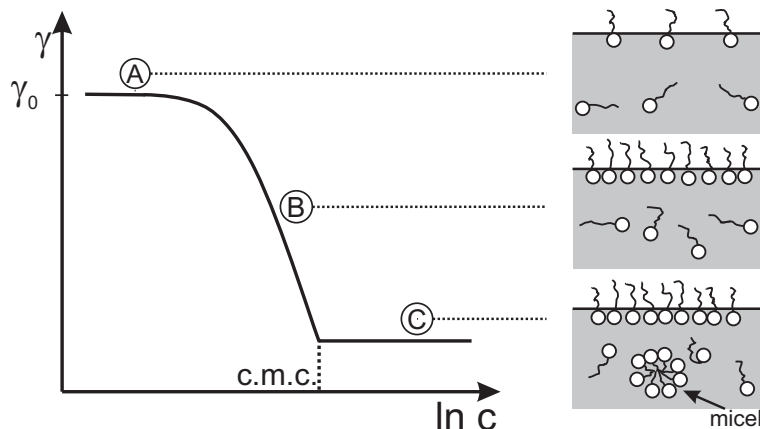


Figure 2.2: Characteristic change of the interfacial tension as a function of surfactant concentration. The dashed vertical line indicates the critical micelle concentration, cmc.

2.2 Micelles: The critical micelle concentration (cmc)

In this treatment I will follow Debye, [1]. Forming a micelle containing n surfactant monomers can be described as the equilibrium



In the above equilibrium, A stands for surfactant monomers and A_n for a surfactant aggregate (micelle) containing n surfactant molecules. Typically the value of n is 50-100 for spherical micelles. Now Debye's arguing goes as follows. Define the equilibrium constant as

$$K = \frac{x_n}{x_1^n} \quad (2.2)$$

where x_1 is the concentration (molefraction) surfactant monomers, and x_n the concentration (molefraction) micelles. In general the dimension of the equilibrium constant as defined by eq. 2.2 is *concentration*⁽¹⁻ⁿ⁾. We use this dimensional argument to *define* the concentration

$$x_0 = K^{\frac{1}{1-n}} \quad (2.3)$$

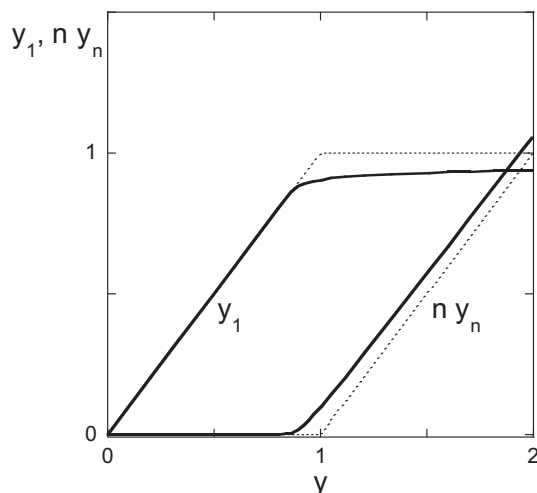


Figure 2.3: Iterative solution of Eq. 2.5. The surfactant concentration y_1 and the micelle concentration ny_n with $n = 65$ as a function of the total surfactant concentration, y , in the system, in reduced units. Below the c.m.c. ($y = 1$) micelles are barely present, whereas above the c.m.c. the monomer concentration is virtually constant. The dashed lines represent the limiting case for $n \rightarrow \infty$, given by Eq. 2.6

Now the total concentration of surfactant molecules in the system is the sum of monomeric surfactant molecules, and surfactant molecules in the form of micelles. In other words, the total surfactant concentration, x , follows by *mass conservation*

$$x = x_1 + nx_n \quad (2.4)$$

Writing $x_n = x_1^n K = x_1^n / x_0^{n-1}$, and defining the reduced concentrations $y = x/x_0$, $y_1 = x_1/x_0$, and $y_n = x_n/x_0$ eq. 2.4 becomes

$$y = y_1 + ny_1^n \quad (2.5)$$

with the typical values of $n \sim 50 - 100$, Eq. 2.5 can only be solved iteratively. It can be verified from eq. 2.5, that with typical values of n stated above, we have

$$y_1 \begin{cases} = y, & \text{if } y < 1; \\ \approx 1, & \text{if } y > 1. \end{cases} \quad (2.6)$$

The results of a numerical calculation using $n = 65$ has been shown in Fig. 2.3.

The crossover from the behaviors described by eq. 2.6 occurs around $y=1$, as can be seen in Fig. 2.3. The value of $y=1$, therefore, corresponds to a *critical point*. $y = 1$ implies that $x = x_0$. Therefore, x_0 is defined as the *critical micelle concentration*. As long as $x < x_0$, all surfactant is present in the form of monomers. But if $x > x_0$, micelles are being formed; the monomer (x_1) concentration remaining (almost) constant.

2.3 Thermodynamics of micelle formation

In section 2.2 we presented a *phenomenological* description: we *presumed* that micelles of size n form, and subsequently studied their properties. We now address the question: what is the thermodynamic condition for the formation of micelles of size n ? We return to eq. 2.1, but leave the value of n unspecified. We address the question as to what the size distribution of micelles is, on the basis of thermodynamics. The general thermodynamic condition for chemical equilibrium is

$$\sum_i \nu_i \mu_i = 0, \quad (2.7)$$

where ν_i are the stoichiometric coefficients and μ_i the chemical potentials. Applying eq. 2.7 to the equilibrium 2.1 we get

$$\mu_n = n\mu_1 \quad (2.8)$$

In this equation, the subscripts 1 and n again refer to surfactant monomers, and micelles consisting of n surfactant molecules, respectively. As long as monomers and micelles are dilute, we may write the chemical potentials as

$$\mu_i = \mu_i^0 + kT \ln x_i \quad (2.9)$$

where μ_i^0 is the standard chemical potential ($\mu_i = \mu_i^0$ iff $x_i = 1$), k and T are Boltzmann's constant and absolute temperature, and i in this case can be monomer ($i = 1$) or micelle (n mer: $i = n$). Combining eqs. 2.8 and 2.9 leads to the distribution of micelles of size n

$$x_n = x_1^n \exp\left(\frac{-(\mu_n^0 - n\mu_1^0)}{kT}\right) \quad (2.10)$$

First of all, note that the cmc is related to the above expression by (compare with eqs. 2.2 and 2.3

$$x_0 \equiv x_{cmc} = K^{1/(1-n)} = \exp\left(\frac{\mu_n^0 - n\mu_1^0}{(n-1)kT}\right) \quad (2.11)$$

In order for the system to have a cmc of $x_0 < 1$ (note that $x_0 > 1$ is *unphysical*; in that case there will be no cmc at all), it follows from Eq. 2.11 that there must be a value of n , or a range of values, such that

$$\mu_n^0 < n\mu_1^0 \quad (2.12)$$

In other words, for micelles of size n to form, it follows from eq. 2.10 that the function $\frac{\mu_n^0 - n\mu_1^0}{kT}$ should have a (deep) minimum at n .

2.4 Influence of molecular properties of the surfactant on the cmc

First of all we write the argument of the exponent in Eq. 2.11 as

$$\frac{\mu_n^0 - n\mu_1^0}{(n-1)} \equiv \Delta\mu^\theta = (\Delta\mu^\theta)_{\text{head}} + (\Delta\mu^\theta)_{\text{tail}}. \quad (2.13)$$

In order to form micelles it is required that $\Delta\mu^\theta < 0$, as has been discussed below Eq. 2.11. The head groups will be closely packed upon micelle formation, which is in general unfavorable compared to the situation where surfactant molecules are monomers. We may therefore expect $(\Delta\mu^\theta)_{\text{head}} > 0$. The packing will be favorable for the hydrophobic tails and hence $(\Delta\mu^\theta)_{\text{tail}} < 0$. Since micelle formation requires $\Delta\mu^\theta < 0$, we find $|(\Delta\mu^\theta)_{\text{tail}}| > |(\Delta\mu^\theta)_{\text{head}}|$.

Despite the vast amount of literature on the calculation of $\Delta\mu^\theta$, we restrict ourselves to observed trends in c.m.c. and the subsequent conclusions for $(\Delta\mu^\theta)_{\text{head}}$ and $(\Delta\mu^\theta)_{\text{tail}}$.

2.4.1 Influence of chain length on cmc

Upon increasing chain length, it is expected that $(\Delta\mu^\theta)_{\text{tail}}$ gets more negative and the critical micelle concentration decreases. Experimental values in Table 2.1 confirm this expectation. The cmc is lowered by roughly a factor of 2 for each added CH_2 -group in anionic surfactants. According Eq. 2.11 this implies that $\Delta\mu^\theta$ decreases by (per mole!) $RT \ln 2 \approx 1.72 \text{ kJ/mole}$ per added CH_2 -group. The critical micelle concentration decreases stronger for non-ionic surfactants for each additional CH_2 -group; roughly a factor of 3. This in turn implies that $\Delta\mu^\theta$ decreases approximately 2.72 kJ/mol for each additional CH_2 tail-unit .

Table 2.1: The c.m.c. and $\Delta\mu^\theta = RT \ln x_{\text{cmc}}$ of four types of surfactants as a function of the number of C-atoms n_C in the alkyl tail at 298 K.

	R	c_{cmc} [mol/l]	x_{cmc}	$\Delta\mu^\theta$ [kJ/mol]
$RCOO^-Na^+$: $\Delta\mu^\theta = 0.65 - 1.66n_C \text{ kJ/mol}$	C_{12}	2.3×10^{-2}	4.2×10^{-4}	-19.3
	C_{14}	6.0×10^{-3}	1.1×10^{-4}	-22.5
	C_{16}	1.5×10^{-3}	2.7×10^{-5}	-26.0
	C_{18}	4.0×10^{-4}	7.3×10^{-6}	-29.2
$ROSO_3^-Na^+$: $\Delta\mu^\theta = -1.35 - 1.70n_C \text{ kJ/mol}$	C_8	1.3×10^{-1}	2.3×10^{-3}	-15.0
	C_{10}	3.3×10^{-2}	6.0×10^{-4}	-18.3
	C_{12}	8.3×10^{-3}	1.5×10^{-4}	-21.7
	C_{14}	2.1×10^{-3}	3.8×10^{-5}	-25.2
$R(CH_3)_3N^+Br^-$: $\Delta\mu^\theta = 0.59 - 1.74n_C \text{ kJ/mol}$	C_{10}	6.5×10^{-2}	1.1×10^{-3}	-16.8
	C_{12}	1.6×10^{-2}	2.9×10^{-4}	-20.2
	C_{16}	9.2×10^{-4}	1.7×10^{-5}	-27.2
$R - .O(C_2H_4O)_6.H (C_{n_C}E_6)$: $\Delta\mu^\theta = 0.40 - 2.80n_C \text{ kJ/mol}$	C_8	7.6×10^{-3}	1.4×10^{-4}	-22.0
	C_{10}	8.0×10^{-4}	1.4×10^{-5}	-27.6
	C_{12}	8.3×10^{-5}	1.5×10^{-6}	-33.2
	C_{14}	8.7×10^{-6}	1.6×10^{-7}	-38.8

The change in standard chemical potential of a surfactant with tail length n_c can according to the experimental results be described empirically by the Klevens equation [2]

$$\Delta\mu^\theta = RT \ln x_{\text{cmc}} = A - Bn_c \quad (2.14)$$

The value of A is dominated by the nature of the head group. Generally one finds $-3.1 < A < +3.7$ kJ/mol. B values are typically found in the range $1.5 < B < 2.9$ kJ/mol. The Klevens equation for some characteristic examples is given in the left column of Table 2.1.

The Klevens equation, 2.14, only holds for $n_C \lesssim 16$, presumably because for larger tail lengths the alkyl tail will fold to prevent hydrophobic interactions. On the other hand, $n_C \gtrsim 8$ to have enough thermodynamic driving force for micelle formation, i.e., $|(\Delta\mu^\theta)_{\text{tail}}| > |(\Delta\mu^\theta)_{\text{head}}|$.

2.4.2 Effect of salt on the cmc

We expect $(\Delta\mu^\theta)_{\text{head}} > 0$ as a consequence of the interactions between charged or polar head-groups. The charges of the head groups are screened by the addition of an indifferent salt which decreases the interactions between the head groups. Therefore, we expect $(\Delta\mu^\theta)_{\text{head}}$ to decrease upon increasing electrolyte concentration. From Table 2.2 it is verified that this is indeed the case.

Table 2.2: The c.m.c. and $\Delta\mu^\theta = RT \ln x_{\text{cmc}}$ of sodium octyl sulphate, $\text{H}(\text{CH}_2)_8\text{OSO}_3^- \text{Na}^+$, as a function of salt concentration at 298 K.

	c_{cmc} [mol/l]	x_{cmc}	$\Delta\mu^\theta$ [kJ/mol]
water	0.134	2.4×10^{-3}	-14.9
water + 0.01 mol NaCl/l	0.121	2.2×10^{-3}	-15.2
water + 0.03 mol NaCl/l	0.102	1.8×10^{-3}	-15.6
water + 0.1 mol NaCl/l	0.069	1.2×10^{-3}	-16.6
water + 0.3 mol NaCl/l	0.035	6.3×10^{-4}	-18.3

The critical micelle concentration as a function of salt concentration generally depends on the valence of the added ions, in particular that of the counter ions. Addition of salt increases the sensitivity of the cmc with increasing tail-length. That is, the cmc decreases steeper with longer carbon tails and, at very high ionic strength, may even resemble the behaviour of non-ionic surfactants. There is almost no influence of salt on the critical micelle concentration of non-ionic surfactants.

2.5 Geometry of surfactant molecules and micellar shape.

What is the physical origin of the minimum of the function $\Delta\mu^\theta$ as a function of n in eqs. 2.11, 2.13? Note that the quantity $\Delta\mu^\theta$ equals the difference in Gibbs free energy of a molecule inside a micelle containing n surfactant molecules, and a freely moving surfactant monomer. Thus, the position of the minimum suggests that at that particular value of n , the surfactant molecules are most comfortably packed in a micelle. This suggests that the geometry of surfactant molecules the relative size of their headgroups, the lengths of their hydrophobic tails, may have something to do with it. Indeed, packing cones in the form of a sphere will naturally lead to a

number of cones that are close packed in a sphere. Squeezing in more cones than the number corresponding to close packing will lead to repulsion, and the function $\Delta\mu^\theta$ will rise with n . Other shapes of the surfactant molecules will lead to different structures of the aggregates. See Fig 2.4, taken from Ref. [3]. Referring to this Figure, we will now derive the geometrical conditions (on surfactant molecules) for aggregate shapes.

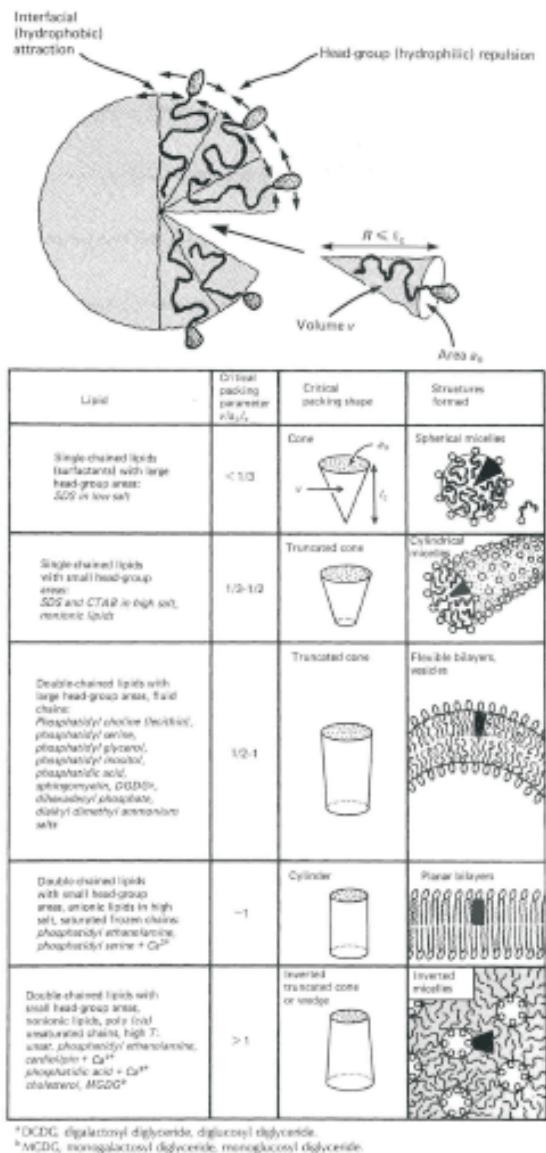


Figure 2.4: Relation between surfactant parameter and micelle shape - from Ref [3]

The three geometrical parameters defined in Fig. 2.4 are the effective molecular headgroup area a_0 , the effective length of the hydrophobic tail l_0 , and the effective volume of the surfactant molecule, v_0 . Note that these parameters are not fixed for a certain surfactant molecule: they depend on conditions such as the ionic strength and temperature. That particularly applies to a_0 : this quantity includes the effect of the electrical double layer around the headgroup (if the headgroup is charged)

We start with the condition for spherical micelles: In that case the volume V_m and surface area A_m of a micelle of radius R are

$$V_m = \frac{4\pi}{3}R^3 = nv_0 \quad A_m = 4\pi R^2 = na_0 \quad (\text{spherical micelle}) \quad (2.15)$$

From eq. 2.15 we may write n in two ways as

$$n = \frac{4\pi}{3v_0}R^3 = \frac{4\pi}{a_0}R^2 \quad (\text{spherical micelle}) \quad (2.16)$$

The above eq. is true iff

$$R = \frac{3v_0}{a_0} \quad (\text{spherical micelle}) \quad (2.17)$$

Since obviously, we also have that $R \leq \ell_0$, we arrive at the geometrical condition for spherical micelles

$$\frac{v_0}{a_0\ell_0} < \frac{1}{3} \quad (\text{spherical micelle}) \quad (2.18)$$

The quantity $\frac{v_0}{a_0\ell_0}$ is often referred to as the surfactant parameter. The number of surfactant molecules in a micelle can now be estimated by $n = \frac{36\pi v_0^2}{a_0^3} = \frac{4\pi\ell_0^3}{3v_0}$. For the surfactant sodium dodecyl sulfate (SDS), the values of ℓ_0 and v_0 are approximately 1.93 nm and 0.4 nm^3 , respectively [3], leading to $n \approx 75$ being in fair agreement with experiments.

Now lets investigate the condition for cylindrical micelles. For a cylinder of radius R and length L we have

$$V_m = \pi R^2 L = nv_0 \quad A_m = 2\pi R L = na_0 \quad (\text{cylindrical micelle}) \quad (2.19)$$

By the same reasoning as in the case of spherical micelles we arrive at the condition $R = 2v_0/a_0$. Using again that $R \leq \ell_0$, we get $\frac{v_0}{a_0\ell_0} < \frac{1}{2}$. Combination with the condition for spherical micelles, eq. 2.18 finally gives

$$\frac{1}{3} < \frac{v_0}{a_0\ell_0} < \frac{1}{2} (\text{cylindrical micelle}) \quad (2.20)$$

Micelles also come in plate shapes; in that case we have, for plates with thickness d and interfacial area A

$$V_m = Ad = nv_0 \quad A_m = 2A = na_0 \quad (\text{plates}) \quad (2.21)$$

So in case of plates we get $d = 2v_0/a_0 < 2\ell_0$, so that

$$\frac{1}{2} < \frac{v_0}{a_0\ell_0} < 1 (\text{plates}) \quad (2.22)$$

Finally, it is easy to see that the condition for *inverse micelles* is that $\frac{v_0}{a_0\ell_0} > 1$.

2.6 Problems

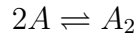
1. Caloric experiments show that the cmc is almost independent of temperature (typically $|\frac{d \ln x_{cmc}}{dT}| \approx 10^{-3} \text{ K}^{-1}$). Is micelle formation an enthalpically or entropically dominated process?

Hint: Make use of the relation between $\Delta\mu^\theta$ and x_{cmc} as well as Tables 2.1 and 2.2. Use (and verify if it looks alien to you) the thermodynamic relation

$$\left(\frac{\partial \Delta\mu^\theta / T}{\partial T}\right)_p = -\frac{\Delta h^\theta}{T^2},$$

where Δh^θ is the molar enthalpy of micelle-formation.

2. Consider the formation of dimers from single molecules via



Let the total mole fraction be x , the monomer mole fraction x_1 , and the dimer mole fraction x_2 .

a. Show that at equilibrium, $x_2 = x_1^2 \exp(-\Delta\mu^0/kT)$. Here, $\Delta\mu^0 = \mu_2^0 - 2\mu_1^0$, with μ_i^0 the standard chemical potential of $i \in \{1, 2\}$.

b. Show that for small x (more specifically: $x e^{-\Delta\mu^0/kT} \ll 1$), $x_1 = x$. Also show that for large x (more specifically: $x e^{-\Delta\mu^0/kT} \gg 1$), $x_1 \propto \sqrt{x}$. Hint: use mass conservation.

c. How does the behavior under b. compare to the the formation of surfactant micelles?

Chapter 3

Microemulsions

3.1 Introduction

Microemulsions are thermodynamically stable mixtures of oil and water. The stability is due to the presence of fairly large amounts (several %) of surfactants. Microemulsions are often transparent, but scattering of light, X-rays, etc. indicate that oil and water are not molecularly dispersed, but are more coarsely mixed. By coarse in this case we mean that oil and water are present in domains of a few to over a hundred nanometers in size. A schematic view of microemulsion droplets is provided by Fig. 3.1.

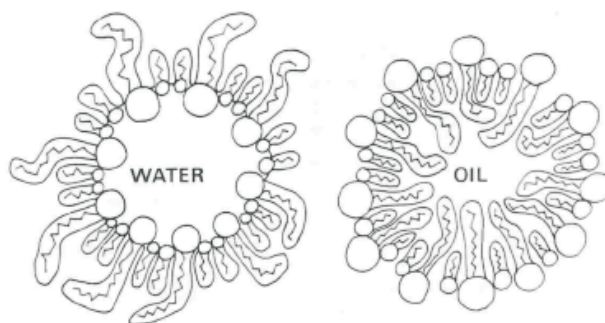


Figure 3.1: Schematic view of water droplets in oil (left) and oil droplets in water (right). In this case two types of surfactant molecules adsorb at the oil-water interface.

Microemulsions contain huge oil-water interfacial areas and to allow stability the interfacial tension must be quite low, usually $\ll 1\text{mN/m}$. In that case the entropy of mixing, although small on account of the coarseness of the mixture, may be large enough to compensate the positive interfacial free energy and to give the microemulsion a free energy lower than that of the unmixed components. A rough estimate of the value of the interfacial tension, γ where spontaneous emulsification occurs is by the condition $4\pi R^2\gamma = kT$, in other words the work to create a drop of radius R should be on the order of the thermal energy kT .

Microemulsions can have various textures, such as oil droplets in water, water droplets in oil, (random) bicontinuous mixtures, ordered droplets or lamellar mixtures with a wide range of phase equilibria amongst them and with excess oil and/or

water phases. This great variety is governed by variations in the composition of the whole system and in the structure of the interfacial layers. The situation for relatively small surfactant concentrations and equal volumes of oil and water is shown in Fig. 3.2, showing the transition from Winsor I (oil droplets in water coexisting with excess oil) to Winsor III (bicontinuous structure with excess water and oil phases) to Winsor II (water droplets in oil with excess water).

Qualitatively the thermodynamics of microemulsions is well understood as the interplay between a small interfacial free energy and a small entropy of mixing. However, because of these contributions being small, other small effects, such as the influence of curvature on the interfacial tension, and the influence of fluctuations, become important. In the following we will derive the generalized Laplace equation to illustrate the consequence of curvature contributions to the (interfacial) free energy. Subsequently, we introduce the curvature free energy put forward by Helfrich. The curvature free energy is an important conceptual tool in understanding the physics of (surfactant) monolayers and membranes. It will be used here to explain the structural transitions of microemulsions as a function of temperature and ionic strength. In the last part, we will estimate the value of the interfacial tension of the flat interface between microemulsions and excess phase (see Fig. 3.2) and compare it to the situation without surfactant.

3.2 Experimental facts

The situation for relatively small surfactant concentrations and equal volumes of oil and water is shown in Fig. 3.2, showing the transition from Winsor I (oil droplets in water coexisting with excess oil) to Winsor III (bicontinuous structure with excess water and oil phases) to Winsor II (water droplets in oil with excess water).

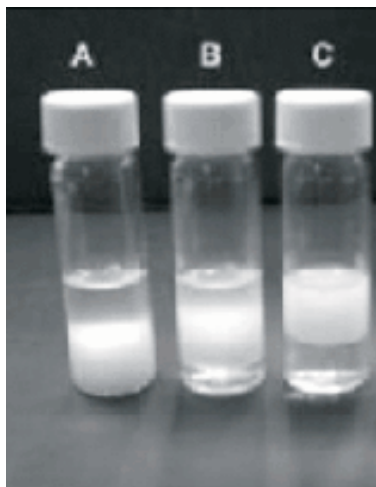


Figure 3.2: A: Oil droplets in water with excess oil (Winsor I); (B) bicontinuous with excess oil and water (Winsor III); (C) water droplets in oil with excess water (Winsor II). From A to C the ionic strength in the system is being increased

At higher surfactant concentrations, the excess water and oil phases are taken up by the microemulsion phase, ultimately leading to single-phase microemulsions.

Upon further increase of surfactant concentrations, excluded volume effects become important, leading to phase transitions to lamellar liquid crystals. The situation for non-ionic surfactants is sketched in Fig. 3.3.

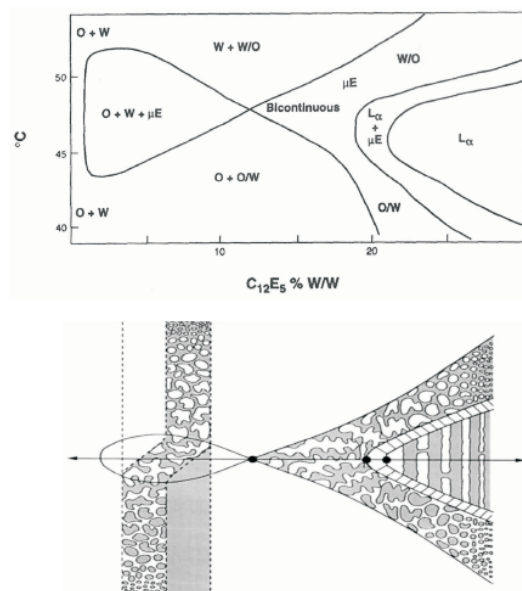


Figure 3.3: Experimental (Top) phase diagram of non-ionic surfactant at equal volumes of oil and water and varying temperature (vertical axis) and surfactant concentration (horizontal axis). An artistic impression of the situation has been shown at the bottom.

3.3 Generalized Laplace equation

Consider the formation of a liquid drop of radius R . It (hopefully) is well-known that inside the drop the pressure is higher than it is outside. The pressure difference, Δp , is referred to as the Laplace pressure and is given by $\Delta p = 2\gamma/R$, with γ the interfacial tension between the drop and its environment (e.g., gas, another liquid).

Now suppose interfacial tension depends on curvature, that is, the droplet radius. Mechanical equilibrium requires that the pressure difference Δp times an infinitesimal change in volume of the drop, dV , equals the change in interfacial free energy $d(\gamma A)$, with A the interfacial area of the drop. In other words, $\Delta p dV = d(\gamma A) = \gamma dA + Ad\gamma$. For a spherical drop this leads to

$$\Delta p = \frac{2\gamma}{R} - \frac{2c}{R^2} \quad (3.1)$$

In this equation, the bending moment

$$c = \frac{\partial \gamma}{\partial (2/R)} \quad (3.2)$$

Eqs 3.1 is the generalized Laplace equation. Obviously it reduces to the classical Laplace equation if the absolute value of the second term is much smaller than the

first one, being the case if $c/R \ll \gamma$, implying small bending moment and/or large value of R .

3.4 Curvature free energy

Helfrich [4] deduced the free energy associated with deformations around a flat surface up to second order in the translational and rotational invariants. The result is

$$F_c = \int_A \left[\frac{\kappa}{2} (c_1 + c_2 - 2c_0)^2 + \bar{\kappa} c_1 c_2 \right] dA. \quad (3.3)$$

In this eq., c_1 and c_2 are the principle curvatures, c_0 the preferred curvature, κ the bending elastic modulus, and $\bar{\kappa}$ the modulus associated with Gaussian curvature. The last quantity often is referred to as 'Gaussian bending (elastic) modulus'. For a sphere of radius R we have $c_1 = c_2 = 1/R$.

Eq. 3.3 often is written in terms of mean curvature $H = (c_1 + c_2)/2$ and Gaussian curvature $K = c_1 c_2$, i.e.,

$$F_c = \int_A [2\kappa(H - c_0)^2 + \bar{\kappa}K] dA. \quad (3.4)$$

The first term proportional to κ in Eqs. 3.3, 3.4 is analogous to the expression of the potential energy of a harmonic spring. The second term is a topological invariant. Without the second term, it can easily be verified that the curvature free energy of, e.g., spheres and cylinders is degenerate. The Gauss-Bonnet theorem states that

$$\int_A K dA = 4\pi(1 - g) \quad (3.5)$$

In this eq., g is the genus of a surface being defined by the number of holes. A sphere has $g = 0$, a cylinder and torus have $g = 1$, while torus-like objects with N holes have $g = N$.

The Gaussian modulus $\bar{\kappa}$ can be smaller or larger than zero. Combination of the result Eq. 3.5 with Eq. 3.4 reveals that the sign of $\bar{\kappa}$ reflects the tendency of the surface to form certain topologies: if $\bar{\kappa} < 0$, the second term in Eq. 3.4 is minimal if g is as small as possible, which corresponds to spheres. On the other hand, if $\bar{\kappa} > 0$, large g will minimize the second term. Of course the second term competes with the first one in the curvature energy, and also with the configurational entropy of the objects.

Let's consider the situation where $\kappa, \bar{\kappa} \gg kT$, so that the role of configurational entropy is negligible, and $c_0 = 0$. If $\bar{\kappa} = 0$, Eq. 3.4 implies that the curvature free energy of a flat object with $c_1 = c_2 = 0$ equals the curvature free energy of objects where at every point in space $c_1 = -c_2$. The last type of object has been sketched in Fig. 3.4. It is referred to as the 'Schwartz minimal surface' or the 'plumbers nightmare'.

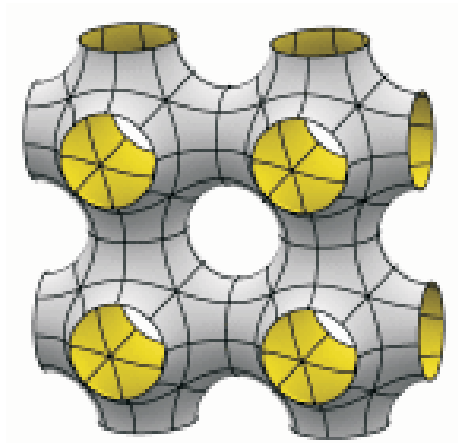


Figure 3.4: Schwartz minimal surface of 'plumbers nightmare'. The surface can be surfactant monolayers separating oil and water, or bilayers with water on both sides of the surface.

Now under the conditions described above, it is the sign of $\bar{\kappa}$ that determines whether plates are stable or the 'plumbers nightmare'. This is relevant for the structure of the 'bicontinuous' microemulsion, i.e., the middle phase in Fig. 3.2B and schematically in the 'head of the fish' in Fig. 3.3.

Away from the 'head of the fish', at small surfactant concentrations, oil droplets in water are stable or water droplets in oil, depending whether temperature is increased or decreased. It is generally accepted that in nonionic surfactants, preferred curvature depends on temperature. The microscopic reason is that temperature influences the level of hydration of the surfactant molecules on the water sides, thereby influencing the sign and absolute value of preferred curvature.

In case of ionic surfactants, the value (and sign) of c_0 is determined by the balance between excluded volume interactions between the surfactant chains on the oil side of the surfactant layer, and the electrostatic (screened- Coulomb) interactions between the charged 'heads' of the surfactant molecules at the water side of the surfactant monolayers. By increasing the ionic strength, as in Fig. 3.2, preferred curvature will be more and more towards the water side of the oil-water interface. The reason is that ions screen the electrostatic repulsion between the surfactant headgroups. The values of the bending elastic moduli depend on surfactant chain-length, charge density and ionic strength.

3.5 A microscopic model for curvature elasticity: incompressible spring model

In this section a simple microscopic model will be analyzed that will allow some physical insight into the meaning of the curvature elastic moduli. This part is based on chapter 6 in [5]. We model the monolayer of adsorbed surfactant molecules (Fig. 3.1) as springs with spring constant k_s and equilibrium spring length ℓ_s . The actual stressed or compressed spring length is denoted by ℓ . The springs are supposed to be incompressible and assume a fixed area per chain at the interface equal

to Σ_0 . In reality, this value is determined by properties of the polar head group. The constant value of Σ_0 implies that interactions that act on the polar head group are much stronger than the chain stretching energies. The (harmonic) energy per chain is

$$f = \frac{k_s}{2}(\ell - \ell_s)^2, \quad (3.6)$$

and the incompressibility of the chains implies a constant volume of the surfactant layer. In case of a flat layer we have $\Sigma_0\ell = v_0$, with v_0 the molecular volume (volume occupied per chain). In case of a curved layer, it can be shown that

$$v_0 = \Sigma_0\ell\left(1 + \ell H + \frac{\ell^2}{3}K\right), \quad (3.7)$$

We now impose the incompressibility condition: put Eq. 3.7 equal to the volume per chain in a flat layer, i.e., $v_0 = \Sigma_0\ell_0$, with ℓ_0 the layer thickness of a flat layer. Solving for ℓ and expanding to third order in ℓ_0 leads to

$$\ell = \ell_0 - \ell_0^2 H + 2\ell_0^3 H^2 - \frac{\ell_0^3}{3}K, \quad (3.8)$$

Note that in general, in the flat monolayer the chain stretching energy Eq. 3.6 is not minimal as $\ell_0 \neq \ell_s$. Thus, in general, the flat layer will have a preferred curvature related to the imposed ℓ_0 and the preferred ℓ_s . Plugging Eq. 3.8 into Eq. 3.6 and keeping the lowest order terms leads to

$$f = \frac{k_s\ell_0^4}{2}[(H - c_0)^2 - \frac{2c_0\ell_0}{3}K]. \quad (3.9)$$

In this Eq., we defined

$$c_0 = \frac{1}{\ell_0}\left(1 - \frac{\ell_s}{\ell_0}\right) = \frac{v_0 - \ell_s\Sigma_0}{\Sigma_0\ell_0^2}. \quad (3.10)$$

Eq. 3.9 is equivalent to the Helfrich form of the curvature free energy, Eq. 3.4. The bending modulus (the coefficient of H^2 in eq. 3.9) and the Gaussian modulus (the coefficient of K) both increase as a power of the chain length. Obviously, the spring constant k_s also depends on the equilibrium spring length ℓ_s . In polymers, and in the limit of small curvatures we have $k_s \sim 1/\ell_s \approx 1/\ell_0$. In that case the bending modulus $\kappa \sim \ell_s^3$. The result that the bending modulus varies with the cube of the thickness also is characteristic for a bent solid elastic plate, see the textbook of Landau and Lifshitz on elasticity theory, ref. [6].

There is a simple physical interpretation of c_0 that emerges from the model, eq. 3.10. Any deviation of that quantity from zero arises because of a mismatch of the preferred length ℓ_s and the imposed length ℓ_0 . The imposed length, in turn, is set by the imposed head area Σ_0 as compared to the 'optimal' area v_0/ℓ_s . If $\Sigma_0 > v_0/\ell_s$, preferred curvature is negative and the system prefers to pack with the heads on the 'outside'. The free energy in that case is lower than that of the flat interface: the system accomodates part of the strain induced by the mismatch between the heads and the chains by bending.

3.6 Interfacial tension between microemulsion- and excess phase

In this section we calculate the interfacial tension, γ_∞ , of the macroscopic interface between a droplet-type microemulsion and excess oil or water phase, see Fig. 3.2. Obviously, that quantity is related to the tension of the droplet (of radius R) interface, γ_R . It should also contain the work related to 'un-bending' the drop into a flat layer. In particular,

$$\gamma_\infty = \gamma_R + \int_{2/R}^0 \frac{\partial \gamma}{\partial (2/R)} d(2/R). \quad (3.11)$$

Combination of Eqs. 3.2 and 3.3 leads to

$$\frac{\partial \gamma}{\partial (2/R)} = c = \frac{\partial^2 F_c}{\partial A \partial (2/R)} = \frac{1}{R} (2\kappa + \bar{\kappa}) - 2\kappa c_0. \quad (3.12)$$

The radius that minimizes the bending energy is

$$R = R_0 \left(1 + \frac{\bar{\kappa}}{2\kappa}\right), \quad (3.13)$$

with $R_0 = 1/c_0$. Here it has been assumed that curvature contributions dominate the total free energy of the system. That only is true if $(2\kappa + \bar{\kappa}) \gg kT$. In practice, the values of the bending moduli are on the order of kT , and entropy effects are significant. In case of dilute systems, this leads to contributions to the free energy that are logarithmic in the number density of the microemulsion droplet. For a discussion see Ref. [7] and references therein. However, these contributions only lead to corrections to eq. 3.13 (and the ones that follow) that are logarithmic in the number density of the microemulsion droplets.

Carrying out the intergration eq. 3.11 and using eqs. 3.12, 3.13 leads to

$$\gamma_\infty = \gamma_R + \frac{2\kappa}{R_0 R} = \gamma_R + \frac{2\kappa + \bar{\kappa}}{R^2} \quad (3.14)$$

In general, it is expected that $\gamma_\infty \gg \gamma_R$ so that $\gamma_\infty \sim R^{-2}$. This is indeed what is to be expected, see the brief discussion on the condition for spontaneous emulsification in the Introduction. In case of liquid-gas interfaces, the interfacial tension $\gamma \sim 1/d^2$ with d a molecular diameter. Interestingly, for microemulsion the size of the emulsified objects sets the interfacial tension.

3.7 Problems

1. Show that for a sphere of radius R , the curvature free energy reads $4\pi(2\kappa + \bar{\kappa}) - 16\pi\kappa c_0 R + 8\pi\kappa c_0^2 R^2$.
2. Prove Eq. 3.13.
3. Verify Eq. 3.5 for a sphere and for a cylinder.

4. What sign of $\bar{\kappa}$ stabilizes the 'plumbers nightmare', Fig. 3.4?
5. Verify Eq. 3.7 by considering the volumes of a spherical and a cylindrical layer.
6. Derive Eq. 3.8 for a sphere of radius R . First verify that the (real) root of the incompressibility condition on Eq. 3.7 for a sphere is given by $\ell \rightarrow R [(3\ell_0/R+1)^{1/3}-1]$

Bibliography

- [1] P.J.W. Debye. *Ann. NY Acad. Sci.*, 51:575–592, 1949.
- [2] H. B. Klevens. *J. Am. Oil Chem. Soc.*, 30:74, 1953.
- [3] J. Israelachvili. *Intermolecular & Surface Forces*. Academic Press, San Diego, 2 edition, 1992.
- [4] W. Helfrich. *Z. Naturforsch.*, 28c:693, 1973.
- [5] S. A. Safran. *Statistical thermodynamics of surfaces, interfaces and membranes*. Perseus, Cambridge, MS, 1994.
- [6] L. D. Landau and E. M. Lifshitz. *Theory of elasticity; 2nd edition*. Pergamon, NY, 1970.
- [7] W. K. Kegel, J. Th. G. Overbeek, and H. N. W. Lekkerkerker. *Thermodynamics of Microemulsions p.13*. Microemulsions, Fundamental and Applied Aspects. Marcel Dekker, NY, 1999.

7. Polymers

Gert Jan Vroege
Van 't Hoff Laboratory
Utrecht University

1. INTRODUCTION

As is well known polymers are long molecules consisting of simple building blocks, the monomers, generally connected through covalent bonds. A simple example is polyethene (figure 1) typically consisting of a 100 to 10000 ethene groups which after polymerization form single C-C bonds around which the polymer can more or less freely rotate. The thus formed chain is an example of a flexible polymer chain, which changes its direction on a length scale of 1 nm because of its rotational freedom around the C-C bonds. Therefore, this polymer is not elongated in solution but it forms a kind of randomly curled coil. Another example is DNA with its double-helix structure, in which 2 DNA-strands are connected through hydrogen bonds (figure 2). DNA can contain up to 10^{10} monomers, leading to a length of up to 1 m if it were to be completely stretched. This polymer is much stiffer, but it also changes its direction gradually (on a scale of 100 nm) through small fluctuations in bond angles and bond lengths. At sufficient length stiff chains also form random coils (in absence of specific interactions, for instance with proteins which can induce very specific DNA conformations in vivo).

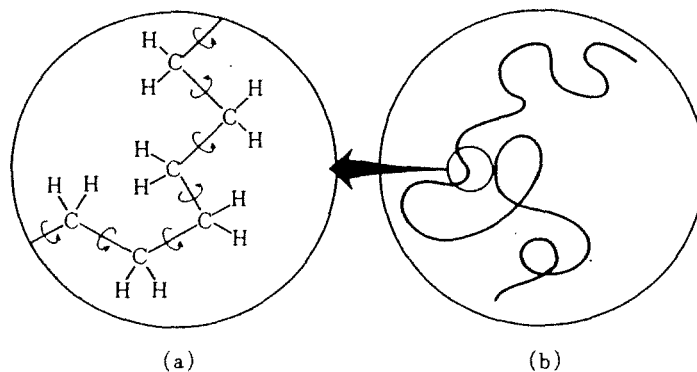


Figure 1. (a) The atomic structure of a polyethene molecule. (b) A schematic representation of a complete molecule. There is rotational freedom around each C-C bond: the molecule forms a long, flexible chain.

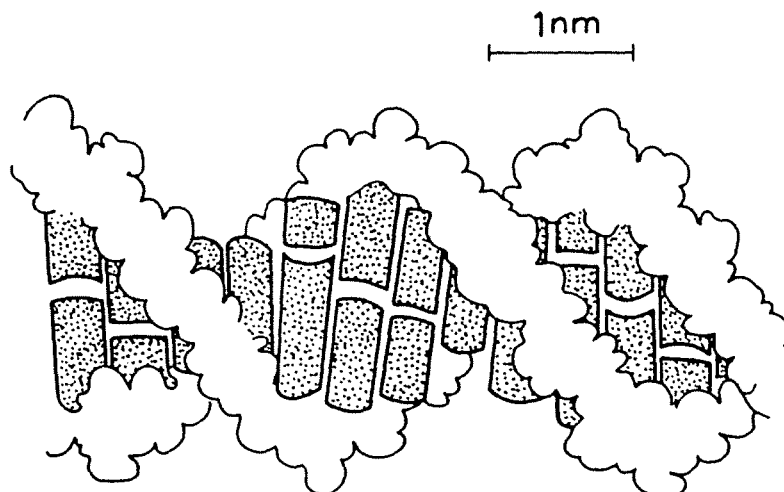


Figure 2. A double helix of DNA in its right-handed B form. Both saccharide-phosphate chains are connected via H-bridges between complementary base pairs.

Polymers can be found everywhere around us. The natural polymers comprise e.g. polysaccharides (like starch and cellulose), DNA and proteins (the last 2 also contain *information* through an alternation of different monomers; this may lead to very specific effects which we will not consider in these lecture notes). Semi-synthetic polymers entered on the scene about a hundred years ago with viscose (chemically modified cellulose, which was used to produce fibres). Totally synthetic polymers were developed in particular after the acceptance of Staudinger's hypothesis (in the twenties and thirties) that polymers consisted of covalently bonded, linear chains of monomers (until then a common notion was that polymers were colloidal aggregates of monomers). Staudinger received the 1953 Nobel prize in Chemistry. During the second world war polymer chemistry became more and more important, an important project being the development of artificial rubber (necessary for some countries because they were cut off from the supply of natural rubber). After the war the production of polymers expanded more and more and now forms a very important part of chemical industry.

Historically, physical chemistry played an important role in characterizing polymers (e.g. through osmotic pressure and viscosity measurements, light scattering and sedimentation), which led to the acceptance of the hypothesis of linear chains, and the concomitant developments of theories. An important name in this context is P.J. Flory (1974 Nobel Prize in Chemistry). In more recent years theoretical developments are increasingly performed by physicists applying general concepts of theoretical physics; for this P.G. de Gennes obtained the 1991 Nobel Prize in Physics.

In these lecture notes we aim at giving a universal description of simple linear flexible polymers. In contrast to synthetic chemists who consider polymers in a very specific way (viz. as built up from specific types of monomers coupled together with a specific type of chemical bond), within physical chemistry polymers are modelled with as few parameters as possible. An indispensable tool is statistical mechanics since one polymer chain consists of a very large number of units and already forms a statistical mechanical system in its own right. In many cases this leads to universal behaviour, which will be illustrated here with comparatively simple calculations.

From statistical mechanics we will mainly use 2 formulas by Boltzmann. The first expresses the entropy of a system in terms of the total number of states W that the

system can assume (at fixed energy):

$$S = k_B \ln W \quad (1.1)$$

and the second the probability P_i of a certain state i with energy E_i (at fixed temperature T):

$$P_i = \frac{e^{-E_i/k_B T}}{Z}$$

In this equation k_B is Boltzmann's constant and Z the partition function:

$$Z = \sum_i e^{-E_i/k_B T} \quad (1.2)$$

The formula can also be written as

$$Z = \sum_j G_j e^{-E_j/k_B T} \quad (1.3)$$

where the sum now runs over the different energies instead of the different states and the degeneracy G_j represents the number of states of the same energy. The partition function Z forms the connection with thermodynamics through the (Helmholtz) free energy A :

$$A = -k_B T \ln Z \quad (1.4)$$

2. IDEAL CHAINS

2.1. The freely jointed chain

When we want to study the universal properties of polymer chains it is useful to consider a simplified model. Here, so-called segments (often point particles) are connected by "bonds" with certain properties. In the simplest possible model, the so-called *freely jointed* model (figure 3), segments are connected through bonds of fixed length b but with completely arbitrary mutual angles.

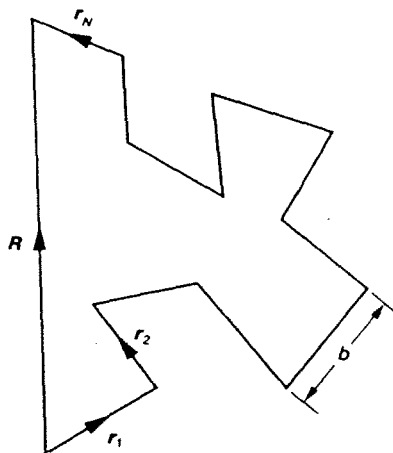


Figure 3. The freely jointed chain.

We can now represent the chain as a sequence of N vectors \mathbf{r}_i , each with a length b . The total length of the (completely stretched) chain, also indicated as the *contour length*, is $L = Nb$. The vector connecting the endpoints of the conformation in space is:

$$\mathbf{R} = \sum_{i=1}^N \mathbf{r}_i$$

From this we can derive the average value of \mathbf{R} :

$$\langle \mathbf{R} \rangle = \sum_{i=1}^N \langle \mathbf{r}_i \rangle = 0$$

Since every bond vector \mathbf{r}_i has an arbitrary direction, every average $\langle \mathbf{r}_i \rangle = 0$ and also the end-to-end vector \mathbf{R} does not have a preferential direction. To characterize the size of the chain it is therefore more adequate to use the (square root of) the mean

square of \mathbf{R} :

$$\langle \mathbf{R}^2 \rangle = \sum_{i=1}^N \sum_{j=1}^N \langle \mathbf{r}_i \cdot \mathbf{r}_j \rangle = \sum_{i=1}^N \langle \mathbf{r}_i^2 \rangle + \sum_{i=1}^N \sum_{j \neq i}^N \langle \mathbf{r}_i \cdot \mathbf{r}_j \rangle \quad (2.1)$$

The last step is taking $\langle \mathbf{r}_i \cdot \mathbf{r}_j \rangle = 0$ if $i \neq j$, since the direction of each bond vector is completely independent of the direction of other bond vectors. Hence we end up with

$$\langle \mathbf{R}^2 \rangle = Nb^2 \quad (2.2)$$

The result of (2.2) is very important. The square root of $\langle \mathbf{R}^2 \rangle$ forms a useful measure for the size of the chain. According to (2.2) the size is proportional to $N^{1/2}$, whereas the contour length is proportional to N : the chain is strongly curled in space. Note that there is no restriction within this model to place two segments at the same position in space; this is a characteristic of a so-called ideal chain.

2.2. The Gaussian distribution

The mean square end-to-end distance is only one property describing the conformation of a chain. It is possible to calculate the complete probability distribution of the end-to-end distance. Therefore we make use of the following equation for the probability $P(\mathbf{R}, N)$ to find an end-to-end vector \mathbf{R} for a polymer of N segments:

$$P(\mathbf{R}, N) = \langle P(\mathbf{R} - \mathbf{r}_N, N - 1) \rangle_{\mathbf{r}_N} \quad (2.3)$$

This equation tells that the end-to-end distribution of a chain of N segments can be determined by stepping back one segment within the chain (in space a step \mathbf{r}_N) and averaging over all possible steps \mathbf{r}_N . In the appendix a derivation is given showing that for large N this leads to a differential equation for $P(\mathbf{R}, N)$:

$$\frac{\partial P}{\partial N} = \frac{1}{6} b^2 \Delta P \quad (2.4)$$

where Δ represents the Laplacian (note that we write $\mathbf{R} = (x, y, z)$):

$$\Delta = \frac{\partial^2}{\partial x^2} + \frac{\partial^2}{\partial y^2} + \frac{\partial^2}{\partial z^2}$$

This equation is identical to the well-known diffusion equation (Fick's second law)

$$\frac{\partial c}{\partial t} = D \Delta c \quad (2.5)$$

using the following correspondence:

$$\begin{aligned} \text{segment number } N &\longleftrightarrow \text{time } t \\ \text{position } \mathbf{R} &\longleftrightarrow \text{position } \mathbf{R} \\ \text{probability } P &\longleftrightarrow \text{concentration } c \\ \frac{1}{6} b^2 &\longleftrightarrow \text{diffusion coefficient } D \end{aligned} \quad (2.6)$$

An ideal chain can thus be compared to a diffusion problem of a particle starting to diffuse from the origin at time $t = 0$ with diffusion coefficient D . The fanciful

trajectory such a particle traverses in time (increasing t) is completely comparable to the conformation consecutive segments of an ideal polymer (increasing N) form within space. A larger typical steplength b leads according to (2.2) to a larger mean square of the end-to-end distance; application of the correspondence (2.6) gives for the analogous diffusion problem:

$$\langle \mathbf{R}(N)^2 \rangle = Nb^2 \longleftrightarrow \langle \mathbf{R}(t)^2 \rangle = 6Dt$$

This is the well-known Einstein formula that tells that a diffusing particle (on average) moves with the square root of time (instead of linearly if the particle would always move in the same direction). Now it is also intuitively clear why (2.2) only applies to an ideal polymer: the polymer must have the opportunity to intersect itself. For a diffusing particle there is after all not a single impediment to return to the same place in space at a later time. In reality this is not possible for a polymer and this may lead to drastically different behaviour. As we will see later there are certain circumstances under which an ideal chain may be a good representation for a polymer.

The solution of (2.4) can be found by applying the correspondence (2.6) to the well-known solution of (2.5) for the analogous diffusion problem (or use Fourier transforms, see appendix 7.2):

$$P(\mathbf{R}, N) = \left(\frac{3}{2\pi Nb^2} \right)^{3/2} \exp \left(-\frac{3\mathbf{R}^2}{2Nb^2} \right) \quad (2.7)$$

Here $\mathbf{R}^2 = \mathbf{R} \cdot \mathbf{R} = x^2 + y^2 + z^2$. This solution may be verified by substitution into the differential equation (2.4). Such a distribution function is called a Gaussian distribution. The form (2.7) is normalized:

$$\int P(\mathbf{R}, N) d\mathbf{R} = \int_{-\infty}^{+\infty} \int_{-\infty}^{+\infty} \int_{-\infty}^{+\infty} P(\mathbf{R}, N) dx dy dz = 1$$

as can be easily verified using the integrals given in appendix 7.4. With this probability distribution also other properties than $\langle \mathbf{R}^2 \rangle$ can be easily calculated, like the standard deviation of \mathbf{R}^2 :

$$\sigma_{\mathbf{R}^2} = \sqrt{\langle \mathbf{R}^4 \rangle - \langle \mathbf{R}^2 \rangle^2} = \sqrt{2/3} Nb^2 \quad (2.8)$$

We see that the deviation in the size of the polymer coil is of the same order of magnitude as the size itself: an ideal coil is a strongly fluctuating object.

2.3. The freely rotating chain

The so-called freely rotating chain is a more realistic model in the sense that there is now a fixed angle θ between consecutive steps (figure 4). The model is called freely rotating because the chain is free to rotate around each bond (though retaining fixed bond angles $\pi - \theta$).

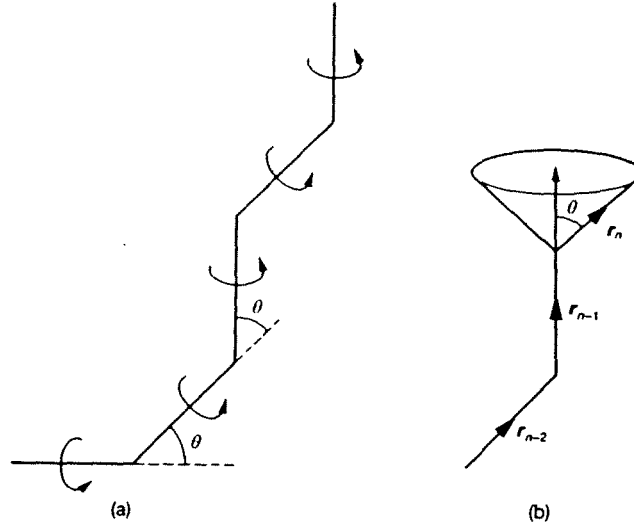


Figure 4. (a) The freely rotating chain. (b) The average of \mathbf{r}_n at fixed \mathbf{r}_{n-1} gives $\cos \theta \mathbf{r}_{n-1}$.

If we now average over all possible directions of a bond, there remains a factor $\gamma \equiv \cos \theta$ in the direction of the previous bond, so that

$$\langle \mathbf{r}_i \cdot \mathbf{r}_{i+1} \rangle = b^2 \gamma$$

while at every next bond an additional factor γ appears because of the averaging over the possible directions of that bond (see figure 4(b))

$$\langle \mathbf{r}_i \cdot \mathbf{r}_j \rangle = b^2 \gamma^{|i-j|}$$

We can use this to calculate the mean square end-to-end distance. To this end we further apply the approximation that most segments are located far from the ends of the chain (if N large) so that in (2.1):

$$\sum_{j \neq i} \langle \mathbf{r}_i \cdot \mathbf{r}_j \rangle \approx 2 \sum_{i-j=1}^{\infty} b^2 \gamma^{|i-j|} = b^2 \frac{2\gamma}{1-\gamma}$$

where we used the summation formula of a geometric series. Substituted in (2.1) this ultimately gives:

$$\langle \mathbf{R}^2 \rangle \approx Nb^2 \frac{1+\gamma}{1-\gamma} = Nb^2 \frac{1+\cos \theta}{1-\cos \theta} \quad (2.9)$$

The most important result is that $\langle \mathbf{R}^2 \rangle$ is still proportional to N , albeit with a proportionality factor larger than for the freely jointed chain (as long as we keep $\theta < \pi/2$).

2.4. More general considerations

We now found for two simple models that $\langle \mathbf{R}^2 \rangle$ is proportional to N . This property has a much wider generality and is a consequence of the so-called *central limit theorem*

in mathematics. In a nutshell this theorem says that a variable (say x), itself a sum of a large number (say N) identical, independent, stochastic variables, is distributed according to a normal (=Gaussian) distribution $\exp(-x^2/2\langle x^2 \rangle)$ and that $\langle x^2 \rangle \propto N$. A polymer chain complies to this if it has a short-range memory (i.e. the position of a certain segment only depends on the positions of a limited number of neighbouring segments within the chain). Then, a chain has "forgotten" where it came from after a limited number of segments. The consequence is that also for a more complex and realistic polymer model the mean square end-to-end distance remains proportional to N (for large N)

$$\langle \mathbf{R}^2 \rangle = Nb_{\text{eff}}^2 \quad (2.10)$$

The proportionality constant obviously has a dimension (length)² and defines the effective step length b_{eff} . For the freely jointed chain we find (see equation (2.9))

$$b_{\text{eff}} = b \sqrt{\frac{1 + \cos \theta}{1 - \cos \theta}}$$

As could be expected the effective step length is larger than b if $\theta < \pi/2$. In the remainder we generally write b instead of b_{eff} . The concept of an effective segment length was first introduced by Kuhn. In order to be independent of the rather arbitrary division into segments (2.10) is now written as

$$\langle \mathbf{R}^2 \rangle = Ll_K \quad (2.11)$$

where L is the length of the polymer if it were completely stretched and l_K is called the *Kuhn length*.

Also the Gaussian distribution (2.7) remains valid in the case of more general short-range models and therefore forms one of the basic formulas of polymer theory. In the end it is not so very important how we exactly model a chain since all (short-range) models give the same results for large chain length. A widely used class of models are the so-called *lattice models*, where chain segments are placed on the lattice points of a space filling lattice (see later).

2.5. The entropy of an ideal coil

The end-to-end distribution $P(\mathbf{R}, N)$ is directly proportional to the number of possible realizations $W(\mathbf{R})$ of an ideal chain at a given end-to-end vector (and at a given number of segments N). From this we can derive an expression for the *entropy* of such an ideal chain via (1.1):

$$S(\mathbf{R}) = k_B \ln W(\mathbf{R}) = \text{cst} - \frac{3k_B}{2Nb^2} \mathbf{R}^2 \quad (2.12)$$

Later we shall use this formula a number of times. At this point we shall use it to show the analogy of a polymer coil with a spring. First we form a (Helmholtz free) energy from this entropy

$$A(\mathbf{R}) = U(\mathbf{R}) - TS(\mathbf{R}) = -TS(\mathbf{R}) = \text{cst} + \frac{3k_B T}{2Nb^2} \mathbf{R}^2 \quad (2.13)$$

Note that $U = 0$ for an ideal chain. The interesting point of this formula is its quadratic form similar to the potential energy of a spring. If the endpoints of a

polymer chain are brought apart, it experiences (on average) a retracting force

$$\mathbf{f} = -\frac{\partial A}{\partial \mathbf{R}} = -\frac{3k_B T}{Nb^2} \mathbf{R}$$

The spring constant is $3k_B T/Nb^2$. This entropic effect forms the basis for the elasticity of rubber, which consists of a network of interconnected polymer chains. Note that the above formula predicts that the spring constant of rubber increases with temperature (in strong contrast to most other materials). This is also found experimentally and is sometimes called the *Guch-Joule* effect. The formula tells further that the material can be stretched more easily if the number of segments between consecutive linking points in the network N is larger.

2.6. Further models of a flexible polymer chain

Since different parts of an ideal chain do not have any interactions, a part of the chain can itself be described by a Gaussian distribution. We then have to use a generalized version $G_N(\mathbf{R}|\mathbf{R}')$ for the probability of a chain of N segments starting at a position \mathbf{R}' and ending at \mathbf{R} (so $P(\mathbf{R}, N) = G_N(\mathbf{R}|0)$). Let us for instance consider a chain on which we also want to fix segment ν at position \mathbf{R}'' . Since both parts of an ideal chain are independent the probability for such a configuration is then given by the product of both probabilities, $G_{N-\nu}(\mathbf{R}|\mathbf{R}'')G_\nu(\mathbf{R}''|\mathbf{R}')$. Integrating over all possible positions of the ν th segment, gives back the original end-to-end distribution:

$$G_N(\mathbf{R}|\mathbf{R}') = \int G_{N-\nu}(\mathbf{R}|\mathbf{R}'')G_\nu(\mathbf{R}''|\mathbf{R}') d\mathbf{R}''$$

This relation can be verified easily using (7.4) and the convolution theorem in Fourier space.

A widely used model, the *standard Gaussian or Gaussian bond model* retains this Gaussian property up to the level of each single bond (assuming the distribution is still valid if we set $N = 1$ in (2.7)). This is frequently justified since we saw that many results do not depend on the specific details of the local structure of the chain.

If we compare this with the previous section this also implies that each bond is a spring with spring constant $3k_B T/b^2$. This forms the basis of another model the *bead-spring model*, in which a polymer is modelled as a string of beads connected by springs. This model is especially used in describing polymer dynamics (Rouse/Zimm model).

The ultimate consequence of the Gaussian model is a continuous model where we do not have separate segments anymore, but a continuous line. This leads to path integrals.

2.7. Gaussian chains in an external field

Here we consider a slightly more general case than before by placing a polymer chain in an external field. We define $\varphi(\mathbf{R})$ as the energy a segment obtains at place \mathbf{R} due to the interaction with this external field. In appendix 7.3 is shown that differential equation (2.4) then takes the form

$$\frac{\partial G}{\partial N} = \frac{1}{6}b^2 \Delta G - \frac{\varphi(\mathbf{R})}{k_B T} G \quad (2.14)$$

where we now formulate the differential equation in terms of $G = G_N(\mathbf{R}|\mathbf{R}')$. It is shown in the appendix that the general solution to this equation can be written as a so-called bilinear expansion:

$$G_N(\mathbf{R}|\mathbf{R}') = \sum_n \psi_n(\mathbf{R}')\psi_n(\mathbf{R}) \exp(-\lambda_n N) \quad (2.15)$$

where $\psi_n(\mathbf{R})$ and λ_n are the eigenfunctions and eigenvalues of the following equation (very similar to the time-independent Schrödinger equation in quantum mechanics):

$$-\frac{1}{6}b^2 \Delta \psi_n + \frac{\varphi(\mathbf{R})}{k_B T} \psi_n = \lambda_n \psi_n \quad (2.16)$$

The solution critically depends on the type of eigenvalues found. In some cases these may take a continuous range of values (a continuous spectrum), which corresponds to a scattering state in quantum mechanics. An example of this is the case with $\varphi(\mathbf{R}) = 0$, corresponding to a free particle in quantum mechanics. In appendix 7.3 is shown that (2.15) leads back to a Gaussian coil (as expected).

Another possibility is a discrete spectrum of eigenvalues. In that case one of the eigenfunctions may dominate the problem for long chains. Let the smallest eigenvalue be $\lambda_0 < \lambda_1, \lambda_2, \dots$. If we make N very large, the exponential term containing λ_0 will be by far the largest in (2.15) and will dominate the solution (*ground state dominance*):

$$G_N(\mathbf{R}|\mathbf{R}') \sim \psi_0(\mathbf{R}')\psi_0(\mathbf{R}) \exp(-\lambda_0 N) \quad (2.17)$$

This result seems reasonable for a long chain: both endpoints get completely uncorrelated. A state like this is called a *bound state*. The parallel with quantum mechanics gets even stronger if we calculate the segment density $c(\mathbf{R})$ for (2.17). We then have to integrate over all segment numbers ν in the chain that must be located at \mathbf{R} , irrespective of the position of the beginning \mathbf{R}' and end of the chain (here taken as \mathbf{R}''):

$$c(\mathbf{R}) = \frac{\int_0^N d\nu \int d\mathbf{R}' \int d\mathbf{R}'' G_\nu(\mathbf{R}|\mathbf{R}') G_{N-\nu}(\mathbf{R}''|\mathbf{R})}{\int d\mathbf{R}' \int d\mathbf{R}'' G_N(\mathbf{R}''|\mathbf{R}')}$$

The numerator is a normalizing factor. Using (2.17) for large N simply gives:

$$c(\mathbf{R}) \sim N \psi_0^2(\mathbf{R}) \quad (2.18)$$

So $|\psi_0(\mathbf{R})|^2$ is the probability to find one of the segments at position \mathbf{R} , much like in quantum mechanics.

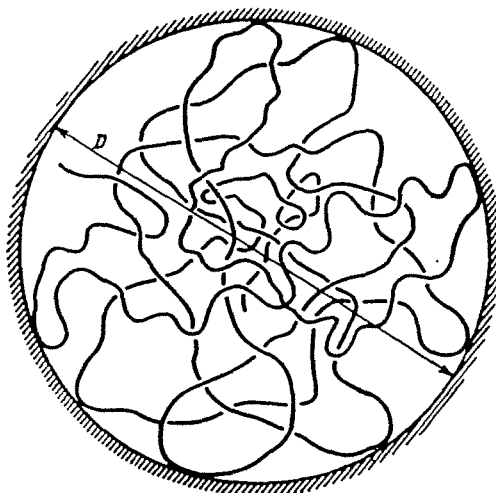


Figure 5. A polymer chain in a spherical cavity of diameter D .

An example of this situation is a polymer chain confined to a spherical cavity of diameter D (see figure 5). For this spherical symmetry we can express the Laplacian in terms of the distance to the origin R :

$$\Delta \dots = \frac{1}{R} \frac{d^2}{dR^2} (R \dots)$$

If we now solve equation (2.16) with $\varphi(\mathbf{R}) = 0$ within the cavity, but all eigenfunctions = 0 outside (since the chain obviously cannot be there), we find as the lowest eigenvalue and (normalized) eigenfunction:

$$\lambda_0 = \frac{2\pi^2 b^2}{3D^2} \text{ and } \psi_0 = \frac{1}{R\sqrt{\pi D}} \sin\left(\frac{2\pi R}{D}\right)$$

Giving a segment density like in figure 6. This is an example of a chain in a globular state.

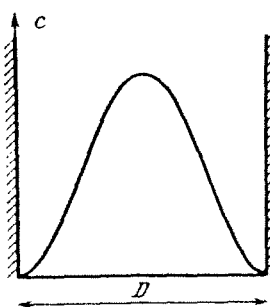


Figure 6. Segment density of a very long ideal polymer in a spherical cavity of diameter D .

2.8. Lifshitz entropy

For a polymer in a bound state it is possible to derive an expression for the entropy. Here, we only consider the situation of ground state dominance (N large). The total partition function would now be:

$$Z = \int d\mathbf{R}' \int d\mathbf{R}'' G_N(\mathbf{R}''|\mathbf{R}')$$

since $G_N(\mathbf{R}''|\mathbf{R}')$ takes into account all chain configurations and Boltzmann weights in the external field and the integrals all possibilities of its beginning and end points. Substituting (2.17) simply gives

$$Z \sim \exp(-\lambda_0 N) \left(\int d\mathbf{R} \psi_0(\mathbf{R}) \right)^2$$

and a concomitant free energy from (1.4)

$$A \sim k_B T \lambda_0 N \quad (2.19)$$

Apart from unimportant end terms this expression is proportional to N and is therefore an extensive property, like in a true macroscopic system.

Note that this expression still depends on the external field $\varphi(\mathbf{R})$, since λ_0 is the lowest eigenvalue of (2.16). Remarkably however, it is possible to eliminate the externally imposed field if we calculate the entropy of the chain. To show this we write

$$S = \frac{U - A}{T} = \int \frac{\varphi(\mathbf{R})}{T} c(\mathbf{R}) d\mathbf{R} - \frac{A}{T}$$

Using (2.18) and (2.19) this reduces to

$$S = N \int \frac{\varphi(\mathbf{R})}{T} \psi_0^2(\mathbf{R}) d\mathbf{R} - k_B \lambda_0 N$$

The integral in this expression can now also be obtained by taking (2.16) for $n = 0$, multiplying by $\psi_0(\mathbf{R})$ and integrating over \mathbf{R} :

$$-\frac{1}{6} b^2 \int \psi_0 \Delta \psi_0 d\mathbf{R} + \frac{1}{k_B} \int \frac{\varphi(\mathbf{R})}{T} \psi_0^2(\mathbf{R}) d\mathbf{R} = \lambda_0$$

Combining these last 2 equations eliminates both $\varphi(\mathbf{R})$ and λ_0 :

$$S = N k_B \frac{1}{6} b^2 \int \psi_0 \Delta \psi_0 d\mathbf{R}$$

In terms of the segment density $c(\mathbf{R})$ from (2.18) this can be written as

$$S[c(\mathbf{R})] = k_B \frac{1}{6} b^2 \int c^{1/2}(\mathbf{R}) \Delta c^{1/2}(\mathbf{R}) d\mathbf{R} = \text{const} - k_B \frac{1}{6} b^2 \int (\nabla c^{1/2}(\mathbf{R}))^2 d\mathbf{R} \quad (2.20)$$

This is the *Lifshitz entropy* of a single chain. We see that this entropy is connected to concentration gradients and therefore the spatial inhomogeneity of the segment distribution. We could say that spatial inhomogeneity is unfavorable for the entropy,

because in the presence of a concentration gradient, the chain is forced to bend in certain directions more often than in others. This restricts the total number of allowed conformations and therefore decreases the entropy.

When there are many chains, their conformational entropies add up and $c(\mathbf{R})$ represents the total concentration of segments of all chains. In fact an ideal translational term should be added, but this is very small since for every chain a very large number of segments N are connected together to form only one translational unit. Therefore, the conformational entropy which as a rule is insignificant for low-molecular-weight substances (compared to the translational entropy) becomes predominant for many properties of polymers.

2.9. Self-consistent field method

The results in the last section are useful for the so-called self-consistent field (SCF) method for polymers. In statistical physics we try to describe systems in terms of a restricted number of macroscopic variables instead of specifying all positions and momenta of individual particles. In the limit of a very large system (thermodynamic limit) we expect that the free energy shows a very sharp minimum when varying the values of these macroscopic variables. This sharpness justifies the usual procedure of minimizing the free energy with respect to these macroscopic variables to find its equilibrium value. However, this neglects the possible influence of fluctuations.

In the case of our polymer system the form of (2.20) suggests to take $c(\mathbf{R})$ as our (quasi)macroscopic variables. The entropy $S[c(\mathbf{R})]$ is now a functional of $c(\mathbf{R})$ (i.e. it is a function of a function: its variables are the values of the segment density at *all* positions \mathbf{R} in the system, but this already is an average over many microscopic configurations). The important point is that in (2.20) the external field $\varphi(\mathbf{R})$ has been eliminated, so its form is independent of the forces that cause this macroscopic state. The next step to obtain an SCF theory would be to add interactions between segments in the form of an energy term $U[c(\mathbf{R})]$, giving

$$A[c(\mathbf{R})] = U[c(\mathbf{R})] - TS[c(\mathbf{R})]$$

The equilibrium distribution $c_{eq}(\mathbf{R})$ is obtained by functional minimization of A with respect to $c(\mathbf{R})$. Since in many polymer systems the segment concentrations are low, an often used approximation for $U[c(\mathbf{R})]$ is to take the corresponding expressions for disconnected segments (a non-ideal gas), although omitting the translational (ideal gas) term since segments are connected here.

To get the most probable end-to-end distance we minimize this free energy by taking the derivative with respect to R and equating it to 0:

$$-\frac{2}{R} + \frac{3}{Nb^2}R = 0 \Rightarrow R_0^* = \sqrt{\frac{2}{3}}\sqrt{Nb^2} \quad (3.3)$$

This procedure gives us an ideal chain dimension R_0^* (NB the procedure followed is not entirely correct but gives a reasonable estimation). We can also use this formula to estimate the average volume fraction of segments within the coil $\phi \approx N\nu_c/R_0^{*3} \approx N\nu_c/(b\sqrt{N})^3 \approx N^{-1/2}$; this obviously gets very small for large N .

3.1. An excluded volume chain

We now consider the simplest type of long-range interaction, where a once occupied lattice point cannot be occupied by a second polymer segment. In analogy with the diffusion problem this type of conformation is also called a SAW (=Self-Avoiding Walk). To describe the resulting conformation qualitatively we assume that the polymer coil swells to a different size R but that the internal structure of the chain is retained (such that we can still apply expression (3.1)). We further assume that encounters between segments take place independently and that only pair interactions are important. We account for this by multiplying (3.4) by a correction factor $p(R)$ which represents the probability that a given conformation is allowed (i.e. we did not place one single segment on the same position as one of the others). The probability that, if we place a segment on a specific lattice point, this is already occupied by another segment, is given by the volume of 1 segment ν_c divided by the total volume of the coil (approximately R^3). There are $N(N-1)/2$ of this kind of possible (pair) contacts within a coil of N segments, so that

$$p(R) \approx \left(1 - \frac{\nu_c}{R^3}\right)^{N(N-1)/2} \approx \exp\left(\frac{N(N-1)}{2} \ln(1 - \nu_c/R^3)\right) \approx \exp\left(-\frac{N^2\nu_c}{2R^3}\right)$$

Multiplying (3.1) by this factor we get the number of configurations with excluded volume:

$$W(R) \propto z^N 4\pi R^2 \exp\left(-\frac{3R^2}{2Nb^2} - \frac{N^2\nu_c}{2R^3}\right) \quad (3.4)$$

The free energy now gets

$$\frac{A(R)}{k_B T} = -\ln W(R) = \text{cst} - 2 \ln R + \frac{3}{2Nb^2}R^2 + \frac{N^2\nu_c}{2R^3} \quad (3.5)$$

and a similar minimization procedure as for (3.3) now gives

$$-\frac{2}{R} + \frac{3}{Nb^2}R - \frac{3N^2\nu_c}{2R^4} = 0$$

Combined with R_0^* from (3.3) this leads to the following equation for the chain size R^* of an excluded-volume chain (first given by Flory):

$$\left(\frac{R^*}{R_0^*}\right)^5 - \left(\frac{R^*}{R_0^*}\right)^3 \approx \frac{\nu_c}{b^3}N^{1/2} \approx N^{1/2} \quad (3.6)$$

To emphasize we are performing a qualitative calculation we left out a factor of $\sqrt{243/128}$. For large N we can neglect the cubic term and the solution is:

$$\frac{R^*}{R_0^*} \approx N^{1/10} \Rightarrow R^* \approx bN^{3/5} \quad (3.7)$$

R^*/R_0^* is often called the *expansion factor* α . In comparison to the ideal chain (3.3) the coil swells and it does so the stronger when the chain is longer. It is essential to realize the difference with a chain with short-range interactions: with short-range interactions the chain may also swell but in this case because of an increased effective step length b_{eff} , while the ideal dependence on N persists. With a long-range excluded-volume interaction the exponent of N changes. The above-described model is strongly simplified. More extensive calculations and computer simulations give for large N :

$$R^* \approx bN^\nu \text{ with } \nu \approx 0.588$$

which does not differ much from the Flory exponent $3/5$ in (3.7).

3.2. A chain in solution

Up to now we only counted conformations to describe a polymer chain, i.e. we only took into account the entropy using formula (1.1). This was made possible by the fact that energy did not play a role. In actual life this never occurs since a polymer chain will always be suspended in a solvent, so different conformations may have different energies. We now account for this in a crude way by adding an (average) energy term $\bar{E}(R)$ to the entropic term in the free energy :

$$\begin{aligned} A(R) &= U(R) - TS(R) \Rightarrow \\ \frac{A(R)}{k_B T} &\approx \frac{\bar{E}(R)}{k_B T} - \ln W(R) \end{aligned}$$

We can determine $\bar{E}(R)$ in the above-used lattice model by again viewing the polymer coil as an object of N segments in a volume R^3 and hence a volume fraction $\phi(R) \approx N\nu_c/R^3$. The lattice points not occupied by the polymer are now occupied by a solvent molecule (see figure 8).

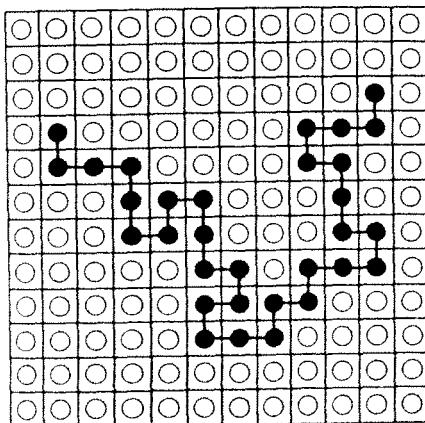


Figure 8. The lattice model of a chain in solution. Black cirkels represent polymer segments and white cirkels solvent molecules.

We now suppose only interaction between neighbouring lattice points, viz.

$$\begin{aligned}
\text{polymer segment-polymer segment} & : -\varepsilon_{pp} \\
\text{polymer segment-solvent molecule} & : -\varepsilon_{ps} \\
\text{solvent molecule-solvent molecule} & : -\varepsilon_{ss}
\end{aligned} \tag{3.8}$$

There are Nz neighbouring points next to the polymer, each with a probability ϕ to be a polymer segment and $1 - \phi$ to be a solvent molecule. The average energy of the coil is then:

$$\bar{E}(R) \approx Nz \left[\frac{1}{2}\phi(-\varepsilon_{pp} + \varepsilon_{ss}) + (1 - \phi)(-\varepsilon_{ps} + \varepsilon_{ss}) \right]$$

The factor $1/2$ appears to avoid double-counting of polymer-polymer interactions and we have chosen the pure solvent as the reference state (for each contact with a polymer segment a solvent-solvent contact is broken). We can rewrite this as:

$$\begin{aligned}
\bar{E}(R) & \approx \text{cst (independent of } R) - Nz\phi(R) \left[\frac{1}{2}(\varepsilon_{pp} + \varepsilon_{ss} - 2\varepsilon_{ps}) \right] \\
& \approx \text{cst} - \frac{N^2\nu_c}{R^3} z \left[\frac{1}{2}(\varepsilon_{pp} + \varepsilon_{ss} - 2\varepsilon_{ps}) \right] \\
\frac{\bar{E}(R)}{k_B T} & \approx \text{cst} - \frac{N^2\nu_c}{2R^3} 2\chi
\end{aligned} \tag{3.9}$$

The last step introduces the so-called *chi-parameter* χ , which we consider more closely in the next section. The reason to write (3.9) as in the last line is clear if we compare this term with the last term of (3.5): the effect of the energetic interaction with the solvent has the same functional form as the excluded volume interaction between segments. We can therefore immediately use the results from the previous section after transforming

$$\nu_c \rightarrow \nu \equiv \nu_c(1 - 2\chi) \tag{3.10}$$

The Flory equation (3.6) now gives:

$$\left(\frac{R^*}{R_0^*} \right)^5 - \left(\frac{R^*}{R_0^*} \right)^3 \approx \frac{\nu}{b^3} N^{1/2} \tag{3.11}$$

The difference is that in this case the right-hand side is not necessarily large. This now depends on the value of χ . We will differentiate between several regimes which we discuss in the next section.

3.3. Good, bad and ideal solvents

The chi-parameter in (3.9) is given by

$$\chi \equiv \frac{z\Delta\varepsilon}{k_B T} = \frac{z(\varepsilon_{pp} + \varepsilon_{ss} - 2\varepsilon_{ps})}{2k_B T} \tag{3.12}$$

where $2\Delta\varepsilon$ represents the energy change at the formation of 1 polymer segment-polymer segment contact (see figure 9).

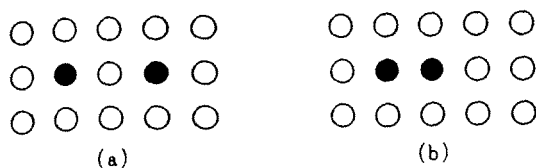


Figure 9. The effective interaction between two polymer segments. If the polymer segments (indicated by black cirkels), originally separated as in (a), are brought together, as in (b), the energy of the system decreases with an amount

$$2\Delta\varepsilon = \varepsilon_{pp} + \varepsilon_{ss} - 2\varepsilon_{ps}.$$

A simple rule of thumb for (London-van der Waals) dispersion forces gives for the interaction energy between two molecules i and j :

$$\varepsilon_{ij} = k \alpha_i \alpha_j$$

Proportionality constant k is generally positive and the α s are (segmental) polarizabilities (note that in the definition of the ε s (3.8) appears a $-$ sign: $k > 0$ implies attraction). Therefore, the energy difference $\Delta\varepsilon = \frac{1}{2}(\varepsilon_{pp} + \varepsilon_{ss} - 2\varepsilon_{ps}) = \frac{1}{2}k(\alpha_p - \alpha_s)^2$ is > 0 in most cases. Consequently, χ is also usually positive. We differentiate between 3 regimes:

- $\chi \ll 1$ This implies that the energy change at immersing a polymer segment in its solvent is much smaller than $k_B T$ (see (3.12)). We expect little influence from energy effects. This also appears from (3.10): $\nu \approx \nu_c$; the coil is swollen as in the previous section. In this case, the solvent is called a *good solvent*. When χ increases, energy effects are getting more important and the polymer coil starts to shrink.
- $\chi = 1/2$ In this special case (3.10) gives $\nu = 0$. The Flory equation (3.11) now gives $R^* = R_0^* \approx bN^{1/2}$, so that the chain behaves like an ideal chain. This is caused by two opposing tendencies. The unfavourable energy change at immersing the polymer segments in solvent wants to contract the coil, while the excluded volume of the segments (and the higher entropy of an expanded coil) leads to swelling of the chain. At $\chi = 1/2$ these two effects just compensate. In this case the solvent is called an *ideal solvent*, a *theta solvent* or sometimes a *marginal solvent*. An important parameter to vary χ is the temperature. The temperature at which the coil behaves ideally, is called the *theta temperature* θ . The term marginal solvent is connected to the fact that $\chi = 1/2$ is a value where the polymer remains only just soluble. At a slightly higher value of χ energy effects are going to dominate.
- $\chi \gtrsim 1/2$ At these values the polymer changes its structure rather abruptly. The higher entropy of the coil structure is not sufficient anymore to compensate unfavourable energy effects, the solvent is expelled and the coil collapses (see figure 10). The chain now forms a rather compact structure, a so-called *globule* (an example is formed by the globular proteins), where $R^* \propto N^{1/3}$. At about the same time different globules in the solution tend to prefer being in mutual contact rather than with the solvent, so that the polymer precipitates (or does not dissolve). In this regime the solvent is called a *bad solvent*.

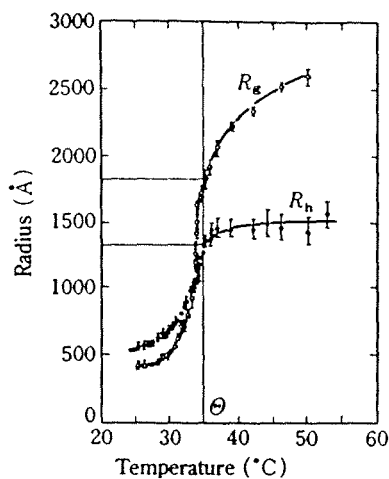


Figure 10. The coil-globule transition in a solution of polystyrene in cyclohexane. The radius of gyration R_g and the hydrodynamic radius R_h undergo a dramatic change when the temperature passes the θ -temperature.

A last remark about the free energy used, (3.5) with transformation (3.10), is in order. When we look at the last term of (3.5) we can write it slightly differently in terms of the segment concentration $c \approx N/R^3$:

$$\frac{N^2\nu}{2R^3} \approx Nc\frac{1}{2}\nu$$

Written in this form the term strongly resembles the second virial term in the expansion of the free energy of a non-ideal gas as a series of concentration c . This is no coincidence since the above model describes the interaction between the polymer segments in terms of two-particle interactions and as if the segments can move independently within the coil. The factor $\frac{1}{2}\nu$ corresponds with the second virial coefficient. In the case of excluded-volume interactions only it is equal to $\frac{1}{2}\nu_0$, half the excluded volume of one segment as in the case of gases. We now see the close connection with the remarks made in section 2.9.

4. CONCENTRATED POLYMER SOLUTIONS

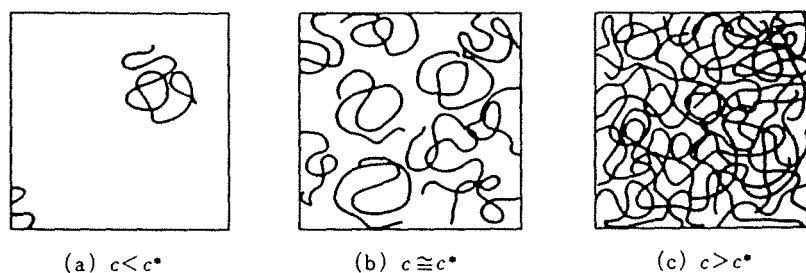


Figure 11. (a) A dilute polymer solution; (b) a solution at the overlap concentration c^* ; (c) a more concentrated solution.

If we increase the concentration of a polymer solution separate coils will start to overlap at a certain point (see figure 11). The corresponding segment concentration is called the *overlap concentration* c^* . We can easily make an estimate of c^* since at that point the total space will be completely filled by coils touching each other. This implies that c^* is equal to the (average) segment concentration within 1 isolated coil:

$$c^* \approx \frac{N}{R^{*3}} \approx \frac{N^{1-3\nu}}{b^3} \quad (4.1)$$

Note that, ν lying between $1/2$ and $3/5$, c^* can be very small for long polymers (large N). Polystyrene at a molecular weight of 1,000,000 can have its c^* at 0.5 weight %. This means that polymer chains can be strongly entangled and will have a strong mutual interactions. The limit is formed by molten polymers (called a polymer melt), where a solvent is completely absent, and which are very important for industrial applications of plastics.

4.1. The Flory-Huggins approximation

A conceptually important description of polymer solutions is the well-known *Flory-Huggins approximation*. A derivation is given in Appendix 7.5. This theory is an example of a so-called mean-field theory, where polymer segments are assumed to be randomly distributed in space and the interaction is calculated on the basis of averaged concentrations in the system. Fluctuations in segment concentrations are completely neglected, although they can be large especially for polymers (if only because of the fact that segments are attached to each other). The Flory-Huggins approximation is therefore better suited for concentrated solutions (far above c^*). Here we are mainly interested in qualitative effects of the degree of polymerization N .

We consider a system of n_p polymers of N segments and n_s solvent molecules (occupying $\Omega = n_p N + n_s$ lattice positions) thus having a volume fraction $\phi = n_p N / \Omega$.

The (Helmholtz) free energy of mixing A_m within the Flory-Huggins approximation is

$$A_m(\Omega, \phi) = \Omega k_B T f_m(\phi) = \Omega k_B T \left[\frac{1}{N} \phi \ln \phi + (1 - \phi) \ln(1 - \phi) + \chi \phi(1 - \phi) \right] \quad (4.2)$$

The first two terms are the entropy of mixing. Here the factor $1/N$ is noticeable (in the "polymer" term), which is absent for low molecular weight liquids. The last term represents the internal energy of mixing analogous to the model considered previously for the single chain (see (3.8)) and contains the same chi-parameter

$$\chi \equiv \frac{z \Delta \varepsilon}{k_B T} = \frac{z(\varepsilon_{pp} + \varepsilon_{ss} - 2\varepsilon_{ps})}{2k_B T} \quad (4.3)$$

4.2. Phase separation in polymer solutions

To be able to predict from the Flory-Huggins free energy whether a polymer solution remains homogeneous or that phase separation occurs, we use a graphical method. If we plot the free energy per lattice point, $f_m(\phi)$ (see (4.2)), against the volume fraction ϕ we could for instance obtain a picture like figure 12.

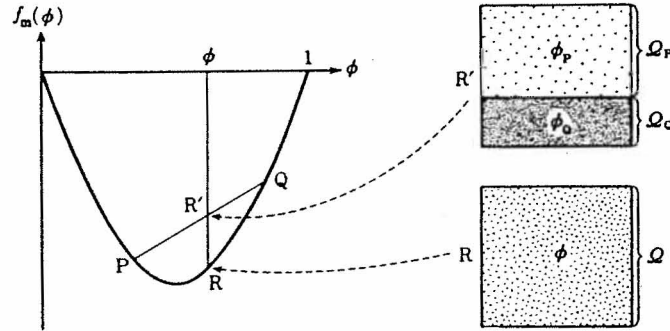


Figure 12. The free energy of mixing for a system without phase separation. Situation at R: a homogeneous phase with volume Ω and volume fraction ϕ . (Imaginary) situation at R': separation in two phases with concentrations ϕ_P , ϕ_Q and volumes Ω_P , Ω_Q .

If this system is homogeneous, the free energy per lattice point at volume fraction ϕ is given by the value of $f_m(\phi)$ at point R (here we consider all energies in units $k_B T$). However, if we would suppose that the system separates in 2 phases P and Q of volume fractions ϕ_P and ϕ_Q , we first have to determine the volumes Ω_P and Ω_Q of both phases from the following conservation conditions of mass and volume:

$$\begin{aligned} \Omega_P \phi_P + \Omega_Q \phi_Q &= \Omega \phi \\ \Omega_P + \Omega_Q &= \Omega \end{aligned}$$

Its solution is:

$$\Omega_P = \frac{\phi_Q - \phi}{\phi_Q - \phi_P} \Omega \quad (4.4)$$

$$\Omega_Q = \frac{\phi - \phi_P}{\phi_Q - \phi_P} \Omega \quad (4.5)$$

Hence the free energy per lattice point of the phase-separated system is

$$\begin{aligned} \frac{A_m^{separated}}{\Omega k_B T} &= \frac{\Omega_P}{\Omega} f_m(\phi_P) + \frac{\Omega_Q}{\Omega} f_m(\phi_Q) \\ &= \frac{\phi_Q - \phi}{\phi_Q - \phi_P} f_m(\phi_P) + \frac{\phi - \phi_P}{\phi_Q - \phi_P} f_m(\phi_Q) \end{aligned}$$

A more precise consideration of this expression shows that its value (per lattice point) in figure 12 lies on the line connecting P and Q at a volume fraction of ϕ , i.e. at R' (expressions (4.4) and (4.5) represent the lever rule for the relative volumes). In this case the free energy of the phase-separated system is higher than the homogeneous system. For an upward concave function like in figure 12, this is true for every possible way of separating the system in 2 phases and the homogeneous system is always the most stable.

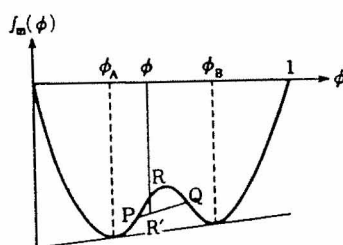


Figure 13. The form of the free energy of mixing for a case of phase separation. Solutions at $\phi_A < \phi < \phi_B$ find their lowest free energy if the system separates in 2 phases of concentrations ϕ_A and ϕ_B .

A very different situation occurs when there is a convex part in the graph, like in figure 13. Here R' lies clearly below R. P and Q can be chosen in many different ways. However, the lowest possible point is situated on the double tangent to the curve and this is therefore the equilibrium state with the two coexisting phases as the tangent points (this well-known double-tangent construction also assures that both tangent points have equal osmotic pressure and chemical potentials).

In (4.2) the value of χ determines the form of the $f_m(\phi)$ -curve. At low values of χ (usually at high temperatures T) its form is upward concave and the system remains homogeneous. At higher values of χ (low T) 2 minima appear and phase separation takes place. This is represented in figure 14 for different values of T .

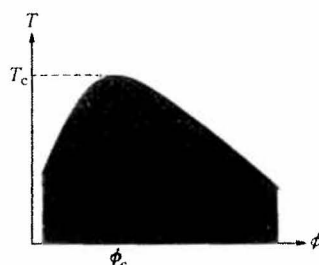


Figure 14. A typical phase diagram for a polymer solution. In the cross-hatched region phase separation occurs.

The χ value at which phase separation first occurs can be found from the fact that both minima in figure 13 shift towards each other and merge at this specific value ($\chi = \chi_c$). This requires:

$$\frac{\partial^2 f_m}{\partial \phi^2} = 0 \text{ and } \frac{\partial^3 f_m}{\partial \phi^3} = 0$$

This point is called the *critical point* and can easily be determined from (4.2):

$$\phi_c = \frac{1}{1 + \sqrt{N}}$$

$$\chi_c = \frac{1}{2} \left(1 + \frac{1}{\sqrt{N}} \right)^2$$

If N increases, these formulas predict that χ_c approaches $1/2$ so that the critical temperature $T_c = z\Delta\varepsilon/k_B\chi_c$ rises and the critical volume fraction decreases. This tendency is clearly visible in figure 15. However, no quantitative agreement with experiments is found. This is understandable, since in the neighbourhood of a critical point particularly strong concentration fluctuations take place, whence a mean-field theory can not be expected to give a good description.

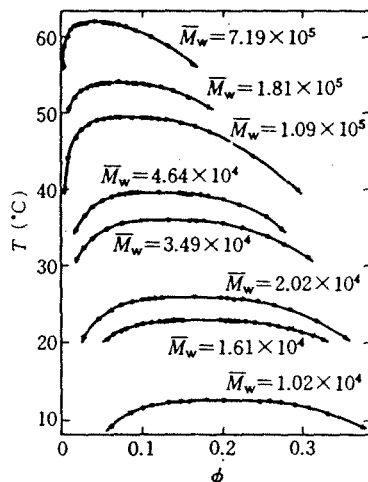


Figure 15. Coexistence curves for a solution of polystyrene in methylcyclohexane. The θ -temperature in this system is 70.3°C .

A further indication of the failing of the Flory-Huggins theory is the osmotic pressure. This can be derived from the Helmholtz free energy:

$$\Pi = \frac{k_B T}{\nu_c} \left[-\ln(1 - \phi) + \frac{\phi}{N} - \phi - \chi\phi^2 \right] \quad (4.6)$$

$$\approx \frac{k_B T}{\nu_c} \left[\frac{\phi}{N} + \left(\frac{1}{2} - \chi \right) \phi^2 + \dots \right]$$

In figure 16 the experimental osmotic pressure is plotted for a number of molecular weights of the same polymer. Note that Van 't Hoff's law (the first term in (4.6)) is only reached at the lowest molecular weight (in this representation the curve should be

horizontal in that regime). At higher concentrations the second term dominates and does not depend on the molecular weight according to (4.6). This is in fact observed but the slope is larger than predicted by Flory-Huggins. This effect is attributed to fluctuations which we shall discuss later.

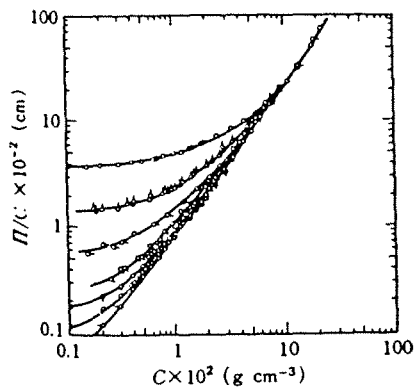


Figure 16. The concentration dependence of the osmotic pressure of poly(α -methylstyrene) molecules of different molecular weights dissolved in toluene. From the top to the bottom molecular weights of: 7×10^4 , 20×10^4 , 50.6×10^4 , 7×10^4 , 119×10^4 , 182×10^4 , 330×10^4 , 747×10^4 .

5. SCALING THEORY

We shall conclude these lecture notes with a more qualitative discussion, where we give an indication of a number of more modern ideas within polymer theory. If we look at the Gaussian distribution function (2.7) for a chain of N segments with step length b , it is striking that N and b enter only as a fixed combination Nb^2 . One could say that there exists a length scale $N^{1/2}b$ that determines the total distribution and therefore also all equilibrium properties on the level of the total chain. The same combination is found within the expression for the entropy of the chain (2.12). An ideal Gaussian coil has the particular property that its structure reproduces itself at different magnifications (see figure 17). This is the property of self-similarity of a so-called *fractal* object.

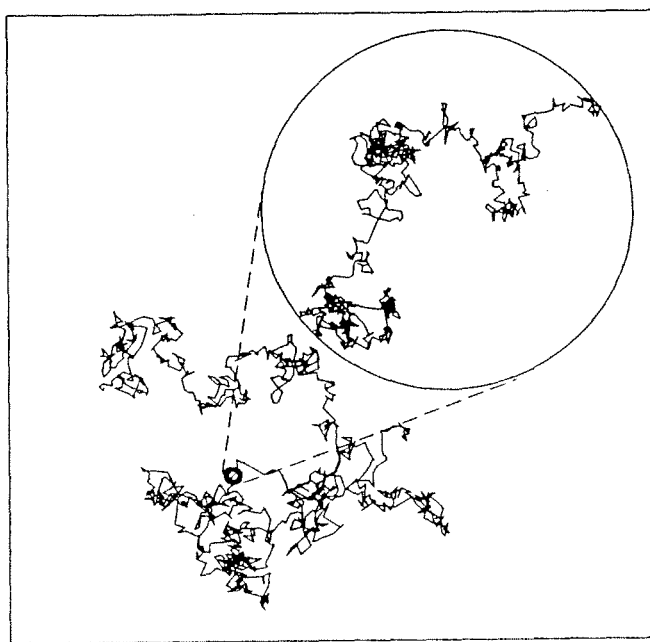


Figure 17. A computer simulation of a "random walk" of 10^6 random steps. In the figure every 10^3 steps are represented as one segment. The inset zooms in on one such segment and represents all steps. The structure of the chain at both levels is completely analogous (self-similar or fractal).

The picture is getting clearer when we ask ourselves whether the monomers within a polymer chain are really determined unequivocally. From a chemical point of view the monomer will of course be the smallest repetition unit within the chain, but we may as well combine several monomers and subsequently use these as the building

block of the polymer ending up with the same polymer. To be more concrete: a chain of N segments and step length b has an average end-to-end distance $N^{1/2}b$. But if we first combine g segments into a new building block, the (average) distance the chain spans within each building block will be $b_g \equiv g^{1/2}b$ which now forms our new step length. On the other hand we only have $N_g \equiv N/g$ of these new building blocks. Our newly built coil is a random walk of the new building blocks (see figure 18) for which we determine the average end-to-end distance in the usual way: $N_g^{1/2}b_g$. The transformation may be summarized as follows:

$$\begin{aligned} \text{step length} & : b \longrightarrow b_g \left(\equiv g^{1/2}b \right) \\ \text{number} & : N \longrightarrow N_g \left(\equiv N/g \right) \\ \text{end-to-end distance} & : N^{1/2}b \longrightarrow N_g^{1/2}b_g \left(= N^{1/2}b \right) \text{ invariant!} \end{aligned}$$

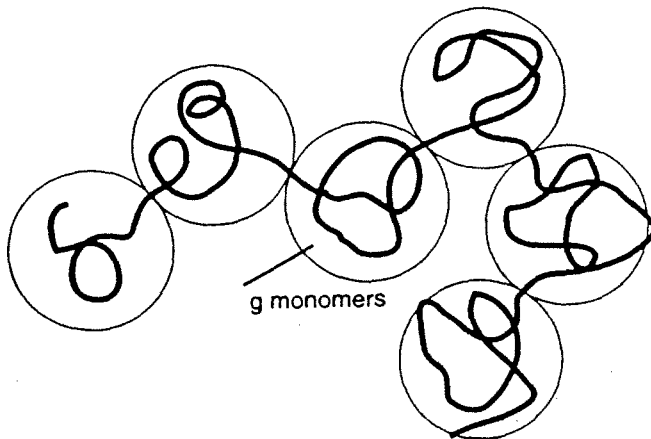


Figure 18. An arbitrary number of segments g in a polymer chain may be thought of as a new segment.

The same story also holds for a non-ideal chain with end-to-end distance $N^\nu b$. P.G. de Gennes applied this type of ideas to determine all kinds of properties of polymers in a simple fashion. Consider for instance the situation that we put a polymer chain in a good solvent ($\nu = 3/5$) into a capillary of diameter D . Can a simple expression be given for the length L which the polymer will occupy within the capillary? We have seen that the size of the building blocks of the polymer can be chosen at will. In this case de Gennes chose the step length equal to the capillary diameter: $bg^{3/5} = D$ so that $g = (D/b)^{5/3}$. The N/g new building blocks of size D will have an excluded-volume interaction like the original segments, so that they only fit into the capillary one behind the other. This gives as the total length of the chain within the capillary:

$$L \approx D \left(\frac{N}{g} \right) \approx ND^{-2/3}b^{5/3} \quad (5.1)$$

It is striking that this calculation is supported by much more involved calculations and simulations. Two limiting cases of the formula can be immediately checked. Firstly, if we consider a wide capillary with a diameter equal to the size of a coil outside the capillary, or $D = N^{3/5}b$. Substitution in (5.1) now gives $L \approx N^{3/5}b$,

hence in a wide capillary the chain is not distorted (for even larger values of D (5.1) of course no longer applies). The second limit is a very narrow capillary of diameter $D = b$. Now the chain is prevented from folding back and can only lie completely stretched. Formula (5.1) indeed gives $L \approx Nb$. The behaviour of L as a function of D is schematically represented in figure 19.

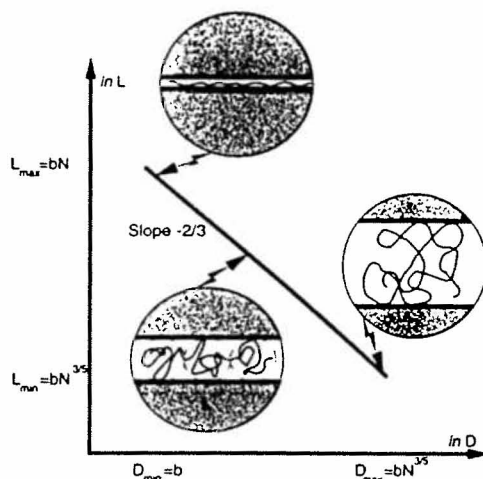


Figure 19. A double-logarithmic plot of length L occupied by a chain in a capillary of diameter D (see text).

As we have seen from (2.8) a polymer coil is a strongly fluctuating object. This kind of fluctuations is completely neglected in mean-field theory, since there only averaged segment concentrations are used. In scaling theory fluctuations are taken along. More formal scaling theory uses an analogy between the behaviour of systems near to a critical point in phase transitions (which also show large fluctuations) and polymer systems (where $1/N$ is comparable with the relative distance to the critical point). One of its ingredients is the above-described procedure of redefining the segments of a chain (also called renormalization). A typical feature in these theories is the prediction of all kinds of power laws containing the relative distance to the critical point. In that sense an expression like

$$R^* \approx bN^\nu \text{ where } \nu \approx 0.588$$

is such a power law where $1/N$ is raised to the power -0.588 (the critical exponent). On the basis of this type of theories a much simpler description of scaling laws (=power laws) is built, using simple physical considerations in a more intuitive way. Nobel prize laureate P.G. de Gennes has been the pioneer of this approach. In the next section we apply this description to semi-dilute solutions.

5.1. Semi-dilute solutions in a good solvent

As we have seen in chapter 4 coils start to overlap around

$$\phi^* = c^*b^3 \approx Nb^3/R^{*3} \approx N^{1-3\nu} \approx N^{-4/5}$$

(note that also c^* is only determined by a global length scale R^*). Since every coil is a strongly fluctuating object, we also expect strong fluctuations in a semi-dilute solution near ϕ^* . Therefore the mean-field description (4.6) is no longer applicable. The scaling expression for the osmotic pressure is now:

$$\Pi = k_B T \frac{c}{N} f(\phi/\phi^*) \quad (5.2)$$

We recognize the ideal law (Van 't Hoff's law) valid at very small ϕ , multiplied by a function f of the relative distance to the overlap concentration ϕ/ϕ^* . For $\phi \rightarrow \phi^*$ this function approaches 1 and at higher concentrations it follows a power law with exponent m :

$$f(x) \sim x^m \quad (5.3)$$

This form is justified by the above-mentioned more extensive theories. The symbol \sim is used for scaling relations and implies that prefactors are left out. Note that $f(x)$ goes to 1 for $x \rightarrow 1$ (or $\phi \rightarrow \phi^*$). Exponent m is now determined from an additional physical condition, i.e. that Π can not depend on N far into the semi-dilute region. An entangled collection of very long polymers contains after all a very small concentration of end points, so that variation in their number can only have a very small influence on the osmotic pressure. Combining the 3 previous equations then gives $m = 1/(3\nu - 1) = 5/4$ and

$$\Pi \sim \frac{k_B T}{b^3} \phi^{9/4} \quad (5.4)$$

This law corresponds to the region in figure 16 where all curves coincide (indeed independent of N) and shows a stronger dependence on ϕ than the mean-field result, which is also found experimentally.

The above derivation shows the typical structure used to derive a scaling law. The unknown quantity is written as a known law in the trivial regime (here Van 't Hoff's law in very dilute solutions) times a scaling function f . Now a characteristic parameter is assumed (here the segment concentration), which serves as an argument in the scaling function f , and the law is written analogously to equation (5.2). The scaling function f has the form of a power law (5.3) and connects to the trivial regime. An additional physical argument (here the independence on N) finally fixes the value of the exponent.

A similar derivation can be given for the characteristic length scale ξ in a semi-dilute solution:

$$\xi = N^\nu b f(\phi/\phi^*) \quad (5.5)$$

As we have seen before the characteristic length scale in the dilute regime is $N^\nu b$. We again suppose a power law:

$$f(x) \sim x^m \quad (5.6)$$

We use the same physical argument that the structure far into the semi-dilute solution does not depend on N . This now leads to $m = -\nu/(3\nu - 1) = -3/4$, whence we find

$$\xi \sim b\phi^{-3/4} \quad (5.7)$$

5.2. Physical picture of a semi-dilute solution

Both results (5.4) and (5.7) are very important to understand a semi-dilute solution. In this section we try to elaborate upon this picture. The *mean-field* result for long polymers in a semi-dilute solution in a good solvent ($\chi = 0$) is given by (4.6)

$$\Pi \approx \frac{k_B T}{\nu_c} \left[\frac{\phi}{N} + \frac{1}{2} \phi^2 + \dots \right] \sim \frac{k_B T}{b^3} \phi^2 \quad (5.8)$$

The osmotic pressure is mainly determined by interactions between segments (the ideal part of the entropy is very small because segments are connected into very large units). The square of ϕ in the above expression represents the probability of contacts (mainly pair contacts), viz. the probability ϕ to find 1 segment times the probability ϕ to find a second segment nearby.

Scaling theory (5.4) now gives the probability to find a second segment not as ϕ but as $w \sim \phi^{5/4}$: a smaller number. This comes about because around one segment in a polymer chain there is always a "cloud" of other segments (of the same chain) that reduces the probability of finding a second segment: at a given contact between 2 segments the surrounding segment clouds also have to come in contact leading to a stronger repulsion.

Given this probability $w \sim \phi^{5/4}$ of a contact between 2 segments we can immediately calculate how many segments g will lie between 2 encounters of one specific chain with other chains:

$$g \sim \phi^{-5/4}$$

If we use this to calculate the ("end-to-end") distance between consecutive encounters in a good solvent this gives

$$g^\nu b \sim b \phi^{-3/4}$$

This "mesh size" of the polymeric network is equal to the characteristic length ξ (5.7). A chain part of g segments with total size ξ was called a "blob" by de Gennes (see figure 20).

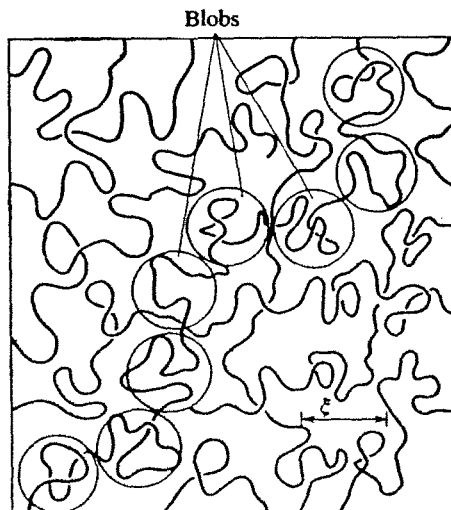


Figure 20. A realization of the conformations in a semi-dilute polymer solution as a network with mesh size ξ or as a system of blobs.

Let us determine the segment concentration within such a blob. This is simple: there are g segments in a volume ξ^3 which makes the concentration $g/\xi^3 \sim \phi/b^3$. However, this is equal to the average segment concentration c , so we conclude that blobs do touch each other but do not overlap. This picture is confirmed if we rewrite the osmotic pressure (5.4):

$$\Pi \sim \frac{k_B T}{b^3} \phi^{9/4} \sim k_B T \frac{c}{g} \sim \frac{k_B T}{\xi^3}$$

A semi-dilute polymer solution is an ideal gas of blobs! ξ apparently also can be interpreted as a “*screening length*” for the excluded-volume interaction: after a chain comes into contact with another polymer chain it seems as if it forgets which segments are on the same chain and which on neighbouring chains. Beyond this length scale ξ the chain will be ideal.

We can now calculate the end-to-end distance for 1 chain: there are N/g blobs with “step length” ξ that themselves form an ideal chain. This implies

$$R \sim \left(\frac{N}{g} \right)^{1/2} \xi \sim N^{1/2} b \phi^{-1/8} \quad (5.9)$$

This relation with the volume fraction is experimentally verified. Note that this expression approaches the completely ideal expression $R \rightarrow N^{1/2} b$ when $\phi \rightarrow 1$. The same is seen from (5.7): $\xi \rightarrow b$. This is caused by the fact that in a melt no concentration fluctuations are possible and there is already an encounter with a different chain after a single step, so that the chain loses its memory right away. The fact that a polymer chain in a melt behaves ideally is also called *Flory's theorem*.

6. SUMMARY

To end these lecture notes it is appropriate to give the following diagram from de Gennes' book, which summarizes many of the results we encountered:

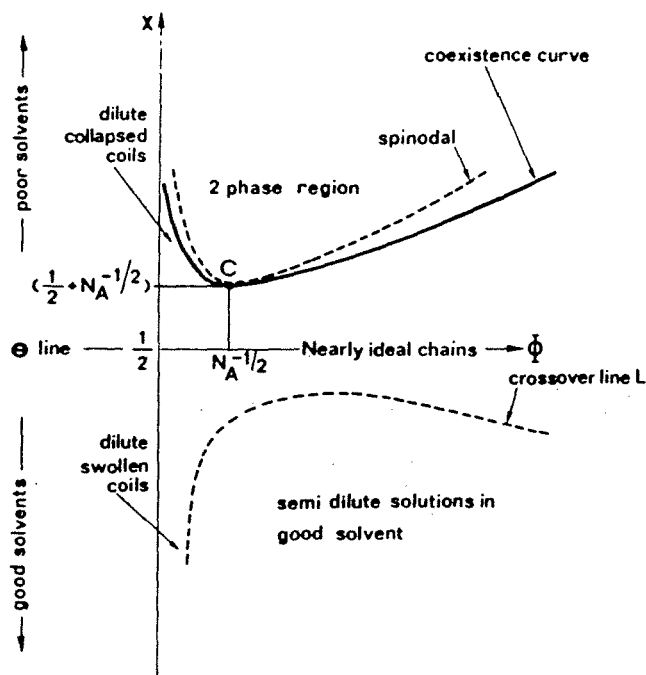


Figure IV.8.

Phase diagram for a polymer-solvent system. χ is the Flory interaction parameter, and Φ is the volume fraction occupied by the polymer. The condition $\chi = 1/2$ defines the Flory Θ temperature. In usual cases such as polystyrene-cyclohexane, χ is a decreasing function of the temperature T ; high temperatures correspond to the lower part of the diagram.

7. APPENDIX

7.1. Derivation of the diffusion equation for an ideal chain

In order to derive from relation (2.3)

$$P(\mathbf{R}, N) = \langle P(\mathbf{R} - \mathbf{r}_N, N - 1) \rangle_{\mathbf{r}_N} \quad (7.1)$$

an expression for $P(\mathbf{R}, N)$, we use the fact that N is large. This implies that 1 is small with respect to N and \mathbf{r}_N is small with respect to \mathbf{R} , so that $P(\mathbf{R}, N)$ varies only gradually and it makes sense to make a Taylor expansion of the function on the right-hand side around $\mathbf{R} = (x, y, z)$ and N :

$$\begin{aligned} P(\mathbf{R} - \mathbf{r}_N, N - 1) \approx & P(\mathbf{R}, N) + \frac{\partial P}{\partial N}(-1) + \sum_{\alpha=x,y,z} \frac{\partial P}{\partial \alpha}(-\mathbf{r}_{N,\alpha}) \\ & + \frac{1}{2} \sum_{\alpha=x,y,z} \sum_{\beta=x,y,z} \frac{\partial^2 P}{\partial \alpha \partial \beta}(-\mathbf{r}_{N,\alpha})(-\mathbf{r}_{N,\beta}) + \dots \quad (7.2) \end{aligned}$$

Since this function actually depends on 4 variables (N, x, y, z) with respect to which we expand, this simple Taylor expansion looks slightly terrifying (we only write down those terms that we ultimately need; i.e. to quadratic order for the derivatives with respect to \mathbf{R} since the linear term turns out to cancel). We must now average this expression over all directions of \mathbf{r}_N , using the fact that there is no preferential direction for \mathbf{r}_N :

$$\begin{aligned} \langle \mathbf{r}_{N,\alpha} \rangle &= 0 \quad (7.3) \\ \langle \mathbf{r}_{N,\alpha} \mathbf{r}_{N,\beta} \rangle &= \langle \mathbf{r}_{N,\alpha} \rangle \langle \mathbf{r}_{N,\beta} \rangle = 0 \text{ als } \alpha \neq \beta \\ \langle \mathbf{r}_{N,x}^2 \rangle &= \langle \mathbf{r}_{N,y}^2 \rangle = \langle \mathbf{r}_{N,z}^2 \rangle = \frac{1}{3} \langle \mathbf{r}_N^2 \rangle = \frac{1}{3} b^2 \end{aligned}$$

Combining (7.1), (7.2) and (7.3) finally leads to the following differential equation for $P(\mathbf{R}, N)$:

$$\frac{\partial P}{\partial N} = \frac{1}{6} b^2 \Delta P$$

where Δ indicates the Laplacian:

$$\Delta = \frac{\partial^2}{\partial x^2} + \frac{\partial^2}{\partial y^2} + \frac{\partial^2}{\partial z^2}$$

Note that this derivation would in fact also be valid if we would not go back just one but several steps along the chain (although a small number compared to the total number of segments) as long as conditions (7.3) can be fulfilled. This is the case for a chain with a so-called short-range memory. Now b represents an effective segment. This substantiates the statements of the opening section of 2.4.

7.2. Solution for the probability of a Gaussian chain

If we want to find the solution for (2.4), this can be easily done by using Fourier transformation

$$P(\mathbf{k}) \equiv \int e^{i\mathbf{k}\cdot\mathbf{R}} P(\mathbf{R}) d\mathbf{R}$$

and its reverse

$$P(\mathbf{R}) \equiv \frac{1}{(2\pi)^3} \int e^{-i\mathbf{k}\cdot\mathbf{R}} P(\mathbf{k}) d\mathbf{k}$$

Taking the Fourier transform of (2.4) gives a simple differential equation for its Fourier transform

$$\frac{\partial P(\mathbf{k}, N)}{\partial N} = -\frac{1}{6} b^2 \mathbf{k}^2 P(\mathbf{k}, N)$$

with the simple solution

$$P(\mathbf{k}, N) = \exp\left(-\frac{N b^2 \mathbf{k}^2}{6}\right) \quad (7.4)$$

which reduces to (2.7) on reverse transformation.

7.3. The differential equation for a Gaussian chain in an external field

Here we consider a slightly more general case than in section 7.1 by placing a polymer chain in an external field. We define $\varphi(\mathbf{R})$ as the energy a segment obtains at place \mathbf{R} due to the interaction with this external field. We now have to modify (7.1) by taking into account the Boltzmann factor connected with this energy:

$$P(\mathbf{R}, N) = \langle P(\mathbf{R} - \mathbf{r}_N, N - 1) \rangle_{\mathbf{r}_N} \exp(-\varphi(\mathbf{R})/k_B T)$$

In a Taylor expansion like (7.2) we must now also linearize this Boltzmann factor (this means that the segment energy must be much smaller than $k_B T$; however, this may always be achieved by our freedom of dividing the chain into more segments) giving

$$\frac{\partial P}{\partial N} = \frac{1}{6} b^2 \Delta P - \frac{\varphi(\mathbf{R})}{k_B T} P \quad (7.5)$$

Equation (7.5) is similar to a diffusion equation with an external field. In a slightly more general form (where a chain starts at point \mathbf{R}' instead of the origin) P is replaced by the so-called Green function $G = G_N(\mathbf{R}|\mathbf{R}')$, which has the character of a conditional probability: the probability of finding the end of a chain of N segments at point \mathbf{R} given that it starts at point \mathbf{R}' . Δ should be understood to be the second derivative to \mathbf{R} (as opposed to \mathbf{R}'). The negative of this form is

$$-\frac{\partial G}{\partial N} = -\frac{1}{6} b^2 \Delta G + \frac{\varphi(\mathbf{R})}{k_B T} G \quad (7.6)$$

and bears a remarkable resemblance to the time-dependent Schrödinger equation for the wave function $\psi(\mathbf{R}, t)$ (of a particle of mass m in an external potential $V(\mathbf{R})$) in quantum mechanics

$$-i\hbar \frac{\partial \psi}{\partial t} = -\frac{\hbar^2}{2m} \Delta \psi + V(\mathbf{R})\psi$$

with N now in the role of an imaginary time it/\hbar .

We will now follow the lines of argumentation of quantum mechanics in obtaining a number of useful results for our equation (7.6). A standard solution method of a partial differential equation like (7.6), called *separation of variables*, assumes a solution of the form:

$$G = f(N)\psi(\mathbf{R}) \quad (7.7)$$

Substituting in (7.6) and rearranging gives

$$-\frac{1}{f} \frac{df}{dN} = \frac{1}{\psi} \left(-\frac{1}{6} b^2 \Delta \psi + \frac{\varphi(\mathbf{R})}{k_B T} \psi \right)$$

of which the left-hand side only depends on N and the right-hand side only on \mathbf{R} . Since this would imply that both sides can be varied independently. However, they should always be equal so we conclude that both sides must be equal to a constant, say λ :

$$\begin{aligned} \frac{df}{dN} &= -\lambda f \\ -\frac{1}{6} b^2 \Delta \psi + \frac{\varphi(\mathbf{R})}{k_B T} \psi &= \lambda \psi \end{aligned}$$

The solution of the first equation is simply

$$f(N) = c \exp(-\lambda N) \quad (7.8)$$

The second equation is an eigenvalue equation completely analogous to the *time-independent Schrödinger equation*:

$$-\frac{\hbar^2}{2m} \Delta \psi + V(\mathbf{R})\psi = E\psi$$

so we must now find the eigenvalues λ_n and eigenfunctions $\psi_n(\mathbf{R})$ for this equation, obeying

$$-\frac{1}{6} b^2 \Delta \psi_n + \frac{\varphi(\mathbf{R})}{k_B T} \psi_n = \lambda_n \psi_n \quad (7.9)$$

Here we review a number of properties of the eigenfunctions of such an equation, for simplicity restricting ourselves to the case that the eigenfunctions are real. It is possible to construct a complete set of orthonormal eigenfunctions, with the property

$$\int \psi_n \psi_m d\mathbf{R} = \delta_{nm} \quad (7.10)$$

($\delta_{nm} = 1$ if $n = m$ and 0 otherwise). This can be easily proved for different eigenvalues $\lambda_n \neq \lambda_m$ using (7.9):

$$\begin{aligned} (\lambda_n - \lambda_m) \int \psi_n \psi_m d\mathbf{R} &= \int (\psi_m \lambda_n \psi_n - \psi_n \lambda_m \psi_m) d\mathbf{R} \\ &= -\frac{1}{6} b^2 \int (\psi_m \Delta \psi_n - \psi_n \Delta \psi_m) d\mathbf{R} \\ &= 0 \end{aligned}$$

The last step is obtained by integration by parts. Since $\lambda_n \neq \lambda_m$ this proves that $\int \psi_n \psi_m d\mathbf{R} = 0$. Further proof can be found in books about quantum mechanics.

Combining (7.7), (7.8) and the solutions to (7.9) gives:

$$G_N(\mathbf{R}|\mathbf{R}')_n = c_n(\mathbf{R}')\psi_n(\mathbf{R}) \exp(-\lambda_n N)$$

where $c_n(\mathbf{R}')$ indicates that the integration constant may be different for every n and can also depend on \mathbf{R}' . Since (7.6) is a homogeneous, linear equation, linear combinations of its solutions are also solutions:

$$G_N(\mathbf{R}|\mathbf{R}') = \sum_n c_n(\mathbf{R}')\psi_n(\mathbf{R}) \exp(-\lambda_n N)$$

which is the general solution, since the ψ_n s form a complete set. This expression can be further simplified since a chain starting at \mathbf{R}' must have the same probability of ending at \mathbf{R} as a chain starting at \mathbf{R} to end at \mathbf{R}' : the expression must not change upon interchanging \mathbf{R} and \mathbf{R}' . This implies

$$G_N(\mathbf{R}|\mathbf{R}') = \sum_n a_n \psi_n(\mathbf{R}')\psi_n(\mathbf{R}) \exp(-\lambda_n N)$$

In the limit of very short chains ($N \rightarrow 0$) of this expression, we must require that the chain ends at the same position where it starts

$$\lim_{N \rightarrow 0} G_N(\mathbf{R}|\mathbf{R}') = \sum_n a_n \psi_n(\mathbf{R}')\psi_n(\mathbf{R}) = \delta(\mathbf{R} - \mathbf{R}')$$

Multiplying with $\psi_m(\mathbf{R})$, integrating over \mathbf{R} , and applying (7.10) gives $a_m = 1$ for all m . So our final expression is:

$$G_N(\mathbf{R}|\mathbf{R}') = \sum_n \psi_n(\mathbf{R}')\psi_n(\mathbf{R}) \exp(-\lambda_n N) \quad (7.11)$$

If we allow complex eigenfunctions we have to insert a complex conjugate *:

$$G_N(\mathbf{R}|\mathbf{R}') = \sum_n \psi_n^*(\mathbf{R}')\psi_n(\mathbf{R}) \exp(-\lambda_n N) \quad (7.12)$$

We can check this formula for the known case of $\varphi(\mathbf{R}) = 0$. Then the solutions of (7.9) are:

$$\begin{aligned} \psi_{\mathbf{k}}(\mathbf{R}) &= \exp(i\mathbf{k} \cdot \mathbf{R}) \\ \lambda_{\mathbf{k}} &= \frac{1}{6}b^2\mathbf{k}^2 \end{aligned}$$

valid for every value of \mathbf{k} . This means that there is a continuous spectrum of eigenvalues and the sum over n in (7.11) reduces to an integral over \mathbf{k} :

$$G_N(\mathbf{R}|\mathbf{R}') = \int \exp(i\mathbf{k} \cdot (\mathbf{R} - \mathbf{R}')) \exp(-\frac{1}{6}b^2\mathbf{k}^2 N) d\mathbf{k}$$

which is the Fourier transform of the usual Gaussian distribution.

7.4. Gaussian integrals

Integrals containing Gaussian functions $\exp(-Ax^2)$ can be derived in a simple way from the following standard integral

$$I(A) \equiv \int_{-\infty}^{+\infty} e^{-Ax^2} dx = \sqrt{\frac{\pi}{A}}$$

By taking its derivative with respect to A we obtain integrals of the product with even powers of x , e.g.

$$\int_{-\infty}^{+\infty} x^2 e^{-Ax^2} dx = -\frac{dI(A)}{dA} = -\frac{d}{dA} \sqrt{\frac{\pi}{A}} = \frac{1}{2} \frac{\pi^{1/2}}{A^{3/2}}$$

and by taking higher derivatives we generate the higher even powers. Odd powers of x give 0 since the integrand is odd in that case:

$$\int_{-\infty}^{+\infty} x^{2n+1} e^{-Ax^2} dx = 0$$

Using these formulas, averages can be calculated quite easily, e.g.

$$\langle x^2 \rangle = \frac{\int_{-\infty}^{+\infty} x^2 e^{-Ax^2} dx}{\int_{-\infty}^{+\infty} e^{-Ax^2} dx} = \frac{1}{2A}$$

From this last relation we can express A in terms of $\langle x^2 \rangle$. A normalized Gaussian distribution (in 1 dimension) is therefore also written like

$$P(x) = \sqrt{\frac{A}{\pi}} \exp(-Ax^2) = \frac{1}{\sqrt{2\pi \langle x^2 \rangle}} \exp(-x^2/2 \langle x^2 \rangle)$$

7.5. The Flory-Huggins approximation

In a concentrated solution polymer chains are interpenetrating, so that a description at the level of individual chains does not apply. Here, we use the same lattice model as in 3.2 to determine the free energy in such a concentrated system. We follow the derivation of M. Doi in his *Introduction to Polymer Physics* (Clarendon Press, 1996). We assume that n_p polymers each occupy N consecutive lattice positions and the remainder of the Ω lattice positions are occupied by $n_s = \Omega - n_p N$ solvent molecules (each occupying 1 lattice position). Therefore, the polymer volume fraction in the system is $\phi = n_p N / \Omega$. If we now write:

$$Z = \sum_i \exp(-E_i/k_B T) \approx W \exp(-\bar{E}/k_B T)$$

the Helmholtz free energy is approximated as:

$$\frac{A}{k_B T} = -\ln Z \approx \frac{\bar{E}}{k_B T} - \ln W \quad (7.13)$$

So, like we did for the single chain, we should determine the total number of configurations of the system W and its average energy \bar{E} . For the average energy we again assume random mixing and interaction between adjacent lattice positions only, like in (3.8). In total the number of nearest-neighbour contacts is $\Omega z/2$, each partner in a contact having a probability ϕ to be a polymer segment and $(1 - \phi)$ to be a solvent molecule. This gives:

$$\bar{E}(\Omega, \phi) \approx -\frac{\Omega z}{2} [\varepsilon_{pp}\phi^2 + \varepsilon_{ps}\phi(1 - \phi) + \varepsilon_{ps}(1 - \phi)\phi + \varepsilon_{ss}(1 - \phi)^2] \quad (7.14)$$

The total number of polymer configurations W is harder to establish. Let us place the polymer chains on the lattice segment by segment. The first segment of the first polymer can be placed in Ω ways and each following segment at approximately $z - 1$ positions with respect to the previous one. This gives w_1 , the number of realizations for the first polymer:

$$w_1 = \Omega(z - 1)^{N-1}$$

For the $j + 1^{\text{st}}$ polymer to be placed the number of possibilities to place its first segment is already less, viz. $\Omega - Nj$, and for each of its next segments we must account for the probability that a lattice point is already occupied (for simplicity we assume that this is the same for every segment within one polymer, viz. $(1 - Nj/\Omega)$). This leads to the following expression for the number of realizations for the $j + 1^{\text{st}}$ polymer, w_{j+1} ,

$$w_{j+1} \approx (\Omega - Nj) \left[(z - 1) \left(1 - \frac{Nj}{\Omega} \right) \right]^{N-1} \approx w_1 \left(1 - \frac{Nj}{\Omega} \right)^N$$

The total number of ways to place n_p polymers on the lattice is therefore

$$W = \frac{1}{n_p!} \prod_{j=1}^{n_p} w_j$$

The factor $n_p!$ corrects for the fact that the polymer molecules are indistinguishable. The logarithm of W can be calculated simply by transformation to an integral:

$$\begin{aligned} \ln W &= \sum_{j=1}^{n_p} \ln(w_j/j) \\ &= \int_0^{n_p} dj \left[\ln \left(\Omega(z - 1)^{N-1} \left(1 - \frac{Nj}{\Omega} \right)^N \right) - \ln j \right] \\ &= \Omega \left[\frac{\phi}{N} - \frac{\phi}{N} \ln \frac{\phi}{N} - (1 - \phi) \ln(1 - \phi) + \phi (\ln(z - 1) - 1) \right] \quad (7.15) \end{aligned}$$

Combining (7.13), (7.14) and (7.15) now gives an expression for the free energy of a system of volume fraction ϕ occupying Ω lattice points, $A(\Omega, \phi)$. In general, the free

energy of mixing A_m is used, from which the free energy of the components before mixing has been subtracted

$$A_m(\Omega, \phi) = A(\Omega, \phi) - A(\Omega\phi, 1) - A(\Omega(1 - \phi), 0)$$

This now leads to the celebrated *Flory-Huggins* expression:

$$A_m(\Omega, \phi) = \Omega k_B T \left[\frac{1}{N} \phi \ln \phi + (1 - \phi) \ln(1 - \phi) + \chi \phi(1 - \phi) \right] \quad (7.16)$$

Note that in this case the usual solute term of the entropy of mixing $\phi \ln \phi$ is multiplied by a factor $1/N$ and the energy of mixing $\chi \phi(1 - \phi)$ contains the same chi-parameter as the energy for a single coil (3.9):

$$\chi \equiv \frac{z\Delta\varepsilon}{k_B T} = \frac{z(\varepsilon_{pp} + \varepsilon_{ss} - 2\varepsilon_{ps})}{2k_B T}$$

7.6. Literature

These lecture notes are largely based upon a number of standard books about polymer theory. A modern book on a very basic level is:

- A.Yu. Grosberg/A.R. Khokhlov, *Giant Molecules* (1997, Academic Press, San Diego)

Several concepts are described in a relatively simple way in:

- M. Doi, *Introduction to Polymer Physics* (1996, Clarendon Press, Oxford)

Two classical books by Flory are:

- P.J. Flory, *Principles of Polymer Chemistry* (1953, Cornell University Press, Ithaca)
- P.J. Flory, *Statistical Mechanics of Chain Molecules* (1969, Interscience Publishers, New York)

Another older but useful book is:

- H. Yamakawa, *Modern Theory of Polymer Solutions* (1971, Harper and Row, New York)

The classical book about scaling theories is:

- P.G. de Gennes, *Scaling Concepts in Polymer Physics* (1979, Cornell University Press, Ithaca)

The first chapters of the following book give a short introduction to static properties:

- M. Doi/S.F. Edwards, *The Theory of Polymer Dynamics* (1986, Clarendon Press, Oxford)

Finally, the Russian school of polymer physics is very well described in:

- A.Yu. Grosberg/A.R. Khokhlov, *Statistical Physics of Macromolecules* (1994, AIP Press, New York)

8. DLVO theory & Measurement of Interaction Forces

Alfons van Blaaderen
Soft Condensed Matter, Debye Institute
Utrecht University

Contents

1. THE DLVO POTENTIAL	04
1.1 Van der Waals forces between two molecules	05
1.2 Van der Waals forces between two spheres: Hamaker approach	08
1.3 Van der Waals forces between two spheres: Modern Theory	10
1.4 Overlap of flat double layers: Debye-Hückel approximation	08
1.5 Double layer overlap between two spheres	15
1.6 Summation of forces	16
1.7 Deviations from DLVO	18
2. MEASURING INTERACTION POTENTIALS	19
2.1 Surface Force Apparatus (SFA)	19
2.2 Atomic Force Microscopy (AFM)	23
2.3 Total Internal Reflection Microscopy (TIRM)	25
2.4 Direct Imaging	26
<i>Appendix A</i> The Principle of Archimedes: Effect of the suspension medium	45
<i>Appendix B</i> Derjaguin Approximation	46
<i>Appendix C</i> Optical Tweezers or Single-beam gradient optical traps	48
REFERENCES	56
REFERENCES ADDENDUM:	
Controversies Continue Feb. 1998- Feb. 2000	60

1. THE DLVO POTENTIAL

It should always be remembered that the origin of forces between colloidal particles is molecular of origin. And although we will soon turn, as one of the many approximations necessary to arrive at results, to a continuous description of matter, it is instructive to write down the different contributions to the interaction potential V between two molecules:

$$V = \text{overlap repulsion (1) + electrical multipole - electrical multipole (2) +} \quad (1) \\ \text{electrical multipole - induced electrical multipole (3) + dispersion (4)}$$

Clearly, all these interactions can in principle be calculated exactly by solving the quantum mechanical Schrödinger equation for the two molecules under consideration. Such a calculation would give both the absolute intramolecular energies and charge distributions. However, this equation can only be solved in (very) simple cases and it is more convenient to interpret the total interaction potential as the sum of the contributions given in Eq. (1). Each contribution depends on molecular properties that can be derived from the Schrödinger equation as well, but some of these terms can also be expressed in a more intuitive (semi) classical form.

Contribution (1) can only be understood in quantum mechanical terms as it represents the repulsion that occurs when the electron clouds of two closed-shell molecules start to overlap. In order to really let that happen the Pauli exclusion principle forbids more than 2 electrons in the same molecular orbital and thus forcing the electrons into excited state orbitals upon approach. This produces a strong increase in energy with the repulsion being approximately proportional to the square of the overlap and increases very strongly as the separation between the molecules decreases. This effect determines a molecule's size (σ), and also a distance of closest approach in a continuum description of matter. Usually, this overlap repulsion is described as a power law in the distance: $V(r) = (\sigma/r)^n$. For $n = 12$, we obtain the repulsive term in the Lennard-Jones potential and for $n = \infty$, we are in the limit of hard spheres.

Electrical multipole-electrical multipole interactions (2) occur between two molecules that possess net charges or an asymmetrical distribution of electrons or nuclei. This term can be (approximately) described by classical electrostatics.

Electrical multipole-induced multipole interactions (3) occur between a molecule with a permanent electrical multipole and a polarizable molecule, a term which can be described semi classical.

Also the dispersion term (4) can only be described in quantum mechanical terms. It represents the coupling between a spontaneous dipole-induced dipole interaction.

In Eq. (1) there is formally a fifth term that describes charge-transfer interactions between two molecules if they are very close together and if one of the molecules acts as a donor of electrons to the accepting molecule with an electron deficiency. For colloidal interactions this term is unimportant and we will not consider it further.

In the following section we will give some (simplified) expressions for the terms 1-4 from Eq. (1) in the case of two neutral molecules. The mono-pole moments that will be part in the case of charged molecules will not be considered but will be deferred to Section 1.4 and 1.5. Taken together these three simplified terms constitute the Van der Waals forces: the Keesom interactions, the Debye interactions and the London interactions.

1.1 Van der Waals forces between two molecules

Before turning to two spheres consisting of so many molecules that we will take their distribution as continuous, we will first consider the Van der Waals forces between two polar and polarizable molecules. As pointed out above, we will only keep simplified expressions. In terms of Eq. (1), we will only consider the second order terms in the full multipole expansion; the mono pole terms are zero because the molecules are uncharged.

But first a few words about the origin of the names associated with these interactions that will turn out all to have an $1/r^6$ dependence on the intermolecular distance r .

It was already Newton in 1686 in his *Principia*, as pointed out by Sparnaay [13], who discussed the attraction between two molecules separated by a distance r , in terms of a force, proportional to r^{-n} , where $n > 4$. He did of course not know the origin of such a force, but could show that if n would be smaller than four the interaction energy of a molecule with a large plate would turn out to be infinitely large. Van der Waals made in 1873 another major step when he treated the equation of state of a gas in his famous thesis [14] and separated out the short-range repulsive forces (term 1 in Eq. (1)), resulting in the excluded volume term (b), from the long range attractive forces that are described by the constant a :

$$\left(P + \frac{n^2 a}{V^2} \right) \cdot (V - nb) = nRT \quad (2)$$

This is how the term Van der Waals forces came into being and in the beginning of the previous century several workers sought an explanation for these long range forces. The three contributions that turned out to be the most important are named after their inventors Keesom, Debye and London forces.

Keesom interactions are Boltzmann-averaged interactions between two permanent dipoles (term 2 in Eq. (1)). It follows from simple electro statics that two dipoles placed head to toe are in their lowest energy configuration which is given by:

$$V(r) = -\frac{m_1 m_2}{2\pi\epsilon_0 r^3} \quad (3)$$

with m the dipole moment of the molecules and ϵ_0 the dielectric permittivity of vacuum. To give some idea of the magnitudes of these interactions: two opposite elementary charges separated by a distance of 0.1 nm gives a dipole moment $m = (0.1 \text{ nm}) \times (1.6 \times 10^{-19} \text{ C}) = 1.6 \times 10^{-29} \text{ C.m} = 4.8 \text{ D}$. The Debye is often used for dipole moments and equals $3.336 \times 10^{-30} \text{ C.m}$. Permanent dipole moments occur in asymmetric molecules and thus not in single atoms. Water has a dipole moment of 1.85 D. Two dipoles with $m = 1 \text{ D}$ in their lowest energy configuration have in vacuum an energy of $k_B T$ (with k_B Boltzmann's constant and T the absolute temperature) at a separation distance of 0.36 nm. These figures indicate that dipole-dipole interactions in liquids, where the interactions are reduced by a factor ϵ the relative dielectric constant (80 for water), are not strong enough to lead to substantial mutual alignment. Therefore, the interaction energies between two dipolar molecules

can be (Boltzmann) averaged rotationally in order to arrive at the following free energy $w(r)$ (see e.g. [7, 5] for the derivation):

$$w(r) = -\frac{m_1^2 m_2^2}{3(4\pi\epsilon\epsilon_0)^2 k_B T r^6} \quad (4)$$

From the above it will be no surprise that the interaction between a polar molecule with a polarizable other molecule with polarizability α also has to be (Boltzmann) orientationally averaged leading to the so-called Debye or induction interactions:

$$w(r) = -\frac{m_1^2 \alpha_2}{(4\pi\epsilon\epsilon_0)^2 r^6} \quad (5)$$

Or, more generally if we consider two polarizable molecules with two dipole moments:

$$w(r) = -\frac{m_1^2 \alpha_2 + m_2^2 \alpha_1}{(4\pi\epsilon\epsilon_0)^2 r^6} \quad (6)$$

In order to get an intuitive idea of the origin and magnitudes of the (electronic) polarizability α , let us imagine a one-electron atom whose electron (charge e) circles the nucleus at a distance R , which also defines the radius of the atom. If under the influence of an external electric field E the electron orbital is shifted by a distance l from the original orbit around the nucleus (see Figure 1), then we get for the induced dipole moment:

$$m_{\text{ind}} = \alpha \cdot E = l \cdot e \quad (7)$$

The *external* force on the electron due to the field E is given by:

$$F_{\text{ext}} = e \cdot E \quad (8)$$

which must be balanced at equilibrium by the attractive force between the displaced electron orbit and the nucleus and is given by the Coulombic force $e^2/4\pi\epsilon_0 R^2$ projected along the direction of the field (see Figure 1). The *internal* restoring force thus becomes:

$$F_{\text{int}} = \frac{e^2}{4\pi\epsilon_0 R^2} \cdot \sin(\theta) \approx \frac{e}{4\pi\epsilon_0 R^3} \cdot m_{\text{ind}} \quad (9)$$

At equilibrium $F_{\text{ext}} = F_{\text{int}}$ and thus

$$m_{\text{nd}} = 4\pi\epsilon_0 R^3 E = \alpha \cdot E \quad (10)$$

whence we obtain for the polarizability:

$$\alpha = 4\pi\epsilon_0 R^3 \quad (11)$$

The unit of (the electronic) polarizability is therefore $4\pi\epsilon_0 \times (\text{volume})$ or $\text{C}^2 \cdot \text{m}^2 \cdot \text{J}^{-1}$ and it is of the order of $4\pi\epsilon_0 \times (\text{molecular radius})^3$. For example, water has $\alpha/4\pi\epsilon_0 = 1.48 \times 10^{-30} \text{ m}^3$, which would lead to a molecular size of 0.114 nm, where 0.114 nm is about 15 % less than the real radius of a water molecule (0.135 nm) [5].

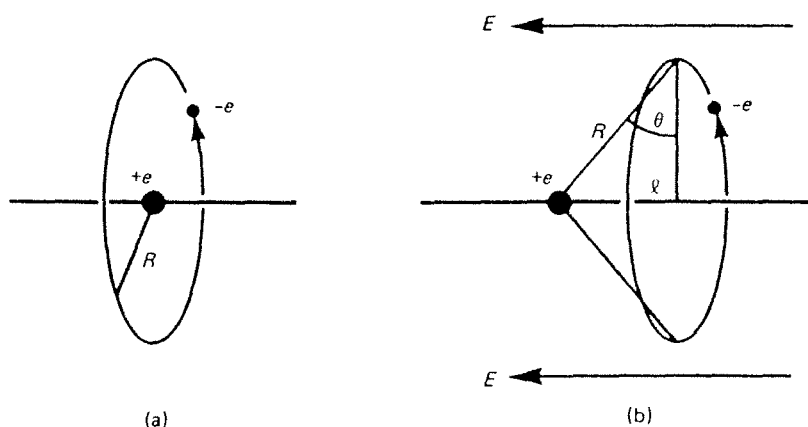


Figure 1 Induced dipole in a one-electron atom: a) no external electric field, b) in an external electric field with magnitude E which shifts the orbital a distance l from the nucleus, so that the induced dipole moment is $m_{\text{ind}} = l.e = \alpha.E$, where the polarizability is given by: $\alpha = 4\pi\epsilon_0 R^3$ [5].

The London or dispersion forces are conceptually the most difficult contribution to the Van der Waals forces because they are of quantum mechanical origin. They could therefore only be derived after the advent of this theoretical framework. Intuitively, their origin may be understood from realizing that for a non polar molecule the time average of its dipole moment might be zero, at every instant there exists a finite dipole moment because the electronic charge and the nuclear proton charge do not reside at the same position in space. This instantaneous dipole moment can induce by polarization a dipole in a nearby neutral molecule (or in other words the two fluctuating dipoles will couple). The resulting interaction between the two dipoles gives rise to an instantaneous attraction between the nonpolar molecules with a time average that is not zero. For getting even a semi quantitative feeling of this interaction we take an example from Israelachvili's book on interaction forces [5].

Let us consider the dispersion interactions between two Bohr atoms. In the Bohr atom one electron is orbiting a proton. The smallest distance (that there is a smallest distance and its size follow only from quantum mechanics) between the electron and the proton is known as the first Bohr radius a_0 . At this radius the Coulomb energy of the system, $e^2/4\pi\epsilon_0 a_0$ is equal to $2h\nu$, or,

$$a_0 = e^2/2(4\pi\epsilon_0) h\nu = 0.053 \text{ nm} \quad (12)$$

where h is the Planck constant and ν the orbiting frequency of the electron. For a Bohr atom, $\nu = 3.3 \times 10^{15} \text{ s}^{-1}$ and thus $h\nu = 2.2 \times 10^{-20} \text{ J}$. This is the energy of an electron in its first Bohr radius and equals the energy to ionize the atom, i.e., the first ionization potential I . As argued above the Bohr atom has no permanent dipole moment, but at

any moment the instantaneous dipole moment m is given by: $m = a_o \cdot e$ whose field will polarize a nearby other neutral apolar atom giving rise to an attractive interaction that is completely analogous to the dipole-induced dipole interaction discussed above. The energy of interaction is therefore given by (see Eq. (6)):

$$w(r) = -u^2 \alpha / (4\pi\epsilon_o)^2 r^6 = - (a_o \cdot e)^2 \alpha / (4\pi\epsilon_o)^2 r^6 \quad (13)$$

here α is the polarizability of the second Bohr atom, which from Eq. (11) is approximately given by $4\pi\epsilon_o a_o^3$. Using this expression for α and Eq. (12) gives:

$$w(r) \approx -\alpha^2 h\nu / (4\pi\epsilon_o)^2 r^6 \quad (14)$$

Apart from a numerical factor Eq. (14) is equal to the result that London derived in the 1930's using quantum mechanical perturbation theory. London's expression for the dispersion interaction between two different molecules is:

$$w(r) = -\frac{3}{2} \frac{\alpha_1 \alpha_2}{(4\pi\epsilon_o)^2 r^6} \cdot \frac{h\nu_1 \nu_2}{(\nu_1 + \nu_2)} = -\frac{3}{2} \frac{\alpha_1 \alpha_2}{(4\pi\epsilon_o)^2 r^6} \cdot \frac{I_1 I_2}{(I_1 + I_2)} \quad (15)$$

Although London's equation has of course been followed by more exact, and more complicated, expressions (see section 1) it gives fairly accurate numbers, though somewhat on the low side compared with more rigorous values. The 'derivation' of Eq. (14) also demonstrates that although the dispersion forces arise from quantum mechanical effects (which gave the strength of the instantaneous, but fluctuating dipole moments), the interaction itself can still be seen as essentially electrostatic. The name *dispersion* force stems from the relation of the forces to the dispersion of light in the visible and UV part of the spectrum (as exemplified by ν in Eq. (15)). A more thorough account of molecular Van der Waals forces can be found in [5, 15].

1.2 Van der Waals forces between two spheres: Hamaker approach

All contributions to the Van der Waals forces, induction, orientation and dispersion, have the same functional form and can be taken together as:

$$w_{VDW}(r) = -C_{VDW}/r^6 = -[C_{ind} + C_{orient} + C_{disp}]/r^6 \quad (16)$$

where the constants C can be taken from Eqs. (4), (6) and (15). From tabulations of the constants given in Eq. (16) it becomes clear that in almost all cases the dispersion forces are the most important, except for small polar molecules like water.

The simplest approach to calculate the Van der Waals forces between macroscopic bodies (macroscopic in the sense that we will treat them as consisting of continuous matter) is to assume that the molecular contributions given above are pairwise additive. (Which as it turns out is for most substances not such a bad approximation). We can then obtain interaction energies from simple integration an approach first taken by a Dutch physicist called Hamaker [16]. The interaction energy dU_{12} between two infinitesimal volume elements $dV_1 = dx_1 dy_1 dz_1$ and $dV_2 = dx_2 dy_2 dz_2$ inside bodies 1 and 2 respectively becomes then:

$$(17)$$

$$dU_{12} = \frac{-C_{12}\rho_1\rho_2 dV_1 dV_2}{\{(x_2 - x_1)^2 + (y_2 - y_1)^2 + (z_2 - z_1)^2\}^3}$$

where the ρ 's are the number densities of the molecules in the material 1 and 2. It is now a matter of algebra (or a numerical calculation) to obtain the interaction energies between the two bodies. An interesting feature of the 6th power dependence is that the resulting energies are scale invariant. (That means that two colloids at a separation of 10% of their distance, say 10 nm, have the same interaction energy as two apples a few cm apart.). We will first present the interaction energy U_{12} between two infinite half-spaces at a distance h (because the half-spaces are infinite the energy is given per area of the half-spaces):

$$U_{12} = \frac{-A_{12}}{12\pi} \cdot \frac{1}{h^2} \quad (18)$$

where we have combined (for historical reasons) $2\pi C_{12}\rho_1\rho_2$ to form the Hamaker constant A_{12} . (There is a very nice anecdote connected to this derivation (see [17])). The integration has turned the short range r^{-6} dependence into a quite long range h^{-2} dependence! Integration of Eq. (17) between two spheres of size $2R$ gives [16]:

$$U_{12} = \frac{-A_{12}}{12} \cdot \left(\frac{1}{x^2 - 1} + \frac{1}{x^2} + 2 \ln \left(\frac{x^2 - 1}{x^2} \right) \right) \quad (19)$$

where $x = r/(2R)$ is the reduced distance between the spheres.

Equations like Eq. (18) are still of not too much use in the description of interactions between two colloidal particles, because these are always dispersed in a dispersion medium and Eq. (18) describes interactions in vacuum. The very nice feature of the pairwise summation assumption is that it leads in a straightforward way to the interactions between two bodies 1 and 3 dispersed in a medium 3. The same principle behind the derivation therefore holds also for other forces that can be summed in a pairwise fashion (like gravity) and the principle behind it is therefore also called the principle of Archimedes (see Appendix A). From this principle it follows directly that by immersion of the two bodies into a third medium not the geometrical terms are changed but instead only the Hamaker constant according to the following equation (see Appendix A):

$$A_{123} = A_{13} + A_{22} - A_{12} - A_{23} \quad (20)$$

Similarly as for the case which Archimedes made famous with his outcry of 'Eureka', the combined Hamaker constant can both be positive and negative. For interactions between two similar bodies Eq. (20) reduces to:

$$A_{121} = A_{11} + A_{22} - 2A_{12} \quad (21)$$

If we look at Eq. (16) it can be shown that A_{121} can be positive only and equals A_{212} indicating that Van der Waals forces between two bodies of the same material are always attractive! As mentioned for most substances the most important contribution

(certainly for apolar substances) to the Hamaker constant is given by the dispersion interaction. From Eq. (15) it follows that approximately:

$$A_{12}^2 \approx A_{11} \cdot A_{22} \quad (22)$$

thus Eq. (21) and Eq. (20) become:

$$A_{121} \approx \left(\sqrt{A_{11}} - \sqrt{A_{22}} \right)^2 \quad (23)$$

and

$$A_{123} \approx \left(\sqrt{A_{22}} - \sqrt{A_{11}} \right) \cdot \left(\sqrt{A_{22}} - \sqrt{A_{33}} \right) \quad (24)$$

which is negative if $A_{11} > A_{22} > A_{33}$ or $A_{11} < A_{22} < A_{33}$. This situation occurs most often when a liquid (2) wets a solid surface (1) in air (3). Then $A_{33} \approx 0$ and often $A_{11} > A_{22}$. This explains for instance why liquid helium will be attracted by a wall of a vessel, and form a relative thick film on the container wall. Because of its low viscosity it can even flow out of the container (see for theory about wetting phenomena the lectures by Blokhuis).

Although a lot of approximations have been made these kind of combining relations are quite useful to estimate Hamaker constants between different materials from known values. To give just two examples: the Hamaker constant for a CaF_2 -helium-air interaction would be predicted by Eq. (24) to be: $A_{123} \approx (\sqrt{7.2} - \sqrt{0.057})(0 - \sqrt{0.056}) \times 10^{-20} = -0.58 \times 10^{-20} \text{ J}$. A more rigorous value gives $-0.59 \times 10^{-20} \text{ J}$. Similarly, for a quartz-octane-quartz system Eq. (23) gives: $A_{121} \approx (\sqrt{6.3} - \sqrt{4.5})^2 \times 10^{-20} = 0.15 \times 10^{-20} \text{ J}$ compared to $0.13 \times 10^{-20} \text{ J}$ [5]. Estimates can also be made from the following approximate values for interactions in water:

A_{121} : (30-10 for metals, 3-1 for oxides and halides, ~ 0.30 for hydrocarbons) $\times 10^{-20} \text{ J}$.

1.3 Van der Waals forces between two spheres: Modern Theory

For many situations in colloid science the approximate formulae derived in the previous section are accurate enough. However, it is clear that many approximations were made and that there are many places/levels where improvements can be made.

In a book dedicated to him on the occasion of his retirement Overbeek remarks that it was perhaps his major discovery that he realized that the London-Van der Waals forces must show retardation at separations larger than the London wave length [18]. In the same heuristic way as the dispersion forces were introduced above, it is not hard to understand where such a retardation comes from. It was assumed above that the dipole moments that were present at each instant in time could induce a dipole in the other molecules instantaneously. It is clear that this can not be correct and in reality such an induced interaction can not travel faster than with the speed of light. This means that if the distance between the molecules becomes so large that the dipole moment in the first molecule has already changed, the interaction with the induced dipole moment is reduced. Overbeek asked Casimir whether he saw a way to a theoretical treatment of this problem and Casimir and Polder succeeded in formulating a quantum mechanical theory for these effects in the case of two metals [19]. It turns out that in the retarded limit the $1/r^6$ potential is reduced to a faster decaying $1/r^7$ functional form. (Note that the other contributions to the Van der Waals forces do not show this retardation).

Using advanced quantum field theory combined with statistical mechanics, Lifshitz [20] and later Dzyaloshinskii [21], derived the general case including dielectric materials. In this theory non-additivity effects and retardation are all treated in a natural way. Because the results were so complex it took a long way for them to reach the complex fluids community. This only happened after Van Kampen and others, along the same treatment as was used by Casimir and Polder, had rederived the essential equations using a much simpler (semi classical) approach. It goes very roughly along the heuristic lines indicated above about the coupling of electromagnetic fluctuations traveling from the one body to the other, but is cast completely in terms of the dielectric responses of the bulk materials. Quite a lot of researchers subsequently simplified the equations to such an extent that it is possible to calculate Hamaker constants from just a few relevant dielectric properties of the materials under consideration. Here we will just refer to the standard books on this subject [15, 4, 5, 7, 8, 10]. All geometrical equations of the previous section are obtained as limiting cases though, and the material properties like the Hamaker constant, are not derived from molecular but bulk dielectric properties.

1.4 Overlap of flat double layers: Debye-Hückel approximation

The interactions between a charged surface and the distribution of ions, both from added salt (we will limit ourselves to so-called z - z symmetric salts) and counterions will be treated within the self-consistent mean-field Poisson-Boltzmann approach. In this approach the Poisson equation, which follows directly from the Coulomb law of electrostatics, is combined with the statistic mechanical Boltzmann equation in order to obtain the distribution of ions in the potential field of the plate with a certain surface charge. We will treat the distribution of the ions along one plate first, after Gouy and Chapman who were the first to do this along these lines, and subsequently calculate the free energy difference of bringing two such plates together.

The surface charge is supposed to be of uniform density and the ions are treated as point objects with no size, embedded in a solvent which is approximated as a continuous dielectric medium. The surface charge on the plate sets up a potential ψ in the solvent, which depends on the distance from the plate and which puts the free ions in the solution at an electrical potential energy. Conversely, the distribution of ions determines the local potential. The iterative or self-consistent way in which these dependencies are expressed is a combination of the Poisson equation, which relates the local charge density to the local potential, and the Boltzmann equation which describes the probability of finding an ion at a certain (electrical) free energy. The Poisson equation is given by:

$$\text{div}(\text{grad } \psi) = \nabla^2 \psi = \frac{-\rho}{\epsilon \epsilon_0} \quad (25)$$

here ρ is the local volume density of charge, i.e., the number of charges per unit volume:

$$\rho = \sum_i n_i z_i e \quad (26)$$

where the summation is over all the species of ion present with valency z_i and number density n_i , here z_i includes the sign of the charge.

The Boltzmann equation reads for an ion at potential ψ :

$$n_i = n_{oi} \exp(-w_i / k_B T) \quad (27)$$

where w_i represents the work done in bringing an ion i up from the bulk, where its number density is n_{oi} , to a point in the double layer where the potential is ψ . The amount of work w_i is now approximated as $w_i = z_i e \psi$. In other words the only work done that is taken into account is the electrical work done on or by the ion when it is brought into the double layer. This ignores work done to move other ions away or create a hole in the solvent, or any effect the ion has on the structure of the solvent or the distribution of the other ions. As stated above the ion is simply treated as a point charge.

Combining Eqs. (25)-(27) gives the Poisson-Boltzmann equation (PB):

$$\nabla^2 \psi = \frac{-1}{\epsilon \epsilon_o} \sum_i n_{oi} z_i \exp(-z_i e \psi / k_B T) \quad (28)$$

If the electrical energy is small compared to the thermal energy ($|z_i e \psi| < k_B T$) it is possible to expand the exponential in this non-linear equation. Neglecting all but the first two terms:

$$\nabla^2 \psi = \frac{-1}{\epsilon \epsilon_o} \left(\sum_i z_i e n_{oi} - \sum_i z_i^2 e^2 n_{oi} \psi / k_B T \right) \quad (29)$$

The first summation must be zero because of charge neutrality in the bulk solution, thus:

$$\nabla^2 \psi = \left(\frac{\sum_i z_i^2 e^2 n_{oi}}{\epsilon \epsilon_o k_B T} \right) \cdot \psi = \kappa^2 \psi \quad (30)$$

where

$$\kappa = \left(\frac{e^2 \sum_i z_i^2 n_{oi}}{\epsilon \epsilon_o k_B T} \right)^{1/2} \quad (31)$$

This linearization of the PB equation is called the Debye-Hückel (DH) approximation because it was used by these workers in their theory of strong electrolytes. Eq. (30) can be solved easily and one obtains:

$$\psi = \psi_o \exp(-\kappa \cdot x) \quad (32)$$

with ψ_o the surface potential. The quantity κ^{-1} the *Debye-Hückel screening length* plays an important role in the theory of the double layer. From Eq. (32) it can be seen why, as in this approximation it determines the extension of the double layer and the region at which the potential around a colloid is different from that of the bulk where it is zero. Apart from some fundamental constants, κ depends only on the temperature and the ionic strength I defined as: $I = (1/2) \sum_i c_i z_i^2$ where c_i is the ionic concentration

in mol/l. A useful rule of thumb is obtained by filling in the constants for water at room temperature (25 °C):

$$\kappa = 3.288 \sqrt{I} \text{ [nm}^{-1}\text{]} \quad (33)$$

Thus for a solution of 1:1 electrolyte at 10^{-3} M the double layer thickness is 9.6 nm. At 10^{-6} M it is 304 nm.

For flat plates the non-linear PB equation can be solved analytically using a mathematical trick. However, in these notes we are more concerned with spherical double layers so we will refer to the literature for this result [2, 4, 9]. Without giving the full result it is easy to see that even in the case of high surface potentials at large distances ψ becomes small and the long distance tail of the potential takes on the exponential form given by Eq. (32), but now with a different scaling factor which is determined by the full solution. Because an other particle will only sample the not too high potential regions the exponential form is often used.

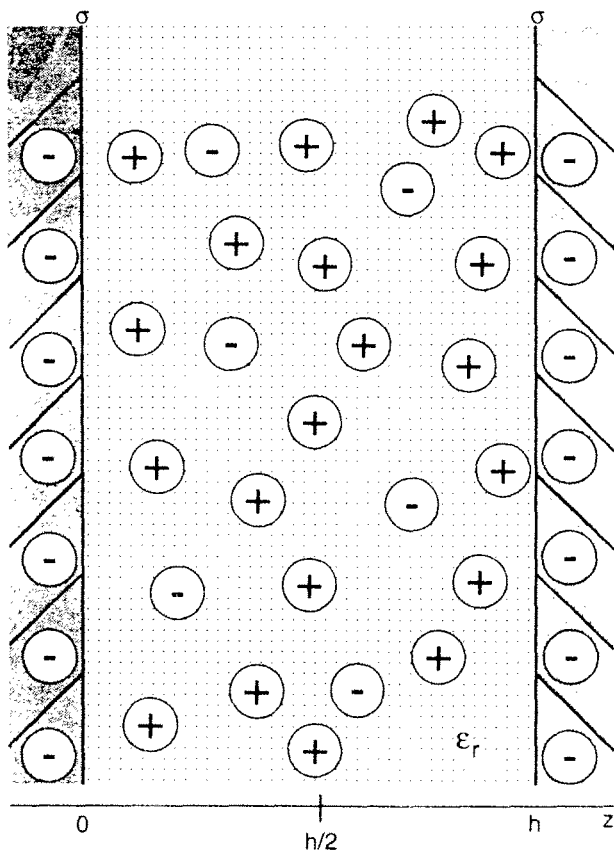


Figure 2 Two interacting negatively charged surfaces separated by h experience a repulsive force as they are pushed together.

Before turning to the much more difficult problem of a double layer around a sphere, we will first give one thermodynamic path of how to obtain the amount of work done if two flat double layers are brought in each others neighborhood and start to overlap, i.e., the free energy as a function of distance between two infinitely large spheres. In the case of overlapping double layers the mechanism of surface charge regulation becomes of importance. There are several mechanisms by which a surface can obtain and regulate a surface charge, some of the most important are: 1) A very small imbalance in the amount of crystal lattice anions or cations (e.g., as in

the case of AgI crystals in water). 2) Surface dissociation. 3) Crystal lattice defects. 4) Surface absorption of ionic species. The problem of how the surfaces regulate their charge on the surface on overlap of two double layers is complicated and also depends on the mechanism of charge generation and maybe even the speed of approach. This problem has not yet been solved unambiguously [9]. However, it can be shown that

real systems will lie within the borders of a constant surface charge upon approach and a constant surface potential, for the moment we will assume the latter.

One other subject that is still to this date a matter of controversy in the literature is the experimental determination of the surface charge or potential. Again going into this would lead us much too far astray, but it should be mentioned that a lot of experimental observations are not yet explained satisfactorily [7, 9].

Lets now turn to the work required to bring two plates from infinity to a separation distance x in the limit where we can use the DH approximation. There are several ways to obtain this free energy difference of double layer overlap V_{dlo} in the case of flat plates [1-2], here we will only go into one, called the 'force method' by Overbeek [2]. If the plates are brought together reversibly all the forces on the system should cancel because a reversible path goes through equilibrium states. We can use this balancing of forces to recognize that the free energy difference can be obtained by integrating the osmotic pressure Π difference (compared to the bulk) at the midplane between the plates from infinity to the separation distance h :

$$V_{dlo} = - \int_{\infty}^h \Pi dx \quad (34)$$

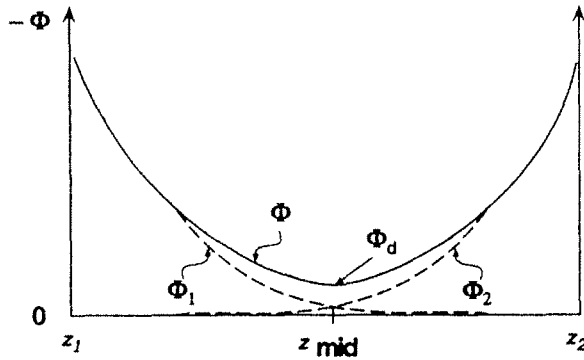


Figure 3 Superposition approximation for two similarly charged surfaces. If the surface charges on the surfaces on the plates are thought to be unaffected by the overlapping double layers, the resulting charge distribution is the sum of the two and by the linearity of the Poisson equation the resulting potential at the midplane will also be the sum of the unperturbed potentials, which can be related to an osmotic pressure at the midplane by the Boltzmann equation.

The rationale behind Eq. (34) is that symmetry dictates that at the midplane the electrical forces on the ions are equal and thus there is no excess charge at this position as well, both because the potential has a minimum here. In the PB approach there are no correlations between the ions so the osmotic pressure of the non interacting ions is simply given by the 'ideal gas' value:

$$\Pi = k_B T ([\sum n_i]_{midplane} - [\sum n_i]_{infinity}).$$

In the linearized DH approximation of small potentials one can take the potential at the midplane as twice the potential of the single plate potential as given by Eq. (32), see Figure 2. This leads to the following double layer overlap potential:

$$V_{dlo} = 2\epsilon\epsilon_o\kappa\psi_o^2 \exp(-\kappa \cdot h) \quad (35)$$

Similarly as stated above, in the limit of large separations also the curves with high surface potential will adopt a limiting form similar to Eq. (35), again with a different 'apparent' surface potential, see Figure 4. It should be remarked that even in the

'simple' two plate geometry the general case can not be treated analytically anymore and all kind of approximate formula's or numerical schemes have to be used (see for more details [2, 9]).

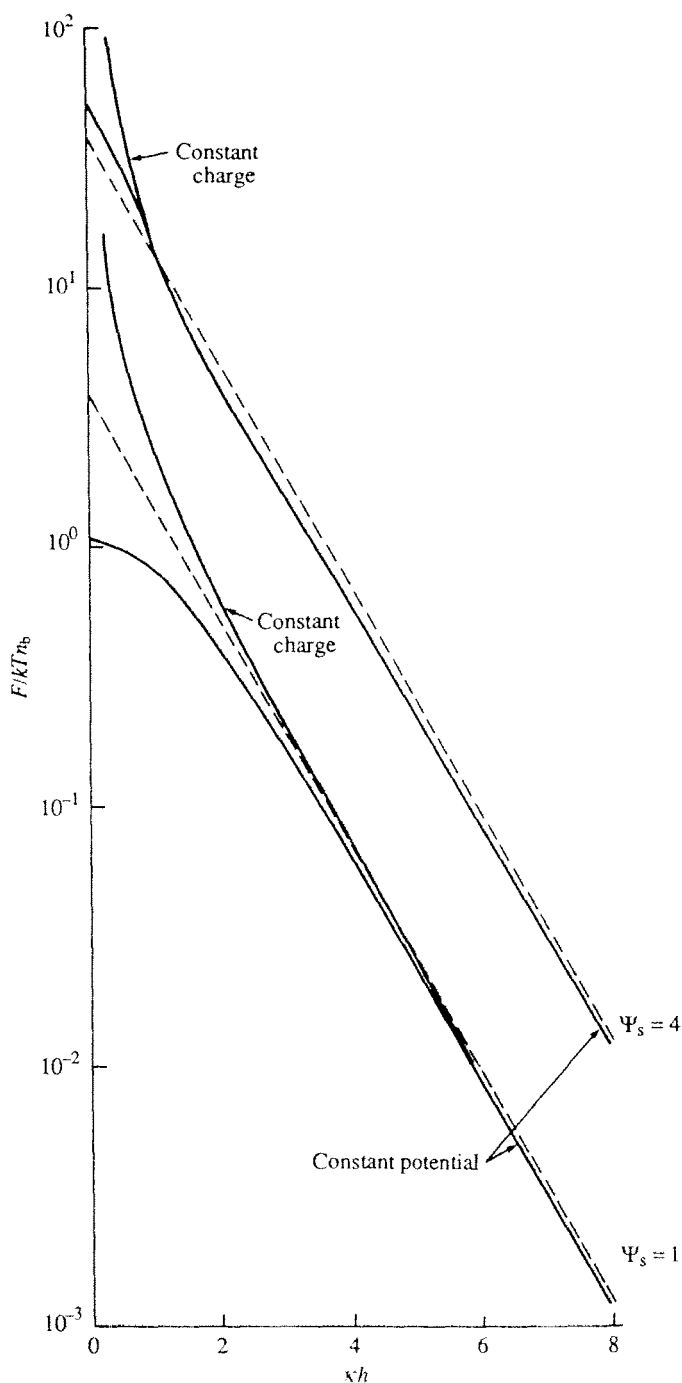


Figure 4 Two identical overlapping flat double layers immersed in an ionic solution. Results are shown in reduced units and as force curves for two different surface potentials and assuming both a constant charge and constant surface potential. The curves are calculated using the exact theory also indicated are approximate results along the lines of Eq. (35). At large separations the approximate results are quite good [4].

1.5 Double layer overlap between two spheres

It will be no surprise that in the much more awkward geometry of two spheres analytical results are even harder to obtain. Not even for a single double layer around a sphere are there analytical results that hold for a reasonable range of parameters and

semi-empirical equation's have been proposed [9]. Only in the case of the DH approximation one obtains an analytical result. Because of the symmetry of the problem the PB equation can best be given in spherical coordinates. In these coordinates the Laplace operator takes the form:

$$\frac{1}{r^2} \frac{d}{dr} \left(r^2 \frac{d\psi}{dr} \right) = \Delta\psi = \frac{-1}{\epsilon\epsilon_0} \sum_i n_{oi} z_i \exp(-z_i e\psi / k_B T) \quad (36)$$

linearizing the exponential ($e^{-x} \approx 1 - x$) leads to (compare with Eq. (30)):

$$\Delta\psi = \kappa^2 \psi \quad (37)$$

Solving Eq. (37) gives a screened Coulomb or Yukawa potential:

$$\psi = \psi_0 \frac{a}{r} \exp[-\kappa(r-a)] \quad (38)$$

where a is the sphere size.

At double layer overlap the situation is even worse. Only for very thin double layers compared to the sphere size it is possible to use the so-called Derjaguin approximation. This approximation comes down to using the results obtained between flat plates to derive equations for large interacting bodies. For interactions between two colloidal spheres the limit of very thin double layers is totally uninteresting. However, because the Derjaguin approximation can also be used with other potentials and is useful in interpreting measurements done with the surface force measurements it is given in Appendix B.

For smaller values of κa (< 5) the Derjaguin procedure breaks down. Verwey and Overbeek have shown that for low surface potentials and if an error of up to 40% can be tolerated approximate formulae in the spirit of Eq. (35) (i.e., by taking sums of potentials) can be derived resulting in again a Yukawa or screened Coulomb form:

$$V_{dl0} = \pi\epsilon\epsilon_0 \kappa a \psi_0^2 \frac{\exp[-\kappa a(x-1)]}{x} \quad (39)$$

here $x = r/a = r/2R$.

1.6 Summation of forces

The combination of the forces resulting from the overlap of two double layers treated theoretically within the assumptions behind the PB equation and the Van der Waals forces constitute the DLVO potential:

$$V_{DLVO} = V_{vdW} + V_{dl0} + V_{Pauli} \quad (40)$$

In this equation we have added the forces that determine the closest distant of approach of two colloids through a strong and steep repulsion caused by the Pauli exclusion principle of electrons in filled orbitals (see Eq. (1)). This repulsion is also quite naturally taken up into a closest distance of approach in the Van der Waals

forces that would otherwise diverge. For two spheres of the same size and using the approximations for the interactions as used in these notes the DLVO potential becomes:

$$V_{DLVO} = \pi\epsilon\epsilon_0\kappa a\psi_0^2 \frac{\exp[-\kappa a(x-1)]}{x} + \frac{-A_{12}}{12} \cdot \left(\frac{1}{x^2-1} + \frac{1}{x^2} + 2\ln\left(\frac{x^2-1}{x^2}\right) \right) \quad (41)$$

One can find numerous forms of DLVO equations, even within the PB approach, it is therefore important to look at which of the many approximations have been used and for what situations the equations are valid.

In a schematic way the different potential shapes, depending on the constants, Eq. (41) can give rise to are given in Figure 5.

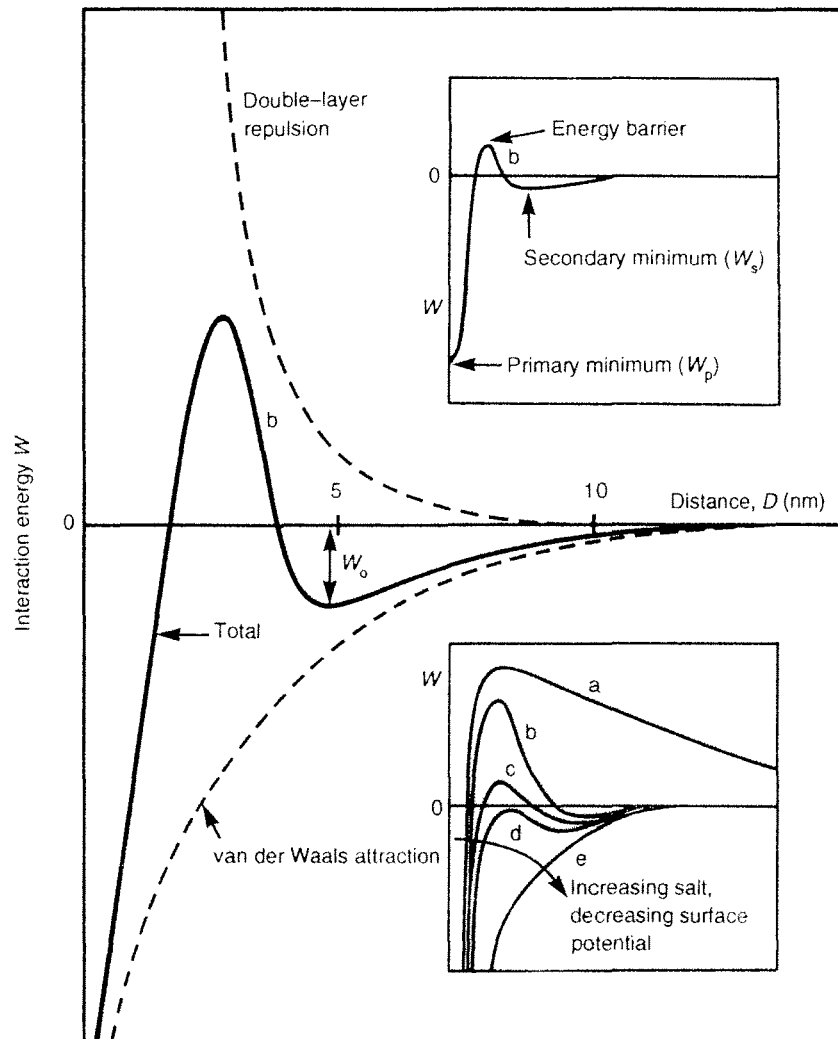


Figure 5 Schematic interaction potentials between two charged colloidal spheres according to Eq. (41) [5].

1.7 Deviations from DLVO

Most of the shortcomings of the Van der Waals forces have already been discussed and with sufficient effort they can at the moment be calculated to great accuracy. The most serious problems arise from the fact that the Lifshitz treatment is a continuum approach and thus if effects that are a consequence of the molecular discreteness are involved the theory fails. For most colloidal interactions there are no indications though that these effects are very important.

There are more (known) problems with the PB description of the double layer interaction potentials. Already mentioned is that in this equation the finite size of the ions and correlations among them are completely neglected. Finite size corrections were realized quickly and the ‘Stern’ layer of closest approach of hydrated ions is one of the earliest examples to remedy this neglect. It has not been until the advent of computer simulations, however, that both new theoretical improvements and the accuracy of the PB approach could be explored fully. It goes too far to discuss these matters in length here (see e.g. Refs. cited in [7, 22]). One of the most important conclusions is that for 1-1 electrolytes at not too high surface potentials and not too close separations the PB equation gives a fair to good description. (It is also relevant in preparation of what follows to remark that between two equal surfaces no attractions have been observed). If the coupling between ions becomes stronger, like for higher valency ions, PB breaks down and qualitatively different behavior is observed [7, 22].

It also seems that equations that are derived under the DH approximation are relatively useless because in practice surface potentials are often higher than ca. 25 mV. However, it is already discussed that this assumption also gives a good description at larger separations if an adjusted surface charge or potential is used. Furthermore, it has been shown theoretically that the DH approximation results in a description that is thermodynamically consistent and can be derived as a limiting case within the framework of liquid state theories (see e.g., the lectures of Briels). This thermodynamic consistency is *not* achieved by solutions obtained from the full non-linear PB equations! Both theoretical work and computer simulations have given additional justification to the use of potentials of the Yukawa form. For instance, Alexander *et al.* have shown through calculations of salt and counterion profiles in a spherical Wigner-Seitz cell that also for strong interactions between the colloids an effective Yukawa pair interaction is obtained if the volume fraction of the particles is not too high. The charge must be renormalized and the double layer thickness adjusted compared to the DH value [23]. Furthermore, Löwen and Krampposthuber have shown from *ab initio* theory that screened Coulomb potentials can be used in many instances as good approximations, but that both the screening length and effective charge have to be adjusted. Moreover, it turns out that in these strongly interacting systems the effective surface charge and screening length become dependent on the phase as well [24].

Now that we have some understanding of the ideas, approximations and limitations behind the DLVO potential(s) it is time to see what experimental methods have been developed over the years to measure these interactions in a direct way. A development which recently has been speeded up, partially from new input from the related field of biology inspired physics and from recent experimental findings that will be described in Section 3.

2. MEASURING INTERACTION POTENTIALS

In this Section we will limit ourselves to a qualitative description of *direct* methods to measure interaction forces. With '*direct*' is meant that the measurements give force-distance curves in an unambiguous way. This excludes methods like osmotic pressure measurements, where only information of a thermodynamic nature is obtained, which can not be directly translated into a force law, or methods that determine only a certain aspect of the force distance relationship like adhesion measurements or coagulation studies. We also exclude potential measurements that rely on an inversion of structural information obtained through scattering studies. Although this method is in principal direct in the above sense it is clear that, largely because of experimental limitations, the inversion procedure is 'ill-defined' and does not give unambiguous potentials (see e.g., [25, 26] and refs. cited).

2.1 Surface Force Apparatus (SFA)

The first attempts to measure both double-layer and Van der Waals forces started in the early fifties in Russia by Derjaguin [27] and in the Netherlands by Overbeek [28] and their coworkers. These studies were performed with set-ups that were essentially similar to what would later be called the surface force apparatus. However, the forces measured were limited to the retarded regime at large surface-to-surface separations because of the roughness of the fused quartz and glass surfaces that were used. It was not until the end of the sixties that Tabor and Winterton started using cleaved mica which made it possible to measure force-distance curves down to molecular separations [29]. Native mica crystallizes in layer structures which can be easily cleaved providing a clay-like atomically smooth surface over a large area, ideally suited for force measurements both in vacuum and in liquids. It is quite remarkable though that just such a 'trivial' matter of obtaining atomically smooth surfaces over large areas has held up the measurement of forces at non-retarded and important range of distances for quite a number of years.

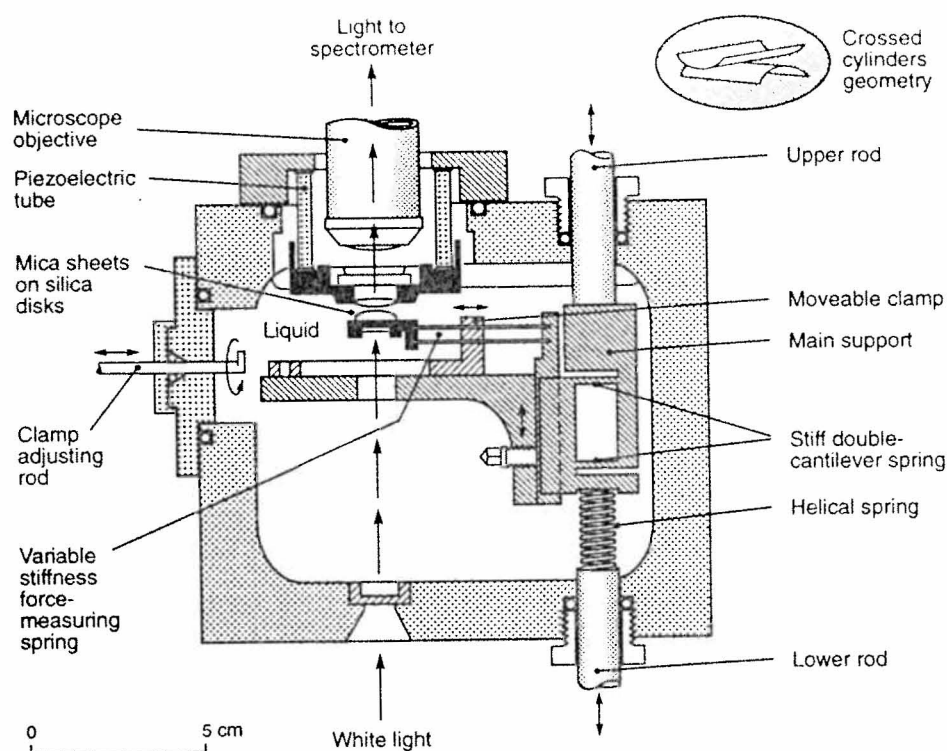


Figure 6. Surface Force Apparatus (SFA) with which force-distance curves can be obtained between molecularly smooth mica sheets with Å (0.1 nm) resolution and a force sensitivity around 10 nN (10^{-8} N) [5].

The modern version of the surface force apparatus is conceptually simple and is depicted in Figure 6 [5]. The separation between the mica surfaces, which are glued onto two quartz pieces with a radius of curvature of 1 cm and are silvered on the back with a partially reflecting silver film, can be determined with an accuracy of 1 Å (0.1 nm). This high accuracy is reached by analyzing the interference that results from multiple reflections of white light by the silver layers on the mica in a spectrometer. Measuring the distance between the surfaces with Å accuracy is only half of the story, it is also necessary to have this accuracy in positioning the surfaces. This is accomplished by a three-stage mechanism. The smallest scale displacements (between 1-10 Å) are achieved by means of a piezoelectric tube that can translate the upper mica surface. In piezo electric materials an electric field can cause the crystal lattice to expand or contract, e.g., by about 1 nm per volt that is applied across the surface of the cylinder wall. Positioning of the lower mica surface on the 1 nm level is achieved by a two spring construction where the difference in stiffness or spring constant between the stiff double-cantilever spring and the helical spring attached to the lower micrometer rod. Therefore, a displacement of the lower micrometer results in a nm displacement of the lower mica surface, in the absence of forces between the mica surfaces. After calibration of this positioning system the actual displacement of this surface can be measured from the interference between the crossed mica surfaces. The difference in displacement can be converted to a force by using the calibrated spring constant of a force measuring spring. The second, lower mica surface is attached to such a force measuring spring of which the stiffness can be varied (by a factor of 1000) by moving a clamp. In this way both attractive *and* repulsive forces can be measured with a sensitivity of about 10 nN (10^{-8} N). Finally, an upper rod can move

the whole section of springs over distances between 1 μm and 1 cm, but it is not used during the actual force measurement. Within the Derjaguin approximation (Appendix B), which is clearly a very good approximation between these macroscopic surfaces, the ratio of the measured force and the radius of curvature, F/R , equals $2\pi U$, where U represents the interaction potential per unit area. Physically, this equivalence means that at a distance h between the curved mica surfaces an average is measured of all interaction forces larger than h . The result of this averaging, the total force equals the sum of the forces between the surface segments from infinity to h , is the energy at h .

In vacuum the forces between the mica sheets are solely due to Van der Waals forces. After all kind of corrections, like change of curvature of the mica sheets due to deformation of the glue by the strong attractive forces, the measured force curves come to within 10 per cent of the calculated curves using the Lifshitz approach over the full range of separations [5]. Immersed in water the mica surfaces obtain a negative surface charge by the dissociation of potassium ions and a double-layer is formed. In this way the DLVO theory was tested at different ionic strengths and potential determining ions (see Figure 8 and Figure 9).

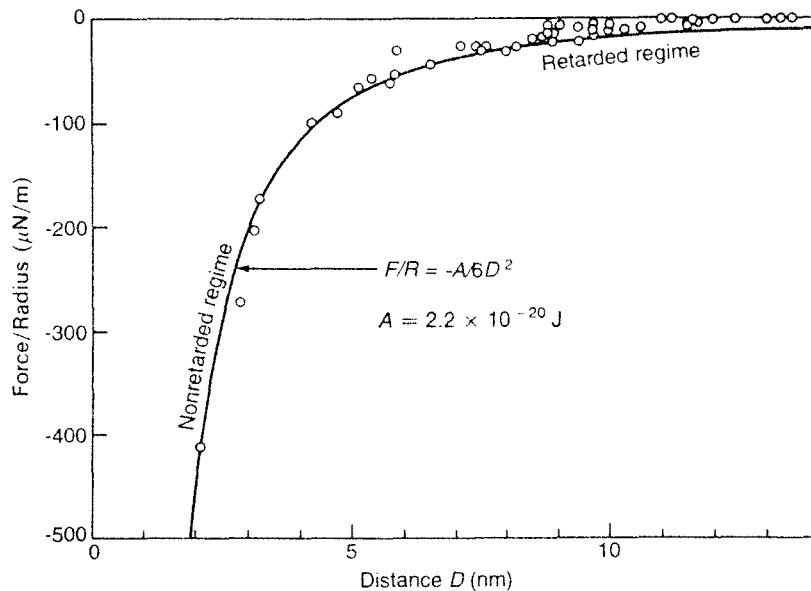


Figure 7 Attractive van der Waals forces between two curved mica surfaces measured in an aqueous electrolyte solution with the SFA [5]. The measured non-retarded Hamaker constant is 2.2×10^{-20} J. Retardation effects become apparent at distances above 5 nm.

At this date the SFA has been quite important in the measurement of all kinds of forces, besides Van der Waals forces and double-layer forces [30, 31], examples are: capillary forces, solvation forces [32], adhesion forces [33], 'hydration' forces [34, 35], depletion forces [36, 37], steric repulsion forces [38, 37], or special 'gel-like short-range' forces on silica [39, 40], and forces that were hardly considered before the experiments, like attractive hydrophobic forces [41, 5] and oscillatory structural forces [5]. All these forces are not elaborated on here, because under conditions under which they are measured it is clear where the assumptions underlying the DLVO potential are not met and/or why the description breaks down. It should be mentioned here that recently these tests are not limited anymore to just one kind of surface, mica in water. For instance, the mica can be used as a substrate to adsorb a thin film of some other material, for example, lipid monolayers, metal films, proteins etc. (see for

Refs. in [5]). In the case of opaque materials a capacitance method replaces the optical technique for measuring distances with similar overall accuracy [42]. Furthermore, Horn *et al.* have finally found a way to make silica surfaces smooth enough so that they could be used in the SFA as well down to molecular levels [43]. The trick is to blow small glass bubbles very fast from the melt so that the surface tension can keep the surface molecularly smooth.

Recently, the SFA measurements have also been extended to the measurement of dynamic interactions and time-dependent effects like the viscosity of liquids in very thin films, measurements which are outside the scope of these lecture notes.

Under circumstances where the assumptions and limitations of the PB approach are met and at distances not too close to contact, no important deviations, that were not expected see Section 1.5, have been reported see e.g. Figs. 7-9.

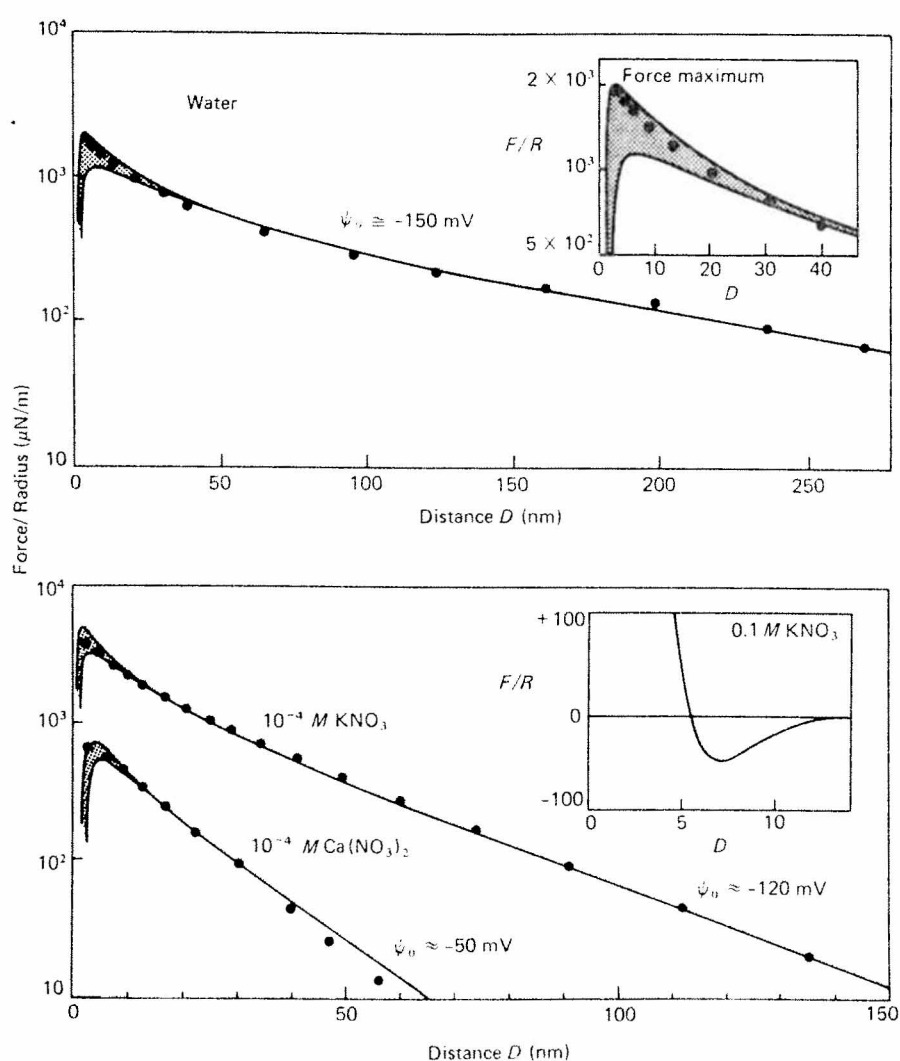


Figure 8 Measured double layer and Van der Waals forces between two curved mica sheets in the SFA in dilute salt solutions [5]. Curves are calculated using a Hamaker constant of 2.2×10^{-20} J (see Figure 7) and the constant charge and potential limits are drawn.

The most serious critique against the SFA apparatus measurements is that it is never clear how well the macroscopic surfaces are representative for the surfaces of colloidal particles was somewhat alleviated by measurements with the SFA between

two surfaces at which colloidal spheres were adsorbed [44]. Of course this kind of approach goes at the cost of accuracy in the distance determination and the geometry becomes less well defined. Also the critique that the time scales of approach are completely different than in the colloidal domain is not alleviated. With the measurement of depletion potentials, where it is also assumed in the theories that one of the colloidal entities is much larger than the other, the measured potentials are probably close to 'true' colloidal potentials. For instance, recent measurements in which depletion forces were measured at a high volume fraction of microemulsion droplets [36]. In this case a true potential of mean-force was measured showing maxima and minima in the force curves as a consequence of the structuring of the droplets by the high volume fraction and the presence of a wall.

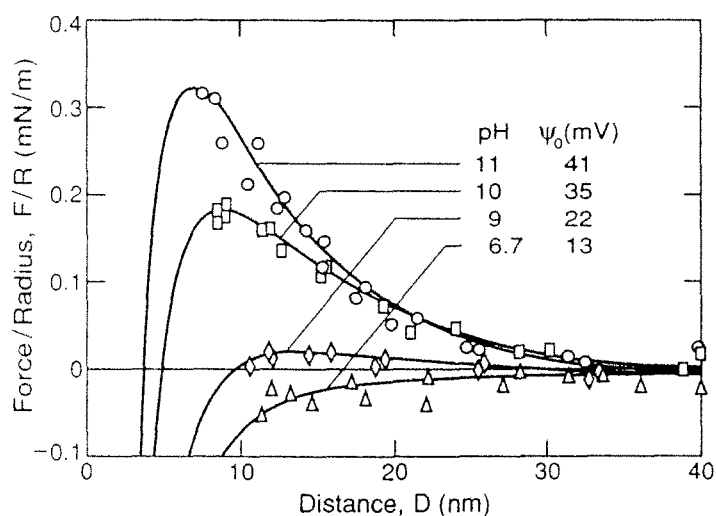


Figure 9 DLVO potentials measured between two sapphire surfaces in 10^{-3} M NaCl solutions at different pH. Full curves have been calculated using the potentials shown and a Hamaker constant of 6.7×10^{-20} J [5].

2.2 Atomic Force Microscopy (AFM)

The development of the atomic force microscope was a direct consequence of the development of the scanning tunneling microscope (STM), but can in retrospect also be seen as a natural continuation of the ideas behind the SFA. The most important difference is that the forces are not measured between two macroscopic bodies, but between a fine tip and a surface [45]. The tip radii can be as small as one atom or larger than $1 \mu\text{m}$. Because of this reduction in size compared to the SFA the spring constants need to be much smaller and the displacements of these springs need to be measured still with high accuracy. Already, spring constants as small as $0.5 \text{ N}\cdot\text{m}^{-1}$ are used and displacements as small as 0.01 nm can be accurately measured. A schematic diagram of a typical set up is given in Figure 10. Position detection of the spring is achieved by reflecting a laser off the back of this spring onto a position-sensitive detector. The tip is moved over the surface by a piezo-scanner (not shown) and the tip deflection is used in a feedback loop operated via another piezoelectric tube to maintain a constant force between the tip and surface by changing the height of the tip. With the tip signal from the feedback loop as a function of position an image of

the surface can be created. Or with the known spring constant force versus distance curves can be obtained.

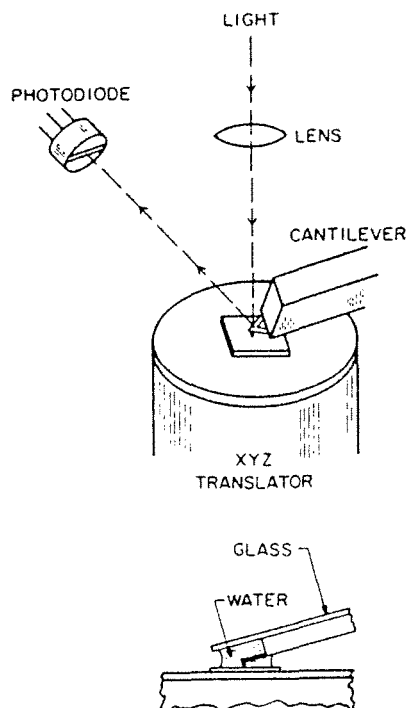


Figure 10 Schematic depiction of an Atomic Force Microscope (AFM). Spring constants as small as 0.5 N.m^{-1} can be combined with position determination of the spring of 0.01 nm to allow for the measurements of forces smaller than 100 pN (10^{-10} N) [7].

Although ‘atomic forces’ can in principal be measured with the AFM we are here more interested in the extension of this technique to the measurement of forces

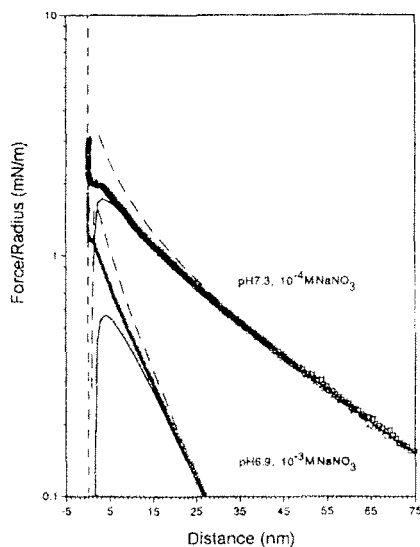


Figure 11 DLVO potentials as measured between a silica sphere (size $5 \mu\text{m}$) and a glass plate in water with added salt measured with an AFM. Surface potentials were taken to be equal for the sphere and plate at values of -105 mV and -42 mV [50].

between a particle in the colloidal size range and a wall. Ducker *et al.* [46] and Butt [47] were among the first to do this between a silica sphere glued to the AFM tip and a flat glass surface in aqueous salt solutions out to surface separations of 60 nm. Similar measurements with silica particles were done by Meagher [48]. Li *et al.* extended the method in the sense that they measured the potential between two polystyrene particles [49] of which one was glued to the tip and one was stuck to a glass surface. All these measurements found fair agreement with potentials derived using the PB approach (some used linear equations others like Butt and Li *et al.* numerically solved the full non-linear equations). Excellent agreement was found by Hartley *et al.* [50] who not only measured the force-distance curves between silica spheres and mica and silica surfaces, but also independently determined the ξ potential of the spheres by electrophoresis measurements and of the surfaces by streaming potential measurements [9]. An example of their careful and accurate measurements is given in Figure 11.

2.3 Total Internal Reflection Microscopy (TIRM)

Prieve and coworkers [51, 52, 53] developed a method to measure the interaction force between a colloidal particle and a wall, which is referred to as total internal reflection microscopy (TIRM). The name is somewhat confusing as it was already used as a general microscopy technique where imaging relied on an evanescent field. When light is incident upon an interface from the more optically dense side (for instance glass) at an angle exceeding the critical or Brewster angle, total internal reflection occurs producing an evanescent wave in the less dense medium (e.g., air or water). If the interface is smooth no light is transmitted normal to the interface into the less dense medium. Imperfections the size of the wavelength or larger will scatter light and appear bright against a dark background. This way of imaging is used to inspect optical surfaces or as a special contrast technique in biology and is also abbreviated TIRM. Prieve *et al.* made use of the fact that the irregularity in the evanescent field could also be a colloidal particle. If such a particle will have a sufficiently large refractive index and is brought within a few thicknesses of the evanescent wave it can start scattering and thus transfer energy from the evanescent field into a propagating wave travelling away from the dense material. This situation is called 'frustrated total internal reflection' and Chew *et al.* [54] solved the Mie scattering problem of a single dielectric sphere by an evanescent wave. This solution can be used to accurately determine the height of a colloidal particle close to a wall.

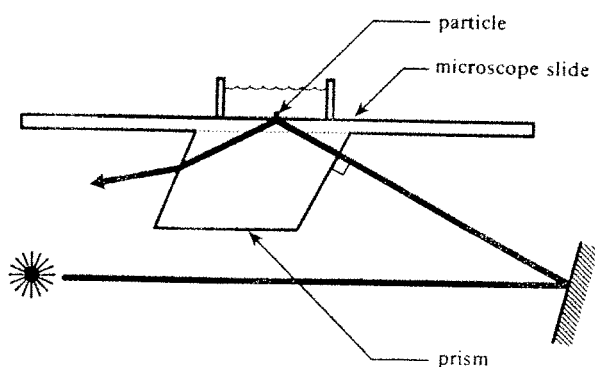


Figure 12 Schematic diagram showing the scattering cell for total internal reflection microscopy (TIRM) measurements on colloidal particles; the (photometric) microscope is not shown [51].

In this method a relatively large colloidal particle, e.g., a silica sphere with a diameter of 10 μm is allowed to sediment until the gravitational pull and the repulsive interaction forces with the wall are of even strength. Because of the Brownian motion, the particle will not be stationary but sample positions around this equilibrium point. These distances are measured as mentioned above and the potential between the particle and the wall can be evaluated around this equilibrium point by assuming a Boltzmann distribution of the distances.

Brown *et al.* extended the technique by combining it with optical tweezers (see Appendix C) which give additional control over where the equilibrium position of the particle could be placed and thus where the potential could be sampled [55, 56, 57]. In addition the tweezers made it possible to measure the absolute separation distance between the sphere and the reflecting surface.

Interaction potentials of polystyrene latex spheres of different size and at different ionic strengths were measured carefully by Bike *et al.* [58, 59]. They did not use tweezers, but were able to get absolute distance measurements. An example of the potentials, which were in good agreement with DLVO potentials, they obtained is given in Figure 13.

Dynamic measurements of the hindered diffusion of the colloid can also quite easily be made by feeding the light to a correlator [51, 60]

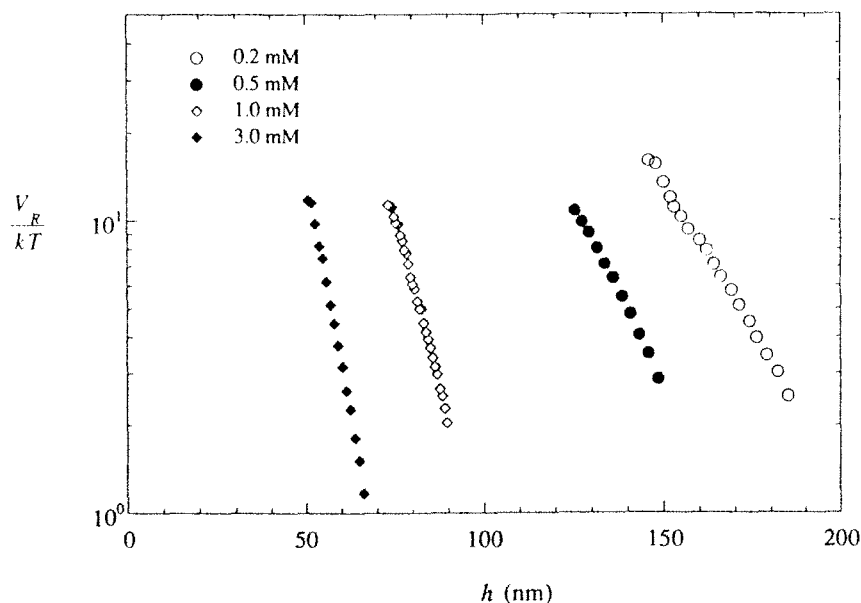


Figure 13 Double-layer potential as measured with TIRM of 15 μm diameter latex sphere above glass as function of the ionic strength [59].

2.4 Direct Imaging

The above mentioned methods always involve one component that is not of a colloidal size. Quite recent methods, almost all relying in some way or another on direct imaging of the particles, finally make it possible to measure force-distance curves between two colloidal particles and have the potential to be used even in the very relevant concentrated regime. However, to this date only a handful of measurements have been reported between two colloidal spheres in 3D in the very or

semi-dilute regime where only a few particles are interacting. It is expected though, that it is only a matter of time before the assumption of pair-wise additivity of colloidal interaction potentials can be tested experimentally under concentrated conditions. In the following we will briefly discuss the papers that have appeared already.

The first papers [61, 62, 63], appeared in 1994 and the interaction potentials were extracted by using digital video analysis to obtain particle coordinates and an analysis based on the radial distribution function, $g(r)$, to obtain the pair-wise inter particle interaction potential $U(r)$ through the relationship:

$$U(r) = -k_B T \ln(g(r)) \quad (42)$$

The radial distribution function essentially gives the chance of observing a particle pair with a separation distance r , see the lectures by Briels. In general $U(r)$ is not the effective pair potential, but the so-called potential of mean-force. This potential describes the potential of a pair of particles in the presence of the interactions with all the neighboring particles as background. Only in the limit of 'infinite' dilution when only isolated pairs of particles interact one obtains the effective pair potential.

Fraden *et al.* analyzed the interactions between two spheres that were confined to an almost two-dimensional (2D) plane by the double layer repulsion of two glass walls separated by only several micron [61, 64]. The only way they could get good statistics was to measure at finite concentrations where more than two particles were interacting at the same time. In order to correct for these effects and obtain a true pair potential they used Brownian dynamics computer simulations in an iterative procedure. Carbajal-Tinocco *et al.* used the same experimental procedure as Fraden *et al.* and also got similar results [65]. They measured also potentials at higher 2D concentrations and used the Ornstein-Zernike equation together with several closures to obtain the effective pair potential from the measured potential of mean force (see the lectures of Briels). These results will be discussed more fully in Section 3.4.

Versmold *et al.* analyzed their potentials at sufficiently low density that three body interactions could be neglected and they analyzed their separations at least 2 micron away from the glass walls [63]. To get good statistics more than 20,000 video pictures were analyzed. (However, they do not describe how it was possible to get accurate distance measurements, because an ordinary microscope was used and the particles were not confined in any way.)

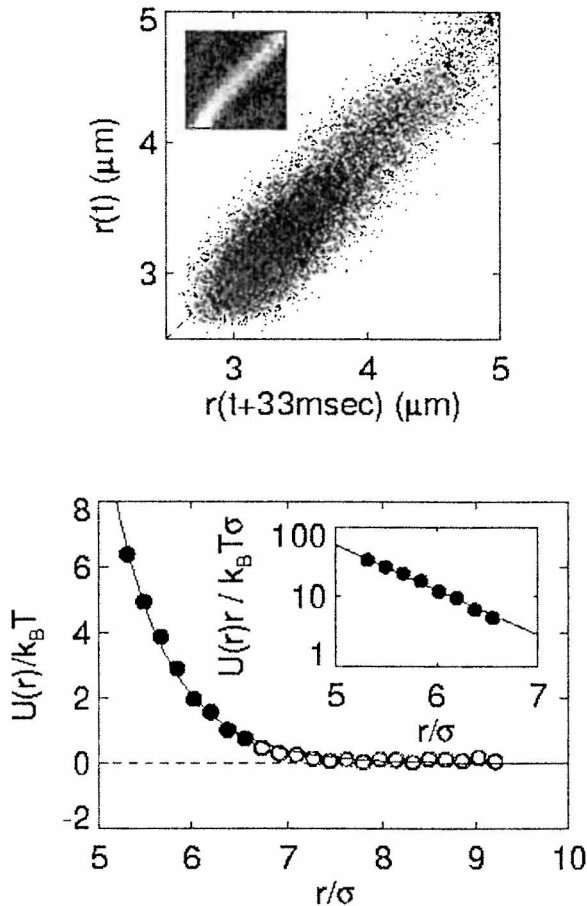


Figure 14 Measurement of pair potential from direct imaging and optical tweezers manipulation [66]. Top: Distribution of particle separations initially at $r(t)$ which evolved to $r(t + 33 \text{ ms})$. Deviations from the line are the result of interactions between the spheres. The density of points does not reflect the probability of finding the spheres at a certain separation, but rather the frequency of which they were put there with the tweezers. Inset shows a histogram of the same data set but now normalized as a propagation matrix. Bottom: sample potential curve between two latex spheres in water. Fit is to a 'charge-regulated' DLVC potential [66, 67].

Also in 1994, Grier *et al.* presented interaction potentials between two charged colloids in water far enough in the bulk to exclude any wall effects [62]. They measured the potential by analyzing the statistics of the displacements of the colloids in a set time interval after they were first put at a specific initial separation with laser tweezers (see Appendix C) [66]. In this way they were sure to measure only pairs and still got good statistics relatively easily. There were also no problems to determine the true separations, because the tweezers confined the particles first in the focal plane. To give some numbers: around 20,000 images of sphere pairs taken in 1/30 sec intervals suffice to measure an interaction potential with a 60 nm spatial resolution and 0.2 kT energy sensitivity over a range of 6 μm [66]. A sample measurement from their paper on the experimental details of the determination of the pair potentials is given in Figure 14 [66]. (It should be mentioned here that some aspects of the procedure Grier *et al.* use in their analysis are unclear [67]).

Of more recent date are measurements performed by Sugimoto *et al.* who did not use Eq. (42) to obtain $U(r)$, but instead used the potential well created in the center of the optical traps (see Appendix C) to obtain the pair potential of latex spheres in water [68]. (Although not the potential of interest for these lectures, depletion forces

induced by polymers between a latex sphere and a glass wall have also been measured with optical tweezers [69]).

The ability to measure interaction forces between *two* colloidal particles both in the bulk of a dispersion and in confinement, have already provided very interesting results, even though almost all were limited to the very dilute regime. These will be discussed in the Section 3.4.

In this section two papers that make use of magnetic forces to measure colloidal force-distance curves are also worth mentioning, despite the fact that this method is at the moment limited to emulsion droplets with quite special properties. The emulsion droplets are filled with a ferrofluid, which can be magnetized in a magnetic field. The magnetic dipolar interactions can subsequently be used to 'handle' the particles in similar ways as can be done with the optical tweezers. Bibette *et al.* used the dipolar interactions to have the ferrofluid droplets, which interact without the magnetic fields as charged particles, self-organize in strings [70]. By changing the field strength the equilibrium distance between the magnetic dipoles could be balanced against the double-layer repulsion. By calibrating the dipole moments and measuring the inter particle distances in the chains through the Bragg reflection (but this could have also been done by imaging) force curves in agreement with DLVO were obtained. Weitz *et al.* used a variation of this method to measure attractive interactions as well. In order to do this they changed the geometry by forcing the particles in a 2D layer between two glass plates [71]. In this geometry the dipoles are repulsive. They obtained the attractive forces drawing the particles together after the magnetic field was switched off by analyzing the (stationary) velocity of the particles as a function of distance and converting this to force vs. distance with the known drag coefficient.

Appendix A The Principle of Archimedes: Effect of the suspension medium

We will calculate the effect of the suspension medium on the Van der Waals forces between two bodies, but the principle used is quite general and we will only use the additivity assumption. In order to calculate the interactions between the two bodies 1 and 2 dispersed in 3 we consider the thermodynamic path depicted in Figure 25. In the initial state bodies 1 and 2 are immersed in 3 but infinitely far apart. We can regard the molecules 3 in the place where body 1 will finally be as constituting a 'ghost-body' 3 as depicted. Now let's remove both body 1 and 3 from the medium to vacuum. The change in free energy for this step is:

$$\Delta F = -F_1 - (F_3 - V_{33}(D) + V_{32}(D)) \quad (44)$$

where D is the distance from 'body 3' to body 2 and F_i is the interaction energy of the isolated body i with a universe of medium 3. The energy change in removing body 3 is not just $-F_3$ but $-(F_3 - V_{33}(D) + V_{32}(D))$ as its environment is not just pure 3. The energy $V_{32}(D) - V_{33}(D)$ represents the change in the interaction energy of body 3 with its environment, when the molecules of 3 that would have occupied the position of body 2 are replaced by body 2. In the second step body 3 and body 1 are placed back into the medium but with their positions changed. The free energy change of this second process is:

$$\Delta F' = F_3 + (F_1 - V_{13}(D) + V_{12}(D)) \quad (45)$$

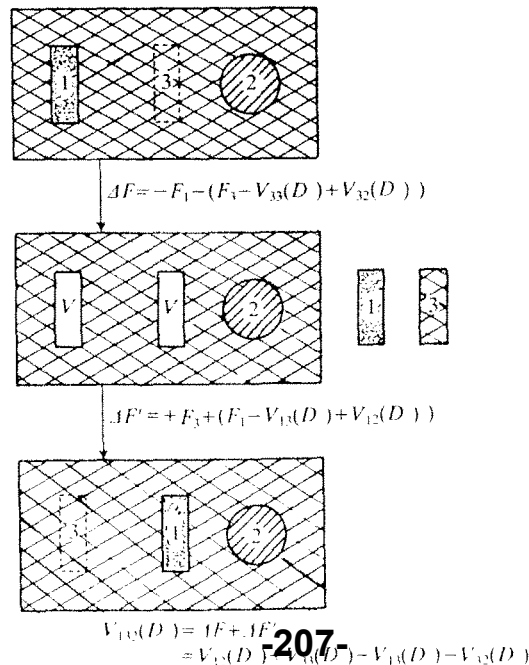
The interaction energy $V_{123}(D)$ of bodies 1 and 2 at separation D immersed in medium 3 is given by

$$V_{123}(D) = \Delta F' + \Delta F = V_{12}(D) + V_{33}(D) - V_{13}(D) - V_{32}(D) \quad (46)$$

Because of the pairwise summation method: $V_{kj}(D) = -A_{kj}V(D)$ where $V(D)$ is a positive function only of the geometry of the system and independent of the nature of bodies 1 and 2 and A_{kj} is the vacuum Hamaker constant. Thus Eq. (20) is obtained in which

$$A_{123} = A_{13} + A_{22} - A_{12} - A_{23} \quad (47)$$

Figure 25 Thermodynamic path for calculating the interaction energy between two bodies 1 and 2 immersed in a third medium 3 [6].



Appendix B Derjaguin Approximation

Derjaguin realized that when surfaces are uniformly curved, their (attractive) force relates to the interaction energy between two planar surfaces. As an example demonstrating this principle (see [7]) we will consider the interaction (here taken to be Van der Waals) between a sphere with radius R at separations $h + R$, which will be taken to be very small, from a half-space as given in Figure 26. Thus we assume in the derivation that $R \gg h$. Then we can calculate the force F acting on the sphere by considering the interaction energy U at two positions displaced by an infinitesimal distance dh :

$$F = \frac{U(h) - U(h + dh)}{dh} \quad (48)$$

When h/R is small, we need only to consider the shell with thickness dh (in the z direction) closest to the half-space; the shell on the other side of the sphere makes a negligible contribution to the force because of the large separation of the interaction potential contribution.

At a lateral distance r from the point of closest approach of the sphere, the shell is at a distance h_1 from the surface. From h_1 to $h_1 + dh$ there exists a circular strip with volume $2\pi r dr dh$. From simple geometry it follows that $h_1 = h + r^2/2R$ as long as $R \gg r$. We know the interaction energy per unit volume as $V_{12}(h)$. As in Eq. (48) we obtain the total force by integrating over r so that

$$\begin{aligned} F_{12} &= \int_0^{R \approx \infty} 2\pi\rho V_{12}(h_1) dr \\ &= 2\pi\rho R \int_h^\infty V_{12}(h_1) dh_1 \end{aligned} \quad (49)$$

Where we have used the geometrical relation between h_1 and r and extended the upper integration limit because we assume $V_{12}(h)$ is negligible for h_1 of order R . If we compare Eq. (49) with the interaction energy between two planar surfaces, Eq. (18). The final integration step leading to Eq. (18) amounts to an integration over planar sheets of thickness dz_2 so that

$$U_{12}(h) = \text{area} \int_0^\infty \rho V_{12}(z) dz \quad (50)$$

with V_{12} is the interaction energy between a molecule and a half-space. The integrals in Eqs. (55) and (50) are the same except for the integration variables and thus

$$F_{12}(h) = 2\pi R \frac{U_{12}(h)}{\text{area}} \quad (51)$$

as long as radius R is large enough compared to the range of $V_{12}(h)$.

In the derivation only the additivity assumption is used, not the interactions self, therefore this result is quite general as long as the potentials are additive and the range is short compared to R . Similar equations can be derived for two crossed cylinders with radii R_1 and R_2 :

$$F(h) = 2\pi\sqrt{R_1R_2} \frac{U(h)}{\text{area}} \quad (52)$$

And for two spheres:

$$F(h) = 2\pi \frac{R_1R_2}{R_1 + R_2} \frac{U(h)}{\text{area}} \quad (53)$$

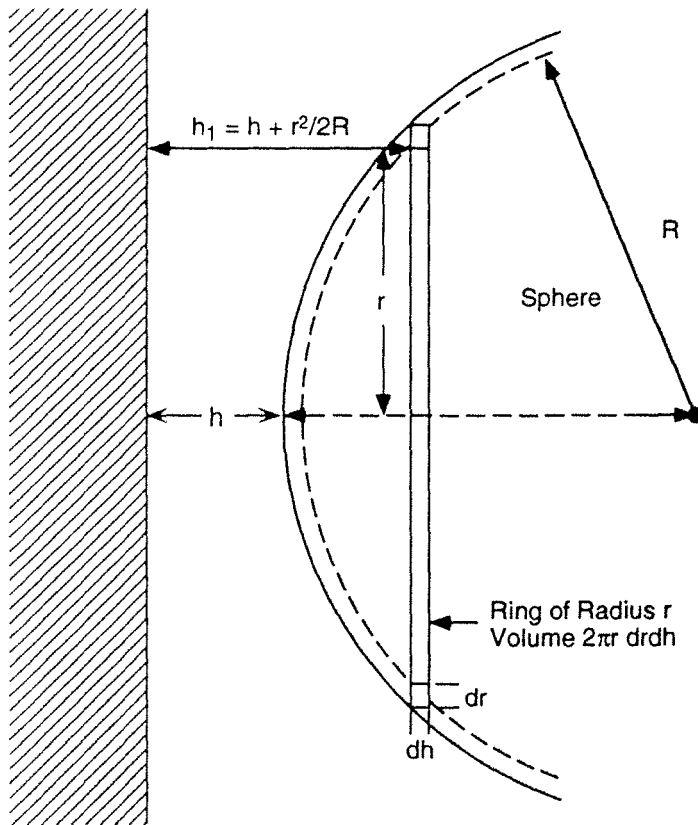


Figure 26 Calculating the force between a sphere and a half-space.

Appendix C Optical Tweezers or Single-beam gradient optical traps

The ability to measure forces in the pN range over nm distances with light was initiated by Ashkin in the early 70's when he showed that it is possible to move and trap atoms and dielectric particles with a highly focused laser beam [134]. The particle refractive index, n_p , has to be higher than that of the dispersion medium, n_m , or, $m = n_p/n_m$, has to be larger than 1. There are several regimes, depending on the ratio of the particle diameter, a , and the wavelength in the medium, λ , and m , in which these forces can be calculated or approximated.

The first regime of electromagnetic radiation interacting with a dielectric sphere is called the Rayleigh regime. A Rayleigh scatterer is a particle with a size much smaller than the wavelength, $a \ll \lambda$. In this regime the particle can be replaced by an effective dipole moment. If we consider the most simple optical trap formed by focusing a laser beam with a Gaussian intensity profile across the beam (e.g., like the fundamental spatial mode of a laser, the TEM₀₀ mode) propagating along the z direction and with polarization in the x direction than we can distinguish for this scattering regime two kinds of forces acting on the particle. These are the gradient and scattering forces. The gradient force tends to pull the particle into the region of highest intensity thus minimizing the energy of the dielectric sphere in the electromagnetic field. In the transverse directions the gradient is due to the Gaussian intensity profile. In the z direction the presence of a focal point creates the gradient. The second force, the scattering force, is due to radiation pressure and destabilizes along the z -direction by pushing the particle out of the trap. There is, however, a small region where the gradient force exceeds the radiation pressure, thus defining the trapping region. Although most particles of interest will not fall in the Rayleigh regime, it is only for this regime that analytical results can be given. We will present these formula's, because they give at least a feeling for the relevant parameters of the problem. Under the above mentioned assumptions the gradient force, \mathbf{F}_{grad} on a particle is given by [135]:

$$\mathbf{F}_{grad} = \frac{4\pi a^3}{c} \left(\frac{m^2 - 1}{m^2 + 2} \right) \cdot \nabla I \quad (54)$$

here c is the velocity of light in vacuum, I the light intensity. The scattering force is given by [135]:

$$\mathbf{F}_{scat} = \frac{I}{c} \frac{128\pi^5 a^6}{3\lambda^4} \left(\frac{m^2 - 1}{m^2 + 2} \right)^2 n_p \mathbf{z} \quad (55)$$

The most important conclusions, which are valid in the other regimes as well, that can be drawn from these equations is that there is an unequal dependence of the forces on the sphere size and refractive index and that there is an *optimal* radius and refractive index difference for trapping of spheres.

On the other extreme are particles that are (much) larger than λ . Here one enters the regime of geometrical optics and the forces can be calculated (numerically) by using ray optics and summing over all directions of the highly focused light. Again the forces can be decomposed in a trapping gradient contribution and a destabilizing

scattering contribution [136]. These calculations can be summarized by stating that the optimal refractive index difference is close to $m = 1.6$. (In this regime the results are not depending on the radius anymore). It is likely that the ray optics calculations still give a reasonable estimate at particle sizes of about 5λ [136].

In the intermediate regime, the most relevant for most applications of the tweezers, the particle size is of the order of the wavelength (m is relatively large) and the interactions with light are called Mie scattering. In this regime the forces are by far the most difficult to calculate and for the geometry of a highly focused light beam these calculations have not yet been done! For Mie scattering in the case of a plane wave of incidence, it is still possible to find an analytical solution, although in the form of a slowly converging series. For most other particle forms or a strongly converging light beam this is not the case.

The development of optical tweezers and very sensitive position detection has benefited a lot from researchers from the biophysical community. In this field there

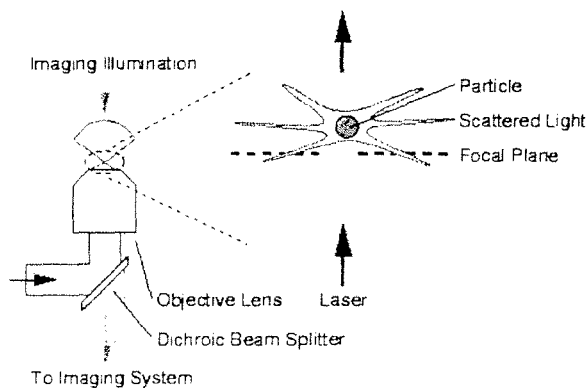


Figure 27 Schematic diagram of a single beam optical trap or a pair of optical tweezers [140].

have already been quite a number of successful measurements of very small forces (~ 1 pN) on bio-molecules and a lot of quite advanced manipulations with the optical tweezers. To build up a simple set of tweezers is not hard and well described in the literature [137, 138, 139]. Recently, tweezers are finding their way to the colloid community as well [140].

REFERENCES

- 1 B. V. Derjaguin, L. Landau, *Acta Physicochim.*, **14**, 633 (1941).
- 2 E. J. Verwey, J. Th. Overbeek, *Theory of the Stability of Lyophobic Colloids*, Elsevier, New York (1948).
- 3 *Ordering and Phase Transitions in Charged Colloids*, eds. A. K. Arora and B. V. R. Tata, VCH Publishers, New York (1996).
- 4 W. B. Russel, D. A. Saville, W. R. Schowalter, *Colloidal Dispersions*, Cambridge Univ. Press, Cambridge (1991).
- 5 J. Israelachvili, *Intermolecular & Surface Forces*, Academic Press, San Diego, 2nd ed. (1991).
- 6 R. J. Hunter, *Foundations of Colloid Science, Volume I and II*, Clarendon Press, Oxford (1989).
- 7 D. F. Evans, H. Wennerström, *The Colloidal Domain, where physics, chemistry, biology and technology meet*, VCH Publishers, New York (1994).
- 8 J. Lyklema, *Fundamentals of Interface and Colloid Science*, Academic Press, Volume I, II, III, IV, V (1995).
- 9 R. J. Hunter, *Zeta potential in colloid science*, Academic Press, London (1981).
- 10 P. C. Hiemenz, *Principles of Colloid and Surface Chemistry*, Marcel Dekker, 2nd Ed., New York, (1986).
- 11 M. J. Vold, R. D. Vold, *Colloid and Interface Chemistry*, Addison-Wesley, Reading (1983).
- 12 D. H. Napper, *Polymeric Stabilization of Colloidal Dispersions*, Academic Press, London (1983).
- 13 J. M. Sparnaay, *J. Colloid Interface Sci.*, **91**, 307 (1984).
- 14 Van der Waals, Thesis
- 15 J. Mahanty, B. W. Ninham, *Dispersion Forces*, Academic Press, New York (1976).
- 16 H. C. Hamaker, *Physica*, **4**, 1058 (1937).
- 17 K. J. Mysels, P. C. Scholten, *Langmuir*, **7**, 209 (1991).
- 18 J. Th. G. Overbeek, *Fifty Years Integration of Forces*, Utrecht University (1981).
- 19 H. B. G. Casimir, D. Polder, *Phys. Rev.*, **73**, 360 (1948).
- 20 E. M. Lifshitz, *Sov. Phys. JETP.*, **2**, 73 (1956).
- 21 I. E. Dzyaloshinskii E. M. Lifshitz, L. P. Pitaevski, *Adv. Phys.*, **10**, 165 (1961).
- 22 B. Jönsson, T. Åkesson, C. E. Woodward in *Ordering and Phase Transitions in Charged Colloids*, eds. A. K. Arora and B. V. R. Tata, VCH Publishers, New York (1996), Chapt. 11.
- 23 S. Alexander, P. M. Chaikin, P. Grant, G. J. Morales, P. Pincus, D. Hone, *J. Chem. Phys.*, **80**, 5776 (1984).
- 24 H. Löwen, G. Kramposthuber, *Europhysics Letters*, **23**, 673 (1993).
- 25 R. Rajagopalan, K. Srinivasa Rao, *Phys. Rev. E.*, **55**, 4423 (1997).
- 26 R. Rajagopalan in *Ordering and Phase Transitions in Charged Colloids*, eds. A. K. Arora and B. V. R. Tata, VCH Publishers, New York (1996), Chapter 13.
- 27 B. V. Derjaguin, A. S. Titijevskaia, I. I. Abrikossova, A. D. Malkina, *Disc. Far. Soc.*, **18**, 24 (1954).
- 28 J. Th. G. Overbeek, M. J. Sparnaay, *Disc. Far. Soc.*, **18**, 12 (1954).
- 29 D. Tabor, R. H. S. Winterton, *Proc. Roy. Soc. Lond. A*, **312**, 435 (1969).

- 30 J. N. Israelachvili, G. E. Adams, *J. Chem. Soc. Faraday Trans. 1*, **74**, 975 (1978).
- 31 J. N. Israelachvili, *Faraday Discuss. Chem. Soc.*, **65**, 20 (1978).
- 32 H. K. Christenson, *J. Chem. Soc. Faraday Trans. 1*, **80**, 1933 (1984).
- 33 J. N. Israelachvili, P. M. McGuiggan, *J. Mater. Res.*, **5**(10), 2223 (1990)
- 34 J. N. Israelachvili, H. Wennerström, *Nature*, **379**, 219 (1996).
- 35 S. Marcelja, *Nature*, **385**, 2689 (1997).
- 36 J. L. Parker, P. Richetti, P. Kékicheff, S. Sarman, *Phys. Rev. Lett.*, **68**, 1955 (1992).
- 37 M. Ruths, H. Yoshizawa, L. J. Fetters, J. N. Israelachvili, *Macromolecules*, **29**, 7193 (1996).
- 38 J. N. Israelachvili, M. Tirrell, J. Klein, Y. Almog, *Macromolecules*, **17**, 204 (1984).
- 39 J. P. Chapel, *J. Colloid Interface Sci.* **162**, 517 (1994).
- 40 G. Vigil, Z. Xu, S. Steinberg, J. N. Israelachvili, *J. Colloid Interface Sci.* **165**, 367(1994).
- 41 H. K. Christenson in *Modern Approaches to Wettability: Theory and Applications*, M. E. Schrader, G. Loeb, eds., Plenum Press, New York (1992).
- 42 J. N. Israelachvili, P. M. McGuiggan, *J. Mater. Res.*, **5**(10), 2223 (1990) and Refs. cited.
- 43 R. G. Horn, D. T. Smith, W. Haller, *Chem. Phys. Lett.*, **162**, 404 (1989).
- 44 D. Atkins, P. Kékicheff, O. Spalla, *J. Colloid Interface Sci.* **188**, 234 (1997).
- 45 P. K. Hansma, V. B. Elings, O. Marti, C. E. Bracker, *Science*, **242**, 209 (1988) and refs. cited.
- 46 A. Ducker, T.J. Senden, R.M. Pashley, *Nature*, **353**, 231 (1991).
- 47 H.-J. Butt, *Biophys. J.*, **60**, 777 (1991).
- 48 L. Meagher, *J. Colloid Interface Sci.* **152**, 293 (1992).
- 49 Y. Q. Li, N. J. Tao, J. Pan, A. A. Garcia, S. M. Lindsay, *Langmuir*, **9**, 637 (1993).
- 50 P. G. Harley, I. Larson, P. J. Scales, *Langmuir*, **13**, 2207 (1997).
- 51 D. C. Prieve, F. Luo, F. Lanni, *Faraday Discuss. Chem. Soc.*, **83**, 222 (1987).
- 52 Dennis C. Prieve, Nasser A. Frej, *Langmuir*, **6**(2), 396 (1990).
- 53 D. C. Prieve, S. G. Bike, Nasser A. Frej, *Faraday Discuss. Chem. Soc.*, **90**, 209 (1990).
- 54 H. Chew, D. S. Wang, M. Kerker, *Appl. Opt.*, **18**, 2679 (1979).
- 55 M.A. Brown, A.L. Smith, E.J. Staples, *Langmuir*, **5**(6), 1319 (1989).
- 56 M.A. Brown, E.J. Staples, *Faraday Discuss. Chem. Soc.*, **90**, 193 (1990).
- 57 M.A. Brown, E.J. Staples, *Langmuir*, **6**, 1260 (1990).
- 58 Scott G. Flicker, Stacy G Bike., *Langmuir*, **9**(1), 257 (1993).
- 59 Scott G.Flicker, Jennifer L. Tipa, Stacy G. Bike, *Journal of colloid and interface science*, **158**(2), 317 (1993).
- 60 S. Tanimoto; H. Matsuoka, H. Yamaoka, *Colloid Polym. Sci.*, **273**, 1201 (1995).
- 61 G. M. Kepler, S. Fraden, *Phys. Rev. Lett.*, **73**, 356 (1994).
- 62 J.C. Crocker, D.G. Grier, *Phys. Rev. Lett.*, **73**, 352 (1994).
- 63 K. Vondermassen, J. Bongers, A. Mueller, H. Versmold, *Langmuir*, **10**, 1351 (1994).
- 64 S. Fraden, G. M. Kepler, *Langmuir*, **10**(8), 2501 (1994).

- 65 M. D. Carbajal-Tinoco, F. Castro-Román; J. L. Arauz-Lara, *Phys. Rev. E.*, **53**, 3745 (1996).
- 66 J.C. Crocker, D.G. Grier, *Journal of colloid and interface science*, **179**, 298 (1996).
- 67 The problem referred to is the influence of hydrodynamic interactions on the displacements measured by Grier et al. in the 1/30 s. They claim to measure equilibrium properties, but this aspect of the measurement is not explained well in their papers and is not understood by the author of these notes.
- 68 T. Sugimoto, T. Takahashi, H. Itoh, S. Sato, A. Muramatsu, *Langmuir*, **13**, 5528 (1997).
- 69 Y.N. Ohshima, H. Sakagami, K. Okumoto, T. Tokoyoda, T. Igarashi, K.B. Shinktaku, S. Toride, H. Sekino, K. Kabuto, I. Nishio, *Phys. Rev. Lett.*, **78**(20), 3963 (1997).
Crocker,
- 70 F.L. Calderon, T. Stora, O. M. Monval, P. Poulin, J. Bibette, *Phys. Rev. Lett.*, **72**(18), 2959 (1994).
- 71 P. Poulin, V. Cabuil, D. A. Weitz, *Phys. Rev. Lett.*, **79**(24), 4862 (1997).
- 72 S. Inoué, K. R. Spring, *Video Microscopy*, 2nd Ed., Plenum Press, New York (1997).
- 73 *Confocal Microscopy*, Wilson Ed., Academic Press, London (1990).
- 74 A. van Blaaderen, P. Wiltzius, *Science*, **270**, 1177-1179 (1995).
A. van Blaaderen, R. Ruel, P. Wiltzius, *Nature*, **385**, 321 (1997).
W. K. Kegel, A. van Blaaderen, *Science*, **287**, 290-293 (2000).
- 75 N. Ise, *Faraday Discuss. Chem. Soc.*, **90**, 62 (1990).
- 76 N. Ise, *Faraday Discuss. Chem. Soc.*, **90**, 182 (1990).
- 77 N. Ise, K. Ito, H. Matsuoka, H. Yoshida, in *Ordering and Phase Transitions in Charged Colloids*, eds. A. K. Arora and B. V. R. Tata, VCH Publishers, New York (1996), Chapt. 5.
- 78 H. Yoshida, J. Yamanaka, T. Koga, N. Ise, T. Hashimoto, *Langmuir*, **13**, 5528 (1998).
- 79 N. Ise, T. Okubo, Y. Hiragi, H. Kawai, T. Hashimoto, M. Fujimura, A. Nakajima, H. Hayashi, *J. Am. Chem. Soc.*, **101**, 5836 (1979).
- 80 N. Ise, T. Okubo, K. Yamamoto, H. Kawai, T. Hashimoto, M. Fujimura, Y. Hiragi *J. Am. Chem. Soc.*, **102**, 7901 (1980);
J. Chem. Phys., **78**, 541 (1983);
J. Chem. Phys., **81**, 3294 (1984)
- 81 J. G. Daly, R. Hasting, *J. Phys. Chem.*, **85**, 294 (1981)
- 82 F. Grüner, W. P. Lehmann, *J. Phys. A: Math. Gen.*, **15**, 2847 (1982).
- 83 A. Arora, R. Kesavamoorthy, *Solid State Commun.*, **54**, 1047 (1985).
- 84 K. Ito, H. Nakamura, N. Ise, *J. Chem. Phys.*, **85**, 6136 (1986)
- 85 K. Ito, H. Nakamura, H. Yoshida, N. Ise, *J. Am. Chem. Soc.*, **110**, 6955 (1988).
- 86 H. Yoshida, K. Ito, N. Ise, *J. Chem. Soc. Faraday Trans.*, **87**, 371 (1991) and Refs. cited.
- 87 A. Kose, M. Ozaki, K. Takano; Y. Kobayashi, S. Hachisu, *J. Colloid Interface Sci.* **44**, 330 (1973).
- 88 N. Ise, H. Matsuoka, K. Ito, H. Yoshida, *Discuss. Faraday Soc.*, **90**, 153 (1990).
- 89 R. Kesavamoorthy. M. Rajalakshmi, C. B. Rao, *J. Phys. Condens. Matter*, **1**, 7149 (1989).

- 90 A. K. Arora, B. V. Tata, A. K. Sood, R. Kesavamoorthy, *Phys. Rev. Lett.*, **60**, 2438 (1988).
- 91 B.V.R. Tata, M. Rajalakshmi, A. K. Arora, *Phys. Rev. Lett.*, **69**, 3778 (1992).
- 92 T. Palberg, M. Würth, *Phys. Rev. Lett.*, **72**, 786 (1994).
- 93 B.V.R. Tata, A. K. Arora, *Phys. Rev. Lett.*, **72**, 787 (1994).
- 94 S. Dosho, N. Ise, K. Ito; et al. *Langmuir*, **9**, 394 (1993).
- 95 K. Ito; H. Yoshida; N. Ise, *Chem. Letters*, **1992**, 2081 (1992).
- 96 K. Ito; H. Yoshida; N. Ise, *Science*, **263**, 66 (1994).
- 97 H. Yoshida, E. Yamahara, P. V. Rajamani, N. Ise, *Phys. Rev. Lett.*, **78**(13), 2660 (1997).
- 98 B.V.R. Tata, A. K. Arora *Phys. Rev. Lett.*, **72**, 787 (1994).
- 99 K. Ito, T. Muramoto, H. Kitano, *J. Am. Chem. Soc.*, **117**, 5005 (1995).
- 100 T. Muramoto, K. Ito, H. Kitano, *J. Am. Chem. Soc.*, **119**, 3592 (1997).
- 101 F. Ghezzi, J. C. Earnshaw, *J. Phys.: Condens. Matter*, **9**, L517 (1997)
- 102 J. Ruiz-Garzia, R. Gamez-Corrales, B. I. Ivlev, *Physica A.*, **236**, 97 (1997).
- 103 A. E. Larsen, D. G. Grier, *Nature*, **385**, 230 (1993).
- 104 A. E. Larsen, D. G. Grier, *Phys. Rev. Lett.*, **76**, 3862 (1996).
- 105 J.C. Crocker, D.G. Grier, *Phys. Rev. Lett.*, **77**, 1897 (1996).
- 106 B.V.R. Tata, A.K. Arora, *Phys. Rev. Lett.*, **75**, 3200 (1995).
- 107 N. Ise, J. Yamanaka, *Phys. Rev. Lett.*, This comment was never published, see [108]
- 108 D. G. Grier, J. C. Crocker, *Phys. Rev. Lett.*, Reply never published. However the text can be read at: <http://rainbow.uchicago.edu/~grier/>
- 109 I. Sogami, N. Ise, *J. Chem. Phys.*, **81**, 6320 (1984).
- 110 J. Th. G. Overbeek, *J. Chem. Phys.*, **87**, 4406 (1987).
- 111 C. E. Woodward, *J. Chem. Phys.*, **89**, 5140 (1988).
- 112 M. V. Smalley, *Molec. Phys.*, **6**, 1251 (1990).
- 113 I. Sogami, T. Shinohara, M. V. Smalley, *Molec. Phys.*, **74**, 599 (1991); **76**, 1 (1992).
- 114 S. Levine, D. G. Hall, *Langmuir*, **8**, 1090 (1992).
- 115 J. Th. G. Overbeek, *Molec. Phys.*, **80**, 685 (1993).
- 116 R. Ettelaie, *Langmuir*, **9**, 1888 (1993).
- 117 I. Sogami, M. V. Smalley, *Molec. Phys.*, **85**, 869 (1995).
- 118 M. V. Smalley, *Langmuir*, **11**, 1813 (1995).
- 119 M. V. Smalley in *Ordering and Phase Transitions in Charged Colloids*, eds. A. K. Arora and B. V. R. Tata, VCH Publishers, New York (1996), Chapt. 12.
- 120 D. G. Hall, *Langmuir*, **12**, 4308 (1996).
- 121 K. S. Schmitz, *Langmuir*, **12**, 1407 (1996).
- 122 K. S. Schmitz, *Langmuir*, **12**, 3828 (1996).
- 123 K. S. Schmitz, *Langmuir*, **13**, 5852 (1996).
- 124 B. V. R. Tata, Akhilesh K. Arora, M. C. Valsakumar, M. C., *Phys. Rev. E.*, **47**, 3404 (1993).
- 125 M. Medina-Noyola, D. A McQuarrie, *J. Chem. Phys.*, **73**, 6279 (1980).
- 126 D. A. McQuarrie, *Statistical Mechanics*, Harper & Row, New York (1973).
- 127 M. D. Carbajal-Tinocco, D. G. Grier, submitted to *J. Chem. Phys.*
- 128 P. Kékicheff, O. Spalla, *Phys. Rev. Lett.*, **75**(9), 1851 (1995).
- 129 O. Spalla, L. Belloni, *J. Chem. Phys.*, **95**, 7689 (1991).
- 130 O. Spalla, L. Belloni, *Phys. Rev. Lett.*, **74**(13), 2515 (1995).

- 131 L. Belloni, O. Spalla, *J. Chem. Phys.*, **107**(2), 465 (1997).
- 132 R. van Roij, J-P. Hansen, *Phys. Rev. Lett.*, **79**(16), 1382 (1997).
- 133 A. Delville, *Langmuir*, **12**, 2605 (1996)
- 134 A. Ashkin, *Phys. Rev. Lett.*, **24**, 156 (1970).
- 135 A. J. Simon, Ph.D. Thesis, University of Chicago (1992).
- 136 A. Ashkin, "Forces of a Single-Beam Laser Trap on a Dielectric Sphere in the Ray Optics Regime", in "Methods in Cell Biology: Laser Tweezers in Cell Biology", Volume 55, M. P. Sheetz ed., Academic Press, San Diego, 1998, pp 1-25.
- 137 "Methods in Cell Biology: Laser Tweezers in Cell Biology", Volume 55, M. P. Sheetz ed., Academic Press, San Diego, 1998, pp 1-25.
- 138 K. Svoboda, Ch. R. Schmidt, B. J. Schnapp, S.M. Block, *Nature*, **365**, 721 (1993).
- 139 K. Visscher, S. P. Gross, S. M. Block, *IEEE J. Selected Topics Quantum Electronics*, **2**(4), 1066 (1996).
- 140 D. G. Grier, *Current Opinion in Colloid & Interface Science*, **2**(3), 264 (1997).
- 141 X. Chu, D. T. Wasan, *J. Colloid Interface Sci.* **184**, 268 (1996).

REFERENCES FEBRUARY 1998 – FEBRUARY 2002

- 141 O. I. Vinogradova, G. E. Yakubov and H. J. Butt, Forces between polystyrene surfaces in water-electrolyte solutions: Long-range attraction of two types? *J. Chem. Phys.* **114**(18), 8124 (2001).
- 142 J. Lyklema, H. P. van Leeuwen and M. Minor, *DLVO-theory, a dynamic re-interpretation. Adv. Colloid Interface Sci.* **83**(1-3), 33 (1999).
- 143 N. V. Churaev, *The DLVO theory in Russian colloid science. Adv. Colloid Interface Sci.* **83**(1-3), 19 (1999).
- 144 B. W. Ninham, *On progress in forces since the DLVO theory. Adv. Colloid Interface Sci.* **83**(1-3), 1 (1999).
- 145 W. Wu, R. F. Giese and C. J. van Oss, *Stability versus flocculation of particle suspensions in water - correlation with the extended DLVO approach for aqueous systems, compared with classical DLVO theory. Colloid Surf. B-Biointerfaces* **14**(1-4), 47 (1999).
- 146 D. Leckband and S. Sivasankar, *Forces controlling protein interactions: theory and experiment. Colloid Surf. B-Biointerfaces* **14**(1-4), 83 (1999).
- 147 P. Attard, *Recent advances in the electric double layer in colloid science. Curr. Opin. Colloid Interface Sci.* **6**(4), 366 (2001).
- 148 M. Dijkstra, *Computer simulations of charge and steric stabilised colloidal suspensions. Curr. Opin. Colloid Interface Sci.* **6**(4), 372 (2001).
- 149 T. J. Senden, *Force microscopy and surface interactions. Curr. Opin. Colloid Interface Sci.* **6**(2), 95 (2001).
- 150 N. Ise, T. Konishi and J. Yamanaka, *X-Ray scattering study of ionic colloidal crystals. Curr. Opin. Colloid Interface Sci.* **6**(2), 126 (2001).
- 151 N. Ise, T. Konishi and B. V. R. Tata, *How homogeneous are "homogeneous dispersions"? Counterion-mediated attraction between like-charged species. Langmuir* **15**(12), 4176 (1999).
- 152 A. K. Arora and B. V. R. Tata, *Interactions, structural ordering and phase*

- transitions in colloidal dispersions. Adv. Colloid Interface Sci. **78**(1), 49 (1998).*
- 153 B. V. R. Tata, *Colloidal dispersions and phase transitions in charged colloids. Curr. Sci. **80**(8), 948 (2001).*
- 154 J. P. Hansen and H. Lowen, *Effective interactions between electric double layers. Annu. Rev. Phys. Chem. **51**, 209 (2000).*
- 155 L. Belloni, *Colloidal interactions. J. Phys.-Condes. Matter **12**(46), R549 (2000).*
- 156 D. G. Grier, *When like charges attract: interactions and dynamics in charge-stabilized colloidal suspensions. J. Phys.-Condes. Matter **12**(8A), A85 (2000).*
- 157 H. Lowen, M. Watzlawek, C. N. Likos, M. Schmidt, A. Jusufi and A. R. Denton, *Phase transitions in colloidal suspensions and star polymer solutions. J. Phys.-Condes. Matter **12**(8A), A465 (2000).*
- 158 V. Vlachy, *Ionic effects beyond Poisson-Boltzmann theory. Annu. Rev. Phys. Chem. **50**, 145 (1999).*
- 159 C. N. Likos, *Effective interactions in soft condensed matter physics. Phys. Rep.-Rev. Sec. Phys. Lett. **348**(4-5), 267 (2001).*
- 160 M. Kardar and R. Golestanian, *The "friction" of vacuum, and other fluctuation-induced forces. Rev. Mod. Phys. **71**(4), 1233 (1999).*
- 161 E. Ruckenstein, *Attraction between identical colloidal particles caused by collective electrostatic repulsion. Adv. Colloid Interface Sci. **75**(3), 169 (1998).*
- 162 J. P. Hansen, D. Goulding and R. van Roij, *Effective interactions between charged colloidal particles: Repulsion, attraction and phase separation. J. Phys. IV **10**(P5), 27 (2000).*
- 163 M. Bostrom, D. R. M. Williams and B. W. Ninham, *Specific ion effects: Why DLVO theory fails for biology and colloid systems - art. no. 168103. Phys. Rev. Lett. **87**16(16), 8103 (2001).*
- 164 E. J. Verwey, J. Th. Overbeek, *Theory of the Stability of Lyophobic Colloids*, Dover, New York (2000).
- 165 T. J. Senden, *Force microscopy and surface interactions. Curr. Opin. Colloid Interface Sci. **6**(2), 95 (2001).*
- 166 J. Yamanaka, H. Yoshida, T. Koga, N. Ise and T. Hashimoto, *Reentrant solid-liquid transition in ionic colloidal dispersions by varying particle charge density. Phys. Rev. Lett. **80**(26), 5806 (1998).*
- 167 G. C. de Leon, J. M. Saucedo-Solorio and J. L. Arauz-Lara, *Colloidal interactions in partially quenched suspensions of charged particles. Phys. Rev. Lett. **81**(5), 1122 (1998).*
- 168 G. C. de Leon and J. L. Arauz-Lara, *Static structure and colloidal interactions in partially quenched quasibidimensional colloidal mixtures. Phys. Rev. E **59**(4), 4203 (1999).*
- 169 J. A. Weiss, A. E. Larsen and D. G. Grier, *Interactions, dynamics, and elasticity in charge-stabilized colloidal crystals. J. Chem. Phys. **109**(19), 8659 (1998).*
- 170 E. R. Dufresne and D. G. Grier, *Interactions, dynamics, and elasticity in charge-stabilized colloidal crystals (vol 109, pg 8659, 1998). J. Chem. Phys. **110**(17), 8845 (1999).*
- 171 T. M. Squires and M. P. Brenner, *Like-charge attraction and hydrodynamic interaction. Phys. Rev. Lett. **85**(23), 4976 (2000).*
- 172 S. H. Behrens and D. G. Grier, *Pair interaction of charged colloidal spheres near a charged wall. Phys. Rev. E **64**05(5), 0401 (2001).*
- 173 J. C. Crocker, J. A. Matteo, A. D. Dinsmore and A. G. Yodh, *Entropic attraction*

- and repulsion in binary colloids probed with a line optical tweezer.* Phys. Rev. Lett. **82**(21), 4352 (1999).
- 174 B. V. R. Tata and N. Ise, *Monte Carlo study of structural ordering in charged colloids using a long-range attractive interaction.* Phys. Rev. E **58**(2), 2237 (1998).
- 175 D. G. Grier and J. C. Crocker, *Comment on "Monte Carlo study of structural ordering in charged colloids using a long-range attractive interaction".* Phys. Rev. E **61**(1), 980 (2000).
- 176 D. G. Grier, *Colloids: A surprisingly attractive couple.* Nature **393**, 621 (1998).
- 177 W. R. Bowen and A. O. Sharif, *Long-range electrostatic attraction between like-charge spheres in a charged pore.* Nature **393**(6686), 663 (1998).
- 178 J. C. Neu, *Wall-mediated forces between like-charged bodies in an electrolyte.* Phys. Rev. Lett. **82**(5), 1072 (1999).
- 179 J. E. Sader and D. Y. C. Chan, *Long-range electrostatic attractions between identically charged particles in confined geometries and the Poisson- Boltzmann theory.* Langmuir **16**(2), 324 (2000).
- 180 J. E. Sader and D. Y. C. Chan, *Long-range electrostatic attractions between identically charged particles in confined geometries: An unresolved problem.* J. Colloid Interface Sci. **213**(1), 268 (1999).
- 181 Y. X. Qian and W. R. Bowen, *Long-range electrostatic interaction between a charged wall and two similarly charged colloidal spheres at low surface potentials,* Journal of Colloid and Interface Science **213**, 316 (1999).
- 182 W. R. Bowen and A. O. Sharif, *Hydrodynamic and colloidal interactions effects on the rejection of a particle larger than a pore in microfiltration and ultrafiltration membranes,* Chemical Engineering Science **53**, 879 (1998).
- 183 W. R. Bowen, A. N. Filippov, A. O. Sharif, *et al.*, *A model of the interaction between a charged particle and a pore in a charged membrane surface,* Advances in Colloid and Interface Science **81**, 35 (1999).
- 184 W. R. Bowen and A. O. Sharif, *Long-range electrostatic attraction between like-charge spheres in a charged pore (vol 393, pg 663, 1998),* Nature **402**, 841 (1999).
- 185 J. J. Gray, B. Chiang, and R. T. Bonnecaze, *Colloidal particles - Origin of anomalous multibody interactions,* Nature **402**, 750 (1999).
- 186 W. R. Bowen and A. O. Sharif, *Long-range electrostatic attraction between like-charge spheres in a charged pore (vol 393, pg 663, 1998),* Nature **402**, 841 (1999).
- 187 R. van Roij, M. Dijkstra and J. P. Hansen, *Phase diagram of charge-stabilized colloidal suspensions: van der Waals instability without attractive forces.* Phys. Rev. E **59**(2), 2010 (1999).
- 188 P. B. Warren, *A theory of void formation in charge-stabilized colloidal suspensions at low ionic strength.* J. Chem. Phys. **112**(10), 4683 (2000).
- 189 D. Y. C. Chan, *Density functional theory of charged colloidal systems - art. no. 061806.* Phys. Rev. E **63**06(6), 1806 (2001).
- 190 D. Y. C. Chan, P. Linse and S. N. Petris, *Phase separation in deionized colloidal systems: Extended Debye-Huckel theory.* Langmuir **17**(14), 4202 (2001).
- 191 B. Beresford-Smith, D. Y. C. Chan and D. J. Mitchell, *The electrostatic interaction in colloidal systems with low added electrolyte.* J. Colloid Interface Sci. **105**, 216 (1985).

- 192 G. Stell, *Criticality and Phase-Transitions in Ionic Fluids*. J. Stat. Phys. **78**(1-2), 197 (1995).
- 193 H. Lowen and E. Allahyarov, *The role of effective triplet interactions in charged colloidal suspensions*. J. Phys.-Condes. Matter **10**(19), 4147 (1998).
- 194 D. Goulding and J. P. Hansen, *Attraction between like-charged colloidal particles induced by a surface: A density-functional analysis*. Europhys. Lett. **46**(3), 407 (1999).
- 195 R. Tehver, F. Ancilotto, F. Toigo, J. Koplik and J. R. Banavar, *Absence of many-body effects in interactions between charged colloidal particles*. Phys. Rev. E **59**(2), R1335 (1999).
- 196 E. Allahyarov, I. D. D'Amico and H. Lowen, *Effect of geometrical confinement on the interaction between charged colloidal suspensions*. Phys. Rev. E **60**(3), 3199 (1999).
- 197 P. Linse and V. Lobaskin, *Electrostatic attraction and phase separation in solutions of like-charged colloidal particles*. Phys. Rev. Lett. **83**(20), 4208 (1999).
- 198 P. Linse, *Structure, phase stability, and thermodynamics in charged colloidal solutions*. J. Chem. Phys. **113**(10), 4359 (2000).
- 199 P. Linse and V. Lobaskin, *Electrostatic attraction and phase separation in solutions of like-charged colloidal particles*. J. Chem. Phys. **112**(8), 3917 (2000).
- 200 V. Lobaskin, A. Lyubartsev and P. Linse, *Effective macroion-macroion potentials in asymmetric electrolytes*. Phys. Rev. E **63**(2), 0401 (2001).
- 201 I. Larson and P. Attard, *Surface charge of silver iodide and several metal oxides. Are all surfaces nernstian?* J. Colloid Interface Sci. **227**(1), 152 (2000).



Soft Condensed Matter

Problem Sets

Utrecht University

February 2013

Soft Condensed Matter 2005 Problems Chapter 1

1) In order to get a feeling of where the formula for the Brownian time (Eq. 1.5) comes from, we can derive it for a simpler case already encountered in the field of the mechanics of point objects. We want to calculate how long it takes if drops a ball with radius R and buoyant mass m in a liquid. Assume that the friction factor f is proportional to the speed v and is given by $6\pi\eta R$.

- What is the terminal velocity of the ball if it is give that the $\eta = 1 * 10^{-2}$ Pa.s and that the buoyant mass of the ball is 1 kg and its radius 1 m ($g = 10 \text{ m/s}^2$).
- Derive an equation for the relaxation time mentioned by solving the second order differential equation that describes this situation.
- What is the relaxation time for the situation mentioned in a)?
- What is the terminal velocity and the relaxation time for a colloidal sphere with a radius of 1 μm , assume a particle density difference of 1 g/cm^3 with the solvent?
- What distance does the particle travel if it is assumed to diffuse Brownian during this time?
- What is the gravitational height of the same colloidal sphere?

2) Let us assume the human lifetime is extended to 10.000 year, what size of particle would one still consider colloidal? What will ultimately limit the size of a colloid?

3) The rotational diffusion constant of a spherical particle with radius 'a' in a medium with viscosity η is given by:

$$D_0^r = \frac{k_B T}{8\pi\eta a^3}$$

What particle size would you choose if you wish to study their rotational diffusion experimentally, for instance in an aqueous ($\eta = 1 * 10^{-2}$ Pa.s [Pa·s]) system?

- 4) a) Show that for colloidal particles dispersed in a liquid, the equilibrium number of particles, N , at a height h above a reference level, h_0 , is given by:

$$N = N_0 \exp[-(m - m')g(h - h_0)/k_B T]$$

where N_0 is the number of particles at height h_0 and m' is the mass of fluid displaced by a particle of mass m .

b) Svedberg (1928) gives the following Table for the sedimentation equilibrium of a gold sol under gravity:

Height (μm)	Number of particles	Height (μm)	Number of particles
0	889	600	217
100	692	700	185
200	572	800	152
300	426	900	125
400	357	1000	108
500	253	1100	78

Assume the particles have radius 21 nm and density $19.3 \text{ g}\cdot\text{cm}^{-3}$ and the temperature is $20 \text{ }^\circ\text{C}$. Estimate the Boltzmann constant, k , from the equation derived in (a) and then calculate Avogadro's number, N_A , assuming $R=8.31 \text{ J}\cdot\text{K}^{-1}\cdot\text{mol}^{-1}$.

c) Repeat the calculation with a radius of 22 nm and note how sensitive the answer is to this variable.

Problems Chapters 2 and 3

1. The First and Second Law of Thermodynamics, and thermodynamic potentials. Consider a thermodynamic system of N identical particles in a volume V with energy E . The temperature is T , the pressure p , and the chemical potential is μ . This system is subject to a process such that the energy changes by a (very small) amount dE due to the uptake of a (very small) amount of heat q , due to the uptake of a (very small) number of particles dN , and due to a (very small) change of volume dV .

 - (a) How are these changes related according to First Law?
 - (b) If we assume that the process is reversible, what is the entropy change dS of the system according to the Second Law?
 - (c) Show that $dE = TdS - pdV + \mu dN$, and conclude/show that the thermodynamic properties of the system such as T , p and μ would follow if the function $E(S, V, N)$ were known. Note that in this picture S , V and N are the independent variables to describe the system, and T , p , and μ follow by differentiation of $E(S, V, N)$.
 - (d) It is not always convenient to deal with S as an independent thermodynamic parameter, in fact one often prefers T as the independent one. Analyse the combination $d(E - TS) \equiv dF$ and show that $F(N, V, T)$ can generate the complete thermodynamics of the system, i.e. μ , p , and S , from the independent variables N , V , and T . Note that F is called the Helmholtz free energy, it is the thermodynamic potential of the independent variables N , V , and T .
 - (e) Which thermodynamic function must be used for independent (N, p, T) ? And (μ, V, T) ? And (N, p, S) ?
2. Phase space of a single particle in 1 dimension Consider a classical point particle that can only move on a 1 dimensional line. We denote the position by x and the momentum by p_x ; the total energy of the particle is E and is assumed fixed —so the system is assumed closed. The mass of the particle is m .

 - (a) Sketch the phase-space trajectory of this particle in the case that it is confined to a "box" with two hard walls, one at $x = 0$ and the other at $x = L$, with L the size of the 1-dimensional box.
 - (b) Sketch the phase-space trajectory of this particle in the case that it is trapped by a harmonic potential $V(x) = Cx^2/2$ with C the spring constant.
3. Partition functions and the Gaussian integral It is well-known that the Gaussian integral is given by $\int_{-\infty}^{\infty} dx \exp[-ax^2] = \sqrt{\pi/a}$ for any $a > 0$.

 - (a) Use this to calculate the canonical partition function Z_1 of a single classical point particle in a 1-dimensional box of length L (see previous question) at temperature T , where Z_1 is defined by
$$Z_1(T, L) = \frac{1}{h} \int_{-\infty}^{\infty} dp_x \int_0^L dx \exp[-p_x^2/(2mk_B T)], \quad (1.1)$$
with h Planck's constant and m the mass of the particle.
 - (b) Rewrite your answer of (a) as $Z_1(T, L) = L/\Lambda$, and give Λ .
 - (c) The free energy of this single particle is given by $F_1 = -k_B T \ln Z_1$, and its entropy by $S_1 = -\partial F_1/\partial T$. Calculate F_1 and S_1 , and also the average energy E_1 using that $F_1 = E_1 - TS_1$.

- (d) Write down the canonical partition function Z_3 for a single particle in a three-dimensional cubic box of volume $V = L \times L \times L$, and show that it equals $Z_3 = Z_1^3$. Calculate the free energy, entropy, and average energy of this three-dimensional case.
4. Virial coefficients of model systems.
- Calculate the second virial coefficient of the hard-sphere (HS) system (diameter σ), and of the square-well (SW) system (diameter σ , well depth $-\epsilon < 0$, and well width $\lambda\sigma$ with $\lambda > 1$). Check for the limiting cases $\epsilon \rightarrow 0$ and $\lambda \rightarrow 1$.
 - Calculate B_3 for hard spheres.
5. The three routes that lead from $g(r)$ to thermodynamics are called the *virial*, the *caloric*, and the *compressibility* route. The first two of these follow from the partition function $Z(N, V, T) = Q(N, V, T)/N!\Lambda^{3N}$, with $Q(N, V, T) = \int_V d\mathbf{r}^N \exp[-\sum_{i < j}^N \phi(r_{ij})/kT]$ the configuration integral.
- Show first that $\beta p = (\partial \log Q / \partial V)_{N, T}$. Go over to scaled Cartesian coordinates $s_{i\alpha} = r_{i\alpha}/V^{1/3}$, i.e. such that $d\mathbf{s}_i = d\mathbf{r}_i/V$, and show that $\beta p = N/V - \frac{1}{6kTV} \int_V d\mathbf{r}_1 d\mathbf{r}_2 r_{12} \phi'(r_{12}) \rho^{(2)}(\mathbf{r}_1, \mathbf{r}_2)$. Reduce this for a homogeneous and isotropic system to the virial-route expression in the notes.
 - Show that $E = \langle H \rangle = -(\partial \log Z / \partial \beta)_{N, V}$, and rewrite this to the expression for the caloric route in the notes.

Note that the virial and caloric route only hold for a pair wise interaction Hamiltonian; the compressibility route is more generally valid.

6. Van der Waals' approximation to the free energy density $f = F/V$ of a one-component system of density ρ and temperature T is given by

$$f = \rho kT \left(\log \frac{\rho \Lambda^3}{1 - b\rho} - 1 \right) - a\rho^2,$$

with a and b positive constants.

- Give the dimension and physical meaning of a and b .
 - Calculate the pressure p and the chemical potential μ from f .
 - Calculate the critical density ρ_c and the critical temperature T_c . Is it crucial that $a, b > 0$?
 - Calculate the critical pressure p_c , and show that $p_c/(\rho_c kT_c) = 3/8$ independent from a, b . Compare this with the experimental values [from: Hirschfelder, Curtis and Bird, "Molecular Theory of Gases and Liquids"]:
- | | | | |
|----------------|-------------------|-----------------|-------------------|
| substance | $p_c/\rho_c kT_c$ | substance | $p_c/\rho_c kT_c$ |
| He | 0.300 | Xe | 0.293 |
| H ₂ | 0.304 | N ₂ | 0.292 |
| Ne | 0.296 | O ₂ | 0.292 |
| Ar | 0.291 | CH ₄ | 0.290 |
- Sketch $p(\rho)$ and $\mu(\rho)$ for $T > T_c$, $T = T_c$, and $T < T_c$. Describe how the condition for gas-liquid equilibrium at $T < T_c$ can be determined, in principle and in practise, from $p(\rho, T)$ and $\mu(\rho, T)$.
7. The hard-sphere direct correlation function $c(r)$ is, within the Percus-Yevick (PY) approximation, given by an expression in the notes.

- Show that the compressibility route can be written as

$$kT \left(\frac{\partial \rho}{\partial p} \right)_T = \lim_{q \rightarrow 0} S(q) = \frac{1}{1 - \rho \int d\mathbf{r} c(r)}.$$

- Combining the PY-form of $c(r)$ with the result of a. yields an expression for the pressure given by $p_c = \rho kT(1 + \eta + \eta^2)(1 - \eta)^{-3}$, where the index "c" denotes that this result stems from the compressibility route. Confirm this result, expand it in powers of η , and compare at which order it no longer agrees with the hard-sphere virial expansion (given in the notes).

c. What is the source of the disagreement with the virial expansion?

A very accurate hard-sphere free energy expression is due to Carnahan and Starling and reads

$$\frac{F_{CS}}{NkT} = \log \rho \Lambda^3 - 1 + \frac{4\eta - 3\eta^2}{(1 - \eta)^2}.$$

d. Calculate the hard-sphere pressure p_{CS} and chemical potential μ_{CS} that follow from F_{CS} .

8. The orientation-averaged second virial coefficient of two hard spherocylinders is given by $B_2^{iso} = 4v_0 + L^2 D / (4\pi)^2 \int d\hat{\omega} d\hat{\omega}' |\sin \gamma|$ with γ the angle between $\hat{\omega}$ and $\hat{\omega}'$. Check this expression, calculate B_2^{iso} , and discuss the importance of the first term $4v_0$ as a function of L/D .

9. In a simple model of a system of rodlike particles one views the particles as rectangular blocks of length L and thickness D , i.e. of the form $L \times D \times D$. A further simplification is to restrict the number of possible orientations of each rod to three, such that the main axes of the rods can only point in the direction of a laboratory frame \hat{x}_α , $\alpha = 1, 2, 3$. A particle with orientation α has its long axis along \hat{x}_α . The interaction between the particles is *hard*, i.e. overlap is not allowed. The Helmholtz free energy F of $N = \rho V$ of such rods in a volume V at temperature T is given, within the second virial approximation, by

$$\frac{F}{VkT} = \sum_{\alpha=1}^3 \rho_\alpha (\log \rho_\alpha \mathcal{V} - 1) + \sum_{\alpha=1}^3 \sum_{\alpha'=1}^3 B_{\alpha\alpha'} \rho_\alpha \rho_{\alpha'},$$

with ρ_α the density of particles with orientation α , and \mathcal{V} the (irrelevant) thermal volume.

- Calculate the second virial coefficients $B_{\alpha\alpha} \equiv B_{\parallel}$ and $B_{\alpha\bar{\alpha}} \equiv B_{\perp}$ for a pair of parallel and perpendicular rods, respectively. [Here $\bar{\alpha}$ stands for “not- α ”, i.e. if $\alpha = 1$ then $\bar{\alpha} = 2$ or 3 , etc.].
- Consider from now the “needle” limit $L/D \rightarrow \infty$. First calculate $B_{\parallel}/L^2 D$ and $B_{\perp}/L^2 D$ in this limit, and then the dimensionless free energy $\psi = FL^2 D / VkT$ as a function of the dimensionless densities $c_\alpha = L^2 D \rho_\alpha$.
- Define the *nematic order parameter* S by $c_3 = c(1 + 2S)/3$ and $c_1 = c_2 = c(1 - S)/3$, with $c = \rho L^2 D$ the total dimensionless density. Explain this nomenclature.
- Calculate $\psi(c, S)$. For a given c one needs to determine S such that it minimises ψ (at the fixed c). Show that $S = 0$ is a solution of $(\partial\psi/\partial S)_c = 0$ for any c . With which phase do you associate $S = 0$?
- The result of d. does *not* guarantee that $S = 0$ yields a minimum of ψ . Argue on the basis of $(\partial^2\psi/\partial S^2)_c$ at $S = 0$ that ψ is minimised by $S \neq 0$ at sufficiently high c . Which phase do you associate with $S \neq 0$?
- Which equations should be solved (numerically) in the determination of phase coexistence of an isotropic phase (density c_I and order parameter S_I) and a nematic phase (density c_N and order parameter S_N)?

4. Problems

- 1) How does equation (4.11) change if the incident light has perpendicular polarization? And parallel?
- 2) Calculate the scattering cross section of a Rayleigh scatterer.
- 3) Derive (4.14).
- 4) *The form factor of a clay particle*
Clay particles have the shape of a uniform, but very small, thin disk. Propose a method to measure the radius R of the disks with light scattering. Derive a formula with which to extract R from the measured data.

5) *Scattering by a Gaussian polymer coil*

Debye pointed out in 1947 that when calculating the scattering by a polymer molecule it is convenient to consider the basic scattering particle to be the statistical chain segment. Interference between waves scattered from different chain segments is then incorporated into the structure factor. The chain segment is usually so small compared to the wavelength of light that it can be considered a point scatterer (*i.e.* its form factor equals unity.) If the polymer solution is dilute then only interference between segments in the same polymer molecule is important. The structure factor (4.27) depends only on the difference vector \mathbf{r}_{jk} between two such segments. For a Gaussian polymer coil the probability density function for this vector is given by (see the Chapter on polymers)

$$p(\mathbf{r}_{jk}) = \left(\frac{3}{2\pi b^2 |j-k|} \right)^{3/2} \exp\left(-\frac{3r_{jk}^2}{2b^2 |j-k|} \right), \quad (\text{P1})$$

where b is the segment length.

- a. Show that the form factor for a Gaussian coil with N segments can be written as

$$P(\mathbf{q}) = \frac{1}{N^2} \sum_j \sum_k e^{-\frac{1}{6}q^2 b^2 |j-k|}. \quad (\text{P2})$$

Hint: Contrary to most problems involving spherical symmetry the integral is best done in normal Cartesian coordinates. The integrals can be performed by completing the squares in the exponent and making use of the integral

$$\int_{-\infty}^{+\infty} e^{-ax^2} dx = \sqrt{\pi/a}.$$

- b. Next, evaluate (P2) by approximating the sums with integrals. Show that

$$P(\mathbf{q}) = \frac{2}{y^2} (e^{-y} - 1 + y), \quad (\text{P3})$$

where

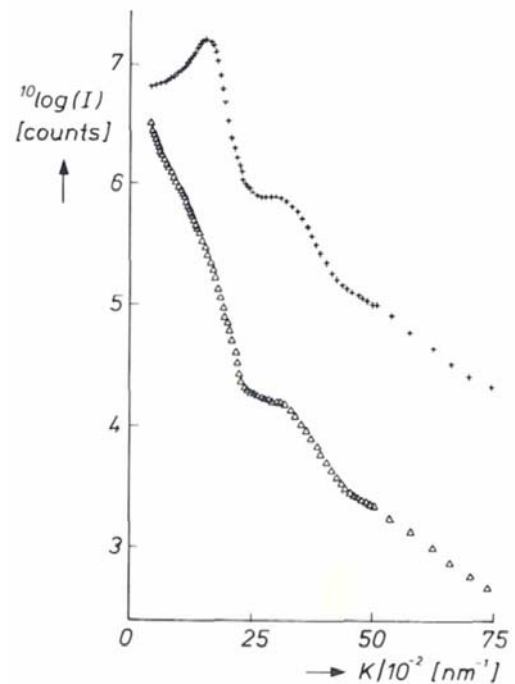
$$y = \frac{1}{6} Nq^2 b^2. \quad (\text{P4})$$

- c. Now derive a lowest order in q approximation for the form factor and confirm that the radius of gyration of a Gaussian chain is given by

$$R_g^2 = \frac{1}{6} N b^2. \quad (\text{P5})$$

6) Determine the systematic vanishings for a body-centered cubic lattice (*bcc*). How would you distinguish *bcc* from *fcc*?

7) The graph shows small-angle X-ray scattering data on two suspensions of colloidal silica spheres in the solvent cyclohexane. The upper curve is a sample with a concentration of 0.714 g/cm³, the lower curve 0.01 g/cm³. The vertical axis shows the scattered intensity *I* and the horizontal axis shows the scattering vector *K* (multiplied by 100).



- Estimate the size of the spheres used in this experiment.
- Explain why the upper curve has a peak in the low-*K* range, while the lower curve does not.
- Why do the curves look almost the same in the high-*K* range?
- Estimate the average distance between the particles in the suspension.
- How would the measured data change if a silica concentration of 1.0 g/cm³ is used?

8) *Brownian motion*

- Find an expression for the probability density function $P(\Delta r, t)$ describing the displacement of a Brownian particle in a time t .
- Show that the mean square displacement is given by $\langle \Delta r^2 \rangle = 6Dt$.

9) *The Random Walk*

Consider the following idealization of a random walk in one dimension. A particle starts in the origin and makes a step of size l_x randomly in the positive or negative x direction, so that:

$$\begin{aligned} x_{i+1} &= x_i + l_x && \text{probability } \frac{1}{2} \\ x_{i+1} &= x_i - l_x && \text{probability } \frac{1}{2} \end{aligned}$$

It is clear that, after a large number N of steps, the expectation value of the x coordinate of the particle is zero.

- Now show that

$$\langle x_N^2 \rangle = Nl_x^2.$$

- Assuming that the particle travels ballistically with a speed v , show that

$$\langle x^2 \rangle = vl_x t.$$

- Next, consider a random walk in three dimensions. Furthermore, allow the random walk step size l to be selected from a probability distribution $P(l)$. Show that

$$\langle r^2 \rangle = vt \frac{\langle l^2 \rangle}{\langle l \rangle}. \tag{0.1}$$

- d. For diffusion of molecules in a dilute gas the pdf for the step size $P(l)$ can be found by considering the collision probability between molecules. Consider an ensemble of molecules that have just undergone a collision. After traveling a distance l there are $N(l)$ molecules left that have gone without colliding a second time. The number of these molecules undergoing another collision in the next dl meters is then proportional to dl and $N(l)$. Verify that this leads to

$$P(l) = \frac{e^{-l/l_{mf}}}{l_{mf}},$$

where $l_{mf} = \langle l \rangle$ is called the *mean-free path* of the molecules.

- e. Finally, show that the diffusion coefficient of these molecules is given by the following formula, which is well known in the kinetic theory of gases:

$$D = \frac{1}{3} v l_{mf}. \quad (0.2)$$

- 10) Suppose that a dilute colloidal dispersion contains equal numbers of two types of spherical particles. One population has a radius of 20 nm, the other 40 nm. Describe the form of the intensity autocorrelation function that one would measure with DLS.

Problems Chapter 5

1

1. The Clausius-Clapeyron equation

$$\left(\frac{dP}{dT}\right)_{1-2\text{coexistence}} = \frac{\ell_{12}}{T(v_1 - v_2)}$$

describes the temperature-pressure relation of phase coexistence of a phase 1 (e.g. a gas) and a phase 2 (e.g. a liquid) of a simple one-component system. Here $\ell_{12} \equiv T(s_1 - s_2)$ is the so-called *latent heat*, which is taken up by the system during the phase transformation from phase 1 to phase 2, and v_i is the volume per particle in phase $i = 1, 2$. Here we derive this.

- a. Two coexisting phases must satisfy the conditions of thermal, mechanical, and chemical equilibrium. What are these conditions?
- b First consider a state (p, T) for which $\mu_1(p, T) = \mu_2(p, T)$, with μ_i the chemical potential in phase $i = 1, 2$. [Recall that $\mu = \mu(p, T)$, e.g. from the Gibbs-Duhem relation.] Now manipulate the condition for phase coexistence at another temperature $T + dT$ and pressure $p + dp$ to obtain the Clausius-Clapeyron equation.

2. Ideal gas

The Hamiltonian for an ideal gas is given by

$$H = \sum_{i=1}^N \frac{p_i^2}{2m} \quad (1)$$

The ideal gas is often used as a reference system of which one can calculate the free energy analytically.

- a. Calculate the canonical partition function $Z(N, V, T)$.
- b. Calculate the Helmholtz free energy, the pressure, the chemical potential, and the averaged energy.
- c. Calculate the averaged energy and show that the energy fluctuations are given by

$$\langle (E - \langle E \rangle)^2 \rangle = \frac{3}{2} N (k_B T)^2 \quad (2)$$

Show that the relative energy fluctuations are small for large N .

3. The three-dimensional hard-sphere fluid is described by the Hamiltonian

$$H(\Gamma) = \sum_{i=1}^N \frac{\mathbf{p}_i^2}{2m} + \Phi(\mathbf{r}^N) \text{ with } \Phi(\mathbf{r}^N) = \sum_{i<j}^N \phi_{HS}(r_{ij}),$$

where $\phi_{HS}(r) = \infty$ for $r < \sigma$ and 0 if $r > \sigma$. The volume of a sphere is $v_0 = (\pi/6)\sigma^3$.

- a. Give the canonical partition function $Z(N, V, T)$ for this system, and perform the momentum integrations. The remaining factor is the configuration integral

$$Q(N, V, T) = \int_V d\mathbf{r}_1 \cdots \int_V d\mathbf{r}_N \exp[-\beta\Phi].$$

- b. Calculate the energy E and the specific heat $C_V \equiv (\partial E / \partial T)_{V, N}$ exactly (!).
- c. In order to obtain the Helmholtz free energy we need to calculate Q . Argue to what extent the following two approximations are reasonable:

$$(i) \quad Q(N, V, T) \simeq V(V - 8v_0)(V - 2 \cdot 8v_0) \cdots (V - (N - 1) \cdot 8v_0);$$

$$(ii) \quad Q(N, V, T) \simeq (V - 4Nv_0)^N.$$

- d. Use approximation (ii) to calculate the pressure p , and compare this with the Van der Waals' equation of state.
- e. Does method (ii) yield the correct hard-sphere virial coefficients B_2 and B_3 ?

4. Carnahan-Starling equation of state for hard spheres The virial expansion for the pressure is given by (see Eq. 3.1):

$$\frac{P}{\rho k_B T} = 1 + B_2 \rho + B_3 \rho^3 + B_4 \rho^3 + \cdots \quad (3)$$

For hard spheres B_2, B_3, B_4 are known analytically, while higher order terms have been calculated by Monte Carlo simulations:

$$\begin{aligned} B_2 &= 4v_0 \\ B_3 &= 10v_0^2 \\ B_4 &= 18.36v_0^3 \\ B_5 &= 28.24v_0^4 \\ B_6 &= 39.53v_0^5 \\ B_7 &= 56.52v_0^6 \end{aligned} \quad (4)$$

with $v_0 = \pi/6\sigma^3$ the volume of a single hard sphere with diameter σ .

- a. Check that the virial coefficients can be approximated remarkably well with $B_{n+1} = (n^2 + 3n)v_0^n$.
- b. Show that by using the expansion:

$$S_0 = \sum_{n=1}^{\infty} \eta^n = \frac{\eta}{1-\eta} \quad (5)$$

one can derive:

$$\begin{aligned} S_1 &= \sum_{n=1}^{\infty} n\eta^n = \frac{dS_0}{d\eta} - 1 - S_0 \\ S_2 &= \sum_{n=1}^{\infty} n^2\eta^n = \frac{d^2S_0}{d\eta^2} + 1 - 3\frac{dS_0}{d\eta} + S_0 \end{aligned} \quad (6)$$

- c. Show that

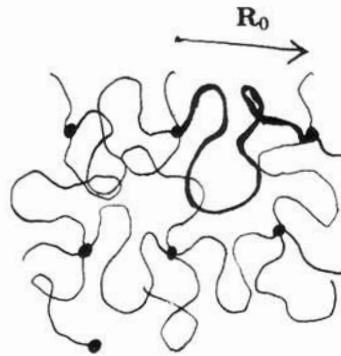
$$\frac{P}{\rho k_B T} = 1 + \sum_{n=1}^{\infty} (n^2 + 3n)\eta^n \quad (7)$$

reduces to the Carnahan-Starling equation of state Eq. (3.54).

7. Polymers: problems

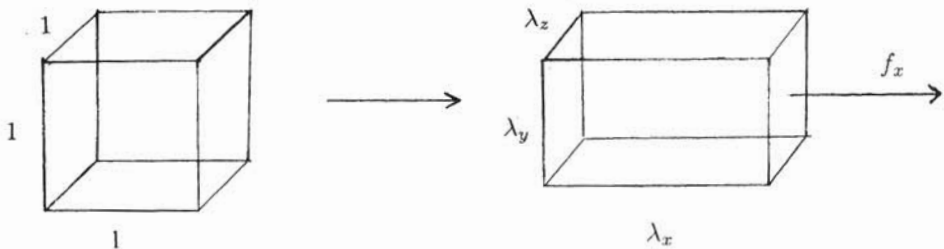
1. In this problem we will have a closer look at some properties of the solution to the diffusion equation.
 - a. Check that probability distribution (2.7) is a solution to equation (2.4).
 - b. Show that this probability distribution is normalized.
 - c. What is the formula corresponding to (2.7) describing a diffusing particle?
 - d. Make a sketch of the formula in c. for different moments in time, for instance as a function of x for $y = z = 0$. What happens if we take $t \rightarrow 0$? What is the physical significance of this?
 - e. Calculate the standard deviation in \mathbf{R}^2 and compare this to $\langle \mathbf{R}^2 \rangle$.

2. This problem tries to describe the elasticity of polymer molecules in a rubber. Rubber consists of molten polymers connected to each other at certain points by so-called *cross links*:



A schematic representation of a rubber.

The concentration of cross links is ν , so there are also on the order of ν subchains per unit volume. \mathbf{R}_0 is the end-to-end distance of a subchain. In a polymer melt (sub)chains practically behave like undisturbed ideal chains, so that we immediately have some formulas to our disposal. When a rubber cube is stretched, there is conservation of volume to a good approximation (after all a polymer melt is a kind of liquid, which are generally incompressible):



Stretching of a unit cube of rubber.

In this picture the so-called stretching factors are λ_x, λ_y and λ_z . Conservation of volume requires $\lambda_x \lambda_y \lambda_z = 1$. Symmetry considerations further give: $\lambda_y = \lambda_z$. We presume that the rubber network deforms in the same way as the total cube:

$$\mathbf{R}_0 = (R_{0x}, R_{0y}, R_{0z}) \xrightarrow{-234-} \mathbf{R} = (\lambda_x R_{0x}, \lambda_y R_{0y}, \lambda_z R_{0z})$$

Now we have sufficient elements to calculate the elastic force.

- What is the change in free energy of one single ideal chain under the deformation described above?
- Argue that the free energy change of the total cube is given by:

$$\Delta A = \frac{k_B T v}{2} (\lambda_x^2 + \lambda_y^2 + \lambda_z^2 - 3)$$

- Let $\lambda_x = \lambda$ and use conservation of volume and symmetry to further simplify this formula.
- Now show that the required force for stretching is given by:

$$f_x = k_B T v \left(\lambda - \frac{1}{\lambda^2} \right)$$

Discuss this formula and the way it depends on the variables involved.

- From a theoretical point of view it is interesting to see how polymers behave in d dimensions. For $d = 2$ one can think of a polymer at a surface. However, also unphysical dimensions $d \geq 4$ are theoretically interesting, since polymer coils turn out to behave always like ideal coils. The most important point is the dependence of the magnitude of the coil on N . A calculation in d dimensions using Flory's lattice model, gives insight into this.
 - Argue that equation (3.5) may be generalized to

$$\frac{A(R)}{k_B T} = -\ln W(R) = cst - (d-1) \ln R + \frac{d}{2Nb^2} R^2 + \frac{N^2 v_c}{2R^d}$$

- Take $v_c = 0$ (ideal chain) first and calculate $R = R_0^*$ where the free energy has a minimum. Compare this with the square root of the mean square $\sqrt{\langle \mathbf{R}^2 \rangle} = bN^{1/2}$ (note that for this part dimension $d = 1$ is not covered by this method).
- Verify that for a non-ideal polymer the minimization leads to

$$\left(\frac{R^*}{R_0^*} \right)^{d+2} - \left(\frac{R^*}{R_0^*} \right)^d \approx \frac{N^2 v_c}{(R_0^*)^d} \approx \frac{v_c}{b^d} N^{2-d/2} \approx N^{2-d/2}$$

We can leave out numerical factors like $d/(d-1)$ and take $v_c/b^d = 1$, since here we are only interested in the dependence on N .

- We can now further analyze this equation. For long chains (large N) it is nearly always possible to neglect one of the terms in the equation with respect to the other two. Use this fact to determine:

$R^* \approx bN^v$	
$d \leq 4$	$v = \frac{3}{2+d}$
$d \geq 4$	$v = \frac{1}{2}$

- Would it have been clear from the start that $v = 1$ for $d = 1$? For 4 dimensions and higher a polymer chain with excluded volume also behaves ideally: think of the reason for this.

Computer simulations give:

d	1	2	3	4
v	1	0.75	0.588	0.50

Compare these results with those of the simple Flory model.

4. At the end of section 3.3 a remark was made about the relation between the free energy of a chain and the second virial coefficient. The second virial coefficient may be better known in the context of the pressure. In this problem the connection is clarified and a relation is made to the free energy of a concentrated polymer solution within the so-called *Flory–Huggins* approximation. The interaction between polymer segments within a single polymer chain is given by the last term of (3.5) using transformation (3.10):

$$\frac{A_{ww}(R)}{k_B T} = \frac{N^2 v}{2R^3} = \frac{v}{2} Nc$$

where segment concentration $c(= N/R^3) = N/V$. From the free energy you can go to the pressure by means of the thermodynamic relation:

$$P = -\left(\frac{\partial A}{\partial V}\right)_N$$

- Use this to show that the interaction term in the free energy leads to a pressure term quadratic in the segment concentration (of which the coefficient is directly related to the second virial coefficient).
- For a more concentrated system of n_p polymers of N segments and n_s solvent molecules (occupying $\Omega = n_p N + n_s$ lattice sites and with a volume $V = \Omega v_c$, where v_c is the fixed volume per lattice site) we have volume fraction $\phi = n_p N / \Omega$ and the (Helmholtz) free energy of mixing A_m (within the Flory–Huggins approximation):

$$A_m(\Omega, \phi) = \Omega k_B T f_m(\phi) = \Omega k_B T \left[\frac{1}{N} \phi \ln \phi + (1 - \phi) \ln(1 - \phi) + \chi \phi(1 - \phi) \right]$$

The free energy of mixing A_m is the difference in free energy between the mixed and unmixed system. The expression for the pressure now also requires a constant number of polymers:

$$P = -\left(\frac{\partial A}{\partial V}\right)_{n_p, N}$$

Could you argue that we obtain the *osmotic* pressure Π of a polymer solution against pure solvent if we take $A = A_m$ within this expression?

- Now calculate Π from A_m . Try to find the following intermediate results:

$$\begin{aligned} \Pi &= \frac{k_B T}{v_c} \left[-f_m(\phi) + \phi \frac{df_m}{d\phi} \right] \\ &= \frac{k_B T}{v_c} \left[-\ln(1 - \phi) + \frac{\phi}{N} - \phi - \chi \phi^2 \right] \end{aligned}$$

- Use this to make a low density expansion. Could you explain the term linear in ϕ ? What is the second virial coefficient and how does it compare to the one found in a.?

5. In this problem we will consider mixtures of 2 types of molten polymers A (N_A segments) and B (N_B segments), so-called *blends*. The second component is now also a polymer, so that the corresponding term in the entropy of mixing within the Flory-Huggins approximation (4.2) must here be divided by the number of segments within this polymer, N_B :

$$f_m(\phi) = \frac{1}{N_A} \phi \ln \phi + \frac{1}{N_B} (1 - \phi) \ln(1 - \phi) + \chi \phi(1 - \phi)$$

with a generalized $\chi \equiv \frac{z(\epsilon_{AA} + \epsilon_{BB} - 2\epsilon_{AB})}{2k_B T}$. We assume that both polymers have the same number of segments ($N_A = N_B = N$).

- Within the above expression for $f_m(\phi)$ compare (qualitatively) the relative importance of the entropy and the energy and try to predict whether the polymers will easily mix.
 - Show that for $N_A = N_B = N$ the expression for $f_m(\phi)$ is symmetric.
 - Determine the positions of the minima and maxima of $f_m(\phi)$. (Hint: show that this implies $\ln(\frac{\phi}{1-\phi}) = -N\chi(1-2\phi)$; assume for one of the solutions to this equation $\phi \ll 1$ and check if this approximation is justified afterwards).
 - Make a sketch of $f_m(\phi)$. Estimate the values of the coexisting volume fractions.
 - Calculate the critical point of this system. What does this tell you about the miscibility of polymers?
 - Could you think of a method to mix these polymers anyway?
6. Describe and explain (within 1 to 2 pages) the different regions and boundaries in the figure displayed on page 31.

8. DLVO Potential & Techniques to Measure Interaction Forces

- 1) Show that if the interaction potential between molecules are of the form C/r^n for all distances, the energy of that molecule will depend on the shape of the container if $n \leq 3$. (Why does the same argument not hold for the free energy?)
- 2) Show that for two weakly interacting dipoles the Boltzmann averaged first order approximation to the energy is of the form $1/r^6$.
- 3a) Show that the interaction energy of an atom A with a permanent dipole with moment m_1 with an atom B with a polarizability α_2 is given by:

$$w(r, \theta) = -\frac{1}{2} \frac{m_1^2 \alpha_2}{(4\pi\epsilon\epsilon_0)^2 r^6} [1 + 3\cos^2 \theta]$$

Where θ is the angle between the dipole and the distance vector r between the atoms.

- 3b) Average this energy rotationally to arrive at the $1/r^6$ term for the induction or Debye forces.
- 4) Calculate the interaction energy between two infinite half-spaces using Hamaker's approach of pair-wise summation of $1/r^6$ interactions (note that this energy needs to be given per unit surface area).
- 5a) Calculate the Van der Waals interaction energy between two identical spheres with radius a a distance h apart using pair-wise summation. Note that in this equation the interaction depends only on h/a (as it should for scale invariant $1/r^6$ potentials).
- 5b) What is the limiting formula for distances $h/a \ll 1$?
- 5c) Show that this limiting form is compatible with the Derjaguin approximation between two spheres.
- 5d) Check how good this limiting formula is by calculating the interaction at a distance $h=0.01a$.
- 6a) Colloidal particles often aggregate in non-polar liquids (hydrocarbons, oils) because of the attractive Van der Waals forces between them. This is often a nuisance but can be prevented by coating the particles with a surfactant or polymer layer whose refractive index matches that of the liquids. Explain this phenomenon.
- 6b) At an ACS conference Dr. X from Colloids Corp. describes a colloidal dispersion of silica spheres (diameter $0.5 \mu\text{m}$, smooth surface) in oil, where by coating the spheres with a 'matching layer' of surfactant, the depth of the potential well was reduced by a factor 10 as ascertained by light scattering measurements. When asked about the thickness of the layer, Dr. X replied that this is proprietary information. What was the thickness of the layer?
- 7a) Show that the non-linear PB equation for a flat plate and 1-1 electrolyte can be written in dimensionless units ($X=x\kappa$, and $\Phi=e\psi/kT$) as:

$$\frac{1}{2} \frac{d}{dX} \left(\frac{d\Phi}{dX} \right)^2 = \frac{d \cosh \Phi}{dX}$$

7b) Solve this equation and show that its solution is:

$$\Phi = 2 \ln \left(\frac{1 + t_0 e^{-x}}{1 - t_0 e^{-x}} \right) \quad \text{with } t_0 = \tanh \left(\frac{\Phi_0}{4} \right)$$

7c) Show that for $\Phi \ll 1$ this equation reduces to the DH limiting case (Eq. 32).

7d) Another interesting limiting case is obtained for large X . Show that in this case the potential can be approximated with:

$$\Phi = 4t_0 e^{-x}$$

7e) Interpret the physical meaning of the (limit of) the prefactor.

8) Use the equation derived at 7d) in combination with the superposition approximation (using the force method) *and* the Derjaguin approximation for spheres to obtain the following free energy of interaction between two identical spheres (for distances $\kappa^{-1} \ll x \ll a$) at a constant surface potential (note the different functional form as compared with Eq. 39):

$$V_{dl0}(h) = 4kT \frac{a}{l_{Bj}} t_0^2 e^{-\kappa h}$$

with the Bjerrum length as defined in Chapter 1 and h the distance between the spheres.

9) If we combine the Van der Waals forces for short distances between spheres (means also in the Derjaguin approximation) with the Equation derived in problem 8 we get for this limit of the DLVO potential:

$$V(h) = 4kT \frac{a}{l_{Bj}} t_0^2 e^{-\kappa h} - \frac{A_{eff} a}{12h}$$

We can now analyze this equation for conditions of stability between the spheres.

9a) First show for what conditions this equation has a maximum.

Let's now analyze a few concrete examples. Example 1: $A_{eff} = 20 \times 10^{-20} \text{ J}$ ($\sim 50 kT$) and $\kappa^{-1} = 10 \text{ nm}$ (10^{-3} M 1-1 electrolyte in water, $\epsilon \sim 80$).

9b) For what surface potentials will there be a maximum in the stability curve?

Example 2: $A_{eff} = 20 \times 10^{-20} \text{ J}$ ($\sim 50 kT$) and $\Phi_0 = 1$.

9b) For what range of 1-1 salt concentration will there be a maximum in the DLVO potential?

9c) Are the values given for 9b still within the approximations made in deriving the DLVO potential used?

